Vol. 59 MARCH, 1955 No. 3

THE JOURNAL OF PHYSICAL CHEMISTRY

(Registered in U. S. Patent Office)

THE JOURNAL OF PHYSICAL CHEMISTRY

(Registered in U. S. Patent Office)

Published monthly by the American Chemical Society at 20th and Northampton Sts., Easton, Pa.

Entered as second-class matter at the Post Office at Easton, Pennsylvania.

The *Journal of Physical Chemistry* is devoted to the publication of selected symposia in the broad field of physical chemistry and to other contributed papers.

Manuscripts originating in the British Isles, Europe and Africa should be sent to F. C. Tompkins, The Faraday Society, 6 Gray's Inn Square, London W. C. I, England.

Manuscripts originating elsewhere should be sent to W. Albert Noyes, Jr., Department of Chemistry, University of Rochester, Rochester 3, N. Y.

Correspondence regarding accepted copy, proofs and reprints should be directed to Assistant Editor, Allen D. Bliss, Department of Chemistry, Simmons College, 300 The Fenway, Boston 15, Mass.

Business Office: Alden H. Emery, Executive Secretary, American Chemical Society, 1155 Sixteenth St., N. W., Washington 6, D. C.

Advertising Office: Reinhold Publishing Corporation, 430 Park Avenue, New York 22, N. Y.

Articles must be submitted in duplicate, typed and double spaced. They should have at the beginning a brief Abstract, in no case exceeding 300 words. Original drawings should accompany the manuscript. Lettering at the sides of graphs (black on white or blue) may be pencilled in, and will be typeset. Figures and tables should be held to a minimum consistent with adequate presentation of information. Photographs will not be printed on glossy paper except by special arrangement. All footnotes and references to the literature should be numbered consecutively and placed in the manuscript at the proper places. Initials of authors referred to in citations should be given. Nomenclature should conform to that used in *Chemical Abstracts*, mathematical characters marked for italic, Greek letters carefully made or annotated, and subscripts and superscripts clearly shown. Articles should be written as briefly as possible consistent with clarity and should avoid historical background unnecessary for specialists.

Symposium papers should be sent in all cases to Secretaries of Divisions sponsoring the symposium, who will be responsible for their transmittal to the Editor. The Secretary of the Division by agreement with the Editor will specify a time after which symposium papers cannot be accepted. The Editor reserves the right to refuse to publish symposium articles, for valid scientific reasons. Each symposium paper may not exceed four printed pages (about sixteen double spaced typewritten pages) in length except by prior arrangement with the Editor.

Remittances and orders for subscriptions and for single copies, notices of changes of address and new professional connections, and claims for missing numbers should be sent to the American Chemical Society, 1155 Sixteenth St., N. W., Washington 6, D. C. Changes of address for the *Journal of Physical Chemistry* must be received on or before the 30th of the preceding month.

Claims for missing numbers will not be allowed (1) if received more than sixty days from date of issue (because of delivery hazards, no claims can be honored from subscribers in Central Europe, Asia, or Pacific Islands other than Hawaii), (2) if loss was due to failure of notice of change of address to be received before the date specified in the preceding paragraph, or (3) if the reason for the claim is "missing from files."

Subscription Rates: to members of the American Chemical Society, $8.00 for 1 year, $15.00 for 2 years, $22.00 for 3 years; to non-members, $10.00 for 1 year, $18.00 for 2 years, $26.00 for 3 years. Postage free to countries in the Pan American Union; Canada, $0.40; all other countries, $1.20. $12.50 per volume, foreign postage $1.20, Canadian postage $0.40; special rates for A.C.S. members supplied on request. Single copies, current volume, $1.00; foreign postage, $0.15; Canadian postage $0.05. Back issue rates (starting with Vol. 56): $15.00 per volume, foreign postage $1.20, Canadian, $0.40; $1.50 per issue, foreign postage $0.15, Canadian postage $0.05.

The American Chemical Society and the Editors of the *Journal of Physical Chemistry* assume no responsibility for the statements and opinions advanced by contributors to THIS JOURNAL.

The American Chemical Society also publishes *Journal of the American Chemical Society*, *Chemical Abstracts*, *Industrial and Engineering Chemistry*, *Chemical and Engineering News*, *Analytical Chemistry*, and *Journal of Agricultural and Food Chemistry*. Rates on request.

THE JOURNAL OF
PHYSICAL CHEMISTRY

(Registered in U. S. Patent Office) (Copyright, 1955, by the American Chemical Society)

VOLUME 59 MARCH 17, 1955 NUMBER 3

THE STRUCTURES OF PHENYLBORON DICHLORIDE, B-TRICHLOROBORAZOLE, AND N-TRIMETHYLBORAZOLE AS DETERMINED BY ELECTRON DIFFRACTION[1]

BY KENNETH P. COFFIN[2] AND S. H. BAUER

Contribution from the Department of Chemistry, Cornell University, Ithaca, N. Y.

Received February 24, 1954

Visual analysis of electron diffraction photographs obtained from gaseous phenylboron dichloride, B-trichloroborazole and N-trimethylborazole permitted the determination of their molecular structures. Within the limits of the data, the first of these was shown to be planar, while the substituted borazoles resemble symmetrically substituted benzene derivatives.

Non-sector electron diffraction photographs were obtained for three boron-containing compounds whose structures are of interest relative to earlier work on boron trichloride and borazole. These are phenylboron dichloride, $C_6H_5BCl_2$; B-trichloroborazole, $B_3Cl_3N_3H_3$; and N-trimethylborazole, $B_3H_3N_3(CH_3)_3$. The materials were received under vacuum in glass tubes furnished with break seals. Two vacuum fractionations were made in all-glass systems in the course of preparing the samples for use in the camera.

The phenylboron dichloride was furnished by A. W. Laubengayer and R. W. Baker (Cornell). The tan color described by Baker[3] as appearing upon standing in the presence of "Apiezon L" was present in these samples, and reappeared in all instances after fractionations under vacuum in entirely glass systems. This indicates that the coloration is the consequence of disproportionation or possibly a polymerization rather than reaction with an impurity. The B-trichloroborazole was furnished by Laubengayer and Brown[4] (Cornell); the sample was a fluffy white solid with a few small crystals and some traces of discoloration. Upon standing, the fractionated material recrystallized into several large colorless crystals. The N-trimethylborazole was furnished by Schaeffer and Anderson[5] (the University of Chicago). This sample appeared as a colorless liquid, with traces of a solid material present. Similar solids were noted after six months or so in the redistilled portions of the sample. Although no physical constants were measured to determine the purity of the materials used for the diffraction studies, we believe these to be as pure as the samples prepared by the original investigators for characterizing these compounds.

The diffraction photographs were taken with electrons of about 47 kv. The nozzle to plate distance of about 19 cm. was calibrated with gold foil for each compound. Intensities were estimated visually and their decrement with angle was adjusted for rough conformity with the criterion $s.I(s)e^{0.0015s^2} \simeq$ constant; in the case of $C_6H_5BCl_2$ this criterion did not appear to be compatible with the photographs, and hence was not rigorously applied. Values of s_0 and the intensities are given in Tables I, II and III. It is regrettable that in spite of several attempts, no rings could be obtained beyond the values of s_0 reported in the tables. Since extended trials and use of a sector were prevented by lack of material and time, we present conclusions derived from the available visual data in view of the interesting structures of the compounds. No attempts were made to revise our original visual intensity estimates after our computation of radial distribution and intensity curves.

Radial Distribution Curves.—Radial distribution curves were calculated by I. B. M. methods according to the equation[6] using the damping cri-

(1) From the doctoral dissertation of Kenneth P. Coffin, Cornell University, 1951.

(2) National Advisory Committee for Aeronautics, Cleveland, Ohio.

(3) R. W. Baker, Thesis submitted to the Graduate School of Cornell University, September, 1948.

(4) C. A. Brown, Thesis submitted to the Graduate School of Cornell University, September, 1948.

(5) G. W. Schaeffer and R. R. Anderson, *J. Am. Chem. Soc.*, **71**, 2143 (1949).

(6) The Cornell procedure is analogous to that of P. A. Schaffer, Jr., V. Schomaker and L. Pauling, *J. Chem. Phys.*, **14**, 659 (1946).

$$rD(r) = K \sum_{q=1}^{q=q_{max}} q \times I(q)e^{-b^2q^2} \sin r\frac{\pi q}{10}$$

terion that $\exp(-b^2q_{max}^2) = 0.1$, where q_{max} equals the observed value of q for the largest ring. The intensity curves were extended to zero angle with the aid of computed curves for reasonable models. The resulting R.D. curves were analyzed to obtain preliminary results; then new intensity curves were computed for the small q values. Finally, the radial distribution calculations were repeated. For each compound, the "improved" R.D. curve was analyzed in order to obtain the "most compatible" model as a basic structure, and as a point of departure for a series of theoretical intensity curves. The method of analysis consisted of systematically "scoring" variations of the distances in the improved model for agreement with the improved R.D.

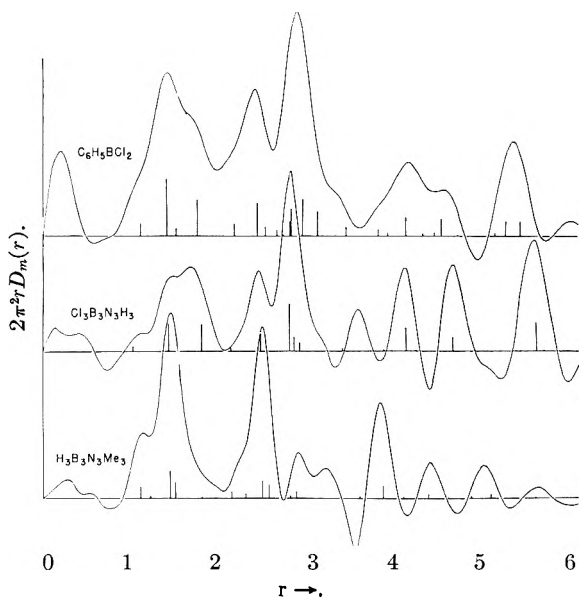

Fig. 1.—Radial distribution curves (improved).

The method is somewhat analogous to the parameter maps based on intensity curves. It requires the calculation of a minimum number of intensity curves, since they are used primarily for confirmatory purposes; advantage is taken of the fact that all the information given in the intensity curve is included in the radial distribution curve, although in a somewhat different form. In particular, for the case of non-sector data, such as were obtained in this case, the method minimizes the great emphasis often put on temperature factors and minor features of the visual pattern. The details of its application to multiparameter problems and nonplanar molecules have not been considered in detail. The testing method used is directly applicable only to a two-variable problem, as is the case for B-trichloroborazole where one wishes to determine the B–Cl and B–N distances after assuming D_{3h} symmetry and the N–H distance, or for N-trimethylborazole, where one wishes to determine the C–N and B–N distances, again assuming D_{3h} symmetry and the B–H and C–H distances. In the phenylboron dichloride, the radial distribution indicates an essentially planar molecule. Then three variables appear: B–C, B–Cl and <ClBCl, assuming an undistorted form for the C_6H_5 group. For the latter compound three values of <ClBCl, 115, 117, and 120° were selected, and the scoring method applied for each model.

The scoring method is as follows. Intervals of each variable are selected (0.02 ångström here), at $A - 0.10$, $A - 0.08$, $A - 0.06$, . . ., A, . . ., $A + 0.08$, $A + 0.10$, etc., and similarly for B, where A and B are the approximate values of the variables under test for the improved model. Each combination of the interval values represents a point of intersection on a two-dimensional grid. For each grid point the various intermolecular distances are determined either graphically or analytically; the relative ease and simplicity in the application of the method result from the high degree of systematization which may be used. Each significant feature of the radial distribution curve is evaluated rather arbitrarily, and a system set up to "score" the corresponding computed feature for each grid point. For example

	Within, Å.	But not within, Å.	Score
Sharp peak, small r	0.01		3
	.02	0.01	2
	.03	.02	1
	.04	.03	0
		.04	Eliminate
Broad peak, large r	0.02		3
	.04	0.02	2
	.06	.04	1
	.10	.06	0
		.10	Eliminate
Composite peak	0.015		2
	.030	0.015	1
		.030	0
Broad peak, medium r	0.03		1

Composite peaks are assumed to be compounded as

$$\sum_{ij}{}' Z_iZ_jr_{ij} \Big/ \sum_{ij}{}' Z_iZ_j$$

By working through the radial distribution curve, peak by peak, using the more symmetric, non-composite peaks, a large number of combinations can be eliminated. The remaining combinations can then be scored completely. The final scores are entered on the grid, and contour lines of constant score are drawn. The center of the contour may reasonably be accepted as the final parameter ratio, subject to the assumed distances and symmetry. The size and shape of the contours give an indication of the probable error. The reliability of the results, of course, is based to some extent on the judgments of the reliability of the individual peaks as reflected in the scoring system.

Figure 1 shows the improved radial distribution curve for each of the compounds. In all cases there is an initial maximum followed by a minimum; for the borazoles these are centered about zero, but for $C_6H_5BCl_2$ the peak is positive and the minimum coincides with the base line. For that compound the entire curve is essentially non-negative; while this is a desirable feature in general, in this case it appears more likely that a low frequency positive loop has been superimposed on the curve. For B-trichloroborazole, the curve has only small negative areas; the peak at 3.55 Å. corresponds to no distance under consideration and has been assumed spurious. The curve for N-trimethylborazole is good except for a spurious peak at 3.10 Å., the deep negative portion immediately to the right, and a spurious peak at 5.55 Å.

Figure 2 shows the contour analyses for these compounds. For $C_6H_5BCl_2$, three contour diagrams appear corresponding to the assumptions of a planar molecule, with $(C-C)_{ring}$ = 1.39 Å. and 115, 117 and 120° for <ClBCl. A molecule with the ClBCl plane at right angles to the plane of the ring would have heavy contributions due to C–Cl distances at about 3.7 and 4.9 Å. At these distances, minima appear in the radial distribution curve; hence, the conclusion that rotation about the C–B bond is highly restricted, the most probable orientation being that with the chlorine atoms in the plane of the ring. All three contours correspond to identical chlorine positions relative to the ring. The indeterminancy arises from the relatively small contribution to the scattering of the distances involving the single boron atom. The Cl–Cl distance is 2.93 ± 0.01 Å. A B–Cl distance in the range 1.69–1.76 Å. is indicated; the centers of the contours being at 1.74, 1.72 and 1.70 ± 0.02 Å., respectively, for 115, 117 and 120°. The corresponding C–B distances are 1.46, 1.50 and 1.55 ± 0.04 Å.

The radial distribution curve suggests that the C–C distances in the ring is somewhat shorter than 1.39 Å., possibly 1.38 or 1.37 Å. Based on the assumption of a 1.37 Å. ring the first radial distribution curve was analyzed, and again, the Cl–Cl distance was found to be 2.93 Å. The three centers of the second set of contours again correspond to identical positions of the chlorine atoms relative to the ring. The over-all length of the molecule is nearly the same for the two cases, the long C–Cl distances being only 0.04 Å. greater for the case of the 1.37 Å. ring and the first radial distribution; this together with the 0.04 Å. difference in ring diameter explains the approximately 0.08 Å. differences in the C–B distance between the two analyses.

<ClBCl, degree	B–Cl, Å.	C–B[C–C, 1.37], Å.	C–B[C–C, 1.39], Å.
115	1.74 ± 0.02	1.55 ± 0.04	1.46 ± 0.04
117	1.72 ± .02	1.58 ± .04	1.50 ± .04
120	1.70 ± .02	1.61 ± .04	1.55 ± .04

Hence, median values based on the scoring method

C–C 1.38 ± 0.01 Å., C–B 1.50 ± 0.08 Å., 115°
1.54 ± 0.08 Å., 117°
1.58 ± 0.08 Å., 120°

The analysis of the contour pattern for B-trichloroborazole is entirely straightforward except that the peak at about 1.68 Å. on the radial distribution curve corresponding to B–Cl is nearly 0.1 Å. too short to be consistent with the remainder of the curve. In this analysis, the 1.68 Å. peak was given only moderate weight as the inconsistency demonstrates that some error must be present in the data. [A computed curve was inverted to make certain there might not be a dislocation inherent in the manner of damping and terminating the intensity curve; none was found.] The result indicated is B–N = 1.41 ± 0.02 Å. and B–Cl = 1.78 ± 0.03 Å.

The physical interpretation of the contour pattern for N-trimethylborazole is somewhat obscured by the fact that the B–N and C–N distances are nearly equal and are weighted quite similarly;

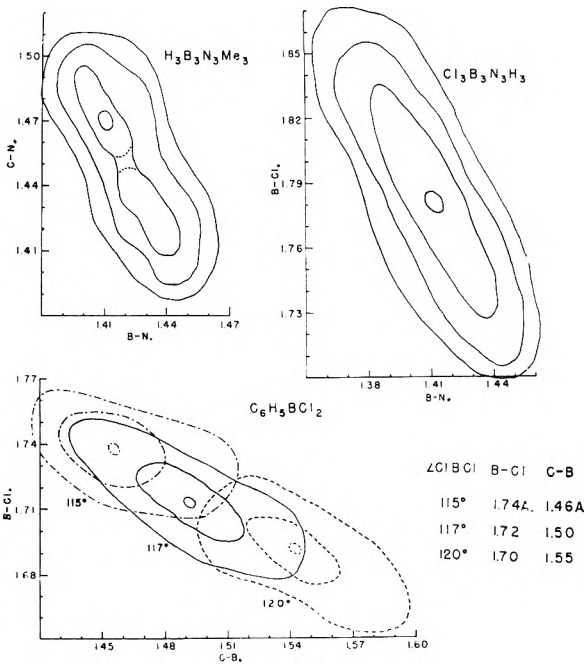

Fig. 2.—Contour analyses of the radial distribution curves. Multiply scales by 1.004 for calibration correction.

the contours are especially elongated and the inner contour seems to indicate the presence of two peaks. Such a possibility seems perfectly reasonable since the two major distances are so nearly equal; however, it seems reasonable to require that C–N be greater than B–N. This assumption dismisses the lower portion of the contour as a geometrical coincidence and shifts the best model from the true center into the lower portion of the upper half, at about B–N = 1.42 ± 0.02 Å. and C–N = 1.48 ± 0.03 Å.

TABLE I

$C_6H_5BCl_2$

Max.	s_0 Min.	q_0	J_{vis}, initial estimate	$J_{2nd\ R.D.}$	$\left(\frac{s}{s_0}\right)_{Bo}$
2.63		8.4	10	8.5	
	4.05	12.9	−15	−18.5	
4.94		15.7	20	29.0	1.012
	5.72	18.2	−12	00.0	1.016
6.23		19.8	15	12.0	1.000
	6.90	22.0	−10	+2.5	0.991
7.38		23.5	10	6.5	0.993
	8.02	25.5	−9	−9.0	0.994
8.59		27.3	8	9.0	1.024
	9.29	29.6	−2	+4.5	1.023
9.71		30.9	5	7.0	0.999
	10.43	33.2	−8	−7.0	0.994
11.06		35.2	6	9.0	1.019
11.64	Sh.	37.1	2	4.0	
	12.73	40.5	−4	−5.5	0.982
13.72		43.7	4	5.5	Error
	14.94	47.6	−3	−3.5	1.004
15.77		50.2	3	4.0	0.998
		(55.5)	−2	−4.5	
18.77		59.7	2	2.4	0.999
				Ave.	1.003
				Mean dev.	0.010

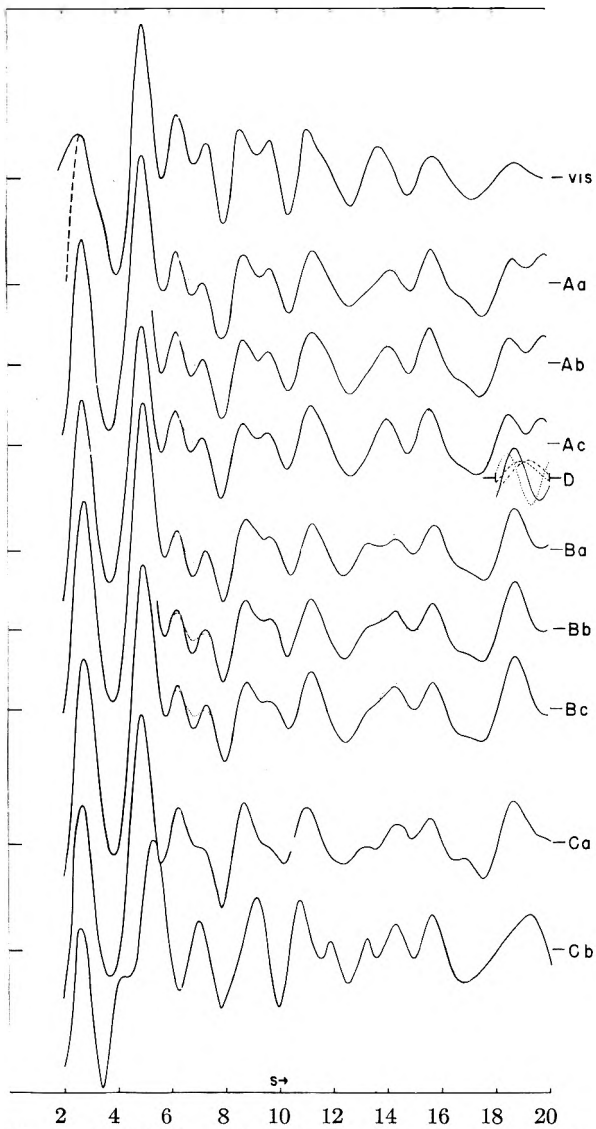

Fig. 3.—$C_6H_5BCl_2$; assumed: symmetrical phenyl group, C—H = 1.09 Å., planar molecule except in Cb.

Curve	Models C–C, Å.	B–Cl, Å.	C–B, Å.	<ClBCl, degree
Aa	1.37	1.69	1.60	120
Ab	1.37	1.71	1.57	117
Ac	1.37	1.73	1.54	115
Ba	1.39	1.69	1.54	120
Bb	1.39	1.71	1.49	117
Bc	1.39	1.73	1.45	115
C	1.39	1.74	1.56	120

Ca Planar.
Cb Plane of ClBCl perpendicular to ring.
No temperature factors are included; all H terms included in A and B, except where dotted lines indicate the effect of damping the long H terms by including only C–H and C–C–H terms.
D (———), long C–Cl distances } combine to a single
(– – – –), 1.39 C–C ring } peak, as in B curves
. . . . . , short C–Cl distances } combine to twin peaks
.–.–.–, 1.37 C–C ring } as in A curves

Intensity Curves and Final Structures.—Figure 3 shows the visual curve, the intensity curves computed for the various models determined from the contour patterns, and two curves computed for a preliminary model for $C_6H_5BCl_2$. These preliminary curves Ca and Cb correspond to the planar and "anti"-planar configurations, respectively; they confirm conclusively the evidence based on the radial distribution curves regarding the lack of large amplitude rotation (of the order of 45° from the plane). Moreover, even the planar Ca differs sufficiently from the visual curve to justify the elimination of this particular model from further consideration.

TABLE II
$B_3Cl_3N_3H_3$

Max.	s_0 Min.	q_0	J_{vis}, initial estimate	$J_{2nd\ R.D.}$	$\left(\frac{q}{q_0}\right)_{Aa}$
	4.23	13.5	−15	14.5	
4.80		15.3	20	20.0	1.026
5.93	Sh.	18.9	15	5.5	
	6.54	20.8	−15	−15.5	0.986
7.04		22.4	14	9.5	1.013
	7.70	24.5	−6	−6.0	1.000
8.23		26.2	9	6.5	0.989
	8.88	28.3	−10	−8.0	0.978
9.45		30.1	10	8.5	1.007
		(32.9)	−9	−7.5	
11.43		36.4	8	5.5	1.005
		(38.4)	−5	−4.5	
12.70		40.4	5	2.5	0.993
		(42.4)	−6	−6.0	
13.99		44.5	7	6.0	1.002
		(47.8)	−5	−2.5	
16.16		51.4	3	2.5	0.990
		(55.5)	−3	−3.5	
18.56		59.1	4	3.5	1.000
		(62.7)	−1.5	−1.5	
20.86		66.4	1	1.0	0.998
		(71.0)	−2	−2.0	
23.50		74.8	2	1.5	0.984
				Ave.	0.998
				Mean dev.	0.010

Minima beyond $s > 9.5$ could not be measured reliably.

TABLE III
$B_3H_3N_3(CH_3)_3$

Max.	s_0 Min.	q_0	J_{vis}, initial estimate	$J_{2nd\ R.D.}$	$\left(\frac{q}{q_0}\right)_{Aa}$
	4.42	14.1	−10	−12.5	
5.34		17.0	20	18.0	1.024
6.81	Sh.	21.7	10	0.0	
	7.64	24.3	−15	−7.0	0.959
8.88		28.3	15	5.5	1.007
	9.71	30.9	−15	−6.0	0.981
10.45		33.3	15	8.0	0.982
	11.25	35.8	−8	−4.0	
11.85		37.7	6	0.0	
	12.50	39.8	−10	−4.5	0.972
13.54		43.1	10	6.0	1.002
	14.72	46.9	−4	−2.5	1.002
15.52		49.4	4	1.5	
	17.00	54.1	−6	−3.0	0.989
18.38		58.5	5	3.5	1.002
		(62.5)		−2.0	
20.56		65.4	2	1.0	1.004
		(69.4)		−1.5	
23.36		74.4	4	1.5	0.993
		(78.4)		−1.0	
26.19		83.4	1	0.8	
				Ave.	0.993
				Mean dev.	0.014

TABLE IV

Compound	$\frac{C-C}{B-N}$	B–Cl	B–C	$\left(\frac{C-C}{1.545}\right)\left(\frac{B-N}{1.56}\right)$	Ref.
C_6H_6	1.393 (0.01)			0.902	7
$C_6H_5BCl_2$	1.38 (+0.02) (−0.01)	1.72 (0.03)	1.52 (0.07)	.895	C and B
$H_3B_3N_3H_3$	1.44 (0.02)			.923	8
$Cl_3B_3N_3H_3$	1.41 (0.02)	1.78 (0.03)			C and B
	1.413 (0.01)	1.760 (0.015)		.907	9
$H_3B_3N_3Me_3$	1.42 (0.02)			.911	C and B
BCl_3		1.73 (0.02)			10
BMe_3			1.56 (0.02)		10
H_3BCO			1.540		11
(BN)cryst.	1.446			.927	12
Graphite	1.42			.922	13

The differences in general shape at $s = 19$ between the A curves and the B curves are predominantly due to the relatively small differences in the ratio of the ring dimension to the six C–Cl distances in the two models; their contributions are shown separately in curves D. When summed, the (C–Cl/C–C) ratio incorporated in the B curves is definitely favored. Using this latter ratio, the computed curves, based on the C–C = 1.39 Å., ring, checks the visual peak at $s = 19$ more closely than does a 1.37 Å. ring. The Cl–Cl distance is identical for both models and the B–Cl distances are identical for corresponding submodels (a, b and c). The four C–B distances contribute about 7% of the total intensity as compared to 10% for the four C–H distances of the phenyl group; this indicates how difficult any definite assignment of C–B will be, which in turn introduces some difficulty in the assignment of B–Cl and <ClBCl.

The shoulder on Ba at $s = 14$ would tend to exclude that model, but none of the curves fit especially satisfactorily in this region (presumably an error in the visual curve); in all cases the magnitude of the shoulder can be reduced with a temperature factor on the hydrogen contributions. In the region of $s = 17$, Ac is preferred while Aa and Ab and possibly Ba are apparently satisfactory.

Based primarily on the outer maximum, the intensity curves seem to eliminate a ring as small as 1.37 Å. Selection among submodels based on a 1.38 or 1.39 Å. ring and the over-all dimensions from the radial distribution curves apparently require data of greater accuracy than those obtained visually.

Final Structure for $C_6H_5BCl_2$.—Combined radial distribution curve and intensity curve analysis gives

C–C = 1.38 or 1.39 Å.
Cl–Cl = 2.93 ± 0.01 Å.
C–B, B–Cl and <ClBCl such as to be consistent with a long C–Cl = 5.38 ± 0.03 Å.; hence <ClBCl = 118 ± 3°, B–Cl = 1.72 ± 0.03 Å., and C–B = 1.52 ± 0.07 Å.
C–H = 1.09 Å. and a hexagonal ring assumed.

Figure 4 shows the visual curve, three intensity curves for variations of the model selected from the contour pattern, and one intensity curve of the preliminary model used for B-trichloroborazole. Although the B curve contains temperature factors, the model it represents seems somewhat less acceptable, based on general relative intensities, than those represented by the A curves. The region $q = 32$–37 favors Aa and Ab, and similarly at $q = 48$–52; in the region $q = 67$–76, Ac is less accept-

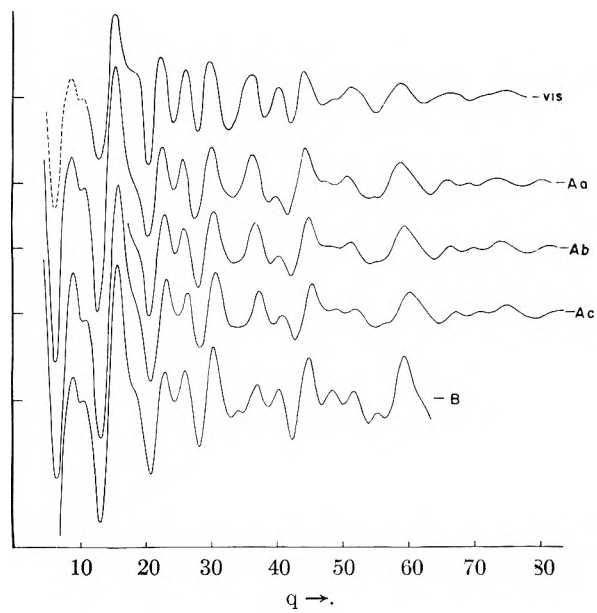

Fig. 4.—$B_3Cl_3N_3H_3$; assumed: D_{3h} symmetry and N–H = 1.01 Å.

Curve	Models B–N, Å.	B–Cl, Å.
Aa	1.41	1.79
Ab	1.41	1.76
Ac	1.41	1.73
B	1.44	1.74

Curve	Bond type	α_{ij}^2
A	Y—Z (except Y—H)	0.0015
	Y—H and X-----Z (except X-----H)	0.0023
	X H and all others	0.0034
B	No temp. factors; only Y—H and X–Y–H hydrogen contributions included	

(7) I. L. Karle, *J. Chem. Phys.*, **20**, 65 (1952).
(8) S. H. Bauer, *J. Am. Chem. Soc.*, **60**, 524 (1938).
(9) D. L. Coursen and J. L. Hoard, *ibid.*, **74**, 1742 (1952).
(10) H. A. Levy and L. O. Brockway, *ibid.*, **59**, 2085 (1937).
(11) W. Gordy, H. Ring and A. B. Burg, *Phys. Rev.*, **78**, 1482 (1951).
(12) R. S. Pease, *Acta Cryst.*, **5**, 356 (1953).
(13) J. D. Bernal, *Proc. Roy. Soc. (London)*, A**106**, 749 (1924).

able than Aa and Ab because of the intensity increases with q in Ac. In general, Aa and Ab seem to be more acceptable.

Final Structure for $B_3Cl_3N_3H_3$.—Combined radial distribution curve and intensity curve analysis gives

B–N = 1.41 ± 0.02 Å.
B–Cl = 1.78 ± 0.03 Å.
N–H = 1.01 Å., and D_{3h} symmetry assumed

Figure 5 contains the visual curve, three intensity curves for variations of the model selected from the contour pattern, and one curve for the preliminary model for N-trimethylborazole. Except for the absence of long hydrogen distances, damping factors and a scale factor, curve B lies close to Ab. Allowing for a visual shift in the feature at q = 50 toward larger values of q, Aa and Ab are favored. At q = 58, Aa shows the largest indication of broadening, and is most compatible with the visual curve.

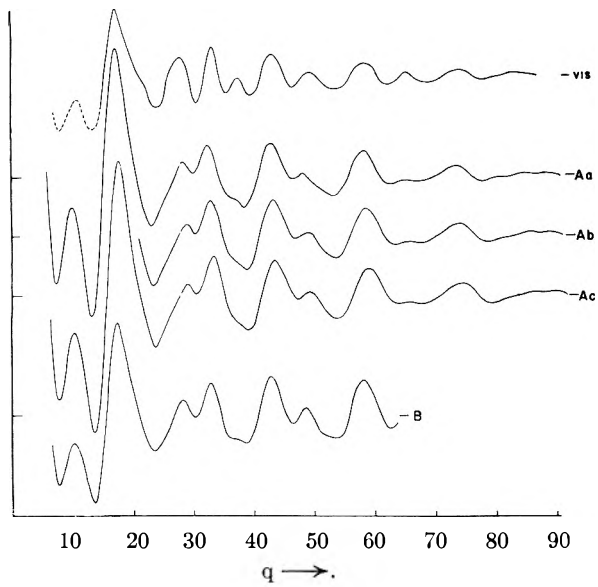

Fig. 5.—$B_3H_3N_3(CH_3)_3$; assumed: D_{3h} symmetry, B–H = 1.20° Å., C–H = 1.09 Å.

Curve	Models B–N, Å.	C–N, Å.
Aa	1.42	1.49
Ab	1.42	1.46
Ac	1.42	1.43
B	1.44	1.47

Curve	Bond type	α^2_{ij}
A	Y—Z (except Y—H)	0.0015
	Y—H and X------Z (except X------H)	0.0023
	X------H and all others	0.0034
	3 rotations, H–CN–B, H–CNB–N and H–CNBN–C introduced as 5 distances	0.0023
B	No temp. factors; only Y–H and X–Y–H hydrogen contributions included	

Final Structure for $B_3H_3N_3(CH_3)_3$.—Combined radial distribution curve and intensity curve analysis gives

B–N = 1.42 ± 0.02 Å.
C–N = 1.48 ± 0.03 Å.
B–H = 1.20 Å.; C–H = 1.09 Å., and D_{3h} symmetry assumed

Discussion

For reference and comparison a summary of the interatomic distances observed in these and related compounds is listed in Table IV.

The B–Cl distance found for $C_6H_5BCl_2$ checks within experimental error that distance determined in the trichloride. The obvious analogous resonance structures may be written for the two compounds. These suggest that the B–C distance should be less in the dichloride than in boron trimethyl. Some estimate of the relative magnitude of the contributions to the ground state of Lewis structures containing $\rangle C{=}B\langle$, may be obtained from the dipole moment determined by Baker[3] for $C_6H_5BCl_2$. He reported 3.07 ± 0.15 debye, using benzene as the solvent. Since the phenyl group and chlorine atoms are not very different in electron sharing properties, resonance contributions from the structures

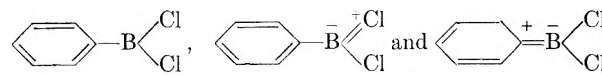

should produce only a small net moment. To account for the large value found, an appreciable contribution from the quinoid structure

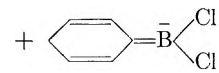

seems necessary.

Attention has been called many times to the expected analogies between the isoelectronic C–C and B–N systems. That the parallels between borazole and benzene, and between boron nitride and graphite may have been over emphasized has been pointed out by Pease.[12,14] Insofar as B-trichloroborazole is concerned, the B–Cl distance does seem to be larger than in BCl_3, which is consistent with the "aromatic" character of the $(B–N)_3$ ring. Part of the ambiguity in the formulation of resonance structures for this ring is due to the difficulty of giving meaning to the term "normal single bond" for the link between adjacent atoms one of which is a good acceptor while the other is a good electron donor. It now appears reasonable to postulate that in $H_2B(NR_2)BBH_2$ [R = CH_3 or H] the B–N bonds are close to "single," and that the B  B is a three-center, two-electron unit.[15] The observed[16] B–N distances [1.55$_4$ ± 0.026 Å. (R = H) and 1.56$_4$ ± 0.026 Å. (R = CH_3)] are consistent with this assumption. Thus, if one accepts the numbers in the table at face value, the fifth column shows that the substituted borazoles approach the

(14) R. N. Pease, *J. Am. Chem. Soc.*, **74**, 4219 (1952).
(15) W. H. Eberhardt, B. Crawford and W. N. Lipscomb, *J. Chem. Phys.*, **22**, 989 (1954).
(16) K. Hedberg and A. J. Stosick, *J. Am. Chem. Soc.*, **74**, 954 (1952).

ratio for a benzene type contraction more closely than does borazole itself.

Further justifications of the assumption made in computing the fifth column rely on spectroscopic and thermochemical data. That the molecular point group symmetry of borazole is D_{3h} has been demonstrated by two infrared studies.[17] In the latter, data on N-trimethylborazole were also obtained. The analysis of the ultraviolet absorption spectrum of borazole[18] was based on the assumed similarity of its electronic structure to that of benzene.[19] Thus, although the first excited electronic level in borazole occurs at 6.5 e.v. above the ground state, compared to 4.9 e.v. for the corresponding level in benzene, the increment was ascribed to the electronegativity differences between the boron and nitrogen.

Rector, Schaeffer and Platt[20] have made a preliminary study of the gain and loss of "aromatic character" on substituted borazoles [N-trimethyl-,[21] B-trimethyl- and B-trichloroborazole] based on shifts in the first ultraviolet absorption band. Their conclusion was that N-substitution increases aromaticity while B-substitution decreases aromaticity (this is due to the corresponding increase and decrease of the negative charge on the boron). The N-trimethyl spectrum resembles that of mesitylene and indicates a nearly completely aromatic compound; the spectrum of the B-trimethyl compound resembles that of the simple addition product of borine and amine absorptions and indicates nearly complete lack of aromaticity. Finally, the spectrum of the B-trichloroborazole was found to be very similar to that of B-trimethylborazole. Hence, these workers argue that the ring in B-trichloroborazole is less aromatic than in borazole itself; their results suggest large double bond contributions of the type $>\bar{B}=\overset{+}{Cl}$ which counter the electron seeking inductive influence of the chlorine atoms. These conclusions, which represent an exception to their general proposition, are not confirmed by the present investigation, which shows the B–N distances of both the N-trimethyl- and B-trichloroborazole to be about the same. At any rate, the ultraviolet absorption spectra of these compounds as well as their general chemical stability support the notion that appreciable aromatic type resonance may be ascribed to the $(B–N)_3$ ring. In contrast, if one were to use 0.80 Å. for the "covalent radius" of boron[22] and the usual Schomaker–Stevenson addition formula, the deduced "single-bond" B–N distance would be 1.45 Å. Then only a negligible amount of aromatic character could be ascribed to the $(B–N)_3$ ring.

A recently determined value for the heat of formation of tris-dimethylaminoborine[23] suggests that the B–N bond in that compound has the same degree of multiple bonding as in B-trichloroborazole. Skinner reports that in $B(NMe_2)_3$ the average bond dissociation energy for B–N is 89.7 kcal. (based on the 96 kcal. value for the heat of sublimation of boron) while a reduction of the heat of formation[24] of $Cl_3B_3N_3H_3$ gives 92.1 kcal. for the corresponding bond, [here $D(N_2)$ = 225.8 kcal.]. In contrast, we point to a rough average bond dissociation energy of about 52 kcal. for B–N in $B_2H_5NMe_2$, based (1) on a preliminary heat of formation for that compound, (2) upon the value for the average bond dissociation energy of the bridge (B–H–B) in diborane,[25] and (3) the assumption that the (B–H–B) bridge bond in $B_2H_5NR_2$ is weaker than those in B_2H_6 by about 6 kcal. This average value for the B–N bond may be interpreted as half the sum of 25 kcal. (for N → B) and 79 kcal. (for a "single bonded" B–B).

This work was supported, in part, by the Office of Naval Research.

(17) (a) B. L. Crawford, Jr., and J. T. Edsall, *J. Chem. Phys.*, **7**, 223 (1939); (b) W. C. Price, *et al.*, *Disc. Faraday Soc.*, No. 9, 131 (1950). See also: R. A. Spurr and S. C. Chang, *J. Chem. Phys.*, **19**, 518 (1951).

(18) J. R. Platt, H. B. Klevens and G. W. Schaeffer, *ibid.*, **15**, 698 (1947); L. E. Jacobs, J. R. Platt and G. W. Schaeffer, *ibid.*, **16**, 116 (1948).

(19) C. C. J. Roothaan and R. S. Mulliken, *ibid.*, **16**, 118 (1948.)

(20) C. W. Rector, G. W. Schaeffer and J. R. Platt, *ibid.*, **17**, 460 (1949).

(21) The N–CH_3 distance in this compound is practically identical with the value reported for $N(CH_3)_3$, 1.47 ± 0.01 Å. V. Schomaker, private communication to P. W. Allen and L. E. Sutton, *Acta Cryst.*, **3**, 46 (1950).

(22) K. Hedberg, *J. Am. Chem. Soc.*, **74**, 3486 (1952).

(23) H. A. Skinner and N. B. Smith, *J. Chem. Soc.*, 4025 (1953).

(24) E. R. Van Artsdalen and A. S. Dworkin, *J. Am. Chem. Soc.*, **74**, 3401 (1952).

(25) Unpublished analyses of various thermochemical and kinetic data involving the borane–diborane equilibrium, S. H. Bauer.

THE RATE OF EVAPORATION OF WATER THROUGH FATTY ACID MONOLAYERS[1]

BY ROBERT JAMES ARCHER[2,3] AND VICTOR K. LA MER

Contribution from the Department of Chemistry, Columbia University, New York, N. Y.

Received June 21, 1954

The influence of fatty acid monolayers on the rate of evaporation of water has been studied by measuring the rate of absorption of water vapor by a solid desiccant supported above the water surface. The data are reported as the specific resistance of the monolayer to evaporation which is equal to the reciprocal of the specific rate constant for condensation through the film. These data establish a contamination effect upon which the retardation of evaporation is strongly dependent and which has introduced serious error in all previous work. Our results give a description, of the rate of evaporation through monolayers, which is fundamentally different from earlier work. The resistance to evaporation of monolayers of the four saturated fatty acids C_{17}, C_{18}, C_{19} and C_{20} was measured as a function of surface pressure, chain length, monolayer phase, subphase composition and surface temperature. In the liquid condensed phase, monolayer resistance is *independent of surface pressure* and subphase *p*H; its logarithm is a linear function of chain length. On the other hand, in the solid phase on an alkaline subphase containing calcium ions, the logarithm of resistance is a linear function of both chain length and surface pressure. The logarithm of the resistance in the liquid condensed phase of C_{19} acid monolayers is a linear function of the reciprocal of the absolute temperature, which substantiates the description of evaporation resistance in terms of an exponential energy barrier. A theory is proposed for the source of the energy barrier; calculation of its magnitude from heats of vaporization data agrees well with the experimental values. All of the monolayers studied decrease the rate of evaporation of water by a factor of about 10^4.

Introduction

Following Hedestrand's[4] unsuccessful attempt to measure the effect of films on the rate of evaporation of water, Rideal[5] showed qualitatively that a fatty acid monolayer decreases the rate. Subsequently, Sebba and Briscoe[6] reported a large dependence of the retardation of evaporation on the surface pressure of the monolayer. About the same time, Langmuir and Schaefer[7] devised an ingenious and simple method for measuring the absolute rate of evaporation through films. Previous techniques measured a relative effect of unknown relation to the absolute rate. Langmuir and Schaefer found a pressure dependence of the same magnitude as observed by Sebba and Briscoe.

The principle of the method of Langmuir and Schaefer was adopted for the present work. However, it was necessary to modify their technique to obtain reproducible measurements and to establish a more reasonable theoretical basis for the method than had been proposed. Although we had misgivings concerning specific points of technique and theory, it was believed, at the outset, that the data of Langmuir and Schaefer (L and S) were essentially valid. Early in the experimental work, however, it was discovered that their monolayers were subject to a source of contamination which produced a reduction of evaporation resistance of such magnitude that their results, particularly the reported pressure dependence, are invalid so far as quantitative conclusions are concerned. This contamination results from the operations involved in a standard technique for forming monolayers and was also present in the work of Sebba and Briscoe. Although L and S's measurements were extensive and posed curious problems, we believe, in the light of the present investigation, that they have little relation to the properties of pure monolayers. Most of the anomalies they reported are traceable to contamination effects or to unexplainable experimental abberrations. The latter comment refers particularly to their finding that the effect of a fatty acid monolayer on evaporation is strongly dependent upon the *p*H of the subphase. We found no such dependence.

(1) A review of previous work and some preliminary results were presented at the Conference on Properties of Surfaces of November 5, 1953, sponsored by The New York Academy of Sciences. The contributions to this conference will appear in Annals of The New York Academy of Sciences, Archer and La Mer, **58**, Art. 6, 807 (1954).

(2) Submitted in partial fulfillment of the requirements for the degree of Doctor of Philosophy in the Faculty of Pure Science of Columbia University, April, 1954. The unabridged dissertation with four appendices of data and calculations will be available as a microfilm through the Dissertation Office of Columbia University Library.

(3) We are indebted to Professor Menelaos D. Hassialis for his kind interest in this work and for recommending one of us (R. J. A.) for a Socony-Vacuum Fellowship for the years 1952-1953 and 1953-1954. For this fellowship, thanks are also extended to the Socony-Vacuum Company and to Columbia University.

(4) G. Hedestrand, THIS JOURNAL, **28**, 1244 (1924).

(5) E. K Rideal, *ibid.*, **29**, 1585 (1925).

(6) F. Sebba and H. V. A. Briscoe, *J. Chem. Soc.*, 106 (1940).

(7) I. Langmuir and V. J. Schaefer, *J. Franklin Inst.*, **235**, 119 (1943), reprinted in "Surface Chemistry," ed. by Forest Ray Moulton, Amer. Assoc. Adv. Sci., No. 21, 1943, pp. 17-39.

I. Technique and Theory of Measurements

Apparatus.—A quantity defined as the specific resistance of the film to the evaporation of water is calculated from the difference between the reciprocals of the rates of absorption of water vapor by a solid desiccant supported above the water surface with and without a monolayer. The measurements are made in the trough of a surface balance so that the resistance to evaporation can be determined as a function of the surface pressure of the monolayer. Figure 1 is a cross-sectional sketch of the components of the apparatus. The desiccant container C is a cylindrical lucite box. The bottom is open except for a membrane M which retains the desiccant but is permeable to water vapor. The thermometer T, inserted through the rubber stopper S, measures the temperature of the desiccant. An airtight lucite lid fits the bottom face when the container is not in use. In making a measurement, the container fits into the lucite ring R and is supported by the extended rim L. The supporting ring is inserted into a circular hole in the square lucite plate P, which rests on the edges of the surface balance trough B, thus holding the bottom face of the container parallel to and about 2 mm. from the water surface. A thermometer is placed just beneath the water surface and another on the floor of the trough. Extensive examination of various possibilities led to the choice of anhydrous lithium chloride for the desiccant and a heavy waterproofed silk cloth for the container membrane. The entire surface balance was enclosed in a large wooden box with glass sides and top and a sliding wooden door.

To determine the rate of absorption, the container, filled with desiccant, is weighed; the lid is removed and the container put into position above the water surface for a definite

time. It is then removed, the lid is replaced and the container is reweighed. The increase in mass divided by the time in position gives the rate of absorption.

Definition and Measurement of Evaporation Resistance.—The transport of water from the liquid phase to the desiccant involves evaporation from the water surface, diffusion through the separating air column and the membrane, followed by condensation or absorption at the desiccant surface. The symbols used in the analysis of this process are defined in Table I.

TABLE I

GLOSSARY OF SYMBOLS

M = mass of water vapor absorbed
t = time of absorption
A = area of the desiccant surface
b = distance between the water and membrane surfaces
b' = thickness of the membrane
T = temp. of the water surface
T' = temp. of the desiccant surface
m = mass of water molecule
Q = $(kT/2\pi m)^{1/2}$
Q' = $(kT'/2\pi m)^{1/2}$
w = concn. of water vapor in equilibrium with the liquid water
w_0 = concn. of water vapor in equilibrium with the desiccant
w' = concn. of water vapor at the water surface
w_0' = concn. of water vapor at the desiccant surface
w_m = concn. of water vapor at the membrane surface
D = diffusion coefficient for water vapor in air
D' = apparent diffusion coefficient for water vapor in the membrane
α = fraction of water molecules impinging on the water surface which condense
β = fraction of water molecules impinging on the desiccant surface which are absorbed

The net rate of evaporation from the water surface is the difference between the absolute rates of condensation and evaporation. If these rates are described as the fraction of the vapor molecules impinging on the surface which condense, the net rate of evaporation is

$$M/t = A\alpha Q(w - w') \quad (1)$$

The rate of diffusion from the water surface to the membrane is

$$M/t = DA(w' - w_m)/b \quad (2)$$

The rate of diffusion through the membrane is

$$M/t = D'A(w_m - w_0')/b' \quad (3)$$

The rate of absorption at the desiccant surface is

$$M/t = A\beta Q'(w_0' - w_0) \quad (4)$$

If these four equations are combined to eliminate w_0', w_m and w', the result is

$$M/At = (w - w_0)/(b/D + b'/D' + 1/\beta Q' + 1/\alpha Q) \quad (5)$$

Equation 5 relates the rate of absorption by the desiccant to the actual rate of evaporation at the water surface in terms of the condensation coefficient α and suggests an analogy to Ohm's law in the form

$$\text{rate} = (\text{driving force})/(\text{resistance}) \quad (6)$$

$$M/t = (w - w_0)/R \quad (7)$$

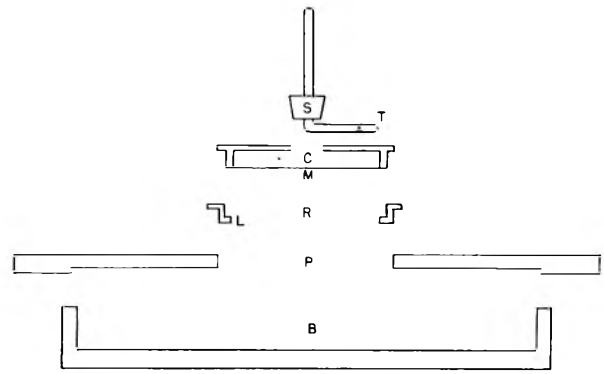

Fig. 1.—Cross-sectional sketch of experimental apparatus.

If specific resistance r is defined by the product of the total resistance and the area of the film under the desiccant

$$r = RA \quad (8)$$

the four terms in the denominator of the right-hand side of equation 5 are, respectively, the specific resistance of the air column, the membrane, the desiccant surface, and the water surface.

The evaporation rate as effected by surface films can be expressed in terms of the specific resistance of the monolayer, which is related to the condensation coefficient of the film covered surface by the expression

$$r = 1/\alpha Q \quad (9)$$

Henceforth, r will refer only to the specific resistance of the water surface with the dimensions sec./cm.

From two determinations of the rate of absorption, one with a monolayer on the surface and one without, the specific resistance of the monolayer is calculated from the expression

$$r = [A(w - w_0)t/M]_{\text{film}} - [A(w - w_0)t/M]_{\text{no film}} \quad (10)$$

which follows from equation 5 when b, T and T' are the same for the two determinations and when the specific resistance of the monolayer is much greater than that for a clean water surface, which is always the case for the films studied.

Temperature Measurement.—In deriving equation 5, it was assumed that the various parts of the system remained at constant temperature during a measurement. Actually, the temperature of the water surface decreases, the desiccant temperature increases, and a varying temperature gradient exists in the air column. It is assumed that the average temperatures of the water surface, the air column and the desiccant surface can be used to determine w, w_0 and D in equation 5. These average temperatures are estimated as follows.

In order to minimize temperature variations in the water surface, water from a thermostat is pumped through a Pyrex glass serpentine tube in the trough. The temperature of the surface is determined from an estimation of the temperature gradient in the water. A thermometer on the bottom of the trough measures a nearly constant temperature T_c. The temperature T_t, measured by another thermometer whose bulb is just beneath the surface, is assumed to be the mean temperature of the gradient between the plane at temperature T_c

and the surface. The temperature of the surface is then given by

$$T_s = 2T_t - T_c \qquad (11)$$

During absorption, the temperature variation in the surface is not great since the cooling effect of evaporation is compensated by a heating effect due to the proximity of the desiccant surface where the temperature is increasing. Since the variation is small, equation 11 gives a reasonable value for T_s within perhaps $\pm 0.1°$.

During a run, a temperature gradient is set up between the lower and upper desiccant surfaces. The temperature of the upper surface is assumed to be that of the thermometer reading at that point. If the contents of the container are mixed and the thermometer bulb submerged in the desiccant, the thermometer approximates the average temperature of the gradient. Therefore, if the temperatures of the lower surface, the upper surface and the average temperature are designated T_s', T_c' and T_t'

$$T_s' = 2T_t' - T_c' \qquad (12)$$

For absorption runs of the duration used, the average temperature and the temperature of the upper surface increase linearly with time, and presumably the lower surface temperature does also. Hence, the average temperature of the lower surface will be the average of the two values of T_s' calculated from equation 12 for values of T_t' and T_c' measured immediately before and after the absorption run.

This method for measuring the desiccant surface temperature is adequate since an uncertainty of as much as $\pm 1°$ produces a small enough effect on the uncertainty in w_0 to be within the precision of the measurements.

Since a temperature gradient exists in the air column with the average temperatures of the bounding surfaces equal to $\bar{T}_s'$ and $\bar{T}_s$, the value taken for the air column is

$$\bar{T}_{air} = (\bar{T}_s + \bar{T}_s')/2 \qquad (13)$$

Correction to M.—There will be a contribution to M from water vapor in the surrounding air. This contribution must be subtracted from the total mass absorbed to obtain the correct value for M for use in the equations developed above. The magnitude of this contribution is determined under the standard conditions by covering the surface with a thin sheet of aluminum foil instead of a monolayer. Under typical experimental conditions with the aluminum foil on the surface, 0.0085 g. of water is absorbed in 3 minutes, 0.0095 g. in 4 minutes, and 0.0125 g. in 8 minutes. For comparison, the amounts of water absorbed without the aluminum foil for times of 3, 4 and 8 minutes are 0.250, 0.333 and 0.666 g. The correction as determined includes the water vapor absorbed while the desiccant container is being put in place above the water surface and the amount absorbed while the container is removed from the supporting ring and the lid is replaced.

If a series of determinations of M as a function of time are made with a clean water surface and constant b and D, the following relation holds.

$$M = \text{constant}\ (w - w_0)t \qquad (14)$$

This requirement was confirmed experimentally.

Test of the Basic Equation.—The validity of equation 5 and of the approximations proposed can be established by measuring one of the specific resistances as a function of $A(w - w_0)t/M$ while holding the other resistances constant. This was done by determining $DA(w - w_0)t/M$ as a function of the distance b between the water surface and the membrane. The distance was varied by introducing supporting rings R of Fig. 1 with varying heights of the rim L. Seven rings were constructed with L varying from 0 to 0.6 cm. in increments of 0.1 cm. The position of the water surface was held constant to within ± 0.001 cm. by means of a hydrophilic point of glass submerged in the trough. When the height of the water decreased, the glass point protruded through the surface. Water was then added until the point just disappeared.

If B is the height of the rim L and b_0 is the constant distance between the water surface and the bottom face of the supporting plate, equation 5 can be written

$$B = DA(w - w_0)t/M - (b_0 + Db'/D' + D/\beta Q' + D/\alpha Q) \qquad (15)$$

So that the second term on the right-hand side of equation 15 will be constant, D is held constant by cooling the desiccant container, when necessary, to such an initial temperature that the average temperature of the air column is constant for a series of determinations.

To test eq. 15, $DA(w - w_0)t/M$ is plotted against B. The data fall on a straight line of unit slope within $\pm 1\%$, which is within the experimental error.[8] Thus, the validity of the technique for measuring specific resistance is established.

Of the quantities on the right-hand side of eq. 15, A, t and M are measured directly and w is taken from standard tables. The diffusion coefficient for water vapor in air is calculated from the expression

$$D = (0.220/p)(T/273)^{1.75}\ \text{cm.}^2/\text{sec.} \qquad (16)$$

from the "International Critical Tables." p is the pressure in atmospheres and T is the temperature in °K.

In these experiments, the desiccant surface became sufficiently moist to behave as a film of saturated solution. A value for w_0 corresponding to the aqueous tension of a saturated lithium chloride solution rather than the one-tenth as large value corresponding to the aqueous tension of the solid monohydrate satisfied eq. 15. Similar results were obtained using calcium chloride, *i.e.*, the aqueous tension of the saturated solution fitted the data, whereas values for the solid hydrates did not. Values for w_0 for lithium chloride are calculated from graphical data published by Bichowsky.[9]

II. Technique for Measuring Resistance of Monolayers

Introduction.—The specific resistances of monolayers of margaric acid, stearic acid, nonadecanoic acid and arachidic acid were studied. These substances will be referred to by the symbol C_n (C_{17} through C_{20}, respectively) where the index indi-

(8) See Appendix I of microfilmed dissertation for detailed data and calculations.

(9) F. R. Bichowsky, *Chem. Met. Eng.*, May, 302 (1940).

cates the number of carbon atoms in the fatty acid molecule. Melting point determinations indicated initial preparations of high purity which were further purified by recrystallization from twice distilled petroleum ether. The water and organic solvents were twice distilled from an all Pyrex glass apparatus. Surface pressure was measured with a surface balance arrangement of the vertical-pull type.[10]

Figure 2 is typical of the pressure–molecular area isotherms for the two states exhibited by compressed fatty acid monolayers.[11] Curve A-B-C is obtained on pure water or acid solutions. On an alkaline subphase which contains calcium ions, or certain other cations which form insoluble soaps, curve D-C results. The more compressible state, A-B, is designated the liquid condensed phase (LC); the state of low compressibility, B-C and D-C, is called the solid phase (S). There are minor variations in the isotherms depending on the chain length of the acid, but they are not important in the present discussion.

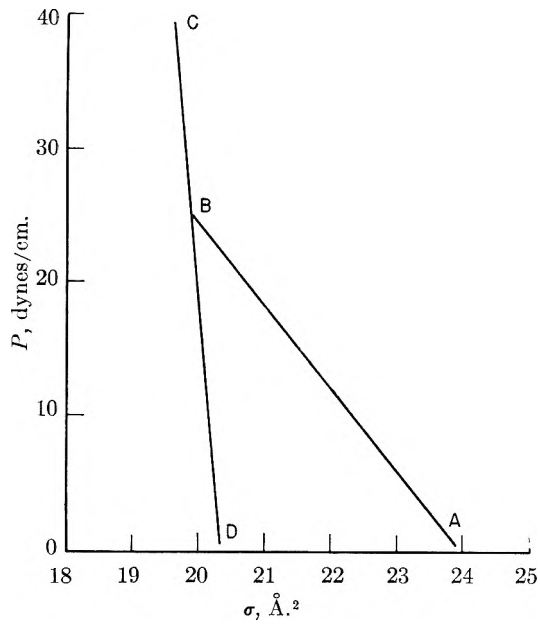

Fig. 2.—Typical pressure–molecular area isotherm for the two phases in which compressed fatty acid monolayers exist. A-B represents the liquid condensed phase and D-C the solid phase.

Dependence of Resistance on Spreading Technique.—The initial experiments to determine the general nature of the resistance of fatty acid films to evaporation were made using monolayers of the C_{19} acid on pure water in the LC phase. These experiments showed that the *characteristics of the plot of specific resistance versus surface pressure are very sensitive to variations in the technique used to spread the film.* The factors determining this sensitivity are (1) the choice of solvent used for the spreading solution, (2) the concentration of the spreading solution, (3) the pressure of the monolayer immediately after spreading, (4) the cleanliness of the water surface immediately before spreading the film, and (5) the presence of paraffin used to coat the inside surfaces and edges of the trough.

The metamorphosis of the *p-r* plot for the C_{19} acid on distilled water at 25°, for specific alterations in technique, is shown in Fig. 3. Each set of data represents typical results for a fixed spreading technique. For curves I through IV, the trough was a chromium plated brass tray coated with paraffin on the inside surfaces and upper edges. It was cleaned by flushing with warm water and the paraffin was renewed periodically.

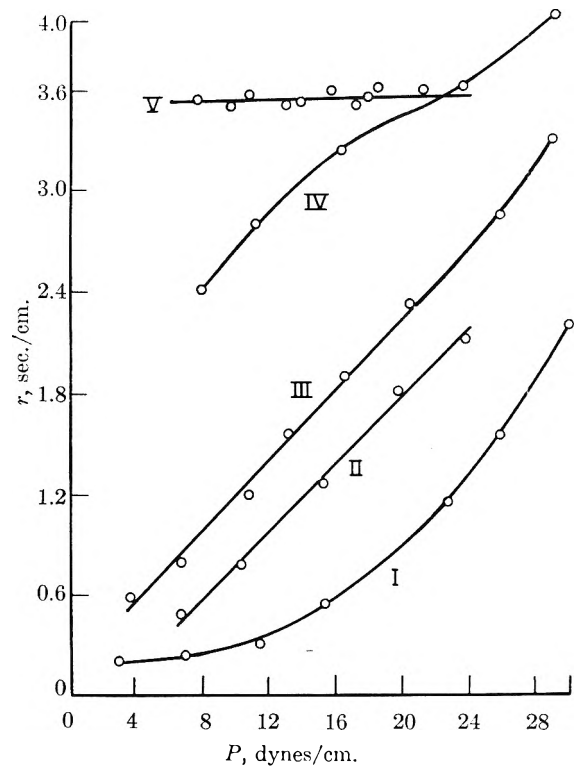

Fig. 3.—Specific resistance for C_{19} acid monolayers in the liquid condensed phase *versus* surface pressure as affected by the spreading technique.

The initial pressure referred to in each case below is the surface pressure of the film before compression. A pressure of zero means that the initial total area must be decreased by at least one-seventh before any change in surface tension is detectable.

Curve I was obtained using benzene as the spreading solvent for a 0.0035 *M* acid solution and zero initial pressure. Curve II resulted from substituting petroleum ether (boiling range 35–40°) as the solvent and using the same concentration and initial pressure. Curve III was obtained by doubling the concentration of the petroleum ether solution. When the concentration was again doubled (now 0.014 *M*), curve IV resulted.

The reproducibility of curves IV and V (the determination of curve V is described below) is contingent upon three other factors of technique: the initial pressure must be 10 dynes/cm. or greater; the water surface must be swept clean *immediately* before spreading the film; and the drops of the spreading solution must be applied rapidly. Using the metal trough, no further variation in technique changes the characteristics of curve IV.

(10) W. D. Harkins, "The Physical Chemistry of Surface Films," Reinhold Publ. Corp., New York, N. Y., 1952, p. 121.

(11) Ref. 10, pp. 116 and 152.

If the concentration of acid in the benzene solution is increased, there is a concomitant displacement of the *p-r* curve upward on the *r*-axis, but the effect is much less marked than with petroleum ether, and in no case is curve IV obtained.

To summarize, *benzene spreading solutions yield consistently low values for specific resistance, and the shape of the p-r curve is approximately exponential. Petroleum ether solutions give larger values for r* and the *p-r* curves *are nearly linear.* Increasing the concentration of the acid in the petroleum ether solutions increases the magnitude of *r* until a limiting concentration of about 0.014 is reached. Finally, if (a) special care is taken to sweep the surface clean before applying the spreading solution, (b) the solution is applied rapidly, and (c) the initial pressure is above 10 dynes/cm., a maximum result is obtained for the paraffined trough.

Explanation of Spreading Technique Effects.—We interpret these variations in the *p-r* plot as caused *primarily* by solvent molecules, occluded in the monolayer when the film is spread, and that the increase of *r* with *p* results from the expulsion of these occlusions on compression of the film. The resistance of monolayers is related to the energy required to form a free site in the film. The magnitude of this energy depends on the potential energy of interaction of a film molecule with its neighbors in the monolayer. Small foreign molecules having relatively meager interactions with the surrounding molecules constitute permanent holes in the film or at least sites of small resistance. Since the total resistance of the monolayer is the resistance of these sites acting in parallel with sites occupied by acid molecules, a small concentration of occluded foreign molecules can produce a large decrease in resistance. The following calculation will illustrate this point.

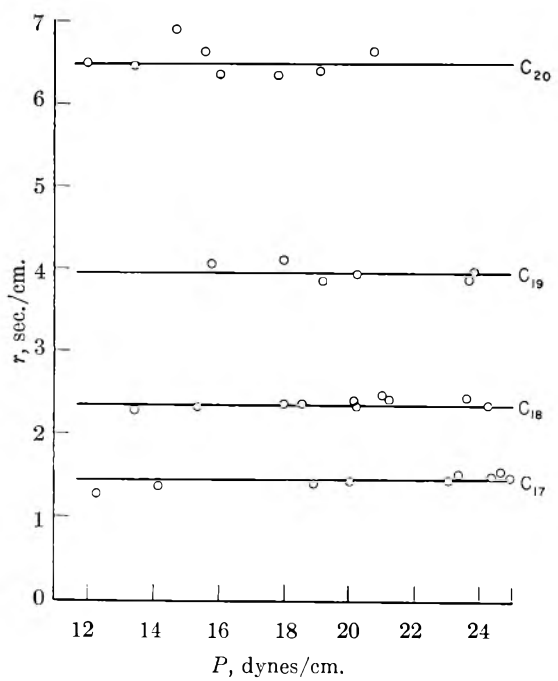

Fig. 4.—Specific resistance *versus* surface pressure for the C_{17}, C_{18}, C_{19} and C_{20} acids in the liquid condensed phase on pure water at 25.1°.

Assuming that the foreign molecules constitute free sites, the specific resistance of these sites is that of a clean water surface, which is given by

$$r_0 = 1/\alpha_0 Q = 1.9 \times 10^{-3} \text{ sec./cm.} \qquad (17)$$

if, after Alty[12] and Baranaev,[13] the value of α_0 is taken as 0.036. As determined below, the specific resistance of the C_{19} acid when occlusion effects are presumably eliminated is 3.94 sec./cm. The observed resistance for contaminated films with small concentrations of occluded molecules is

$$1/r = 1/r_{C_{19}} + n_0/r_0 \qquad (18)$$

where n_0 is the mole fraction of occlusions. Table II shows the variation of resistance with the concentration of occlusions calculated from eq. 18. These values show the large decrease in resistance that accompanies a small number of occlusions; they agree in magnitude with the observed effects of Fig. 4.

TABLE II

DEPENDENCE OF RESISTANCE ON CONCENTRATION OF OCCLUSIONS

n_0	10^{-2}	10^{-3}	10^{-4}	10^{-5}	0
r	0.18	1.3	3.3	3.8	3.94

Since the specific resistances of benzene and petroleum ether molecules probably have about the same magnitude, more molecules must be occluded when benzene is the spreading solvent to account for the lower resistances with this solvent. The relative degree of occlusion will depend on the ability of the occluded molecules to interact both with the neighboring long chain molecules and with the water surface. That this interaction would be greater for benzene follows from the facts that long chain acids are several times more soluble in benzene and that benzene itself will form a monolayer on water with an equilibrium film pressure of about 10 dynes/cm.[14] A further factor favoring the occlusion and retention of benzene is its lower volatility compared to petroleum ether.

Besides the occlusion of solvent molecules, three other sources of impurities are present in the system. These are the subphase water, the air above the surface and the paraffined surfaces of the trough.

The effect of impurities which settle on the water from the air and which are absorbed at the surface from the underlying water before the monolayer is spread will be decreased by cleaning the surface as soon as possible before applying the spreading solution. This experimental precaution yields higher resistance values. Absorption after the film is formed is minimized by maintaining the film at relatively high pressures since the rate of absorption is known to depend on surface pressure.

A likely source of impurities is the large area of paraffined surfaces of the metal trough. The difficulty of cleaning the paraffined surfaces and the possibility of surface-active impurities even in paraffin contribute sources of contamination. To alleviate these possibilities, an all glass trough of the

(12) T. Alty, *Proc. Roy. Soc. (London)*, **A131**, 554 (1931).
(13) M. Baranaev, *J. Phys. Chem. (USSR)*, **11**, 484 (1938).
(14) Harkins, ref. 10, p. 99.

type described by Andersson and others[15] was constructed by sandblasting a cavity 1.5 cm. deep, 65 cm. long and 14 cm. wide in a solid block of Pyrex glass 2.5 cm. thick. It is unnecessary to paraffin the inner surfaces of this trough; it can be cleaned easily with chromic acid cleaning solution. The upper edges of the trough can be made hydrophobic by grinding these surfaces lightly and by applying the paraffin from a stick of the solid and then rubbing with a clean towel until only a thin film is retained. This film is then fused by passing a warm porcelain spatula over the surface.

When resistance measurements were made using the glass trough and the technique of curve IV, curve V of Fig. 3 was obtained.[16] Curve V is effectively independent of the pressure of the film within the range (10–25 dynes/cm.) measured, indicating that the pressure dependent "tail" of curve IV can be eliminated by reducing the absorption of impurities from the paraffined surfaces.

The assumption that measurements employing the technique of curve V give the correct values for the specific resistance of fatty acid monolayers and that this technique is essential for the formation of such monolayers if they are to be free of impurities is substantiated by the reproducibility and the consistency of the data to be presented as well as the simplicity of interpreting the results in respect to temperature and chain lengths.

Fatty acid monolayers are ordinarily spread using about 0.2 ml. of an 0.0017 *M* acid solution, whereas we use 0.025 ml. of an 0.014 *M* solution for resistance measurements. We were unable to construct pressure–molecular area isotherms for films spread using this technique because the drops of concentrated solution evaporate so rapidly after being applied that a small amount of the acid precipitates on the water surface as an island of crystalline acid in the monolayer. As a result, the quantity of material in the film is not known and the molecular area cannot be calculated. Measurement of pressure as a function of the total film area, however, gives, for each of the monolayers, a linear isotherm exhibiting collapse at the transition point. The islands of crystalline acid did not influence the resistance because they were never permitted on that part of the film beneath the desiccant container during an absorption measurement.

In general, the surface pressure remained constant over the period of time in which evaporation resistance was measured. Occasionally, the pressure would decrease by as much as one to two dynes during the entire period of measurement (*ca.* 15 min.), in which case the average pressure is reported.

III. Experimental Results

Liquid Condensed Phase.—Having developed a technique for the reproducible measurement of specific resistance of compressed fatty acid monolayers, we studied the resistances of these films as a function of chain length, subphase composition, state of the monolayer and temperature.

Figure 4 shows the results of the measurements of the resistances of the C_{17}, C_{18}, C_{19} and C_{20} acids on pure water at 25.1° in the LC state. For each acid, resistance depends markedly on the chain length of the molecule but is independent of pressure in the range measured. The logarithms of these resistances are plotted in Fig. 5 as a function of the number of carbon atoms in the acid molecule. The plot is a straight line for which the following expression is valid for C_{17} to C_{20} acids[17]

$$\log r = -3.5355 + 0.21734n \qquad (19)$$

The resistance of the C_{19} acid in the LC phase was also determined on dilute hydrochloric acid solutions. The resistance at *p*H 1 and *p*H 3 is the same, within the experimental error, as given in Fig. 4 on pure water at *p*H 5.8–6.0.

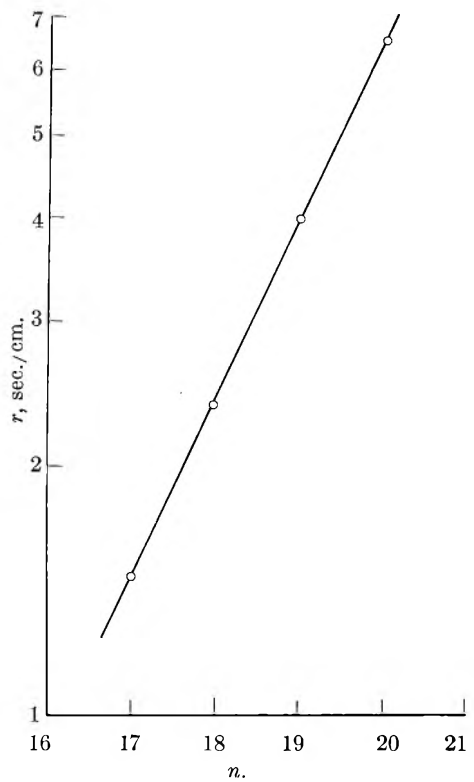

Fig. 5.—The logarithm of specific resistance in the liquid condensed phase as a function of the chain length of the monolayer molecules.

Extension of the measurements on pure water into the S phase indicates that in this range resistance increases with pressure, but the data are insufficiently reproducible to be significant. The poor reproducibility is due to the instability of the films. As soon as the transition point between the LC and S phases is passed, the film begins to collapse. Collapse is indicated by a decrease in pressure with time.

Solid Phase.—A different behavior is exhibited by the S phase on a subphase of 10^{-4} *M* $CaCl_2$ and 10^{-3} *M* $KHCO_3$ at *p*H 8. The resistance of these fatty acid films is greater than on distilled water and now varies significantly with surface pressure.

(15) K. J. I. Andersson, S. Stallberg-Stenhagen and E. Stenhagen, "The Svedberg" (Mem. Vol.), Almqvist & Wiksells Boktryckeri Ab., Uppsala, 1944.

(16) The magnitude of *r* is slightly less in Fig. 3 than in Fig. 4 because a less pure sample of nonadecanoic acid was used in these measurements.

(17) The data are given in the unabridged dissertation, Appendix II.

Data for the C_{18}, C_{19} and C_{20} acids at 25.0° obey the linear relation[18]

$$\log r = -1.9575 + 0.1400n + 6.60 \times 10^{-3}p \quad (20)$$

The data are plotted in Fig. 6. The curves are for equation 20.

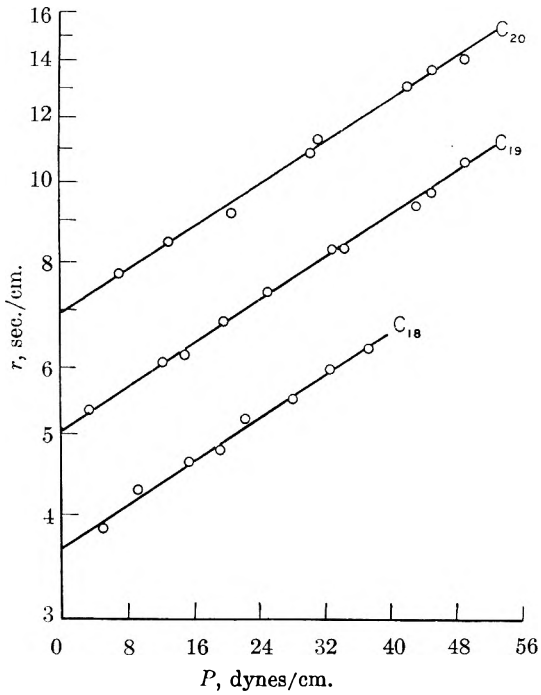

Fig. 6.—The logarithm of specific resistance in the solid phase as a function of surface pressure on a subphase of 10^{-4} M $CaCl_2$ and 10^{-3} M $KHCO_3$ at 25.0° for the C_{18}, C_{19} and C_{20} acids.

It was not possible to obtain reproducible data for the C_{17} acid on the alkaline subphase. This monolayer is unstable and exhibits a rapid collapse even at low pressures. As a general rule, when collapse occurs, specific resistance becomes abnormally low.

Temperature Dependence of Resistance.—As will be discussed below, specific resistance is attributed to an energy barrier to evaporation, E, and can be represented by an expression of the form

$$r = \text{constant} \exp(E/RT) \quad (21)$$

In order to determine the energy barrier and the coefficient of the exponential, the resistance of the C_{19} acid on pure water in the LC phase was determined as a function of the temperature of the surface. Figure 7 is the plot of log r *versus* the reciprocal of the absolute temperature. Each point on this curve is the average of four to six determinations on three different monolayers. The method of least squares yields the following relation for the straight line of Fig. 7.

$$\log r = -10.103 + 3190.7/T \quad (22)$$

At all four temperatures, resistance is independent of surface pressure as in Fig. 4.[19]

Summary.—Table III summarizes the results of the experiments. The last column expresses the data in terms of the actual effect on the evaporation rate by means of the ratio of the rate with a film on the surface to that with a clean water surface. This ratio is

$$v_f/v_0 = r_0/r \quad (23)$$

A fatty acid monolayer decreases the rate of evaporation by a factor of about 10^4.

(18) Ref. 17, Appendix III.
(19) *Ibid.*, Appendix IV.

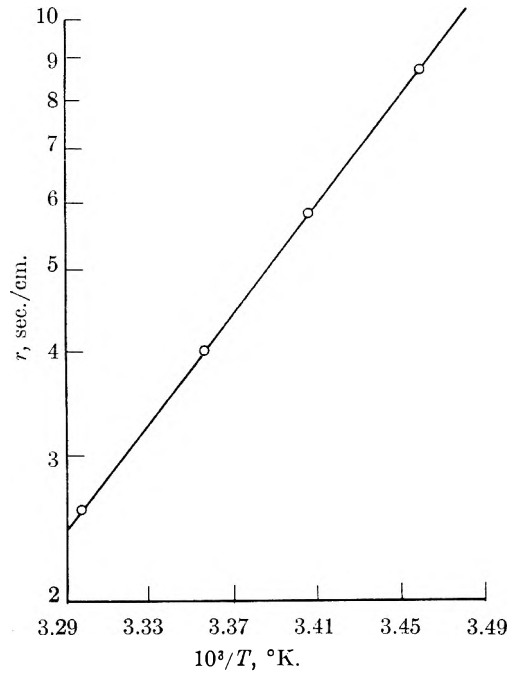

Fig. 7.—Specific resistance of the C_{19} acid monolayer as a function of the reciprocal of the absolute temperature in the liquid condensed phase on pure water.

TABLE III

TABULATION OF DATA

Acid	Subphase	T	r	A.D.[a]	p	10^4 v_f/v_0
		Liquid Condensed Phase				
C_{17}	Water	25.1	1.45	0.03	12–25	13
C_{18}	Water	25.1	2.36	.02	12–25	7.96
C_{19}	Water–HCl	25.1	3.94	.06	12–25	4.77
C_{20}	Water	25.1	6.48	.17	12–25	2.90
C_{19}	Water	30.0	2.64	.06	12–25	7.12
C_{19}	Water	20.4	5.84	.17	12–25	3.20
C_{19}	Water	15.7	8.72	.17	12–25	2.15
		Solid Phase				
C_{18}	10^{-4} M $CaCl_2$	25.0	3.65		0	5.15
	10^{-3} M $KHCO_3$		6.66		40	2.82
C_{19}	10^{-3} M $KHCO_3$	25.0	5.04		0	3.74
			9.24		40	2.04
C_{20}	10^{-3} M $KHCO_3$	25.0	6.95		0	2.70
			12.75		40	1.47

[a] A.D. computed for the 6 to 10 measurements over the pressure range p as plotted in Fig. 4. p is in dynes/cm. r is in sec./cm.

It is of interest to compare specific resistance in the liquid condensed and solid phases at the transition point where the two monolayers have the same surface pressure (about 25 dynes/cm.) and occupy the same area per molecule (about 20 Å.²/molecule). This is done in Table IV. The solid phase resistance is about twice that of the liquid condensed phase value for the three films considered.

TABLE IV

COMPARISON OF LC AND S RESISTANCES AT TRANSITION POINT

Monolayer	r_{LC}	r_S	r_S/r_{LC}
C_{18}	2.36	5.31	2.25
C_{19}	3.94	7.35	1.89
C_{20}	6.48	9.28	1.42

IV. Discussion of Experimental Results

Energy Barrier to Condensation.—A fundamental assumption in deriving the relation between the rate of absorption and specific resistance is that the absolute rate of condensation is proportional to the vapor concentration of water at the surface, and, by definition, the rate of condensation is

$$v_c = w'/r \qquad (24)$$

Since specific resistance is the reciprocal of the specific rate constant, it should obey a relation of the form

$$r = C \exp(E/RT) \qquad (25)$$

where C may be a function of temperature and E is the activation energy for condensation.

The temperature dependence of resistance for the C_{19} acid agrees with eq. 25. Equation 22 written in the form of eq. 25 is

$$r = 7.89 \times 10^{-11} \exp(14{,}595/RT) \qquad (26)$$

The activation energy for the C_{19} acid is 14,595 cal./mole.

Theory of Energy Barrier.—It is postulated that over limited domains the molecules in fatty acid monolayers form a close packed hexagonal array and that an unoccupied site must be formed in the array in order for a water molecule to penetrate the film. The energy required for this process is assumed to be the principal source of the activation energy.

The increase in the potential energy of the film molecules accompanying the formation of a free site is determined as follows. Consider a small area of the monolayer. In the initial state, all sites are occupied, and, if w_{pq} is the potential energy of interaction of a film molecule p with one of its neighbors q, the total interaction energy is the summation

$$\sum_p \sum_q w_{pq} \qquad (27)$$

over all of the molecules in the area. In the final state, one free site is formed, but the number of molecules in the area is assumed to be unchanged. The resultant change in intermolecular separation will be negligible if the area under consideration is sufficiently large. Due to the presence of the unoccupied site, the interaction energy in the final state is less than in the initial state by an amount equal to the interaction of all of the molecules with the molecule formerly occupying the free site, *i.e.*

$$\Delta E = \sum_q w_{aq} \qquad (28)$$

To restate, the increase in the potential energy of the film when a free site is formed is just the interaction energy of a molecule with all of its neighbors in the monolayer.

Assuming that each carboxyl group is associated with two water molecules through two hydrogen bonds, free site formation entails an energy increase equivalent to breaking one hydrogen bond in addition to the lateral interaction of expression 28. From this point of view, the interaction energy of a fatty acid molecule in the monolayer state should be about the same as that in the liquid state except for the relatively small interaction of the non-polar terminal groups with the corresponding overlying groups in the liquid state. Therefore, the energy of formation of a free site should be roughly one-half the energy of vaporization for the liquid state.

Energy Barrier in the Liquid Condensed State.—In order to account for the fact that, for the range reported, resistance is independent of pressure or molecular area in the LC state, the structure of the film and the mechanism of compression must be such that a decrease in molecular area is not accompanied by a decrease in intermolecular separation. Of the current theories of the structure of monolayers, the "tilted chain" theory[20,21] is in best accord with this requirement. This theory postulates that at point A on the pressure–molecular area isotherm (Fig. 2) the film molecules are close packed with their vertical axes parallel but at some angle less than 90° relative to the plane of the water surface. As the monolayer is compressed, the angle of tilt increases and the distance between homologous groups decreases. The perpendicular distance between molecules, however, is unchanged. Therefore, the interaction energy is about the same for molecules perpendicular to the surface and tilted relative to the surface. There is some variation of interaction with tilt for the end groups, but for the methyl groups the change is negligible compared to the total energy, and the change in the carboxyl group interaction is assumed to be compensated by an increase in interaction with surface water molecules as the angle of tilt decreases.

It is consistent with the above theory for the energy barrier to write eq. 25 in the form

$$\log r = \log C + E'/2.3RT + (n-2)E(CH_2)/2.3RT \qquad (29)$$

where $E(CH_2)$ is the increment in the energy barrier per CH_2 group and E' is the residual energy. This expression agrees with eq. 19 written

$$\log r = -3.1008 + 0.21734(n-2) \qquad (30)$$

The experimental value for $E(CH_2)$ calculated from eq. 30 is 296.6 cal./mole.

As a check on the consistency of experimental equations 19 and 22, equations 29 and 30 can be equated, the value for C from equation 22 is inserted, and the resultant expression solved for E'. If this is done

$$E' = 9555.6 \text{ cal./mole}$$

and

$$E = E' + (n-2)E(CH_2) = 14{,}597 \text{ cal./mole} \qquad (31)$$

in perfect agreement with the value 14,595 cal./mole for C_{19} acid from eq. 22.

The magnitude of the activation energy and of the methylene group increment can be estimated from energies of vaporization as noted above. An

(20) D. G. Dervichian, *J. Chem. Phys.*, **7**, 931 (1939).

(21) C. G. Lyons and E. K. Rideal, *Proc. Roy. Soc. (London)*, **A124**, 322 (1929).

approximation of these values can be obtained from Lederer's[22] evaluation of the constants in Nernst's[23] empirical relation for the heat of vaporization. At 25°, which is extrapolating below the melting point of the acids in question, Lederer's data give the following values for the heats of vaporization of the long chain fatty acids.

$$\lambda = 14{,}345 + 703n - 1.51n^2 \text{ cal./mole} \quad (32)$$

Taking the energy barrier to condensation as one-half the heat of vaporization, the total barrier for the C_{19} acid is 13.7 kcal./mole and the increment per methylene group is 323 cal./mole. These values agree well with the experimental values of 14.6 and 297 cal./mole. The good agreement exceeds the gross uncertainties in the heats of vaporization as calculated and must be partly fortuitous. Nevertheless, it substantiates the theory proposed for the energy barrier.

Energy Barrier in the Solid State.—Resistance for S phase monolayers on an alkaline calcium ion subphase is given by

$$\log r = -1.6776 + 0.1400(n - 2) + 6.60 \times 10^{-3}p \quad (33)$$

Since the coefficient of p does not involve n, $E(CH_2)$ is constant and independent of compression. The structure of S films may, therefore, be described in terms of the "tilted chain" theory as for the LC phase. From the coefficient of n in eq. 33, $E(CH_2)$ is 191.0 cal./mole. Assuming that C has the same value for both phases, the residual energy is

$$E' = 11{,}517 + 9.00p \text{ cal./mole} \quad (34)$$

and the total energy barrier for the C_{19} acid at zero pressure on this subphase is 14,764 cal./mole.

The increment in the energy barrier per CH_2 group in the S phase is only $^2/_3$ the LC phase value, whereas the total energy for the C_{19} acid at zero pressure is 168 cal./mole greater than the LC energy. A qualitative explanation of these differences follows.

At the pH of these experiments, the S monolayers are calcium soaps. The condensation of these films, *i.e.*, the absence of the LC phase, is due to the formation of soap bonds. This association may be the formation of $Ca(R\text{-}COO)_2$ molecules or coördination bonding in which each calcium ion is attached to four carboxylate ions and four water molecules. In either case, it is supposed that when the soap bonds are formed, the chains of the acid molecules are forced close enough together for repulsive forces to become important. As a result, the interaction energy per CH_2 group is decreased and the lowered value for $E(CH_2)$ follows.

The increase in the residual energy of 2 kcal./mole is due to the energy required to break a soap bond when the free site is formed. The magnitude of this energy should increase as the separation between carboxylate ions decreases, thus causing the observed dependence of resistance on pressure.

The Condensation Coefficient.—Comparison of equations 9 and 26 shows that the fraction of the impinging vapor molecules which penetrate the monolayer and condense is

$$\alpha = 8.56 \times 10^5 \exp(-E/RT) \quad (35)$$

Clearly, C of eq. 25 is a function of temperature since the maximum value of α is unity. On simple theory, α could be considered to be the fraction of the impinging molecules with an energy available for penetration equal to or greater than E. Or, from another point of view, α might be described as the fraction of the monolayer sites which are unoccupied. Either description should give α approximately as a Boltzmann distribution, and the large value of C in equation 35 remains unexplained.

Postulating an intermediate surface phase in the process of condensation and evaporation may offer an explanation of the large coefficient. Wyllie[24] has discussed this mechanism for a clean liquid surface at some length. If it is postulated that the water molecules in condensing and evaporating pass through an intermediate phase in which they are adsorbed on the monolayer under conditions such that the fraction of adsorption sites occupied is small, the condensation coefficient is given by

$$\alpha = k_e/(k_e + wQ) \quad (36)$$

where k_e is the rate of transfer of water from the liquid phase through the monolayer to the adsorbed phase on the monolayer. From eq. 35 and an empirical relation for w in terms of the energy of vaporization of water E_v, k_e is found to be

$$k_e = 1.4 \times 10^{13} \exp[-(E + E_v)/RT] \text{ g./cm.}^2 \text{ sec.} \quad (37)$$

The energy barrier in this case includes the energy of vaporization as would be expected since evaporation is being described.

(22) E. L. Lederer, *Seifensieder-Z.*, **57**, 67 (1930).

(23) W. Nernst, "Theoretische Chemie," Verlag von Ferdinand Enke, Stuttgart, 1921 p. 796.

(24) G. Wyllie, *Proc. Roy. Soc. (London)*, **A197**, 383 (1949).

ELECTRON DIFFRACTION DETERMINATION OF LATTICE PARAMETERS OF POLYCRYSTALLINE SPECIMENS GIVING BROAD DIFFRACTION PEAKS. I. DISCUSSION OF TECHNIQUE AND ANALYSIS OF ERRORS

BY G. G. LIBOWITZ[1] AND S. H. BAUER

Department of Chemistry, Cornell University, Ithaca, N. Y.

Received August 18, 1954

The various errors which arise in the measurement of lattice parameters of compounds giving broad electron diffraction peaks have been considered. These were found to be (1) the shifting of diffraction peaks by the sharply sloping background, (2) visual difficulty in locating the true center (maximum density) of a peak, (3) overlap of the tails of adjacent peaks, and (4) spottiness of the diffraction rings. The magnitudes of these errors, and methods of correcting them are discussed. It was found that the use of a rotating sector was especially advantageous in such cases. A technique of preparing powder samples for electron diffraction studies of compounds containing impurities is given.

Introduction

In the course of an electron diffraction study of polycrystalline nickel oxide, it was discovered that several systematic errors, though not apparent in the measurement of sharp diffraction rings, enter into the determination of broad (half-width >300 μ) diffraction rings. The four chief causes of these errors were found to be (1) a sharply sloping background, (2) visual difficulty in locating the true center (maximum density) of a diffraction peak, (3) overlap of the tails of adjacent peaks, and (4) spottiness of the diffraction rings. Aside from instrumental factors which can be eliminated by proper camera design,[2] the widths of the diffraction peaks depend on the crystallite size of the specimen, refraction of the electron beam,[3] and variation of lattice parameter within a particular sample due to imperfections in the crystal lattice.[4] Because of the interest in semi-conductors and the presence of minute amounts of impurities and defects in crystals, it was necessary to investigate the errors arising in the measurement of broad diffraction peaks.

Experimental Procedure

The electron diffraction camera used in these investigations has been described by Hastings and Bauer.[5] The camera length was increased from 20 cm. to 50 cm. in order to increase the dispersion and to some extent the resolution, and to permit greater precision in measuring the diffraction rings. The sample support was a $^5/_{16}$ inch brass rod, with five $^1/_4$ inch holes to support the grids on which the samples were deposited. The holes were positioned in the path of the electron beam by moving the rod (which was lightly greased with Apiezon N grease) through a rubber gasket having a slightly smaller diameter than the rod. No break was made in the vacuum during change of samples; only a slight leak appeared when the rod was withdrawn for reloading.

The patterns were recorded on Kodak Lantern Slide Contrast or Medium Plates; contrast plates were found to be preferable because of their finer grain size. The plates were developed for 7–9 minutes at 13–16° with Kodak D-11, with continuous agitation in a tray. The development was carried out at low temperatures (and therefore required longer times) in order to obtain maximum contrast and minimum grain size.

Preparation of Samples.—The samples studied were polycrystalline nickel oxide containing varying amounts of lithium oxide as an added impurity. In preparing powder specimens for diffraction photographs, the usual method of evaporation and re-crystallization could not be used since the distribution of crystal defects or impurities would be changed. It was necessary to devise a procedure for evenly distributing the specimen in its original state in a well dispersed condition so that a maximum amount of surface would be exposed to the electron beam. A satisfactory apparatus is shown in Fig. 1. It consists of a glass tube, 135 cm. in length and 1.6 cm. in diameter, with a piece of coarse sintered glass at the bottom and a side-arm at the top. The sample was placed onto the sintered glass and a stream of dry air was passed through the stopcock. This produced a churning of the powder on the sintered glass, and a large number of particles was slowly carried up the tube by the stream of air. The particles were deposited on a 400-mesh nickel grid which had previously been covered by a 50 or 100 Å. dried collodion film. The grids were $^1/_4$ inch in diameter and rested on a small platform at the end of a brass rod which was placed in the side-arm at the upper end of the tube. A very fine distribution of particles on the grid was thus obtained. As far as could be determined, there did not seem to be a variation in particle size throughout a sampling run. For a sample requiring a controlled atmosphere, an inert gas can be used instead of air, and stopcocks A and B can be closed before shutting off the gas stream.

In order to prevent loss of sample when transferring the grid to the electron diffraction camera, the powder was pressed into the collodion film by placing the grid between two small stainless steel bars which had been ground flat, and pressing in a small vise. For some samples, the stream of air failed to agitate the powder because minute channels were formed. This was eliminated by adding some inert substance of considerably larger particle size. For example, porcelain ground to 80–100 mesh was found to be satisfactory. Smaller particles of porcelain could not be used, since they were carried up in the stream and gave rise to their own electron diffraction pattern.

Measurement of the Diffraction Photographs.—Thallous chloride[6] was used as an internal standard, and was distributed on the grid in the same manner as the sample. Although an internal standard introduces additional lines thus enhancing the possibility for overlap of some of the lines of the standard with those of the sample, for the determination of precision lattice parameters the advantages of using an internal standard far outweigh the disadvantages. Errors due to plate processing, ellipticity of the rings, and measurement of the rings off center are completely eliminated. The plates were measured with both a travelling microscope and with a microphotometer. The travelling microscope (Gaertner Scientific Corp. No. 3231) has a magnification of about 9× and a 10 mm. field. The linear scale could be read to 0.001 mm. and has a range of 100 mm. The positions of the maxima were also read from microphotometer records (Leeds and Northrup Recording

(1) Now at Department of Chemistry, Tufts College, Medford, Mass.

(2) J. Hillier and R. F. Baker, *J. App. Phys.*, **17**, 12 (1946); R. S. Page and R. G. Garfitt, *J. Sci. Inst.*, **29**, 398 (1952); J. M. Cowley and A. L. G. Rees, *ibid.*, **30**, 33 (1953).

(3) J. M. Cowley and A. L. G. Rees, *Proc. Phys. Soc.*, **59**, 287 (1947).

(4) A. L. G. Rees and J. A. Spink, *Nature*, **165**, 645 (1950).

(5) J. M. Hastings and S. H. Bauer, *J. Chem. Phys.*, **18**, 13 (1950).

(6) F. W. C. Boswell, *Phys. Rev.*, **80**, 91 (1950).

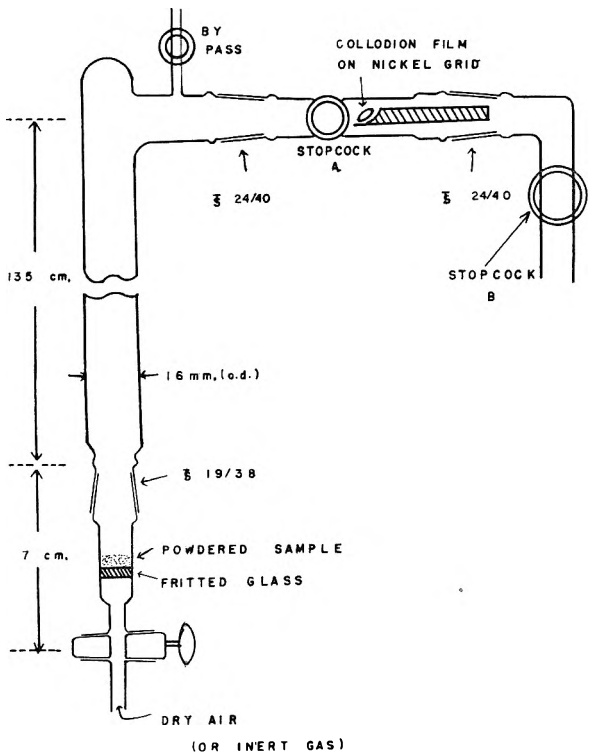

Fig. 1.—Apparatus for preparing powder samples for electron diffraction.

Microphotometer) Patterns recorded at a linear magnification of 26× were used. The position of the maximum for each peak was determined by finding the mid-point along lines of equal density for the two ends of a diffraction peak and drawing the best vertical straight line through them. The diameter of each ring was then determined by measuring the distance between corresponding peaks on opposite sides of the center with a millimeter rule which could be read to 0.1 mm. With a magnification of 26×, the actual reading error was of the order of 0.004 mm.

Background Effect

In studying the molecular structure of gases by the radial distribution method, the background characteristic of all electron diffraction photographs can be corrected for so as to obtain true intensity values. However, in the determination of lattice parameters by the powder method, where only the diameters of the rings need be measured, the effect of the background has usually been considered negligible. This is true for very sharp peaks[7]; for the case of relatively broad peaks, however, the change of slope of the background across the half-width of a peak is sufficient to cause an appreciable shift of the position of the maximum in the direction of greater background intensity. Before discussing methods of correcting for this shift, it is interesting to consider the factors which give rise to the background.

The usual expression given for the intensity of primary scattered electrons by a randomly oriented powder sample, at an angle θ to the incident beam is

$$I(s) = \kappa\left(\frac{\rho_N t}{R^2 s^4}\right)\left\{\begin{matrix}\text{coherent}\\ \text{atomic}\\ \text{scatter}\end{matrix} + \begin{matrix}\text{incoherent}\\ \text{atomic}\\ \text{scatter}\end{matrix} + \begin{matrix}\text{structure}\\ \text{dependent}\\ \text{scatter}\end{matrix}\right\} \quad (1)$$

where ρ_N is the number of scattering units per unit volume of sample, t is the thickness of the sample (assumed uniform), R is the distance from the sample to photographic plate and $s = (4\pi/\lambda)\sin\theta/2$. It is recognized that an appreciable background appears due to the first two terms. All terms are functions of the angle s, but the steepest dependence on that variable is due to the factor s^{-4}. However for sufficiently dense matter (most gases above 10 mm. of Hg and, of course, liquids and solids), secondary and higher order scattering becomes significant, and eq. 1 no longer provides a sufficient description of the observed intensity function.[8] As expected, it was experimentally established that the slope of the background did depend on the size of the powder crystallites. As the magnitude of the secondary and higher order scattering increased with larger crystallite sizes, the slope of the background decreased.

In addition to the above terms, scattering from the supporting nickel grid and collodion film must be taken into account. An experimental determination showed that although the supporting grid (400 mesh nickel) obscured 73% of the beam, it contributed nothing to the diffraction pattern. Preliminary measurements by Andersen[9] indicated that for a thickness of collodion under 150 Å., the intensity of the beam transmitted along the incident ray declined roughly exponentially with thickness; *i.e.*, $J_0/P_0 = \exp(-\mu t)$; where J_0/P_0 is the ratio of intensities of the primary electron beam after and before passing through the collodion film; t is the thickness of the film in Å., and $\mu \cong 2.8$ to 2.5×10^{-3}.

A complete expression for the intensity function would therefore also include terms for the scattering produced by the collodion, and for multiple scattering. Although the first two terms in eq. 1 and the contribution of the collodion can be calculated, there is no available theory or straightforward experiment which permits the correction of the pattern for multiple scattering. Indeed, the shape of the background varied from one sample to the next since the packing of powder particles could not be reproduced. For this reason, it was necessary to develop an empirical procedure for making appropriate background corrections. The actual form of the background was obtained, therefore, empirically from the microphotometer record of each photograph. The background intensity curve was sketched in using points remote enough from peaks so that it was not influenced by the tails of these peaks. Microphotometer records of pure collodion films were used to assist in the drawing of the shape of the background at the broad collodion peaks.

The correction for the effect of the background on the diffraction maxima could now be determined by dividing the total intensity curve by the empirically obtained background. Actually, a more exact correction would be obtained by subtracting the background due to the collodion film and multiple scattering and dividing by $[\Sigma_i f_i^2 + \Sigma_i G_i]/s^4$,

(7) In this discussion the term *peak* is defined as any portion of the total intensity curve rising above the background; and the term *maximum* refers to the point of maximum density of one of these peaks.

(8) R. B. Harvey, F. A. Keidel and S. H. Bauer, *J. App. Phys.*, **21**, 860 (1950)

(9) P. Andersen, private communication.

the coherent and incoherent atom form factors. Since there is no way of determining what fraction of the background to subtract, the total intensity curve was divided by the total apparent angular function. That this does not cause any appreciable error will be shown below, eq. 4. Four methods were used for making background corrections. These will be described, and a comparison between them will be made.

Direct Division or Subtraction.—Direct division was carried out on a microphotometer record by taking various points along the total intensity curve and dividing the density value at each point by the density of the background at that point; or, in the case of subtraction, by subtracting the density of the background from the corresponding density of the total curve. Although this method of correcting for the background is the most obvious one, it is not the simplest or most accurate, since it is a lengthy and laborious process which requires re-drawing of the corrected curve to permit location of the true maxima, and in turn introduces additional errors in estimating the positions of the maxima.

This method was tested on a large number of curves, and it was found that, although the positions of the maxima did not depend appreciably on whether the background was subtracted or divided, the shapes of the peaks were consistently more symmetrical for the division operation.

Correction Equations.—If a Gaussian shape is assumed for the diffraction peaks, which was very nearly the case for the samples studied in this investigation, the equation for a peak superimposed on a background of unit intensity is (taking $x = 0$ at the position of the true maximum)

$$F(x) = F_M \exp(-\alpha^2 x^2) + 1$$

This is represented by the solid curve in Fig. 2. Upon designating the empirically determined background multiplying function as $B(x)$, the observed intensity curve can be represented by

$$I(x) = B(x)F_M \exp(-\alpha^2 x^2) + B(x)$$

the dashed curve in Fig. 2. Maximizing this expression gives the shift of the maximum from its true position.

$$dI(x)/dx = [-2\alpha^2 x B(x)F_M \exp(-\alpha^2 x^2) + F_M \exp(-\alpha^2 x^2)\{dB(x)/dx\} + dB(x)/dx]_{at\, x_m} =$$

When the magnitude of the shift is small, $\alpha^2 x_m^2 << 1$, and

$$x_m \backsimeq \frac{[dB(x)/dx](F_M + 1)}{2\alpha^2 B(x) F_M}\Big|_{at\ x\,=\,0} \qquad (2)$$

To a good approximation over the width of one peak, the background function was a straight line, represented by CE in Fig. 2. If the slope of the background is not too large, the shift of the maximum due to the background reduces to

$$x_m \doteq S(F_M + 1)/2\alpha^2 F_M I_B; \qquad S = \Delta I_{1/2}/W_{1/2} \quad (3)$$

where S is the slope of the line CE, and $\Delta I_{1/2}$ is the change in intensity of the background across the half-width of the peak, $W_{1/2}$; also, $I_B = B(x = 0)$. The intensity of the background at x_m is only a very small percentage larger than I_B, so that it can be assumed to equal I_B. If I_p is the difference

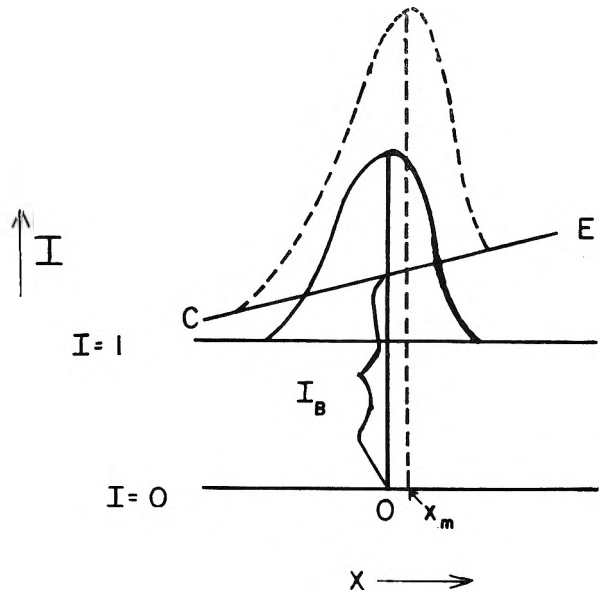

Fig. 2.—The effect of a sloping background on the position of a maximum.

in intensity between the maximum of the shifted peak, and the background line CE, then $I_p = I_B F_M$, and eq. 3 becomes, after substituting the value for $\alpha = 2(\ln 2)^{1/2}/W_{1/2}$

$$x_m \doteq \frac{0.18\Delta I_{1/2}(I_p/I_B + 1)W_{1/2}}{I_p} \qquad (4)$$

This is the shift in the position of a peak due to the multiplicative effect of the background. In a similar manner, the shift due to adding the background to a Gaussian peak is shown to be

$$x_m \doteq \frac{0.18(\Delta I_{1/2} W_{1/2})}{I_p} \qquad (5)$$

This is the "background error" given by Rymer and Butler.[10] These authors also state that the multiplicative constant assumes the values 0.18 ± 0.02 for almost all contours other than Gaussian.

A comparison between eq. 4 and 5 indicates that 4 reduces to 5 when the ratio $I_p/I_B << 1$. For most of the broad peaks in this investigation, this ratio was less than 0.1. For cases where it was larger, the peaks were sufficiently sharp not to be affected by the background. Therefore, for most broad peaks the background may be removed either by division or subtraction. Because of the assumptions made in deriving these equations, they give inaccurate results when the slope of the background is large. In addition, they cannot be used when the shape of the peak is highly unsymmetrical because of overlapping of the peaks, peculiar particle size distributions, or refraction effects.

Geometrical Method.—Subtraction or division by the background can be performed geometrically on microphotometer records of the total intensity curve. For subtraction, a series of lines parallel to the background was drawn (taking into account the non-linearity of the density scale on a microphotometer record) onto the total intensity curve. A vertical line drawn through the mid-points of these lines gave the position of the true maximum. Division by the background was carried out in the

(10) T. B. Rymer and C. C. Butler, *Phil. Mag.*, **36**, 821 (1946).

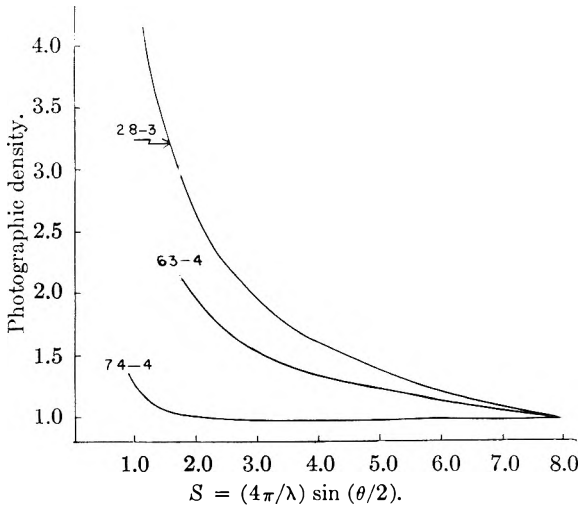

Fig. 3.—Backgrounds with and without sector.

same way, except that the series of lines were not parallel to the background, but were drawn so that any two points with corresponding s values always had the same intensity ratio for each line. This method cannot be used when the peaks are unsymmetrical for reasons other than the presence of a background.

Table I is a comparison of the background corrections obtained on some NiO maxima by the three methods thus far discussed. Since these data were obtained for symmetrical peaks, the values deduced from the geometrical method are the most reliable, in view of the fact that no assumptions had to be introduced, and no re-drawing was necessary. Therefore, it can be seen that, in general, eq. 5 gives slightly low results, although the values are more reliable than those obtained by direct subtraction.

TABLE I

EFFECT OF BACKGROUND ON THE POSITION OF NiO DIFFRACTION MAXIMA

Line	Background shift: By direct subtraction, cm.	Using eq. 5, cm.	By geometric method, cm.
Pl. 1L (200)	0.0004	0.0009	0.0009
Pl. 1R (200)	.0027	.0007	.0011
Pl. 2R (111)	.0023	.0012	.0018
Pl. 3L (220)	.0019	.0030	.0025
Pl. 1R (220)	.0027	.0033	.0036
Pl. 4R (220)	.0038	.0021	.0036

The Use of a Rotating Sector.—A rotating sector multiplies the total intensity curve by the reciprocal of the background function during the recording of the diffraction pattern. Although the rotating sector has been used by many investigators since its introduction[11] to determine molecular structure by the radial distribution method, it has not been used in the determination of lattice parameters of solids since there was no need to evaluate true intensities. However, as shown above, it is necessary to correct for the effect of background in the case of broad diffraction peaks, and the use of a rotating

(11) F. Trendelenburg, *Naturwissenschaften*, **21**, 175 (1933); P. P. Debye, *Physik Z.*, **40**, 66, 404 (1939); C. Finbak, *Avh. norske Vidensk Acad. M.-N. Kl.*, No. 13 (1937).

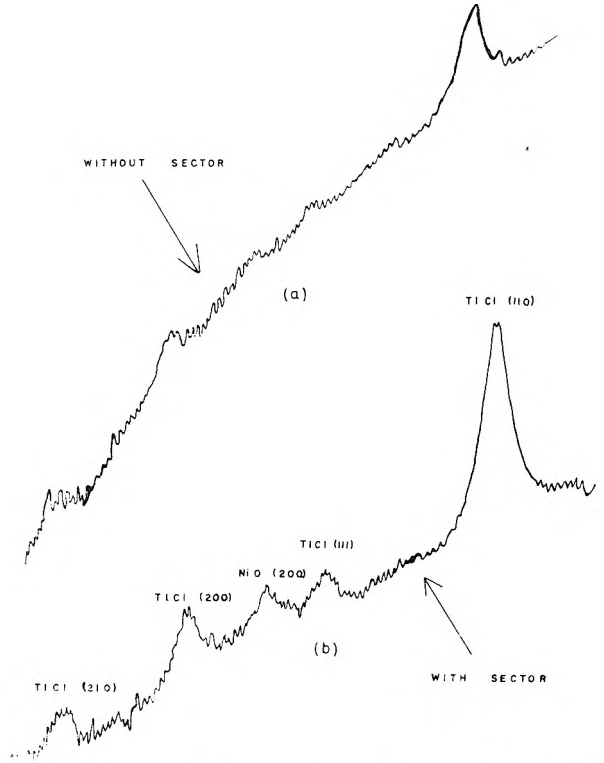

Fig. 4.—The effect of the sector on the shapes of the peaks.

factor was found to be the most convenient method for accomplishing this.

The sector function, in this investigation, was determined empirically from microphotometer records of electron diffraction photographs of typical samples. As mentioned above, the shape of the background depends upon the distribution of the particles on the grid, the particle size, the ratio of the amount of sample to the amount of internal standard used, and the ratio of both of these amounts to the thickness of the collodion film. Since it was impossible to reproduce all these factors for every run, the shape of the background was variable. Therefore, use of the sector did not give a level background on all photographs. However, the slight residual background was easily corrected for by using one of the other three correction methods. Figure 3 demonstrates the effect of the rotating sector on the background function. Curve 28-3 is the background of a photograph taken without a sector. This was the background used to cut the sector employed in these experiments. Curves 63-4 and 74-4 are the backgrounds of photographs from two different samples taken with the sector. The first peak measured occurred at $s = 2.3$, and the last at $s = 7.5$.

A major advantage in using a sector for powder diffraction work is that the peaks can be more clearly seen, both visually and on the microphotometer record. Since the positions of the maxima are determined by measuring the mid-point at several places on a peak, this is a great advantage. It is also a great help in the determination of crystallite sizes from the widths of powder lines. In addition, some peaks which are lost (*i.e.*, are only points of inflection) in the rapidly falling background, be-

come visible in sector photographs. This is illustrated in Fig. 4 which shows two microphotometer records of the same sample. Figure 4a was taken from a non-sector photograph of NiO and TlCl, and Fig. 4b is the same set of peaks from a sector photograph.

A significant method for reducing the background has been introduced by Boersch[12] whereby a filter lens inserted in the camera is used during the recording of the electron diffraction pattern. This prevents the incoherently scattered electrons from reaching the photographic plate.

Visual Error

It was observed that the lattice parameters determined by visually measuring the ring radii with a travelling microscope were consistently lower than those obtained from microphotometer records. The reason for this discrepancy was shown by Viervoll[13] to be as follows. The maximum of a diffraction line is actually determined with a travelling microscope by measuring the position of its mid-point; *i.e.*, by taking the point mid-way between the two edges of the line rather than the location of the point of maximum density. What appears to be an edge of a line to the eye is in fact a point of inflection. When a broad peak is superimposed on a rapidly falling background, this method of estimating maxima positions leads to serious errors as illustrated in Fig. 5. A and B are what appeared to be the edges of an NiO (111) diffraction line when viewed under the microscope. Because of the effect of the sloping background, and adjacent peaks, these were not equidistant from the true maximum. The error in the position of the maximum, when reading this line under a travelling microscope was therefore CD. Since the background was heaviest at the center of the photographic plate and decreased monotonically outwards, the error was always in the direction of high ring radii and therefore this method yielded low values for the lattice parameters. Although this error was in the opposite direction to the background error, the two errors do not cancel each other, since the "visual error" is usually considerably larger. Table II illustrates the magnitudes of the visual error.

TABLE II

ERROR DUE TO VISUAL EFFECT

NiO line	$W_{1/2}$, cm.	$\Delta I_{1/2}$	Visual error, cm.	Error in lattice param., %
Pl. 2L (111)	0.068	0.066	0.022	1.9
Pl. 2L (220)	.093	.037	.019	1.0
Pl. 3R (111)	.045	.038	.017	1.5
Pl. 2R (111)	.026	.024	.010	0.9
Pl. 3L (220)	.053	.022	.009	0.4
Pl. 3R (422)	.071	.016	.000	...

From Table II it is clear that the visual error depends on the slope of the background, $\Delta I_{1/2}$, and only to a small extent, if at all, on the half-widths of the peaks, $W_{1/2}$.

It is possible that the results of Boswell[14] which show a decrease in lattice parameter with decreasing crystallite size may be explained by this "visual error." As crystallite size decreases, the diffraction lines become broader and the slope of the background increases because of reduction in multiple scattering. Since Boswell used an optical comparator for his measurements, it is likely that the visual error increased as the crystallite decreased, thus leading to fictitious lower values for the lattice parameters.

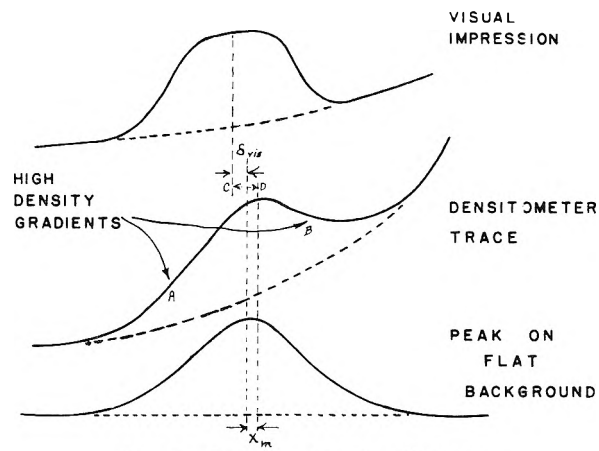

Fig. 5.—Basis for the "visual" error.

Overlapping of Peaks

If two different peaks occur in close proximity, there may be overlapping of their tails thus introducing shifts of their maxima, as illustrated by Archard.[15] For the case where the two overlapping peaks were produced by the same compound, and the relative positions and intensities of the peaks were known from X-ray data, the shifts were determined by adding the known peaks together. When an internal standard or mixture of compounds was used, however, wherein the relative intensities depended on the relative amount of each component, and the relative positions varied with change in lattice parameters of the compounds, the X-ray data for the individual compounds was of no value. For cases where the intensity of one of the peaks was large compared to the other so that only the smaller peak was shifted, the tail of the more intense peak was treated in the same manner as a sloping background with respect to the smaller peak. It was necessary to remove the normal background before making these corrections in order to avoid serious errors from overcompensation. Since removal of the background by direct subtraction introduces its own errors, the use of a rotating sector was especially advantageous in such cases. If both peaks were approximately of equal intensity, the only method of making these overlap corrections was to deduce their true shapes by trial and error. Since this is not a reliable method, it is preferable to discard values from peaks overlapping in this manner.

Spottiness

If in a sample there is an insufficient number of crystallites to give a uniform distribution in orientation, the diffraction rings appear spotty and uneven. Since a spot may occur anywhere over the width of a ring, this may cause large errors in the

(12) H. Boersch, *Z. Physik*, **134**, 156 (1953).
(13) H. Viervoll, private communication.
(14) F. W. C. Boswell, *Proc. Phys. Soc.*, **64A**, 465 (1951).
(15) G. D. Archard, *Brit. J. App. Phys.*, **5**, 19 (1954).

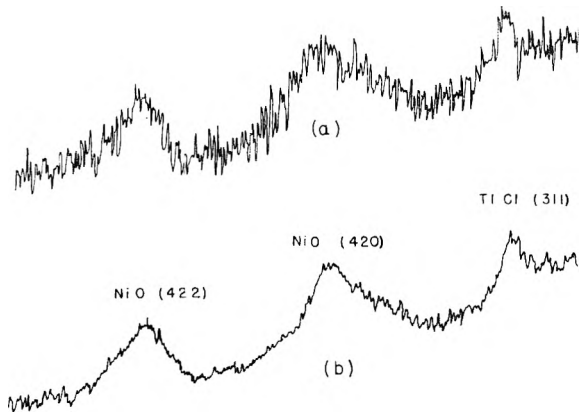

Fig. 6.—The effect of plate oscillations on microphotometer records.

determination of the position of the maximum as read from microphotometer records. The slit of the microphotometer may pass through one or two such intense spots which are off the center of the true maximum, so that the record shows the maximum density at a displaced position. It is obvious that the broader the diffraction peak, the larger the probability and magnitude of such an error. For the case of NiO, where the average peak width was 0.06 cm., the scanning error could be as large as 0.03 cm. which would lead to an error of 2.5% in the lattice parameter as determined from the (111) line.

Oscillation of the sample during the recording of the pattern, which is the usual procedure in X-ray powder work, is impractical for electron diffraction since the duration of the exposure is very short. This error was reduced to some extent, however, by the use of a mechanism which oscillated the electron diffraction photograph through an angle of 10° while it was being scanned in the microphotometer. The angle through which oscillation could be carried out was limited by the ellipticity of the rings. Another advantage in using this oscillating mechanism was the reduction of the effect of the photographic grain thus permitting easier recognition of low peaks. Figure 6a is a microphotometer record of a portion of a plate taken without the oscillating mechanism, and Fig. 6b is the identical portion taken with oscillation.

Application of the above analysis and correcting procedures to a study of nickel oxide, yielded lattice parameters which were precise to within 0.05%, precision being expressed as the standard deviation of the mean value. As shown in the following paper, the lattice parameter for NiO checked the X-ray value to within 0.001 Å., for crystallites in the 80–100 Å. range.

Acknowledgment.—The authors wish to express their appreciation to Dr. Henry Viervoll for the many discussions which were of invaluable aid in this investigation.

ELECTRON DIFFRACTION DETERMINATION OF LATTICE PARAMETERS OF POLYCRYSTALLINE SPECIMENS GIVING BROAD DIFFRACTION PEAKS. II. A STUDY OF NICKEL OXIDE

BY G. G. LIBOWITZ[1] AND S. H. BAUER

Department of Chemistry, Cornell University, Ithaca, N. Y.

Received August 18, 1954

The lattice parameters of powdered samples of nickel oxide containing varying amounts of lithium oxide were determined. With increasing Ni^{+3} content, the lattice parameters decrease, and for the same samples the values as determined by electron diffraction agree with those determined by X-ray back reflection methods to within 0.002 Å. The crystallite size as determined by X-rays and electron diffraction have been compared, and an estimate of the inner potential of NiO was obtained from the measured relative broadening of the (200) and (111), (220) reflections. Conditions which must be met to permit detection of differences between surface and bulk lattice parameters are analyzed.

Introduction

At various times, differences have been reported[2] between lattice parameters as obtained by X-ray and by electron diffraction. It was the purpose of this investigation to determine whether controlled impurities would emphasize such differences, which would arise, of course, if there were a different concentration of impurity at the surface than in the bulk. To study the effect of impurites on lattice parameters, the system nickel oxide with lithium impurity was chosen because of the ease of the preparations, and because of the large effect of Li_2O on the lattice parameter of NiO as observed by Verwey and co-workers.[3]

Verwey[4] has shown that the introduction of lithium oxide into the nickel oxide lattice induces the formation of trivalent nickel according to the equation

$$n\mathrm{Li_2O} + 2(1-n)\mathrm{Ni^{II}O} + n/2\,\mathrm{O_2} \longrightarrow 2\mathrm{Li}_n\mathrm{Ni^{II}}_{1-2n}\mathrm{Ni}_n^{\mathrm{III}}\mathrm{O}$$

Thus, for every Li^+ ion which enters into the lattice, one Ni^{+2} ion becomes converted to a Ni^{+3} ion to maintain electroneutrality. The trivalent nickel ion has a smaller ionic radius and higher charge, so that its effective potential is considerably greater than that of the divalent ion. This causes

(1) Now at Chemistry Department, Tufts College, Medford, Mass.

(2) G. I. Finch and H. Wilman, *J. Chem. Soc.*, 751 (1934); G. I. Finch and S. Fordham, *Proc. Phys. Soc.*, **48**, 85 (1936); J. Gnan, *Ann. Physik*, **20**, 361 (1934); E. Pickup, *Nature*, **137**, 1072 (1936); C. Lu and E. W. Malmberg, *Rev. Sci. Inst.*, **14**, 271 (1943); N. Kato, *J. Phys. Soc. Japan*, **6**, 502 (1951).

(3) E. J. W. Verwey, P. W. Haaijman, F. C. Romeijn and G. W. van Oorterhout, *Philips Research Reports*, **5**, 173 (1950).

(4) E. J. W. Verwey, *Bull. soc. chim. France*, Ser. 5, **16**, D122 (1949).

a contraction of the lattice which shows up in lower values for the lattice parameter as reported by Verwey[3] and Brownlee and Mitchell.[5] It is presumed that the lithium ion has no effect on the lattice parameter since it has the same Goldschmidt ionic radius as divalent nickel.

Experimental

Preparation of Samples.—The samples of NiO were prepared from basic nickel carbonate. The nickel carbonate was prepared from J. T. Baker Analyzed Low Cobalt (0.002%) nickel chloride by the following procedure. A 70% solution of the nickel chloride was heated almost to boiling and a 50% solution of B and A Reagent quality potassium carbonate was slowly added with stirring, in a sufficient amount to satisfy the equation

$$NiCl_2 + K_2CO_3 \longrightarrow NiCO_3 \downarrow + 2KCl$$

Actually, this leaves an excess of potassium carbonate, since a basic nickel carbonate, $NiCO_3 \cdot xNi(OH)_2$ is formed instead of $NiCO_3$.

The solution was filtered through a buchner funnel and washed with warm water. The precipitate of basic carbonate was then transferred to the beaker, washed thoroughly with boiling water, re-filtered, and washed again in the buchner funnel. This procedure was repeated four times so that the precipitate would be completely free of potassium chloride and residual potassium carbonate. The precipitate was then dried in a vacuum desiccator over activated alumina.

Pure NiO (sample no. 5) was obtained from the basic nickel carbonate by decomposing it at high temperatures. Sillimanite boats containing the carbonate were placed in a large quartz tube which rested inside a high temperature furnace. The quartz tube was connected to a vacuum pump through a Dry Ice–acetone trap. The system was pumped down to a pressure of 5×10^{-2} mm. and the quartz tube was heated from room temperature to 1000° over a period of three hours. It was kept at 1000° for five hours and then cooled to room temperature.

The nickel oxides containing Li_2O were prepared as follows. The required amount of lithium carbonate was dissolved in 3 *M* acetic acid and the solution was used to make a paste with the nickel carbonate. The mixture was evaporated on a hot-plate and dried overnight in an oven at 110°. The dried powder was then ground in a mortar for thorough mixing of the carbonate and acetate, and heated in an alundum tube. Sample No. 11 was kept at 1000° for 4.5 hours before cooling to room temperature. The final amount of trivalent nickel in the sample was 0.86%. Sample no. 10 was heated at 600° for 5 hours to decompose the carbonate and acetate, and then cooled and pressed into pellets $^3/_{16}$" in diameter and $^1/_{16}$" to $^1/_8$" thick. These pellets were heated to 1000° for three hours, cooled to room temperature and ground in a mortar. This sample contained 5.31% trivalent nickel.

Chemical Analysis.—The samples were analyzed for trivalent nickel by dissolving in 6 *N* HCl thus forming free chlorine, according to the reaction

$$2Ni^{+3} + 2Cl^- \longrightarrow Cl_2 \uparrow + 2Ni^{+2}$$

The chlorine was passed into a 5% KI solution with a stream of nitrogen, thus oxidizing the iodide to iodine which was then titrated with standard 0.005 *N* sodium thiosulfate solution. The apparatus and procedure were checked by analyzing known amounts of MnO_2 which produces chlorine parallel to the above reaction.

Diffraction Photographs.—X-Ray diffraction photographs (using a Cu target tube) of each sample were taken with a symmetrical focusing back reflection camera having a diameter of 10.007 cm. A nickel filter was used to remove all but the $K\alpha_1$ and $K\alpha_2$ lines. Kodak Type K X-ray film was used and processed as recommended. The sample was dusted onto a celluloid film upon which a thin layer of Lubri-seal had been spread. Although with our camera absolute values of the lattice parameter can be obtained if the proper corrections are made, we decided to use thallous chloride as an internal standard in order to reproduce the conditions used in taking electron diffraction photographs. The positions of the diffraction lines were measured to 0.1 mm. on a millimeter scale which had been photographed onto the film.

The values of the lattice parameter were calculated from the relation

$$a_0 = \frac{(h^2 + k^2 + l^2)^{1/2}\lambda}{2 \cos \frac{x}{4D}}$$

where x is the distance between two lines of the same index, D is the diameter of the camera. In the region of the Bragg angles used, the (420), (421), (332) and (422) thallous chloride lines and the (422) and (333) nickel oxide lines appeared. Since the lines due to $K\alpha_1$ and $K\alpha_2$ radiation are distinctly resolved, there were eight pairs of thallous chloride lines and four pairs of nickel oxide lines which were utilized.

The procedure for taking electron diffraction photographs was described in the previous paper.[6] The results given below have all been corrected for the errors described in that paper.

Lattice Parameters.—The values obtained for the lattice parameters by both methods are given in Table I. The values for pure nickel oxide check the most recent value of 4.177 ± 0.001 Å. given by Swanson and Tatge.[7]

TABLE I

LATTICE PARAMETERS OF NICKEL OXIDE SAMPLES

Sample	Ni^{+3}, %	Lattice parameters (Å.) By X-rays	By electron diff.
5	0.00	4.177 ± 0.001	4.176 ± 0.001
11	0.86	4.175 ± .001	4.173 ± .002
10	5.31	4.168 ± .001	4.167 ± .002

Crystallite Sizes.—The crystallite sizes of these samples were determined using the relation

$$t = K\lambda/\beta \cos \theta \qquad (1)$$

where t is the crystallite size, λ is the wave length of the radiation used, β is the true line broadening in radians, θ is the Bragg angle, and K is the shape factor = 1.0 for cubic crystals.[8] Because of the finite width of the electron beam due to instrumental factors, the observed line widths could not be used directly in eq. 1. In order to eliminate the effect of instrumental design, Jones[9] suggested mixing the sample whose particle size is to be determined with a material having a particle size which is effectively infinite. The maximum crystallite size which can be determined by eq. 1 is 400–500 Å. Therefore, any crystallite size above this value may be considered infinite. Thallous chloride, which was used as an internal standard in the lattice parameter determinations, was also employed as a reference for deducing crystallite sizes of the NiO by electron diffraction; its crystallite size was 610 ± 40 A. as determined by X-ray diffraction using the camera described above. A microscopic examination of the thallous chloride revealed well developed crystals and a nearly uniform particle size distribution.

The true broadening for the unknown sample, β, was obtained from its measured half-width, $W_{1/2}$,

(5) L. D. Brownlee and E. W. J. Mitchell. *Proc. Phys. Soc.*, **65B**, 710 (1952).

(6) G. G. Libowitz and S. H. Bauer, THIS JOURNAL, **59**, 209 (1955).

(7) H. E. Swanson and E. Tatge, National Bureau of Standards Circ. 539 V. I, June, 1953.

(8) A. R. Stockes and A. J. C. Wilson, *Proc. Camb. Phil. Soc.*, **38**, 313 (1942); C. C. Murdock, *Phys. Rev.*, **63**, 223 (1943).

(9) F. W. Jones, *Proc. Roy. Soc. (London)*, **166A**. 16 (1938)

using the method described by Shull.[10] Assuming the peaks to be simple Gaussians, which was very nearly the case in this investigation, Shull found that the true broadening is identical with the expression given by Warren,[11] where

$$\beta^2 = (W_{1/2})^2 - \beta_s^2 \qquad (2)$$

β_s being the half-width of the lines of the reference material. In our case β_s was estimated from the average value of the nearby thallous chloride lines; the crystallite sizes of samples no. 5 and no. 10 were calculated from the NiO (200) peaks using eq. 1 and 2. The (200) peaks were chosen because these do not exhibit additional line broadening due to refraction of the electron beam. It was not possible to estimate the crystallite size of sample no. 11 with any degree of precision from the NiO (200) lines. These were quite weak with respect to the background on all plates, and the shapes of the peaks, and, therefore, the half-widths could not be determined. However, the half-widths of the (220) lines could be measured with a slightly better degree of precision. From the value of the inner potential given below, a rough measure of the crystallite size was deduced for this sample.

The crystallite sizes of these samples were also determined from X-ray diffraction photographs using the same procedure. The results of both methods are given in Table II. The larger values obtained from X-rays is to be expected when a distribution of crystallite sizes is present. X-Rays are singly scattered by large crystals as well as the smaller ones, but the small crystallites produce very broad diffraction maxima (since $\lambda_{X\text{-rays}} \cong 30 \cdot \lambda_{electrons}$) which merge into the background. On the other hand, even quite small crystallites produce clearly measurable maxima by electron diffraction, while the crystals larger than a few hundred ångströms contribute mostly to the background, due to multiple scattering. Therefore, for a broad size distribution, X-ray diffraction would give higher values for the crystallite size than would electron diffraction.

TABLE II

CRYSTALLITE SIZES OF NiO SAMPLES

Sample	Crystallite size, Å. Electron diff.	X-Ray diff.
5	85 ± 11	300
10	93 ± 3	300
11	400 ± 250	>500

Refraction Effect.—It was observed that the broadening of the (220) and (111) lines was appreciably greater than that of the (200) lines, as seen in Table III.

TABLE III

BROADENING OF NiO DIFFRACTION PEAKS

Sample	Peak	Av. β (radians × 10^{-4})
5	(200)	6.8
5	(220)	11.8
10	(200)	6.0
10	(220)	11.2
10	(111)	11.2

(10) C. G. Shull, *Phys. Rev.*, **70**, 679 (1946).

(11) B. E. Warren, *J. App. Phys.*, **12**, 375 (1941).

The increased broadening for (*hhh*) and (*hh*0) lines was due to refraction of the electron beam as explained by Sturkey and Frevel.[12] If the assumption is made that the crystals are of regular shape, so that the (200) lines are not broadened by refraction, the inner potential of nickel oxide can be calculated from the relation[13]

$$P = \frac{E(\beta_{220} - \beta_{200})}{0.60}$$

where P is the inner potential and E is the accelerating voltage of the electrons. Using the values in Table III, the inner potential was calculated to be 38 volts for sample no. 5, and 42 volts for sample no. 10. This average value of 40 volts is considerably higher than the 10 to 20 volts given for most compounds. Since there is no previous determination of the inner potential of nickel oxide in the literature, there is no estimating how reliable this value is. Cowley and Rees[13] found a value of 40 to 50 volts for the (220) reflection of cadmium oxide containing a stoichiometric excess of cadmium. It is possible, therefore, that deviations from stoichiometry (which probably exist[5] even in pure NiO) may cause large deviations in inner potential since the defects present introduce considerable changes in the lattice energy.

Discussion of Results

As seen from Table I, for the samples of NiO prepared in this investigation, there was no difference in the values of the lattice parameter as deduced from X-ray and electron diffraction, within the experimental error of the electron diffraction data. Before discussing this result, it would be interesting to make a comparison of the sampling as observed by electrons and by X-rays.

If the assumption is made that only singly scattered electrons contribute to the structure sensitive part of the diffraction pattern, it is clear that the intensity of single scattering will be a maximum for some thickness of the crystal, since the amount of single scattering will increase with thickness but the fraction lost through multiple scattering will also increase. For transmission experiments, the fraction of singly scattered electrons as a function of the sample thickness, t, is

$$N/N_0 = \frac{1}{R^2}\,\mu_e \rho_a\, t \exp(-\mu_e \rho_a\, t) \qquad (3)$$

where μ_e is an effective extinction coefficient, ρ_a is the atomic density (atoms/cc.) and R is the sample to plate distance. Since the intensity lost by the primary beam is due only to scattering (other causes being negligible), the extinction coefficient, μ_e, is simply the ratio of scattered electrons to incident electrons per unit area for each atom. Thus, if to the desired approximation one may neglect the small interatomic interference terms relative to the much larger atomic scattering, then

$$\mu_e = \left(\frac{8\pi^2 me^2}{h^2}\right)^2 \int_0^{4\pi/\lambda} \frac{(Z - f)^2 + G}{s^4} \left(\frac{\lambda^2}{2\pi}\right) s\, ds$$

where f is the X-ray atom form factor, $s = (4\pi/\lambda) \sin\theta$, G is the incoherent atom form factor, and

(12) L. Sturkey and L. K. Frevel, *Phys. Rev.*, **68**, 56 (1945).

(13) J. M. Cowley and A. L. G. Rees, *Proc. Phys. Soc. (London)*, **59**, 287 (1947).

m, e, h and Z have their usual meanings. For a Thomas-Fermi model for the charge distribution of an atom, Boersch[14] calculated this to be

$$\mu_e = 6.3 \times 10^{-17}\lambda^2 Z^{4/3}, \text{ cm.}^2 \text{ (for } \lambda \text{ in Å.)}$$

The density $\rho_a = \nu/d$ where ν = number of atoms per cm.^{2} in each Bragg plane, d is the interplanar distance. The intensity of the structure sensitive part may be assumed to be proportional to N/N_0. For the case of the (200) planes of nickel oxide, d = 2.1 A., $\nu = 2.3 \times 10^{15}$ atoms/cm.^{2}, $\lambda = 0.056$ Å. and $Z = 18$ [using the average between Ni (28) and O (8)]. Putting these into eq. 3

$$R^2 \frac{N}{N_0} = 0.01t \exp(-0.01t) \qquad (4)$$

For X-rays the fraction of singly scattering photons is

$$\frac{N_0}{N} = \frac{(1 + \cos^2\theta)}{2}\left(\frac{e^2}{mc^2}\right)^2 \frac{\rho_a}{R^2} f^2 t \exp(-\mu_x t)$$

where $((1 + \cos^2\theta)/2)^{1/2}$ is the polarization factor, and μ_x is the absorption coefficient for X-rays (due to photoelectric and Compton effects). For NiO, and copper K radiation, $\mu_x = 3 \times 10^{-6}$. For the range of sizes being considered here, (50 Å. $< t <$ few hundred Å.) and for small angles, ($f = Z$), the above equation can be written

$$R^2 \frac{N}{N_0} = \left(\frac{e^2}{mc^2}\right)^2 \rho_a Z^2 t = 2.7 \times 10^{-8} t \qquad (5)$$

From the graphs of eq. 4 and 5 in Fig. 1, it is seen that the maximum for single scattering for electrons occurs at about t = 100 Å., although single scattering occurs appreciably over a range from 30 to 200 Å. In this region, the intensity of scattering for X-rays increases linearly with t. However, the effective contribution to the X-ray pattern by very small crystallites is less than is indicated by the equation because the diffraction peaks for crystals $\leq$ 100 Å. are broad and tend to merge into the background. Since the average crystallite size was found to be about 100 A., for samples no. 5 and no. 10, it appears that there was no appreciable preferred sampling of the surface in the individual crystallites by electron diffraction. However, since we have indications that a fairly large range of crystallite sizes was present, it also follows from Fig. 1 that the preferential sampling of the small crystallites by electrons will occur, whereas they will be overlooked by X-rays. For sample no. 11, where the crystallite size is larger, this selective sampling would be even more pronounced.

If there is a surface region for which the lattice parameter differs from (is either larger or smaller than) that of the bulk, it is obvious that this would result in an asymmetry of the diffraction peaks. This asymmetry would be a more sensitive criterion for the detection of a difference between surface and bulk lattice parameters than a slight shift in the position of the maxima. Equations for the asymmetry effect have been formulated but not included here because the diffraction peaks studied in this investigation were almost Gaussian in shape, and hence any asymmetry present was less than the error in recording the intensities.

(14) H. Boersch, *Z. Naturforschung*, **2a**, 615 (1947).

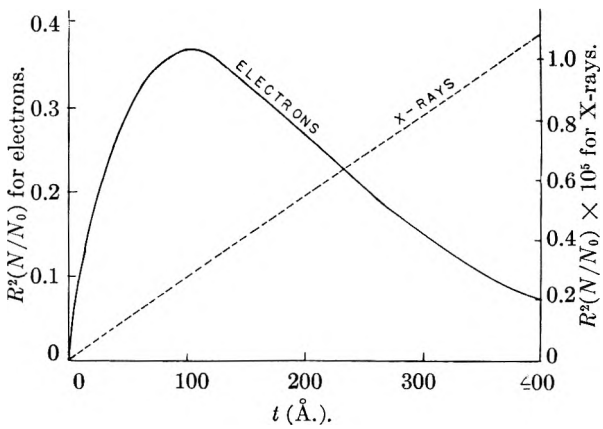

Fig. 1.—The fraction of singly scattered radiation as a function of sample thickness, for electrons and for X-rays.

From purely theoretical considerations Lehovec[15] has shown that an electric potential exists between the surface and the bulk material in ionic crystals containing lattice defects. This is due to an unequal distribution of lattice defects. For sodium chloride at 600°K., he calculated that the surface is 0.01% deficient in chloride ion with respect to the bulk. In view of this estimate and the experimental results reported here, it appears that more precise methods than diffraction by powder specimens must be used in order to detect any difference between surface and bulk lattice parameters. Conversely, the significant fact about the conclusions reached is that small amounts of impurities will cause a negligible difference to appear between the lattice parameters as obtained by X-rays and by electrons. Therefore, the differences which have been reported by previous investigators could not have been due to the presence of impurities, as claimed by some of them. As mentioned in the previous paper,[6] it is also unlikely that variation in crystallite size would cause a difference in lattice parameter. This is supported by the fact that the X-ray value for 300 Å. average crystallites is the same as the electron diffraction value for 90 Å. average crystallites. One is led to the conclusion that many of the differences found by other investigators were due to errors caused by the sharply sloping background in the electron diffraction photographs.[6] It should be pointed out that these results refer to a quantitative variation of the lattice parameter at or near the surface, and not to the existence of a different compound on the surface having its own distinctive diffraction lines which can be detected.[16]

(15) K. Lehovec, *J. Chem. Phys.*, **21**, 1123 (1953).

(16) L. O. Brockway and J. Karle, *J. Coll. Sci.*, **2**, 277 (1947); L. G. Schulz, *Acta Cryst.*, **5**, 130 (1952).

HEAT CAPACITIES AT LOW TEMPERATURES AND ENTROPIES AT 298.16° K. OF CRYSTALLINE CALCIUM AND MAGNESIUM ALUMINATES

BY E. G. KING

Contribution from the Minerals Thermodynamics Branch, Region III, Bureau of Mines, United States Department of the Interior, Berkeley, Calif.

Received August 12, 1954

Heat capacity measurements of crystalline $3CaO{\cdot}Al_2O_3$, $12CaO{\cdot}7Al_2O_3$, $CaO{\cdot}Al_2O_3$, $CaO{\cdot}2Al_2O_3$ and $MgO{\cdot}Al_2O_3$ were conducted throughout the temperature range 51 to 298°K. All five substances showed normal thermal behavior. The entropies at 298.16°K. are, respectively, 49.1 ± 0.3, 249.7 ± 1.5, 27.3 ± 0.2, 42.5 ± 0.3 and 19.26 ± 0.10 cal./deg. mole. The calcium aluminates have unusually high entropies of formation from the oxides.

Introduction

There are several compounds in the calcium oxide–alumina system, of which the more important are $3CaO{\cdot}Al_2O_3$, $12CaO\ 7Al_2O_3$, $CaO{\cdot}Al_2O_3$ and $CaO{\cdot}2Al_2O_3$. In the magnesium oxide–alumina system, only one compound, $MgO{\cdot}Al_2O_3$, is known. Thermodynamic data for these substances have been virtually entirely lacking; in particular, no low temperature heat-capacity data and entropy values are to be found in the literature. This paper reports heat capacity measurements in the range 51 to 298°K. and entropies at 298.16°K. for magnesium aluminate (*i.e.*, magnesium–aluminum spinel) and the four calcium aluminates designated above.

Materials.—The four calcium aluminates were prepared from pure hydrated alumina (obtained from reagent grade aluminum chloride) and reagent grade calcium carbonate. Intimate, stoichiometric mixtures were pressed into pellets and heated for several periods at temperatures specified below, with intervening grindings, mixings, chemical analyses and adjustments of composition.

In preparing tricalcium aluminate, three prolonged heats totaling 39 hours above 1,000°, of which 18 hours was at 1,400–1,450°, were made. The product analyzed 62.25% calcium oxide and 37.84% alumina, as compared with the theoretical 62.26 and 37.74%. The material was completely soluble in hydrochloric acid, and extraction with absolute alcohol showed the absence of any free calcium oxide. The X-ray diffraction pattern agreed with those in the literature.[1,2]

The calcium aluminate of composition $12CaO{\cdot}7Al_2O_3$ required five heats totaling 48 hours at 1,300° and 21 hours at 1,400°. The product analyzed 48.32% calcium oxide and 51.20% alumina, as compared with the theoretical 48.53 and 51.47%. Ferric oxide in amount of 0.10% was present, and also an estimated total of 0.25% magnesia and alkali oxides. No test for free calcium oxide resulted from absolute alcohol extraction. The X-ray diffraction pattern agreed with the work of Brownmiller and Bogue.[3]

Monocalcium aluminate was made by three heats totaling 18 hours at 1,480–1,500°. The product analyzed 35.49% calcium oxide and 64.44% alumina, as compared with the theoretical 35.49 and 64.51%. The X-ray diffraction pattern agreed with the A.S.T.M. catalog.

In preparing calcium dialuminate, five heats totaling 70 hours at 1,400–1,500° were made. The product contained 21.58% calcium oxide and 78.49% alumina, as compared with the theoretical 21.57 and 78.43%. The X-ray diffraction pattern agreed with that obtained by Lagerqvist, Wallmark, and Westgren.[4]

Magnesium aluminate was prepared in a similar manner, except that pure hydrated alumina and reagent grade magnesia were the starting materials. The stoichiometric mixture was heated for several periods including a total of 15 hours at 1,480–1,500°. Analysis of the product gave 28.33% magnesia and 71.62% alumina, as compared with the theoretical 28.34 and 71.66%. The X-ray diffraction pattern agreed with that in the A.S.T.M. catalog.

Measurements and Results.—The heat capacities were measured with previously described apparatus,[5] and the following masses of the substances were employed: 134.91 g. of $3CaO{\cdot}Al_2O_3$, 168.80 g. of $12CaO{\cdot}7Al_2O_3$, 169.90 g. of $CaO{\cdot}Al_2O_3$, 149.98 g. of $CaO{\cdot}2Al_2O_3$, and 147.77 g. of $MgO{\cdot}Al_2O_3$.

The measured values, expressed in defined calories (1 cal. = 4.1840 abs. joules) per deg. mole, appear in Table I. No evidence of any abnormal thermal behavior was observed during the measurements, and it may be seen from Fig. 1 that all five substances have regular heat capacity curves.

Entropies at 298.16°K.—The entropy increments between 51.00 and 298.16°K. were obtained in the usual manner by Simpson rule integrations of C_p against log T plots. The extrapolated portions of the entropies (0–51.00°K.), except in the case of $12CaO{\cdot}7Al_2O_3$, were obtained by use of empirical combinations of Debye and Einstein functions. The following function sums represent the measured heat capacities throughout the range 51 to 298.16°K. to within the limits indicated.

$$3CaO{\cdot}Al_2O_3:\ D\left(\frac{165}{T}\right) + 4E\left(\frac{294}{T}\right) + 5E\left(\frac{642}{T}\right) + E\left(\frac{1,280}{T}\right),\ (0.8\%)$$

$$CaO{\cdot}Al_2O_3:\ D\left(\frac{211}{T}\right) + 2E\left(\frac{326}{T}\right) + 3E\left(\frac{743}{T}\right) + E\left(\frac{1,425}{T}\right),\ (0.9\%)$$

$$CaO{\cdot}2Al_2O_3:\ D\left(\frac{181}{T}\right) + 4E\left(\frac{337}{T}\right) + 4E\left(\frac{715}{T}\right) + 3E\left(\frac{1,249}{T}\right),\ (0.9\%)$$

$$MgO{\cdot}Al_2O_3:\ D\left(\frac{397}{T}\right) + 2E\left(\frac{527}{T}\right) + 2E\left(\frac{667}{T}\right) + 2E\left(\frac{1,040}{T}\right),\ (1.1\%)$$

Because of the very high heat capacity of $12CaO{\cdot}7Al_2O$, the comparison method of Kelley, Parks and Huffman[6] was used to obtain the extrapolated portion of the entropy. The heat capacity values for the other three calcium aluminates were given equal weights in constructing the "standard"

(1) L. J. Brady and W. P. Davey, *J. Chem. Phys.*, **9**, 663 (1941).

(2) H. F. McMurdie, *Natl. Bur. Stands. J. Research*, **27**, 501 (1941).

(3) L. T. Brownmiller and R. H. Bogue, *Amer. J. Sci.*, **23**, 508 (1932).

(4) K. Lagerqvist, S. Wallmark and A. Westgren, *Z. anorg. allgem. Chem.*, **234**, 1 (1937).

(5) K. K. Kelley, B. F. Naylor and C. H. Shomate, U. S. Bur. Mines Tech. Paper 686 (1946).

(6) K. K. Kelley, G. S. Parks and H. M. Huffman, THIS JOURNAL, **33**, 1802 (1929).

TABLE I

HEAT CAPACITIES

T, °K.	C_p, cal./deg. mole	T, °K.	C_p, cal./deg. mole	T, °K.	C_p, cal./deg. mole
		$3CaO \cdot Al_2O_3$ (mol. wt., 270.20)			
53.86	7.024	105.00	20.65	216.23	41.65
58.06	8.073	114.74	23.16	226.03	42.86
58.29	8.117	124.82	25.52	236.29	44.13
62.58	9.297	135.88	28.02	245.83	45.23
62.80	9.331	145.54	30.03	256.54	46.32
67.09	10.54	155.59	32.00	266.41	47.36
71.65	11.77	165.92	33.97	276.33	48.33
76.22	12.99	176.02	35.69	286.51	49.25
81.20	14.38	185.96	37.33	296.54	49.96
86.39	15.78	195.92	38.80	298.16	(50.14)
94.90	18.05	206.35	40.28		
		$12CaO \cdot 7Al_2O_3$ (mol. wt., 1,386.68)			
53.89	35.07	114.69	117.3	216.04	212.6
58.20	40.53	124.87	129.6	225.99	219.3
62.50	46.53	135.98	142.2	235.94	226.0
67.20	53.28	145.55	152.5	245.78	231.9
72.00	59.30	156.38	163.6	256.20	237.7
76.65	66.36	165.74	172.6	266.08	243.3
82.00	73.92	175.78	181.5	276.25	248.8
86.21	79.78	185.56	189.8	286.54	253.9
94.55	91.08	195.72	198.1	296.75	258.3
104.79	104.5	206.15	205.6	298.16	(259.3)
		$CaO \cdot Al_2O_3$ (mol. wt., 158.04)			
53.52	4.073	114.75	12.55	216.32	23.11
57.74	4.341	124.65	13.79	225.97	23.88
61.99	5.269	136.22	15.17	235.98	24.65
66.52	5.945	145.72	16.26	246.07	25.43
71.16	6.516	155.70	17.34	256.37	26.13
75.79	7.264	166.66	18.50	266.38	26.83
80.40	7.923	176.04	19.45	276.71	27.52
84.45	8.505	185.85	20.40	286.54	28.16
94.66	9.313	196.25	21.35	296.30	28.68
106.15	11.43	206.07	22.17	298.16	(28.83)
		$CaO \cdot 2Al_2O_3$ (mol. wt., 260.00)			
53.50	5.358	114.78	19.17	216.13	37.44
57.99	6.310	124.71	21.24	226.25	38.88
62.54	7.357	138.27	24.03	236.04	40.17
67.11	8.406	146.60	25.65	245.88	41.54
71.69	9.470	155.94	27.38	256.26	42.88
76.24	10.49	165.81	29.25	266.25	44.10
80.30	11.45	175.84	30.99	276.42	45.26
84.70	12.46	185.76	32.69	286.60	46.55
94.76	14.75	195.98	34.35	296.35	47.41
104.97	17.00	206.37	35.91	298.16	(47.70)
		$MgO \cdot Al_2O_3$ (mol. wt., 142.28)			
53.55	1.060	114.95	7.384	216.32	20.51
57.72	1.283	124.87	8.737	228.03	21.75
62.19	1.591	135.89	10.29	237.36	22.69
66.84	1.953	146.36	11.69	245.85	23.47
71.51	2.341	156.37	13.11	256.37	24.41
76.17	2.759	165.90	14.43	266.66	25.27
80.80	3.211	175.91	15.74	276.12	26.03
85.02	3.660	185.86	16.98	286.54	26.89
94.43	4.736	196.21	18.22	296.31	27.52
105.62	6.181	206.36	19.38	298.16	(27.71)

heat capacity curve and in obtaining $S°_{51}$ and $H_{51.00} - H_0$ for the hypothetical "standard substance." Comparison of the heat-capacity data for $12CaO \cdot 7Al_2O_3$ and the "standard" then was made and the entropy of the former at 51.00°K. calculated as described by Kelley, Parks and Huffman.

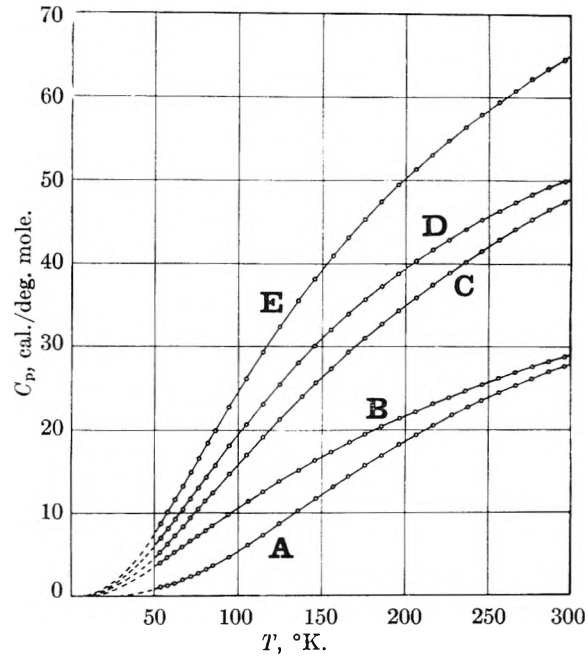

Fig. 1.—Heat capacities: A, $MgO \cdot Al_2O_3$; B, $CaO \cdot Al_2O_3$; C, $CaO \cdot 2Al_2O_3$; D, $3CaO \cdot Al_2O_3$; E, $12CaO \cdot 7Al_2O_3$ ($1/4$ C_p is plotted).

The results of the entropy calculations are in Table II. It should be noted that magnesium aluminate is a member of the regular class of spinels and therefore requires no entropy increment for randomness in its structure. So far as now known, the calcium aluminates also are free of structural irregularities.

TABLE II

ENTROPIES AT 298.16°K. (CAL./DEG. MOLE)

Substance	$S°_{51}$ (extrap.)	$S°_{298.16} - S°_{51}$ (meas.)	$S°_{298.16}$
$3CaO \cdot Al_2O_3$	2.77	46.34	49.1 ± 0.3
$12CaO \cdot 7Al_2O_3$	13.6	236.1	249.7 ± 1.5
$CaO \cdot Al_2O_3$	1.60	25.70	27.3 ± 0.2
$CaO \cdot 2Al_2O_3$	2.17	40.29	42.5 ± 0.3
$MgO \cdot Al_2O_3$	0.32	18.94	19.26 ± 0.10

From the data of Table II, the entropies of calcium and magnesium oxides,[7] and the entropy of aluminum oxide,[8] the following entropies of formation from the oxides at 298.16°K. are obtained: 8.4 ± 0.7 for $3CaO \cdot Al_2O_3$; 50.6 ± 2.9 for $12CaO \cdot 7Al_2O_3$; 5.6 ± 0.3 for $CaO \cdot Al_2O_3$; 8.7 ± 0.4 for $CaO \cdot 2Al_2O_3$; and 0.6 ± 0.2 for $MgO \cdot Al_2O_3$. The ΔS values for the calcium aluminates are unusually high in comparison with those for other interoxidic compounds studied to date. However, the same characteristic, although to a lesser degree, is shown by the calcium ferrites.[9]

(7) K. K. Kelley, U. S. Bur. Mines Bulletin 477 (1950).

(8) E. C. Kerr, H. L. Johnston and N. C. Hallett, *J. Am. Chem. Soc.*, **72**, 4740 (1950).

(9) E. G. King, *ibid.*, **76**, 5849 (1954).

HIGH TEMPERATURE HEAT CONTENTS OF ALUMINATES OF CALCIUM AND MAGNESIUM

BY K. R. BONNICKSON

Contribution from the Minerals Thermodynamics Branch, Region III, Bureau of Mines, United States Department of the Interior, Berkeley, Calif.

Received August 20, 1954

Heat contents of the compounds, $3CaO \cdot Al_2O_3$, $12CaO \cdot 7Al_2O_3$, $CaO \cdot Al_2O_3$, $CaO \cdot 2Al_2O_3$ and $MgO \cdot Al_2O_3$, were measured in the temperature range 298 to 1808°K. Regular behavior was observed except for $12CaO \cdot 7Al_2O_3$ which has an anomaly (heat capacity peak) at 1310°K. Heat content and entropy increments above 298.16°K. are tabulated, and representative heat content equations are derived.

Introduction

A recent paper[1] from this Laboratory reported low-temperature heat capacities and entropies at 298.16°K. for magnesium aluminate ($MgO \cdot Al_2O_3$–spinel) and the more important of the calcium aluminates ($3CaO \cdot Al_2O_3$, $12CaO \cdot 7Al_2O_3$, $CaO \cdot Al_2O_3$ and $CaO \cdot 2Al_2O_3$). The present paper records the results of heat content measurements for the same substances in the temperature range 298 to 1808°K. The only previous similar measurements are those of von Gronow and Schwiete[2] for $3CaO \cdot Al_2O_3$ (293–1573°K.) and $CaO \cdot Al_2O_3$ (293–1673°K.).

Materials and Method.—The substances investigated are portions of the samples used by King[1] in low temperature heat capacity measurements. His paper describes the methods of preparation and gives the results of chemical analyses and X-ray diffractions, so that repetition here is unnecessary. The indicated purity is 99.5% or better in each instance.

The heat content measurements were conducted with previously described[3] apparatus and methods. The samples were held in platinum–rhodium capsules, the heat contents of which were determined by separate experiments. The furnace thermocouple was checked frequently against the melting point of pure gold.

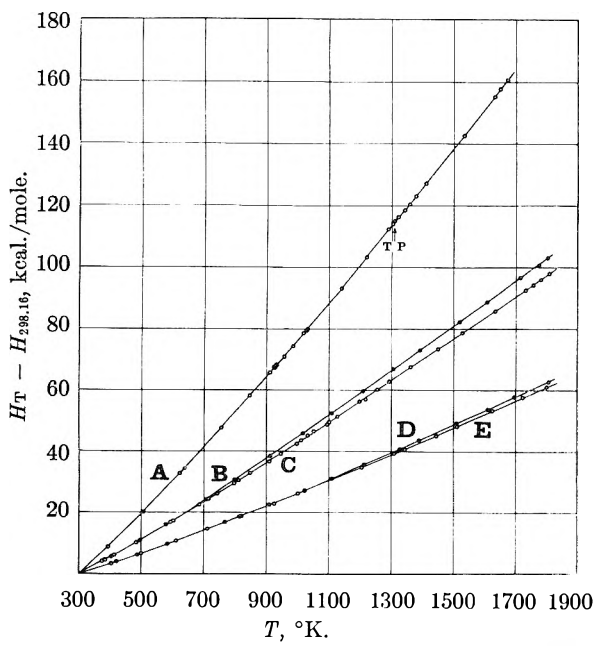

Fig. 1.—Heat contents above 298.16°K.: A, $12CaO \cdot 7Al_2O_3$ ($^1/_3$ mole is plotted); B, $CaO \cdot 2Al_2O_3$; C, $3CaO \cdot Al_2O_3$; D, $MgO \cdot Al_2O_3$; E, $CaO \cdot Al_2O_3$.

Results

The measured heat contents, expressed in defined calories (1 cal. = 4.1840 abs. joules) per mole, appear in Table I and Fig. 1. Molecular weights conform with the 1953 International Atomic Weights.[4] The estimated uncertainty in the measured heat contents is about ±0.2%.

TABLE I

HEAT CONTENTS ABOVE 298.16°K. (CAL./MOLE)

T, °K.	$H_T - H_{298.16}$	T, °K.	$H_T - H_{298.16}$	T, °K.	$H_T - H_{298.16}$
		$3CaO \cdot Al_2O_3$ (mol. wt., 270.20)			
373.6	3,980	742.4	26,290	1127.4	51,430
381.3	4,280	796.9	29,530	1196.5	56,310
383.8	4,380	811.3	30,520	1215.5	56,770
413.2	6,070	812.7	30,410	1253.3	60,070
482.6	10,120	845.9	32,950	1292.1	62,770
495.7	10,920	909.0	36,680	1361.4	67,300
501.9	11,320	944.9	39,190	1449.8	73,210
502.6	11,440	997.4	42,410	1527.8	78,540
592.7	16,880	1010.2	43,610	1632.6	85,550
598.6	17,090	1031.1	45,230	1731.3	92,470
601.6	17,390	1050.0	46,640	1757.4	94.160
684.9	22,630	1093.1	48,710	1780.8	95,890
713.3	24,220	1099.7	49,480	1807.9	97.910
		$12CaO \cdot 7Al_2O_3$ (mol. wt., 1386.68)			
394.4	26,250	983.0	222,480	1322.3	348.900
506.1	60,160	1016.5	235,610	1341.5	355,220
622.0	98,480	1027.9	238,600	1358.0	361.240
637.8	103,540	1029.0	239,810	1378.6	368,870
753.7	142,610	1140.3	279,350	1412.1	381,320
845.4	174,390	1221.3	309,230	1534.4	427,590
908.6	196,640	1290.4	336,550	1632.6	465,050
924.9	202,020	1306.2	342,730	1651.1	472,180
930.3	204,170	1310.3	344,930	1672.6	482,030
954.7	212,300				
		$CaO \cdot Al_2O_3$ (mol. wt., 158.04)			
402.6	3,250	1000.1	26,340	1443.7	44,980
498.2	6,570	1109.8	30,780	1510.7	48,090
611.4	10,820	1204.8	34,820	1623.2	53,230
710.9	14,560	1307.9	39,220	1721.1	57,610
817.4	18,710	1342.5	40,430	1800.2	61,130
922.6	22,930				
		$CaO \cdot 2Al_2O_3$ (mol. wt., 260.00)			
403.7	5,570	1013.9	45,760	1518.7	82,190
494.5	10,800	1108.1	52,440	1608.3	88,670
578.0	16,070	1207.7	59,470	1714.6	96,620
704.7	24,230	1306.4	66,890	1773.8	100,600
797.0	30,700	1392.4	73,040	1801.5	102,860
910.8	38,530				
		$MgO \cdot Al_2O_3$ (mol. wt., 142.28)			
421.0	3,830	909.0	22,570	1388.4	43,630
485.7	6,070	1020.9	27,230	1508.2	49,060
584.5	9,760	1109.9	31,150	1610.1	53,590
767.4	16,870	1212.2	35,690	1695.0	57,770
814.4	18,720	1325.5	40,710	1805.5	62,690

(1) E. G. King, THIS JOURNAL, **59**, 218 (1955).

(2) H. E. von Gronow and H. E. Schwiete, *Z. anorg. Chem.*, **216**, 185 (1933).

(3) K. K. Kelley, B. F. Naylor and C. H. Shomate, U. S. Bur. Mines Tech. Paper 686 (1946).

(4) E. Wichers, *J. Am. Chem. Soc.*, **76**, 2033 (1954).

TABLE II

HEAT CONTENTS (CAL./MOLE) AND ENTROPIES (CAL./DEG. MOLE) ABOVE 298.16°K.

T, °K.	$3CaO \cdot Al_2O_3$ $H_T - H_{298.16}$	$3CaO \cdot Al_2O_3$ $S_T - S_{298.16}$	$12CaO \cdot 7Al_2O_3$ $H_T - H_{298.16}$	$12CaO \cdot 7Al_2O_3$ $S_T - S_{298.16}$	$CaO \cdot Al_2O_3$ $H_T - H_{298.16}$	$CaO \cdot Al_2O_3$ $S_T - S_{298.16}$	$CaO \cdot 2Al_2O_3$ $H_T - H_{298.16}$	$CaO \cdot 2Al_2O_3$ $S_T - S_{298.16}$	$MgO \cdot Al_2O_3$ $H_T - H_{298.16}$	$MgO \cdot Al_2O_3$ $S_T - S_{298.16}$
400	5,380	15.48	27,800	80.0	3,140	9.03	5,340	15.34	3,150	9.05
500	11,180	28.41	58,250	147.8	6,610	16.76	11,200	28.40	6,650	16.85
600	17,280	39.52	90,850	207.2	10,320	23.52	17,480	39.84	10,350	23.59
700	23,570	49.22	124,650	259.3	14,130	29.39	24,050	49.97	14,190	29.51
800	29,990	57.79	158,900	305.0	18,030	34.60	30,830	59.02	18,150	34.79
900	36,510	65.47	193,600	345.9	22,020	39.30	37,760	67.18	22,220	39.59
1000	43,110	72.42	228,750	382.9	26,100	43.59	44,800	74.60	26,390	43.98
1100	49,770	78.77	264,500	417.0	30,260	47.56	51,920	81.38	30,660	48.05
1200	56,460	84.59	301,150	448.9	34,500	51.25	59,100	87.63	35,030	51.85
1300	63,170	89.96	340,250	480.2	38,810	54.70	66,320	93.41	39,490	55.42
1310	...	...	344,500 (α)	483.4	...	...	...	...	...	...
1310	...	...	344,500 (β)	483.4	...	...	...	...	...	...
1400	69,900	94.95	376,700	507.2	43,180	57.93	73,570	98.78	44,030	58.78
1500	76,660	99.61	414,400	533.2	47,610	60.99	80,830	103.79	48,620	61.95
1600	83,460	104.00	452,600	557.9	52,090	63.88	88,100	108.48	53,230	64.92
1700	90,310	108.15	491,400	581.4	56,610	66.62	95,400	112.91	57,850	67.72
1800	97,220	112.10	...	...	61,160	69.22	102,750	117.11	62,480	70.37

No transformations, isothermal or otherwise, were observed, except in the case of $12CaO \cdot 7Al_2O_3$. This substance has a heat capacity peak at 1310°K. The heat capacity increases from 259.3 cal./deg. mole at 298.16°K. to about 391 at 1310°K., then falls abruptly to about 357.5, and finally again increases to about 396 cal./deg. mole at 1700°K.

The heat content of $MgO \cdot Al_2O_3$ is higher than that of $CaO \cdot Al_2O_3$ by amounts ranging from <0.1% at 400°K. to 2.2% at 1800°K. This cannot be considered abnormal as the structures of the substances are different. The magnesium compound has the spinel structure, while the calcium compound has a less symmetrical, although apparently not yet completely determined, structure.

Kelley[5] has examined the data of von Gronow and Schwiete[2] for $CaO \cdot Al_2O_3$ and $3CaO \cdot Al_2O_3$ and has estimated the uncertainty as 3%, which is confirmed by the present work. Their data for $CaO \cdot Al_2O_3$ average about 3% higher than the present values, while those for $3CaO \cdot Al_2O_3$ show agreement to within ±1%.

Table II gives smooth values of the heat content and entropy increments above 298.16°K. The latter were calculated to match the former, using the method recommended by Kelley.[5]

The heat content data of Table II are represented, to within the average limits indicated, by the following equations, which were derived by the method of Shomate[6] and which utilize King's[1] heat capacity values at 298.16°K.

$3CaO \cdot Al_2O_3$:

$$H_T - H_{298.16} = 62.28T + 2.29 \times 10^{-3}T^2 + 12.01 \times 10^5T^{-1} - 22{,}801$$
(0.5%; 298–1800°K.)

$12CaO \cdot 7Al_2O_3(\alpha)$:

$$H_T - H_{298.16} = 301.96T + 32.75 \times 10^{-3}T^2 + 55.30 \times 10^5T^{-1} - 111{,}491$$
(0.6%; 298–1310°K.)

$12CaO \cdot 7Al_2O_3(\beta)$:

$$H_T - H_{298.16} = 228.52T + 49.22 \times 10^{-3}T^2 - 39{,}327$$
(0.1%; 1310–1700°K.)

$CaO \cdot Al_2O_3$:

$$H_T - H_{298.16} = 36.00T + 2.98 \times 10^{-3}T^2 + 7.96 \times 10^5T^{-1} - 13{,}668$$
(0.3%; 298–1800°K.)

$CaO \cdot 2Al_2O_3$:

$$H_T - H_{298.16} = 66.09T + 2.74 \times 10^{-3}T^2 + 17.80 \times 10^5T^{-1} - 25{,}919$$
(0.6%; 298–1800°K.)

$MgO \cdot Al_2O_3$:

$$H_T - H_{298.16} = 36.80T + 3.20 \times 10^{-3}T^2 + 9.78 \times 10^5T^{-1} - 14{,}537$$
(0.2%; 298–1800°K.)

Corresponding heat capacity relationships may be obtained by differentiation.

(5) K. K. Kelley, U. S. Bur. Mines Bulletin 476 (1949).

(6) C. H. Shomate, *J. Am. Chem. Soc.*, **66**, 928 (1944).

MECHANISM OF PEPTIZATION OF ALUMINUM SOAP–HYDROCARBON GELS BASED UPON INFRARED STUDIES[1]

By Willard O. Ludke, Stephen E. Wiberley, Jerome Goldenson and Walter H. Bauer

Department of Chemistry, Walker Laboratory, Rensselaer Polytechnic Institute, Troy, N. Y., and Chemical Corps Chemical and Radiological Laboratory

Received August 23, 1954

The mechanism of peptization of aluminum dilaurate-cyclohexane gels was studied by means of measurement of the changes in infrared absorption attending peptization. Effective peptizers, such as *m*-cresol, ethyl alcohol and *m*-toluidine reduced absorption intensities at 10.1, 6.3 and 2.7 μ, and increased intensities at 5.8 and 3.0 μ. The presence of a proton on the functional group capable of hydrogen bonding was shown to be essential in peptization, and steric factors were found to be more important than relative basicity. It is proposed that aluminum soaps exist as linear polymeric molecules in which aluminum has a coördination of six, the octahedra being joined by coördinate bonding through both hydroxyl groups and carboxylate groups of the fatty acid from which the soap is derived. Evidence is presented to support a mechanism of peptization involving hydrogen bonding of the peptizer to the carboxylate oxygen with the resulting rupture of the polymeric linkage rather than preferential coördination with aluminum.

Introduction

Aluminum soaps are notable for their ability to form soap–hydrocarbon gels of high viscosity. Properties of individual systems have been shown to depend on such factors as the nature of the hydrocarbon and the fatty acid group involved, the temperature, and the presence of peptizers.[2–4] Investigations have shown aluminum soaps to be definite chemical compounds,[5,6] and evidence has been presented that the soaps exist only in the disoap form.[6] Polymeric structure of the aluminum soap molecules[7–10] has been proposed in explanation of their ability to thicken hydrocarbons. Numerous investigators have proposed various structures for aluminum soaps derived mainly from X-ray diffraction and viscosity studies.[11–18] Gray[7] suggested a linear polymer based on octahedral coördination, and this conception was extended by Gray and Alexander,[4] who retained the octahedral coördination with four corners occupied by fatty acid groups. The octahedra were joined through coördinate bonds between aluminum atoms and the oxygen atoms of hydroxyl groups. McGee[9] advanced a structure similar to that of Gray and Alexander with adjacent chains held together by van der Waals forces and hydrogen bonding between the hydrogen of the shared hydroxyl groups and the oxygen atoms of the carboxyl of the adjacent molecules. Infrared studies[5,19] have shown free and no bonded hydroxyl in both aluminum disoaps and the hydrocarbon gels formed therefrom, indicating that hydrogen bonding is not an essential factor in gel formation.

Infrared spectra of all aluminum soaps show characteristic absorption bands at 2.7, 6.3, and 10.1 microns, ascribed to free hydroxyl, stretching vibrations of carboxylate ion, and an aluminum oxygen linkage, respectively. Peptization of aluminum soap–hydrocarbon gels may be caused by such compounds as water, alcohols, amines and phenols.[4] Reduced viscosity of gels and lowered ready solution temperature[20] of the soaps in the presence of peptizers are accompanied by a corresponding decrease in the intensity of the infrared absorption at 10.1 microns.[19] It appeared likely, therefore, that a study of the changes in infrared absorption intensities accompanying peptization of gels would afford information both as to the nature of peptization and the type of linkages in aluminum soap polymer responsible for their gel forming characteristics.

Experimental

Materials.—Lauric acid was Eastman Kodak White Label grade. The purity of this acid was previously determined.[19] Eastman Kodak 2-ethylhexoic acid was purified by distillation at 5 mm. pressure after removal of unsaponifiable material. The fraction used in this investigation had a neutralization equivalent of 144.2. Cyclohexane from Shell Chemical Corporation was dried, filtered and distilled. The fraction used had a boiling point of 80.5–80.6° at 760 mm. pressure. The cyclohexane was stored over metallic sodium in an all-glass dispersing unit. Alcohols, ethers and *m*-cresol were dried over Drierite, and the alcohols and ethers were distilled from calcium hydride. Amines were dried over sodium hydroxide before distillation. Aluminum hydroxy dilaurate and aluminum hydroxy 2-ethylhexoate were prepared as previously described.[19] Aluminum analysis showed that the ratio of moles of fatty acid per mole of aluminum was 1.99 in the laurate, and 2.03 in the 2-ethylhexoate. The laurate soap was precipitated at 50–60°, and the hexoate at 25°.

Gel Preparation.—Aluminum soap–hydrocarbon gels were prepared by the addition of dried, weighed portions of soap to measured weights of solvent in culture tubes. The soaps were dispersed by hand shaking of the aluminum foil covered, capped tubes. After gel formation, the tubes were placed in a rotating mount and aged for 24 hours at 60°. Gels were cooled at 20° for 24 hours prior to use.

(1) Abstracted from W. O. Ludke's Ph.D. Dissertation, Rensselaer Polytechnic Inst., Troy, N. Y., January, 1954.

(2) C. M. Cawley, J. H. G. Carlile, J. G. King and F. E. T. Kingman, *J. Inst. Petroleum*, **33**, 649 (1947).

(3) W. H. C. Rueggeburg, This Journal, **52**, 1444 (1948).

(4) V. R. Gray and A. E. Alexander, *ibid.*, **53**, 9 (1949).

(5) W. W. Harple, S. E. Wiberley and W. H. Bauer, *Anal. Chem.* **24**, 635 (1952).

(6) J. J. Bulloff, Ph.D. Dissertation, Rensselaer Polytech. Inst., April, 1953.

(7) V. R. Gray, *Trans. Faraday Soc.*, **42B**, 196 (1946).

(8) J. W. McBain and R. B. Working, This Journal, **51**, 974 (1947).

(9) C. G. McGee, *J. Am. Chem. Soc.*, **71**, 278 (1949).

(10) H. Sheffer, *Can. J. Research*, **B26**, 481 (1948).

(11) H. S. Seelig, Gunther and Kingston, M.I.T.-MR. No. 192, CWS Development Laboratory, Cambridge, Mass., Sept. 26, 1945.

(12) S. S. Marsden, K. J. Mysels and G. H. Smith, *J. Colloid Sci.*, **72**, 265 (1947).

(13) K. J. Mysels, *Ind. Eng. Chem.*, **41**, 1435 (1949).

(14) S. Ross and J. W. McBain, *Oil and Soap*, **23**, 214 (1946).

(15) S. S. Marsden K. J. Mysels, G. H. Smith and S. Ross, *J. Am. Oil Chem. Soc.*, **25**, 454 (1948).

(16) A. E. Alexander, and V. R. Gray *Proc. Roy. Soc. London*, **A200**, 162 (1950).

(17) T. S. McRoberts and J. H. Schulman, *Nature*, **162**, 101 (1948).

(18) J. C. Arnell, *Chem. in Canada*. **B5**, No. 11, 29 (1953).

(19) F. A. Scott, J. Goldenson, S. E. Wiberley and W. H. Bauer, This Journal, **58**, 61 (1954).

(20) H. S. Jackson, Ph.D. Dissertation, Rensselaer Polytech. Inst., June, 1951.

Appropriate quantities of peptizer, when used, were added to cyclohexane before the gels were prepared. Extreme care was taken to avoid entry of water.

Infrared Absorbance Measurements.—The techniques of absorbance measurements and apparatus have been previously described.[19] For studies at 10.1, 6.3 and 5.8 μ, a sodium chloride prism was used, and at 2.7 and 3.0 μ, a lithium fluoride prism was used. Gels were introduced to the absorbance cell by means of a hypodermic syringe. Values of the absorbance are the logarithm to the base 10 of the reciprocal to the transmittance, p/p_0, where p and p_0 are the intensities of the light transmitted by the solute and solvent, respectively.

Results and Discussion

Absorbance as a Function of Soap Concentration.—A series of gels were prepared in which the concentration of aluminum dilaurate in cyclohexane varied over the range of 0 to 7.5% soap by weight. Infrared absorbances were measured at 10.1, 6.3, with a fixed cell thickness of 0.10 mm., and at 2.7 μ, with a cell thickness of 0.4 mm., and the results are shown in Fig. 1.

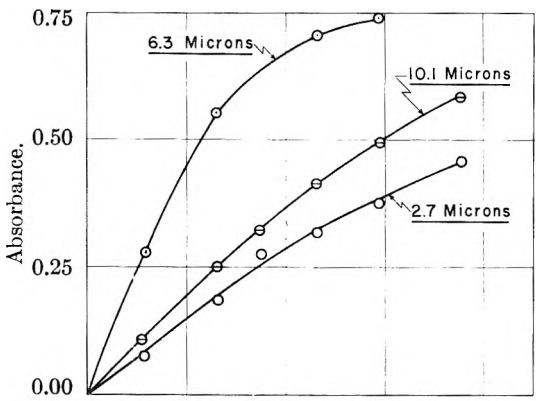

Fig. 1.

Effect of Peptizers.—Absorption intensities at 10.1, 6.3, 5.8 and 2.7 μ were measured on a series of gels containing a fixed weight of aluminum dilaurate in cyclohexane with varying amounts of *m*-cresol, ethyl alcohol, isopropyl alcohol, pyridine and *m*-toluidine. The results of these measurements are shown in Figs. 2, 3, 4 and 5. In addition, a similar study of triethylamine was made, with results similar to those obtained for pyridine and *t*-butyl alcohol. These additives were chosen for study of the effects of steric hindrance and the presence of an available proton. That triethylamine, a

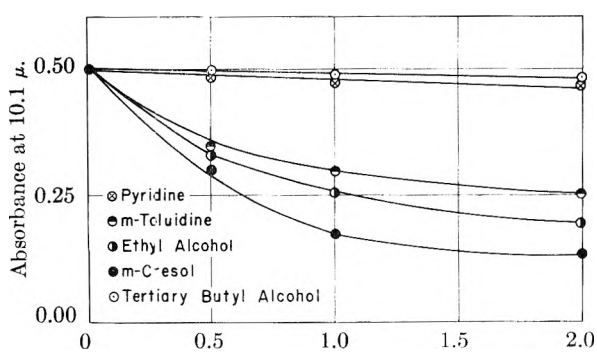

Fig. 2.

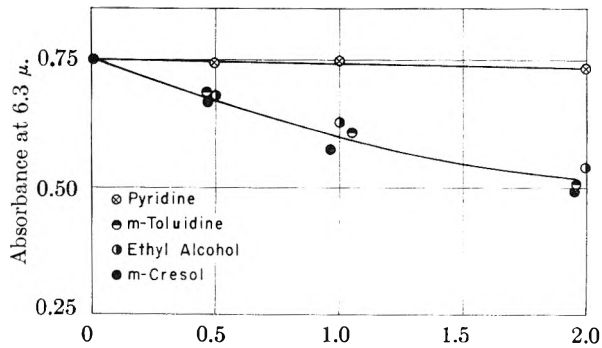

Fig. 3.

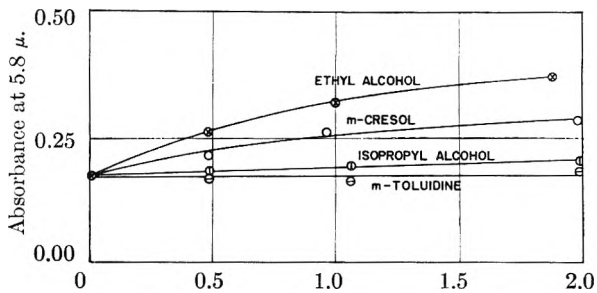

Fig. 4.

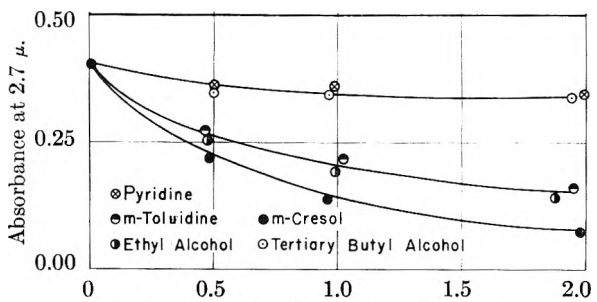

Fig. 5.

poor peptizer, is ineffective as compared to *m*-toluidine is ascribed to steric hindrance. Pyridine, also ineffective as a peptizer, should be less sterically hindered than *m*-toluidine, and thus there remains only the basic difference of lack of an available proton on the functional group to account for the results.

Ethyl alcohol, *m*-toluidine and *m*-cresol were the most effective of the peptizers studied. They gave comparable lowering of the gel viscosities together with a reduction in intensity of absorbance at 10.1, 6.3 and 2.7 μ, and an increase in absorbance at 5.8 μ. Since *m*-toluidine, ethyl alcohol and *m*-cresol produced similar effects on the absorbance at the various wave lengths, it is apparent that the relative basicity was of minor importance in these cases. The effect of steric hindrance is illustrated by the results of measurements in the series of alcohols, ethyl, isopropyl and *t*-butyl, when compared on a molar basis. The decrease of absorption intensity in the series of alcohols is concurrent with decrease in effectiveness as a peptizer.

Effect of Ethers.—Gels of aluminum dilaurate were prepared in cyclohexane with di-*n*-amyl ether and 1,4-dioxane at concentrations of 2 moles of pep-

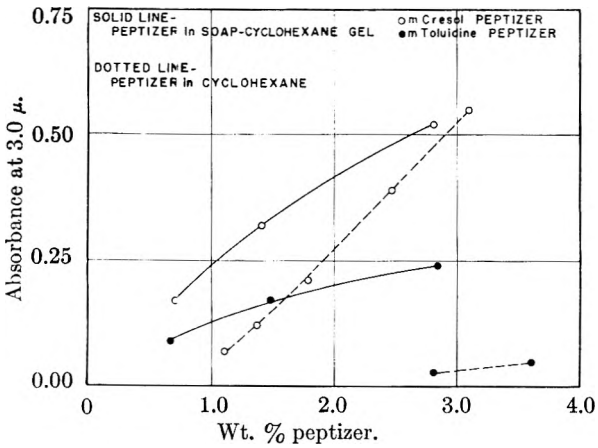

Fig. 6.

tizer per formula weight of soap. No change in viscosity from that of the unpeptized gel was noted, and no decrease in the absorbance at 10.1 and 6.3 μ was found.

Hydrogen Bonded Hydroxyl.—The absorption at 6.3 μ of both aluminum soaps and their cyclohexane gels is attributed to a resonance structure of the carboxylate ion with very little of the carbonyl character found in fatty acids. The acids are largely associated as

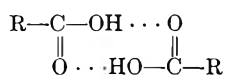

This acid type of carbonyl group shows absorption at 5.8 and 3.0 μ, ascribed to the carbonyl group and the bonded acidic hydrogen, respectively. It appeared likely that one action of a peptizer is to rupture a bond depending on the ionic carboxylate linkage and to modify the carboxylate ion to the type of structure exhibited by associated fatty acids, as the result of hydrogen bonding of the free hydroxyl hydrogen to the carboxylate oxygen. The decrease in absorbance at 2.7 μ, Fig. 5, on peptization is ascribed to the disappearance of the free hydroxyl hydrogen. Accordingly, absorbance measurements were made on all the peptized gels of aluminum dilaurate in cyclohexane, in the region of 3.0 μ, at which wave length the disoap shows only very slight absorbance. In all cases, peptization was accompanied by an increase in absorption at 3.0 μ. In Fig. 6 are shown results for gels peptized by *m*-cresol and *m*-toluidine. All peptizers used, with the exception of *m*-toluidine are highly capable of hydrogen bonding to themselves as their concentration in cyclohexane increases. There is less tendency to form a hydrogen bond of the N–H . . .N type than to form the O–H . . . O type of bond, with the bond energy of an N–H . . .O type falling intermediate between the two.[21] In Fig. 6, hydrogen bonding as shown by absorbance at 3.0 μ is definitely taking place upon peptization of the aluminum dilaurate with *m*-toluidine, and in this case there is no complicating feature of the peptizer molecule bonding to itself. This confirms the supposition that during peptization the free hydrogen of the hydroxyl group is becoming bonded, and that the peptizer molecule is itself acting through hydrogen bonding. Assuming the structure of the aluminum soap polymer to be as shown below, the mechanism of peptization can be illustrated as follows, where the fatty acid ion is represented by 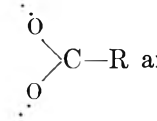 and the peptizer molecule by R'–H

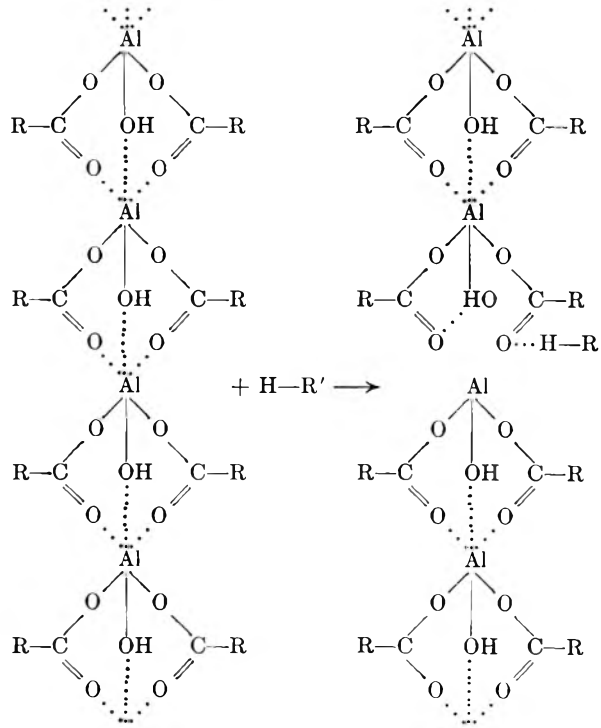

Comparison of Peptizer Effect on Branched and Straight Chain Soaps.—Aluminum hydroxy di-2-ethylhexoate is known to have a higher molar gelling capacity than aluminum hydroxy dilaurate. To compare the action of a peptizer, gels of both soaps in cyclohexane were made up at concentrations of 0.14 molal, based upon the formula Al-OHR_2. A series of gels of this concentration containing ethyl alcohol of varying amounts were also prepared and absorbance measurements were conducted on all gels at 10.1, 6.3, 2.7 and 5.8 μ. Results of these measurements show that ethyl alcohol acting as a peptizer produces much less effect on the 10.1 and 2.7 μ absorbance bands of the aluminum di-2-ethylhexoate gel than on the corresponding bands of aluminum dilaurate gel. On the other hand the decrease in absorbance at 6.3 and the increase at 5.8 μ is nearly the same in each case, as shown in Fig. 7.

Assuming the action of a peptizer presented previously to be correct, the difference in effect at 10.1 and 6.3 μ between the aluminum dilaurate and the aluminum di-2-ethylhexoate may be explained on the basis of the inductive effect of the 2-ethyl group. The strength of the (O–Al) bond of the (C–O–Al) group is increased by the increase of the electron density about the oxygen atom through the inductive effect of the 2-ethyl substituent. This

(21) L. Pauling, "Nature of the Chemical Bond," Cornell Univ. Press, Ithaca, N. Y., 1948, pp. 313-314.

increased strength prevents the rupture of the (O–Al) bond by the peptizer. Thus the breaking of a second and a third (O–Al) bond and the bonding of the hydroxyl hydrogen is prevented. The fact that carboxylate absorption at 6.3 μ and the carboxyl carbonyl absorption at 5.8 μ are affected in the same manner by the alcohol in the case of either dilaurate or di-2-ethylhexoate soap, is ascribed to the hydrogen bonding of the peptizer to the carboxylate oxygen with the resulting loss of resonance in the ion and the modification to a more truly carbonyl structure. Although no actual rupture of bonds is taking place, the resultant effect on the absorbance at 6.3 and 5.8 μ is the same as if the bonds were broken.

The comparatively smaller reduction in absorption at 10.1 μ shown by peptized gels of aluminum di-2-ethylhexoate soaps is in accord with the greater resistance to lowering of gel viscosity on peptization shown by these gels compared to aluminum dilaurate gels, corresponding to less rupture of the polymer linkage –O–Al–O–.

It may be assumed that when peptization occurs bonds associated with the polymeric linkages of the aluminum soaps in a gel must be broken or modified. It is evident from the proposed structure of the aluminum soap polymer that associated with each aluminum atom are six (Al–O) linkages, four involving the carboxylate oxygens and two involving the hydroxyl oxygens. All six are not equivalent. Consideration should be given to the fact that the 10.1 μ absorption may arise from an (Al–O–Al) type of linkage rather than a (C–O–Al) type. Infrared studies of organosilicon compounds by Simon and McMahon[22] have led to the assignment of 9.3 absorption band to an Si–O–Si linkage.

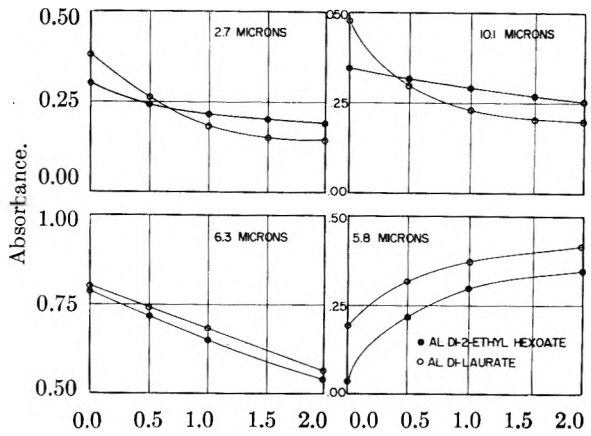

Fig. 7.

Compounds with numerous (SiO) linkages, but without Si–O–Si linkages, showed no absorption in this region. Richter[23] has ascribed an absorption band in the 10 μ region to the Al–O–Al linkage in aluminum oxide. The reduced peptizing action of alcohol on aluminum 2-ethylhexoate soap gels compared to its action on aluminum dilaurate gels in respect to viscosity lowering may indicate that though in each case there is much modification of carboxylate ion linkages, in the case of aluminum di-2-ethylhexoate soap gels comparatively fewer Al–O–Al linkages are broken. The absorption phenomena shown in Fig. 7 are in agreement with this mechanism.

Acknowledgment.—This study was conducted under contract between the Chemical Corps, U. S. Army, and Rensselaer Polytechnic Institute.

(22) I. Simon and H. McMahon, *J. Chem. Phys.*, **20**, 905 (1952).

(23) R. Richter, *Helv. Phys. Acta*, **19**, 21 (1946).

THE INTERACTION OF DEUTERIUM AND SATURATED HYDROCARBONS ON NICKEL CATALYSTS[1]

BY H. C. ROWLINSON, ROBERT L. BURWELL, JR., AND RICHARD H. TUXWORTH

Contribution from the Department of Chemistry, Northwestern University, Evanston, Illinois

Received September 1, 1954

The interaction of deuterium and a variety of alkanes and cycloalkanes on evaporated nickel films and on a reduced nickel oxide catalyst leads to very similar results. Isotopic exchange occurs conveniently at 150–200° to produce species with from one to all hydrogen atoms exchanged. With heptane and 3-methylhexane, the most abundant species are those of extensive but not total exchange. With cyclopentanes, cyclohexanes and 2,3-dimethylbutane, the most abundant is the fully exchanged one. In cycloalkanes no anomaly appears in the concentration of the species in which one-half of the hydrogen atoms are exchanged. Under the experimental conditions, hydrogenolysis of carbon–carbon bonds occurs only with ethylcyclobutane, in which case its rate is comparable to that of exchange. The data seem to require initial adsorption of the hydrocarbon molecule with cleavage of a carbon–hydrogen bond. The point of attachment then shifts in an α-β process with isotopic exchange accompanying each shift. α-α and α-γ shifts are relatively uncommon. A single branch in the carbon skeleton does not impede migration of the point of attachment but a *gem*-dimethyl group blocks it. Since racemization of (+)3-methylhexane is closely correlated with the total number of molecules exchanged, a symmetric intermediate is required during the exchange process.

A recent paper from this Laboratory[2] presented a study of the interaction of hydrogen and deuterium with heptane, (+)3-methylhexane, 3,3-dimethylhexane and 2,2,3-trimethylbutane on a nickel–kieselguhr catalyst. Of those molecules which exchanged, most suffered exchange of many hydrogen atoms. Most of the molecules of (+)3-methylhexane which were exchanged were also racemized. It appeared that initial adsorption of alkane involves dissociative adsorption with rupture of a carbon–hydrogen bond followed by migration of

(1) Presented at the September, 1954, meeting of the American Chemical Society.

(2) R. L. Burwell, Jr., and W. S. Briggs, *J. Am. Chem. Soc.*, **74**, 5096 (1952).

the point of attachment of the alkyl fragment with accompanying isotopic exchange. With (+)3-methylhexane, at some stage a symmetric intermediate is formed. It seemed wise to see in how far these initially rather surprising results are characteristic of nickel catalysts in general. This paper reports a study of eleven alkanes and cycloalkanes on evaporated nickel films, on reduced nickel oxide and on another type of nickel–kieselguhr catalyst.

Experimental

Materials.—The following Phillips Petroleum Company Research Grade hydrocarbons were used without treatment: cyclopentane, methylcyclopentane and methylcyclohexane. Heptane was percolated through silica gel and fractionated in a 50-plate Podbielniak Heli-Grid column, $n^{25}D$ 1.3853. Phillips Pure Grade 2,3-dimethylbutane was similarly treated, $n^{25}D$ 1.3724, as was Eastman Kodak Company cyclohexane, $n^{25}D$ 1.4234. Neopentane was kindly furnished by Professor H. Pines and 1,1-dimethylcyclohexane, 99.9 mole % pure, by Dr. Kenneth Greenlee of the American Petroleum Institute Project 45, Dr. Cecil Boord, director, at the Ohio State University.

3,3-Dimethylpentane was prepared by interaction of *t*-amyl chloride and ethylene in the presence of aluminum chloride at −40°.[3] The resulting 1-chloro-3,3-dimethylpentane was converted to 3,3-dimethylpentane by preparing and hydrolyzing the Grignard reagent. After preliminary distillation, the material was percolated through silica gel and distilled in the 50-plate column, $n^{25}D$ 1.3886.

Ethylcyclobutane was prepared by R. G. Armstrong following Pines, Huntsman and Ipatieff,[4] $n^{20}D$ 1.4018. It was percolated and distilled as above.

(+)3-Methylhexane was prepared from active amyl bromide[5] by reaction of the Grignard reagent of this compound with acetic anhydride at −78°.[6] The resulting 4-methyl-2-hexanone was reduced to the hydrocarbon by the Wolff–Kishner method.[7] The product was distilled, percolated through silica gel and distilled on the 50-plate column. The infrared spectra of several batches were shown identical with those of the Bureau of Standards Standard Sample of this hydrocarbon by a substitution method. This method of preparation is superior to the one formerly described.[2]

Tank deuterium gas was secured from the Stewart Oxygen Company under allocation from the Atomic Energy Commission. Before use it was passed over copper at 450° and then through a Dry Ice trap.

The nickel catalyst was prepared by Mr. W. S. Briggs from nickel carbonate which was precipitated from a solution of nickel nitrate by the rapid addition of sodium carbonate. The precipitate was thoroughly washed by decantation, filtered, dried at 110° and treated with oxygen at 300° for four hours. 20–40 mesh material was selected and reduced at 300° in hydrogen before placing in the catalyst chamber where it was rereduced. Harshaw Chemical Company's nickel–kieselguhr catalyst was crushed and 20–40 mesh material was selected.

Analysis.—Products were examined on the Baird recording infrared spectrograph. The C–D band at 4.6 μ was used to get an immediate estimate of the degree of exchange and to select suitable samples for mass spectrographic analysis.

Mass spectrographic analyses of hydrocarbons of molecular weight of 98 and higher were performed on a Consolidated mass-spectrometer under the direction of D. V. Kniebes at the Institute of Gas Technology, Chicago, Illinois. Those of lower molecular weight were examined on a manual Westinghouse mass-spectrometer in the Department of Chemical Engineering at Northwestern University under the supervision of D. M. Mason. Relatively high pressures of hydrocarbon were used to get as much sensitivity in the determination of the isotopically exchanged species as possible. The % of each exchanged species was computed from the parent peaks save for neopentane in which case mass 57 was employed and 3,3-dimethylpentane, mass 85. The treatment of the mass spectroscopic data was as before.[2]

Evaporated Nickel Films.—Evaporated nickel films were prepared by customary procedures including careful degassing at elevated temperatures. Owing to the necessity of collecting enough 3-methylhexane for polarimetry, the scale of operation was much larger than that generally used by previous workers.

The catalyst chamber was a section of glass tubing 45 mm. in inside diameter and between 50 and 75 mg. of nickel was evaporated onto the inner surface of this tube while the tube was cooled in ice-water. Gaseous mixtures of deuterium and hydrocarbon were prepared by bubbling deuterium gas through a sample of previously degassed hydrocarbon held at a suitable temperature. The mole ratio of deuterium to hydrocarbon was about 3 save with (+)3-methylhexane in which it was about 2. The reactant stream entered at the bottom of the catalyst chamber *via* 8 mm. tubing coiled helically around the large tube. The whole was surrounded by a furnace so that the reactant stream entered the catalyst chamber at reaction temperatures. A furnace surrounded the catalyst tube. A hemispherical shell of glass about 40 mm. in diameter was placed open end up immediately above the joint of the entrance tube to the catalyst tube. This served to start the gas stream up the inner face of the catalyst tube.

The effluent stream was passed into a trap cooled with liquid nitrogen and containing a calibrated section of small bore tubing at the bottom. Flow rates lay between 0.3 and 0.7 cc. of liquid hydrocarbon per hour.

Nickel Catalysts.—Experiments on reduced nickel oxide and on nickel–kieselguhr were run in an apparatus which will be described elsewhere. It is generally similar to that formerly used[2] but contains a positive action pump delivering degassed hydrocarbon into an evaporator provided with deuterium flow. Two cc. of catalyst was employed. Flow rates were about 3.4 cc. of liquid hydrocarbon per hr. and of deuterium, 0.0265 mole per hour. The catalysts were reduced initially at 325°. The catalyst from nickel oxide declined in activity with use. Activity could be restored by repeating the treatment with hydrogen at 325°.

Experimental Results

The activities of the evaporated films and of the reduced nickel oxide were rather similar. Measurements on the former were made at 130–200° and on the latter at 156–210°.

From the data of Beeck, Smith and Wheeler[8] one expects evaporated nickel films to have surface areas of 10 sq. meters per gram at 0°. About 0.22 cc. of vapor (STP) would, then, completely cover the surfaces of our films in adsorption with two point attachment. This would apply to films at 0°, sintering would reduce this figure. It is not surprising that we had some troubles with poisoning. After a run, the hydrocarbon in the evaporator was often replaced by another. Attempt was made to avoid the introduction of oxygen during this process. It was commonly possible to get two runs on the same film and occasionally three before serious loss of activity occurred. Particularly in early runs, there seemed to be some variation in initial activity of different preparations.

Typical exchange distribution patterns are shown in Figs. 1 and 2. (Tabulated data for these and many other runs will be supplied on request to Robert L. Burwell, Jr.). In general, very similarly shaped curves were observed on nickel films and on reduced nickel oxide.

At 86°, on the sample of nickel–kieselguhr previously studied, heptane gave a curve characterized

(3) L. Schmerling, *J. Am. Chem. Soc.*, **67**, 1152 (1945).

(4) H. Pines, W. D. Huntsman and V. N. Ipatieff, *ibid.*, **75**, 2315 (1953).

(5) R. L. Burwell, Jr., and G. S. Gordon, III, *ibid.*, **70**, 3128 (1948).

(6) M. S. Newman and A. S. Smith, *J. Org. Chem.*, **13**, 592 (1948).

(7) Huang-Minlon, *J. Am. Chem. Soc.*, **68**, 2487 (1946).

(8) O. Beeck, A. E. Smith and A. Wheeler, *Proc. Roy. Soc. (London)*, **A177**, 63 (1940).

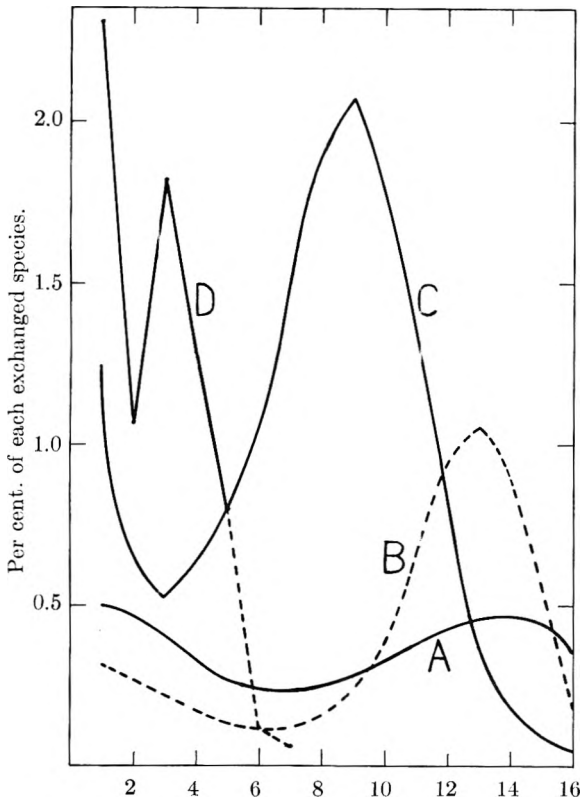

Fig. 1.—Distribution patterns of deuterated alkanes: pattern A, Harshaw nickel–kieselguhr, heptane, 96°; pattern B, reduced nickel oxide, heptane, 176°; pattern C, reduced nickel oxide, 3-methylhexane, 210°; the heptane pattern under these conditions differs mainly in d_1 being but half so great; pattern D, reduced nickel oxide, 3,3-dimethylpentane 210°.

by decline to D_7 followed by relatively constant abundance nearly to D_{16} (Fig. 1 of ref. 2). At 96° another sample of nickel–kieselguhr (Harshaw) exhibits a small maximum in the distribution pattern as shown in Pattern A, Fig. 1.

On reduced nickel oxide at 160–210°, heptane and 3-methylhexane give patterns of the type B and C. The maximum is at D_{15} at 160°. As the temperature is raised, the maximum moves to the left as shown in patterns B and C. The two hydrocarbons give very similar curves under similar conditions.

Nickel films give the same kinds of patterns but less definite statements are possible since fewer comparable runs were made and partial poisoning may partly confuse the issue.

Consequent to isotopic exchange, hydrogen accumulates in the gaseous deuterium. This causes the maximum in the distribution pattern to shift to the left with increasing extent of reaction. The observed shift with increasing temperature is but partly caused by this effect.

The relative extent to which the differences between patterns A and B result from difference in temperature and from difference in particle size is under investigation. Nickel–kieselguhr as reduced at 300° exhibits variation of magnetization with temperature[2] indicative of small particle size.[9] The plot of magnetization against temperature for

(9) P. W. Selwood, T. R. Phillips and S. Adler, *J. Am. Chem. Soc.*, **76**, 2281 (1954).

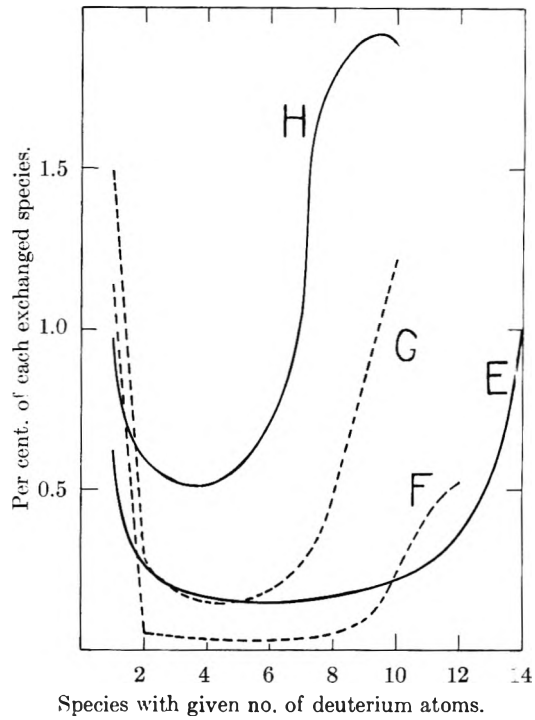

Fig. 2.—Distribution patterns of deuterated hydrocarbons: pattern E, evaporated nickel film, 2,3-dimethylbutane, 200°; pattern F, reduced nickel oxide, cyclohexane, 176°; pattern G, 1,1-dimethylcyclohexane, evaporated nickel film, 201°; pattern H, evaporated nickel film, cyclopentane, 200°.

reduced nickel oxide is very similar to that of bulk nickel.[10] This is indicative of relatively large particle size.

Pattern D (3,3-dimethylpentane) is characteristic of both evaporated nickel and of reduced nickel oxide. The minimum at D_2 is observed on both.

Cycloalkanes exhibit similar patterns on both catalysts. The comparatively large abundance of D_1 seems characteristic of cyclohexane (pattern F). Methylcyclohexane on nickel films and methylcyclopentane on both catalysts gave curves closely resembling the parent cycloalkane but with an exchange pattern extending to two more deuterium atoms.

Passage of ethylcyclobutane and deuterium over an evaporated nickel film at 150° resulted in some hydrogenolysis since some species of mass number greater than C_6D_{12} were observed. The results may be presented as follows, $C_6H_{11}D$, 3.03%; D_2, 1.63; D_3, 1.07; D_4, 0.90; D_5, 1.01; D_6, 1.29; D_7, 1.74; D_8, 2.03; D_9, 2.41; D_{10}, 2.48; D_{11}, 2.26; D_{12}, 1.74; D_{13}, 1.18; D_{14}, 0.68; D_{15}, 0.28; D_{16}, 0.23. It is assumed here that all species have the same sensitivity as ethylcyclobutane.

The relative rates of exchange of heptane, 3-methylhexane, 3,3-dimethylpentane, cyclohexane and methylcyclopentane were determined on the reduced nickel catalyst in order to compare them with the relative rates of exchange of several hydrocarbons published previously.[2] A run on each of the last four hydrocarbons was sandwiched between two runs on heptane. The catalyst was assumed to be in the same state throughout if the

(10) We are indebted to Dr. T. R. Phillips for this determination.

depth of the C–D absorption band in the heptanes was nearly the same. One of the heptanes was examined mass spectroscopically. The percentage of heptane molecules exchanged thus found was corrected to the average values for the two reference runs on the basis of the absorption at the C–D band (4.6 μ). In one case, the heptane runs differed by 10%, in the other cases by no more than 3%. Duplicate agreeing sets of runs are available for 3,3-dimethylpentane and methylcyclopentane.

Where the mass spectroscopic patterns permit unequivocal sorting of the exchange patterns of two different hydrocarbons, a mixture of hydrocarbons may be passed over a catalyst and the relative rates of exchange thus determined. Heptane and 3,3-dimethylpentane exemplify this situation. Since the latter compound has a negligible parent peak, there is no interference with the heptane analysis. 3,3-Dimethylpentane has a large peak at mass 85 and heptane has a small peak the effect of which can be subtracted out. In a run at 200° on an evaporated nickel film, 58.8% of the heptane molecules had exchanged, 21.7% of the 3,3-dimethylpentane.

Data on relative rates of exchange are presented in Table I in terms of the number of molecules of hydrocarbon exchanged referred to heptane as 1.0. It was assumed that the rate of appearance of exchanged molecules was first order in unexchanged molecules. Thus the relative rate is

$$\ln Z/\ln Z_0$$

where Z is the fraction of molecules which has not exchanged and Z_0 that fraction for heptane under the same conditions. Since cyclohexane and methylcyclopentane were fed at the same liquid volume rate as heptane, correction was made for contact time.

TABLE I

RATES OF EXCHANGE RELATIVE TO HEPTANE[a]

	Evaporated nickel films	UOP nickel–kieselguhr[b]	Reduced nickel oxide
Heptane	1.0	1.0	1.0
3-Methylhexane		0.75 (120°)	1.16 (176°)
3,3-Dimethylpentane	0.27 (200°)		0.48 (210°)
3,3-Dimethylhexane		0.36 (86°)	
Cyclohexane			0.52 (176°)
Methylcyclopentane			8.5 (160°)
2,2,3-Trimethylbutane		0.13 (120°)	

[a] The relative rates are followed by the temperature at which the comparison with heptane was made. The ratios are of numbers of molecules of hydrocarbon exchanged. [b] From ref. 2.

On nickel catalysts, the rate of exchange of 3-methylhexane is about the same as that of heptane, that of molecules containing *gem*-dimethyl groups and short side chains is smaller: 3,3-dimethylpentane, 3,3-dimethylhexane, 2,2,3-trimethylbutane. Neopentane exchanges very slowly. Cyclohexane exchanges more slowly than heptane but its isomer, methylcyclopentane, exchanges much more rapidly.

The nickel films were evaporated from 0.020 in. nickel wire manufactured by the Driver-Harris Company. Emission spectroscopy indicated the presence of copper, 0.02%; iron, 0.03%; magnesium, 0.4%; manganese, 0.3% and silicon, 0.02%. Since but 15–20% of the wire was evaporated, one cannot say just what the analysis of the film would have been. Presumably, particularly volatile impurities would concentrate in the first part of the film. In one experiment, about 40 mg. of nickel was evaporated. This film was removed and a film made from the remaining wire. The activity of the second film and the exchange patterns of 3-methylhexane and of cyclohexane were indistinguishable from those of the other films.

Discussion

As previously proposed,[2] the exchange reaction seems to require initial adsorption of the alkane with cleavage of a carbon–hydrogen bond followed by migration of the position of attachment with consequent exchange of one deuterium atom for each such migration.

The propagation reaction (that is, the migration of the position of attachment) is not significantly affected by the presence of a single branch in the alkane. This is clearly shown by the resemblance of the results with heptane with those of 3-methylhexane. Nor do two branches on different carbon atoms interfere as is shown by the exchange pattern of 2,3-dimethylbutane, Fig. 2, pattern E.

However, as previously found for 3,3-dimethylhexane,[2] a double branch on the same carbon atom blocks the propagation reaction. This is shown by 3,3-dimethylpentane in which only one of the ethyl groups exchanges, Fig. 1, pattern D. The slight concentration of species containing more than five deuterons results from double adsorption of the same molecule, the probability of which is $^1/_2X^2$ where X is the fraction of molecules which have exchanged once.[2]

Limitation of the exchange of 1,1-dimethylcyclohexane to ten deuterium atoms (the number of hydrogen atoms attached to the ring) illustrates the same point, Fig. 2, pattern G. These runs show, however, that the double branch does not seriously interfere with exchange of hydrogen atoms attached to the carbon atom adjacent to the branch.

Neopentane exchanges very slowly. The principal species which appears is $C_5H_{11}D$. Concentrations of doubly and trebly exchanged species are small. In one run at 200° on nickel film, the concentrations of $C_5H_{11}D$, $C_5H_{10}D_2$ and $C_5H_9D_3$ were 1.38, 0.12 and 0.08%, respectively. No $C_5H_8D_4$ could be detected. Therefore, α-α migration of the position of attachment is not very frequent. α-γ migration is not the dominant type. It hardly occurs at all past a double branch as shown by 3,3-dimethylpentane and 1,1-dimethylcyclohexane. With cyclohexane were it to occur exclusively, then only the six hydrogen atoms attached to carbon atoms 1 (the atom at which adsorption first occurs), 3 and 5 would exchange. The complete absence of any anomaly in the concentration of $C_6H_6D_6$ proves that this reaction is not dominant at these temperatures, Fig. 2, pattern F.

On the other hand, as shown by multiple exchange in 3,3-dimethylpentane, α-β migration occurs. It seems likely, then, that α-β migration is

the reaction which is principally responsible for multiple exchange.

If cycloalkanes were adsorbed flat and so remained, one would expect an anomaly to appear at the concentration of the species in which half of the hydrogen atoms in the ring were exchanged. No such anomaly appears in cyclopentane, methylcyclopentane, cyclohexane, methylcyclohexane or dimethylcyclohexane at these temperatures. Furthermore, one might expect hindrance to the flat adsorption of the last hydrocarbon, but its exchange pattern closely resembles that of cyclohexane.

The migration of the position of attachment in cyclic systems is relatively stereo-insensitive under the conditions studied. Thus, if migration were to occur exclusively to an adjacent *cis*-position, cyclopentane and cyclohexane would exchange but half of their hydrogen atoms. If migration were to occur exclusively to the *trans*-position, cyclohexane would exchange but six hydrogen atoms.

Furthermore, migration of the point of attachment does not require the hydrogen atom adjacent to the point of attachment to be in a *gauche*- or a *trans*-position since the relatively rigid molecule, cyclopentane, exchanges without difficulty.

On the whole, evaporated nickel films and reduced nickel oxide behave very similarly. Exchange patterns for heptane, 3-methylhexane, 3,3-dimethylpentane, cyclohexane and methylcyclopentane were closely similar on the two catalysts. There is no sign of anything unusual about evaporated nickel films. Once this material *has been exposed to reactant* it behaves in a standard fashion.

Nickel films prepared by evaporation in 1 mm. of nitrogen rather than *in vacuo* gave exchange patterns with 3-methylhexane and with cyclopentane which were of the same general type as those given by films prepared in high vacuum. After Beeck, *et al.*,[8] the crystallites of such films are oriented with the 110 faces parallel to the backing. The oriented film was, however, much more active than any other films both absolutely and relatively since its weight was but about one-fifth that of the unoriented films but it gave nearly twice the conversions of the usual films. As will appear, the ratio of exchange to racemization with (+)3-methylhexane was also the same as with unoriented films. Oriented films are more active in ethylene hydrogenation than are unoriented ones.[8]

Leaving out of consideration the blocking of the propagation reaction, the exchange patterns fall into two groups. 3-Methylhexane resembles heptane while all the cycloalkanes resemble 2,3-dimethylbutane (pattern E). The difference must lie in variation in the ratio of the probability of the propagation reaction to that of desorption. This ratio may also depend upon whether the position of adsorption is in the center or at the end of the acyclic alkanes. However, it is the more compact molecules which give curves with the maximum at the most exchanged species. This would seem to result in some degree from surface steric requirements for completion of the propagation reaction. (Compare, for example, 3-methylhexane and methylcyclohexane.)

One might suggest that multiple exchange results from diffusion of an alkane molecule into a pore in which it has many chances of adsorption with single exchange before it diffuses out of the pore. The possibility of this kind of a diffusion mechanism is often very difficult to eliminate. It can be eliminated unequivocally in the present case. If such a mechanism were to obtain, at low total conversions, at least ten hydrogen atoms of 3,3-dimethylpentane would be subject to exchange instead of but five.

One expects hydrogenolysis of carbon–carbon bonds at temperatures somewhat above those at which exchange starts.[11,2] In our experiments, hydrogenolysis was generally absent. We passed heptane and light hydrogen over a freshly evaporated nickel film at 200°. The infrared adsorption spectra of the products were indistinguishable from those of the reactant. As tested mass spectroscopically no significant amount of methane appeared in the off gas. This experiment was repeated with the same results. With cyclohexanes and cyclopentanes, hydrogenolysis would lead to species of mass numbers greater than those of the fully exchanged alkanes. None was observed.

However, with ethylcyclobutane on an evaporated nickel film, species heavier than C_6D_{12} were observed (see section "Experimental Results"). D_{13}, D_{14}, D_{15} and D_{16} must correspond to exchanged hexanes. Thus, exchange of the cyclobutane ring is accompanied by extensive ring opening to produce mainly 3-methylpentane.[12] On the other hand, the peak corresponding to D_1 must be singly exchanged ethylcyclobutane. If one allows that hydrogenolysis of the ring would necessarily introduce at least two deuterium atoms, then D_2 and D_3 are doubly and trebly exchanged ethylcyclobutane. Whether these one, two and three deuterium atoms are in the ring or in the ethyl side chain could not be ascertained.

By the use of optically active 3-methylhexane, one may determine the stereochemistry of the exchange reaction. If both the production of exchanged species and the loss of rotation proceed as first order reactions, the ratio of the rate of exchange to that of racemization is

$$\ln Z/\ln (\alpha/\alpha_0)$$

where Z is the fraction of molecules which have suffered no exchange.[2] Table II presents the results obtained in the present work. The probable error when small is determined by the % exchange, when larger, by the accuracy of polarimetry.

On the Universal Oil Products Company nickel–kieselguhr used before[2] the ratio was about 1.6, in agreement with that on the Harshaw catalyst. The reduced nickel oxide and particularly the evaporated films give lower values, closer to 1.2. With all catalysts there are some species with but a few deuterium atoms introduced in which exchange has probably not propagated to the optical center and, therefore, would not have resulted in loss of rota-

(11) K. Morikawa, W. S. Benedict and H. S. Taylor, *J. Am. Chem. Soc.*, **58**, 1445 (1936); **58**, 1795 (1936); K. Morikawa, N. R. Trenner and H. S. Taylor, *ibid.*, **59**, 1103 (1937).

(12) V. Haensel and V. N. Ipatieff, *ibid.*, **68**, 345 (1946); but see, also, B. A. Kazanskii and M. Yu. Lukina, *Doklady Akad. Nauk S.S.S.R.*, **74**, 263 (1950).

tion. The fraction of molecules having 3 deuterium atoms or less is listed in Table II. The choice of 3 deuterium atoms is, of course, rather arbitrary.

TABLE II

RATIO OF RATE OF EXCHANGE TO THAT OF RACEMIZATION FOR (+)3-METHYLHEXANE

Catalyst	Run no.	Ratio[a]	Fraction $D_1 + D_2 + D_3$[b]
Harshaw nickel–kieselguhr	107	1.7 ± 0.1	0.24
Reduced nickel oxide	122	1.4 ± .3	.24
	136	1.6 ± .2	.21
	153	1.2 ± .1	.16
Evaporated nickel film	19a	1.1 ± .1	.12
	19b	1.5 ± .3	.19
	22a[c]	1.1 ± .1	.08
	22b[c]	1.2 ± .1	.12

[a] The ratio of the rate of formation of exchanged species to that of loss of rotation. [b] Fraction of total molecules exchanged which had 1, 2 or 3 D-atoms. [c] Oriented film.

The assumption that such molecules are responsible for the ratio exceeding 1.0 is consistent with the exchange patterns. There are relatively more of the less extensively exchanged molecules with nickel–kieselguhr than with the other catalysts. In run 17 of ref. 2 on a nickel–kieselguhr which has been reduced at 250° rather than at 300°, α/α_0 was 0.979, whence the ratio is 3.2 ± 0.6. On this run, there is nearly an exponential decline in concentration with increasing degree of exchange and a much larger proportion of slightly exchanged species.

Our previous conclusion that racemization accompanies substantially all exchange at the tertiary carbon atom applies also to the catalysts studied in this paper.

A study of isotopic interchange between deuterium and ethane[13] and between deuterium and propane and isobutane[14] on a series of evaporated metal films including nickel has been reported. Multiple exchange was observed but, with nickel at 0° and long contact times, considerably less multiple exchange was observed than with the hydrocarbons we have studied at higher temperatures. Whether this difference results from the differences in the hydrocarbons or in the differences in temperature and pressure (Anderson and Kemball worked at much lower total pressures) is not clear. In contrast to our results, oriented and unoriented nickel films give rather different types of exchange patterns with ethane, the oriented film giving less multiple exchange.

Kemball and Anderson interpreted multiple exchange by the same general type of process which had been suggested for nickel–kieselguhr.[2] However, their suggestion that the propagation of the exchange reaction proceeds through

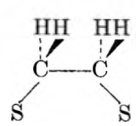

suffers from the difficulty that it cannot explain the racemization of (+)3-methylhexane.[2] Further, it is equivalent to adsorbed ethylene, which, in the presence of deuterium, returns considerable deuteroethylene to the gas phase as is also true of adsorbed butylenes.[15] One would have to assume that no such return would occur in exchange between alkanes and deuterium since, at the temperatures under consideration, the equilibrium concentration of olefin would be infinitesimal. Similar objection can be raised to two of the symmetric intermediates suggested to allow for racemization.[2] This consideration alone, however, is not necessarily fatal since the rate of olefin desorption could vary with surface conditions as influenced by the partial pressure of olefin in the vapor phase.

One symmetric intermediate previously suggested[2] could account for the results and would confine the propagation reaction to an α-β shift. As applied to (+)3-methylhexane it takes the form

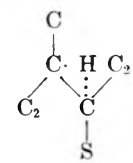

On the other hand, an adsorbed alkyl group might have a less classical structure. Our knowledge of surface orbitals does not seem adequate to specify exactly the nature of an adsorbed radical. If the adsorbed alkyl group was planar and if the plane of the radical was perpendicular to the surface, ad-

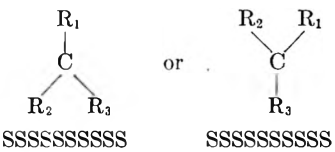

sorbed (+)3-methylhexane would pass through a symmetric form. The details of the exchange of cycloalkanes would also be intelligible. This proposed intermediate is equivalent to a free radical in which the p-orbital interacts with surface orbitals. Addition of a hydrogen atom to the central carbon atom would result in desorption while simultaneous removal of a hydrogen atom from one of the adjacent carbon atoms would result in propagation of exchange. The stereochemistry would be satisfied if the adsorbed alkyl group merely passed through the proposed structure. The adsorbed alkyl group would not necessarily exist mainly in such a form. There is some interrelation between the two possibilities given above since, in the first, either the plane of the non-adsorbed free radical must be perpendicular to the surface or there must be free rotation about the central carbon–carbon bond.

We have derived an expression for the exchange pattern of cyclopentane on a model involving initial adsorption at a single point coupled with random migration of this point of attachment with exchange of a deuterium atom at each shift. This

(13) J. R. Anderson and C. Kemball, *Proc. Roy. Soc.* (*London*), **223A**, 361 (1954).

(14) C. Kemball, *ibid.*, **223A**, 377 (1954).

(15) T. I. Taylor and V. H. Dibeler, THIS JOURNAL, **55**, 1036 (1951). This paper is a leading reference to previous work in the field of olefin hydrogenation and exchange.

model does not confine the propagation reaction to α-β shifts but mathematically it is less refractory.[16] When probability of migration of the point of attachment at any stage is about 0.91 (or the probability of desorption is 0.09), the exchange pattern is one in which all exchanged species have about the same concentration. When the migration probability exceeds 0.91, the concentration steadily increases with increasing exchange, and when it is less than 0.91 it declines with increasing exchange. The exchange pattern of cyclopentane cannot result from such a model. However, if the migration probability was below 0.9 on one crystal face and above 0.93 on another face, then a curve of the observed form Fig. 2, Pattern H would result. Anderson and Kemball[13] treated ethane from a rather similar model with similar conclusions. In any case, considering that many of the exchanges accompanying the propagation reaction would merely replace a deuterium atom by another deuterium atom, the net probability of desorption at any stage must be small in order that exchange of all hydrogen atoms in a substantial fraction of cyclopentane would result.

(16) We are indebted to Mrs. H. C. Rowlinson for the mathematical solution of this combinatorial problem.

Acknowledgment.—This research was supported by the Office of Naval Research. One of us, Richard H. Tuxworth, was the holder of a Visking Corporation Fellowship.

THE SCATTERING OF LIGHT BY SUCROSE SOLUTIONS

BY SAMUEL H. MARON AND RICHARD L. H. LOU

Physical Chemistry Laboratory, Department of Chemistry and Chemical Engineering, Case Institute of Technology, Cleveland, Ohio

Received September 2, 1954

Previously published agreements between the measured turbidities of sucrose solutions and turbidities calculated from osmotic pressure data prove to be fortuitous, and are due to a compensation of calibration errors by neglect of some important corrections, particularly that due to depolarization of the scattered light. Consequently, the turbidities and depolarization ratios of sucrose solutions up to a concentration of 0.59 g. per cc. have been redetermined at 25° and at two wave lengths, 4358 and 5461 Å. The newly observed turbidities are shown to be in very good accord with those calculated from concentration dependence of osmotic pressure, and they yield for the molecular weight of sucrose 338 ± 6 g. per mole, as against the theoretical 342.

Introduction

Debye[1] and Halwer[2] have both measured the turbidities of sucrose solutions, and have presented results to show that the measured turbidities were in satisfactory agreement with those calculated theoretically from the osmotic pressures of the solutions. Debye's measurements were based on the turbidity of the Cornell standard polymer, whose value was taken to be 2.70×10^{-3} cm.$^{-1}$ at 4358 Å. and 25°, a value shown subsequently to be considerably in error[3] and equal actually to 3.50×10^{-3} cm.$^{-1}$. Again, although Halwer employed an opal glass as a turbidity standard, he obtained on a cross-check a value of 2.56×10^{-3} cm.$^{-1}$ for the Cornell standard polymer at 4358 Å., a value which would suggest that his measurements were also based on an incorrect standard. These facts came to light when we attempted to compare the turbidities of sucrose solution as based on Ludox calibration[4] with the published values, and found the former to be invariably higher by a considerable percentage.

The apparent agreement with theory obtained by Debye and Halwer, even though their standards were incorrect, has been found to be due largely to neglect by these authors of the depolarization correction. This correction is, as will be shown below, quite appreciable for sucrose solutions, and its neglect compensates to a large degree for the error in the standards. In view of this situation, we decided to reinvestigate this question of the turbidities of sucrose solutions and their relation to osmotic pressure, because this system offers an excellent means of testing the theory of scattering of light by solutions under conditions where dissymmetry is absent. The results obtained in this study are presented here.

Theoretical Considerations.—Debye[5] has shown that, for a solution of small isotropic particles, the excess turbidity, τ, due to solute is related to the osmotic pressure of the solution, P, by the expression

$$\tau = \left[\frac{32\pi^3\mu_0^2}{3N\lambda^4}\left(\frac{d\mu}{dC}\right)^2\right]\frac{CRT}{(\partial P/\partial C)} \qquad (1)$$

Here μ_0 is the refractive index of the pure solvent, μ that of the solution of concentration C, N is Avogadro's number, T the temperature, R the gas constant, and λ the wave length of the light employed. In deriving this equation Debye introduced the approximation that $(\mu + \mu_0)^2 \approx 4\mu_0^2$. Although this approximation is quite valid for dilute solutions, in sucrose solutions of 0.6 g. per cc. concentration it can introduce an error of *ca.* 4%. Consequently, for our purposes the more exact equation to be used is

$$\tau = \left[\frac{8\pi^3(\mu + \mu_0)^2}{3N\lambda^4}\left(\frac{d\mu}{dC}\right)^2\right]\frac{CRT}{(\partial P/\partial C)} \qquad (2a)$$

$$= \frac{HCRT}{(\partial P/\partial C)} \qquad (2b)$$

(1) P. Debye, THIS JOURNAL, **51**, 18 (1947).

(2) M. Halwer, *J. Am. Chem. Soc.*, **70**, 3985 (1948).

(3) C. I. Carr and B. H. Zimm, *J. Chem. Phys.*, **18**, 1616 (1950); B. A. Brice, M. Halwer and R. Speiser, *J. Opt. Soc. Am.*, **40**, 768 (1950); P. Doty and R. F. Steiner, *J. Chem. Phys.*, **18**, 1211 (1950); H. P. Frank and H. Mark, *J. Polymer Sci.*, **10**, 129 (1953); S. H. Maron and R. L. H. Lou, *ibid.*, **14**, 29 (1954).

(4) S. H. Maron and R. L. H. Lou, *J. Polymer Sci.*, **14**, 29 (1954).

(5) P. Debye, *J. Appl. Phys.*, **15**, 338 (1944).

where H is equal to the quantity in brackets in (2a).

When the solute particles are non-isotropic, and the scattered light is depolarized, equation 2 has to be modified by the introduction of the depolarization correction factor $(6 + 6\rho_u)/(6 - 7\rho_u)$, where ρ_u, the depolarization ratio, is the ratio of the horizontal to the vertical components of the light scattered by the solute at 90° to the direction of the incident unpolarized light. Equation 2 becomes thus

$$\tau = \frac{HCRT}{(\partial P/\partial C)}\left(\frac{6 + 6\rho_u}{6 - 7\rho_u}\right) \qquad (3)$$

and this expression permits then the calculation of τ from the osmotic pressures and the depolarization ratios of the solutions at the various concentrations.

Experimental

The sucrose employed in these studies was the highly purified product supplied by the National Bureau of Standards for calorimetric work, and it was used without further purification. The aqueous solutions of this sucrose showed considerable dissymmetry which could not be removed by filtration through even ultrafine sintered glass filters. To effect the required optical cleanliness of the solutions, the following procedure was finally adopted. The sucrose solutions, adjusted to 25°, were introduced into Corning ultrafine sintered glass filters containing about a 0.5-inch layer of fresh and dry activated carbon powder. The solution and carbon were then thoroughly mixed by shaking, and the mixture filtered under nitrogen pressure directly into the scattering cell kept in an isolated dust-proof atmosphere. The solutions thus obtained were tested then for dissymmetry, and only those which showed none were employed for the light scattering measurements.

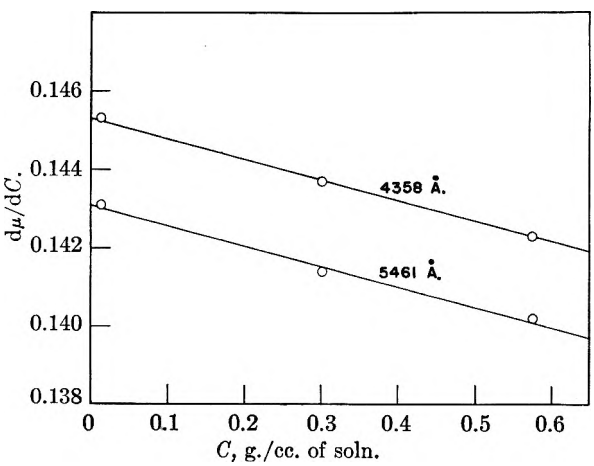

Fig. 1.—Dependence of $d\mu/dC$ of sucrose solutions on concentration at 25°.

Since the above purification procedure may modify the concentrations of the solutions, the latter were checked in all cases by determination of the density of the filtrates. A density–concentration curve prepared from the same sucrose allowed then the establishment of the concentration.

The turbidities of the sucrose solutions were determined by 90° scattering measurements in the manner described before,[4] and are based on calibration of the light scattering photometer with Ludox dispersions.[4] From the observed 90° intensity $i_{90°}$, the intensity of scattering solute, $I_{90°}$ was obtained by the relation

$$I_{90°} = i_{90°}(C_n C_v) - i_{90°\,(solvent)} \qquad (4)$$

where C_n is the correction for refractive index variation, C_v is the correction for the volume observed by the phototube,[6] and $i_{90°\,(solvent)}$ is the intensity observed when the cell was filled with purified water. There is no $C_n C_v$ correction required for the latter quantity because in our case this correction is referred to water as a reference.[6]

The variation of refractive index with concentration, $d\mu/dc$, was determined at 4358 and 5461 Å. with a Phoenix differential refractometer. The refractive index of water at 4358 Å. was taken from the literature, while μ_0 at 5461 Å. was determined by use of a Bausch and Lomb precision refractometer.

The depolarization ratios for the various sucrose solutions were measured in the light scattering photometer as follows. The photomultiplier tube, with a polaroid analyzer mounted in front of it, was set at 0° angle and exposed to the incident light beam attenuated through a suitable set of neutral filters. The dynode voltage was then regulated to give a selected constant reading (corrected for dark current). Next the scattering cell was shifted into the beam, the photomultiplier tube moved to the 90° position, and a reading of intensity taken. The same operation with the same filters and constant setting was repeated to obtain readings for the other plane of polarization. By employing this procedure for every scattering measurement, any errors which may arise from possible shifts in light intensity, fluctuations in photomultiplier sensitivity, and differences in sensitivity of the latter toward different planes of polarization, were minimized. Finally, in order to obtain intensity contribution due only to solute, the solvent readings obtained in identical manner were subtracted from all solution readings.

All the optical measurements described in this paper were performed within about a degree of 25° and hence they can be considered to be applicable to this temperature.

Results and Discussion

In Table I, Column 8, are given the turbidities found in the present study for the series of sucrose solutions at 4358 and 5461 Å. Figure 1, in turn, shows $d\mu/dc$ as a function of concentration. Since these plots are linear within experimental error over the concentration range of interest, we may write

$$\frac{d\mu}{dC} = a - bC \qquad (5)$$

and hence on integration

$$\mu = \mu_0 + aC - \frac{b}{2}C^2 \qquad (6)$$

For the sucrose solutions at 4358 Å. $a = 0.1453$ and $b = 0.0053$, while at 5461 Å. $a = 0.1431$ and $b = 0.0050$. These equations were used to calculate the μ and $d\mu/dc$ values shown in columns 3 and 4 of Table I. A check of μ as given by equation 6 with directly determined refractive index showed the equation to be more than adequate for the purpose at hand.

The $\partial P/\partial C$ values for the various sucrose solutions, shown in column 5 of Table I, were obtained by graphical differentiation of large scale plots of $(P - P_i)$ *vs.* C, where P is the experimentally observed osmotic pressure in atmospheres and $P_i = (CRT/M)$ is the osmotic pressure according to Van't Hoff's law of ideal solutions. From such slopes $\partial P/\partial C$ follows at 25° as

$$\frac{\partial P}{\partial C} = \frac{RT}{M} + \frac{\partial(P - P_i)}{\partial C} = 71.50 + \frac{\partial(P - P_i)}{\partial C} \qquad (7)$$

The differentiation was performed with the aid of a precision tangentimeter made in this Laboratory. Up to 1 molal solutions the osmotic pressure data of Morse[7] at 25° were used after conversion to g. of sucrose per cc. of solution with aid of the densi-

(6) S. H. Maron and R. L. H. Lou, *J. Polymer Sci.*, **14**, 273 (1954).

(7) Morse, Publ. Carnegie Inst. Washington No. 198, 1914, p. 184.

TABLE I

SUMMARY OF LIGHT SCATTERING DATA FOR SUCROSE SOLUTIONS AT 25°

Concn. C, g./cc.	λ, Å.	μ	$\frac{d\mu}{dC}$	$\frac{\partial P}{\partial C}$, atm. cc./g.	$\frac{6+6\rho_u}{6-7\rho_u}$	$\tau \times 10^4$ (cm.$^{-1}$) Eq. 3	Obsd.	$H\frac{C}{\tau}$ $\times 10^3$
0.0000	4358	1.3397	...	...	1.07	...	...	2.81
	5461	1.3339	...	...	1.07	...	...	2.72
.0352	4358	1.3448	0.1451	77.9	1.08	0.689	0.680	2.99
	5461	1.3389	.1429	77.9	1.08	0.269	0.279	2.84
.0614	4358	1.3486	.1450	80.9	1.09	1.17	1.16	3.05
	5461	1.3427	.1427	80.9	1.09	0.457	0.474	2.91
.106	4358	1.3551	.1447	87.5	1.09	1.86	1.86	3.29
	5461	1.3491	.1425	87.5	1.09	0.726	0.775	3.08
.163	4358	1.3633	.1445	98.0	1.11	2.63	2.67	3.54
	5461	1.3571	.1422	98.0	1.11	1.03	1.11	3.32
.251	4358	1.3760	.1440	118.4	1.12	3.38	3.47	4.20
	5461	1.3696	.1418	118.4	1.12	1.32	1.41	4.03
.314	4358	1.3850	.1437	132.8	1.14	3.86	3.80	4.83
	5461	1.3786	.1414	132.8	1.14	1.50	1.53	4.67
.353	4358	1.3907	.1435	143.7	1.14	4.01	3.97	5.20
	5461	1.3841	.1413	143.7	1.14	1.57	1.58	5.11
.434	4358	1.4023	.1430	172.2	1.17	4.22	4.05	6.26
	5461	1.3955	.1409	172.2	1.17	1.65	1.65	6.00
.587	4358	1.4241	.1423	304.6	1.33	3.69	3.66	9.44
	5461	1.4170	.1401	304.6	1.33	1.44	1.52	8.84

ties of water and sucrose, and the volume contraction data given by Morse. For higher concentrations the data employed were those of Frazer and Myrick[8] and of Lotz and Frazer.[9]

Figure 2 shows the results obtained for the depolarization ratio, ρ_u, and the depolarization correction factor, $(6 + 6\rho_u)/(6 - 7\rho_u)$, as a function of the concentration of the sucrose solutions. ρ_u has been found to be identical at the two wave lengths employed, and hence the depolarization correction factor is also the same as for both wave lengths. From Fig. 2 it may be seen that this correction is concentration dependent and varies from 1.07 at zero concentration to 1.37 at a concentration of 0.6 g. of sucrose per cc. Consequently, omission of this correction by both Debye and Halwer introduces errors into the theoretical calculation of τ which amount, depending on the concentration, to from 7–37%. The depolarization correction factors corresponding to the concentrations shown in Table I were read from Fig. 2, and are given in column 6 of the table.

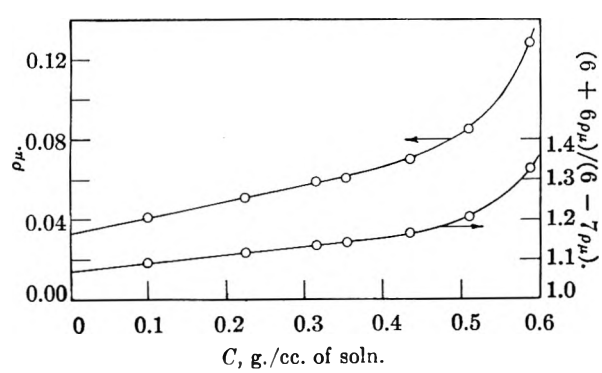

Fig. 2.—Depolarization of scattered light by sucrose solutions at 25°.

(8) J. C. W. Frazer and R. T. Myrick, *J. Am. Chem. Soc.*, **38**, 1907 (1916).

(9) P. Lotz and J. C. W. Frazer, *ibid.*, **43**, 2501 (1921).

Employing the data shown in Table I, τ values corresponding to the various concentrations have been calculated from the osmotic pressure coefficients by means of equation 3, and these are given in column 7 of the table. The calculated τ's are to be compared with the experimentally observed values, and such a comparison is shown in Fig. 3. In this figure the solid lines correspond to the τ's given by equation 3, while the points are τ's measured experimentally. It may be seen that the agreement between the two sets of τ's is very good.

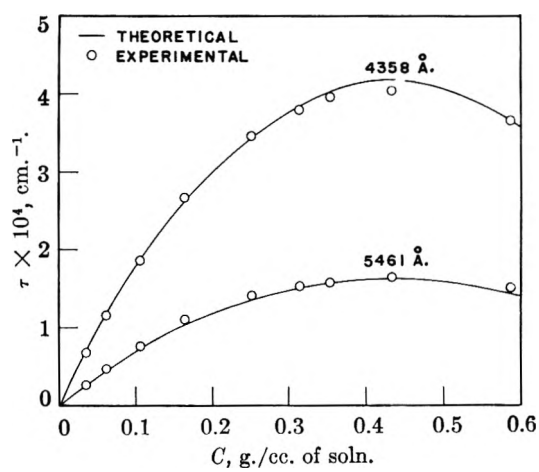

Fig. 3.—Comparison of theoretical and experimental turbidities of sucrose solutions at 25°.

Another way of testing the agreement between osmotic and light scattering theories is by intercomparison of the quantity $(1/RT)(\partial P/\partial C)$, which is based entirely on osmotic measurements, with $(HC/\tau)[(6 + 6\rho_u)/(6 - 7\rho_u)]$, which is a quantity exclusively dependent on optical measurements. According to equation 3 the two quantities should have identical values for a given concentration. In Fig. 4 the solid line gives the plot of $(1/RT)(\partial P/\partial C)$ as a function of concentration, while the

points are the experimentally observed values of (HC/τ) $[(6 + 6\rho_u)/(6 - 7\rho_u)]$ at the two wave lengths. Again the agreement between the two sets of measurements is satisfactory.

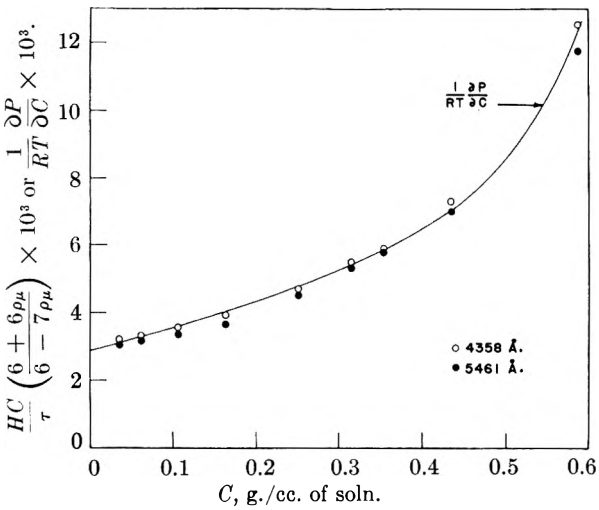

Fig. 4.—Comparison of $(1/RT)(\partial P/\partial C)$ with $(HC/\tau)[(6 + 6\rho_\mu)/(6 - 7\rho_\mu)$ for sucrose solutions at 25°.

Finally, Fig. 5 shows the conventional plot of the experimental HC/τ values, given in the last column of Table I, *vs.* C. From this plot the limiting values of HC/τ are found to be 2.81×10^{-3} at 4358 Å. and 2.72×10^{-3} at 5461 Å. and, hence, the molecular weight of sucrose, M, follows as

$$M = \frac{1}{\left(\frac{HC}{\tau}\right)_0\left(\frac{6 + 6\rho_u}{6 - 7\rho_u}\right)_0} = \frac{1}{1.07\left(\frac{HC}{\tau}\right)_0} \quad (8)$$

Equation 8 yields for M 332 and 344 g. per mole at 4358 and 5461 Å., respectively, or an average of 338 ± 6. This figure is in very good agreement with the theoretical molecular weight of sucrose, namely, 342.3.

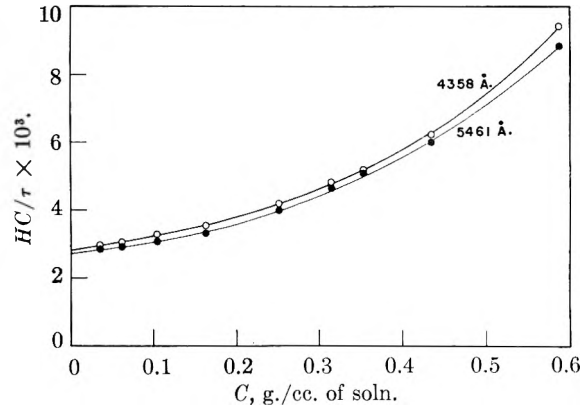

Fig. 5.—HC/τ *vs.* C plot for aqueous sucrose solutions at 25°.

The results presented in this paper confirm the relation between turbidity and osmotic pressure as epitomized by equation 3, and, further, yield the correct value for the molecular weight of sucrose. However, the τ values obtained for the various concentrations of sucrose are in all cases higher than those given by Debye or Halwer, in some instances by as much as 27%. As has been indicated, the low results of Debye and Halwer were due to use of the incorrect value for the turbidity of their standards. Again, the turbidities obtained by these men from the osmotic pressures of sucrose solutions were also low due to neglect of the depolarization correction. The compensation of the two errors gave them an apparent agreement between osmotic pressure and light scattering which was fortuitous, and which resulted in assignment of incorrect turbidities to the sucrose solutions.

Acknowledgment.—The work discussed herein was performed as a part of the research project sponsored by the Reconstruction Finance Corporation, Office of Synthetic Rubber, in connection with the Government Synthetic Rubber Program.

STUDIES ON COÖRDINATION COMPOUNDS. XIV. THE DETERMINATION OF ENTHALPY AND ENTROPY VALUES FOR SEVERAL BIVALENT METAL IONS AND CERIUM(III) WITH THE ACETYLACETONATE ION[1]

BY REED M. IZATT,[2] W. CONARD FERNELIUS AND B. P. BLOCK

Contribution from The College of Chemistry and Physics, The Pennsylvania State University, State College, Pa.

Received September 10, 1954

Thermodynamic stepwise equilibrium formation constants are given for the reaction in aqueous solution of the acetylacetonate ion with Cu^{2+}, Be^{2+}, UO_2^{2+}, Ni^{2+}, Co^{2+}, Zn^{2+}, Mn^{2+}, Cd^{2+}, Mg^{2+} and Ce^{3+} at 10, 20 and 40°. Constants at 30° have been given in previous publications.[4,5] Values of the thermodynamic quantities, ΔH, ΔS and ΔF are given over the temperature range 10 to 40° for the formation of the first complex, $MCh^{(n-1)+}$, in each case (except UO_2^{2+}), of $MCh_2^{(n-2)+}$ in each case (except Zn^{2+} and Cd^{2+}), and of MCh_3^- in the case of Ni^{2+}. Values for these thermodynamic quantities are also given for the dissociation of acetylacetone over the above temperature range. The significance of the values obtained is discussed in the light of the reactions involved. Comparisons are made with other thermodynamic values in the literature involving several of these same ions with other ligand types.

Introduction

This study was undertaken (1) to learn the approximate temperature coefficients of the formation constants for the acetylacetonates of a variety of metal ions and (2) to compare the thermodynamic quantities obtained with those for various other ligands with the same metal ions. The thermodynamic data available on the chelation of metal ions are not sufficient to enable one to draw any extensive conclusions concerning the energy changes which occur. In order that the resulting thermodynamic quantities may be reliable, measurements should be made at more than two temperatures and all molarity quotients should be converted to the thermodynamic constants before calculating ΔF, ΔH and ΔS values. This has not always been done in the past.

Experimental

Stock solutions of the perchlorates of Cu^{2+}, UO_2^{2+}, Ni^{2+}, Co^{2+}, Zn^{2+}, Mn^{2+}, Cd^{2+}, Mg^{2+} and Ce^{3+} and the nitrate of Be^{2+} were prepared and standardized by conventional methods. All perchlorate solutions (except UO_2^{2+}) were prepared by dissolving the metal salt (G. F. Smith Chemical Co.) in water. The $UO_2(ClO_4)_2$ solution was prepared by dissolving UO_3 (Fisher Scientific Co.). in a known amount of $HClO_4$ and diluting to volume with water. The $Be(NO_3)_2$ solution was prepared by dissolving the salt (Brush Beryllium Co.) in water and determining the Be^{2+} in a portion of the solution as the sulfate.[3] Portions of these solutions, except in the case of Cu^{2+}, were mixed with acetylacetone, HCh (Eastman Kodak Co.), and diluted to a known volume. In the case of Cu^{2+} a portion of the $Cu(ClO_4)_2$ was diluted to volume without adding HCh since the blue copper(II) chelate precipitated when the two were mixed under these conditions. Identical portions of each of these solutions were taken and diluted to 100 ml. with water. Following this dilution, a known volume of a standard aqueous HCh solution was added to the Cu^{2+} solution. In each case, the final solution was about 5×10^{-3} M in M^{n+} and 20×10^{-3} M in HCh. These solutions were placed in the water-bath and allowed to come to thermal equilibrium for at least 30 minutes. Potentiometric titrations were carried out using a Beckman Model G pH meter equipped with glass (Beckman Type E. No. 1190–80) and saturated calomel (Beckman 1170) electrodes. The electrodes were periodically checked against standard Beckman buffers (at 10° pH 4.00 and 7.06, at 20° pH 4.00 and 7.02, at 40° pH 4.03 and 6.97). Measurements were made at 10, 20 and 40° with the bath temperature automatically controlled to ±0.1°. While the solutions were stirred continuously, increments of standard NaOH (0.200 N) were added, and the pH was measured after each addition. One set of measurements was made at each temperature in all cases except Cu^{2+}, where four sets were made at each temperature to establish the precision of the results.

The pK_D of the HCh was determined at each temperature. One determination was made at each temperature, and the pK_D values were calculated from five separate points on each titration curve. The pK_D values calculated from these points agreed to ±0.01. The reproducibility of these pK_D values from different determinations, however, would likely not be better than about ±0.02 to 0.03. If it were desired to conduct more detailed studies of these or other metal ion–HCh systems, it would be desirable to obtain more exact pK_D values.

The thermodynamic formation constants involving the reaction of these metal ions with the acetylacetonate ion, Ch^-, at 30° have been given in previous publications.[4,5]

Calculations.—The method used to calculate the thermodynamic formation constants has been given in a previous paper.[4] The free energy, enthalpy and entropy changes involved were calculated by the customary methods. The log K_{f_n} values are tabulated in Table I together with the calculated thermodynamic quantities, ΔH_n, ΔF_n, and ΔS_n. The ± values given for Cu^{++} are the maximum deviation from the average of the four Cu^{++} determinations at each temperature. The plots of log K_{f_n} *vs.* $1/T$ from which ΔH_n was determined are given in Figs. 1 and 2. Thermodynamic quantities were not calculated in cases where good linear relationships were not evident (see the — marks in Table I).

Discussion

The greatest single source of error in these experiments lies in the reading obtained from the pH meter. Under optimum conditions each reading should be accurate to pH ± 0.02. In a previous paper[3] the precision, measured as the 95% confidence interval, for a large number of log K_{f_n} values involving Ni^{2+} and Zn^{2+} with Ch^- at 30° was shown to be about ±0.10 in the log. Since only one determination has been made at each temperature in the present paper, care must be taken in drawing any definite conclusions concerning the data. The

(1) From a portion of a thesis presented by Reed M. Izatt in partial fulfillment of the requirements for the degree of Doctor of Philosophy, August, 1954.

(2) Mellon Institute of Industrial Research, Pittsburgh 13, Pa.

(3) V. Cupr, *Z. anal. Chem.*, **76**, 173 (1929).

(4) R. M. Izatt, C. G. Haas, Jr., B. P. Block and W. C. Fernelius, THIS JOURNAL, **58**, 1133 (1954).

(5) R. M. Izatt, W. C. Fernelius and B. P. Block, *ibid.*, **59**, 80 (1955).

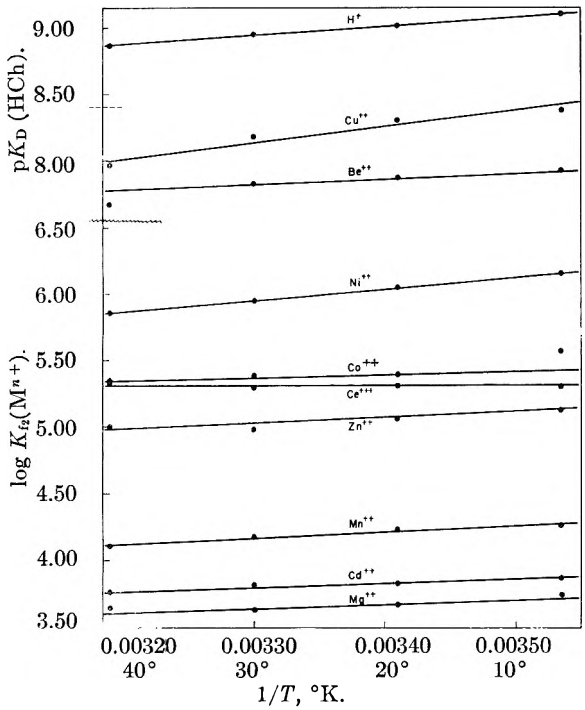

Fig. 1.—Plot of log K_{f1} *vs.* $1/T$ (°K.) for several M^{n+}–HCh systems from 10 to 40°. Also included is a plot of pK_D (for HCh) *vs.* $1/T$ (°K.) from 10 to 40°.

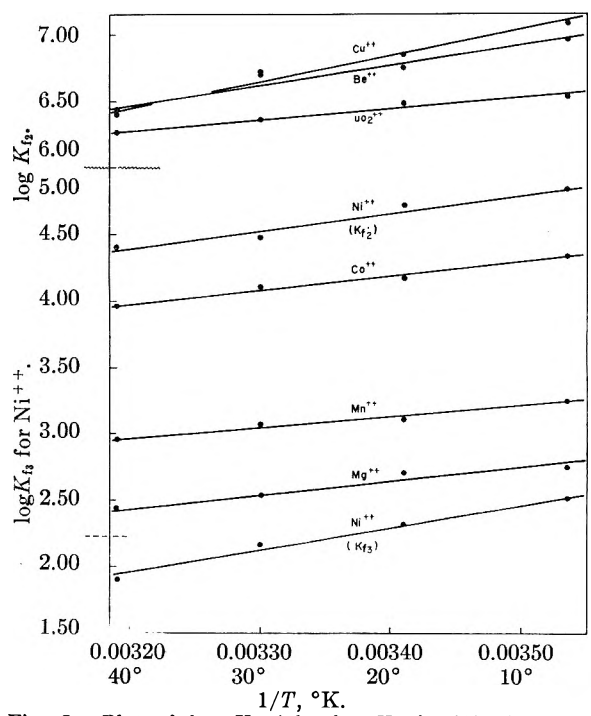

Fig. 2.—Plot of log K_{f2} (also log K_{f3} for Ni^{++}) *vs.* $1/T$ (°K.) for several M^{n+}–HCh systems from 10 to 40°.

purpose of the investigation was to learn whether there was a measurable temperature dependence of log K_m, and it was found that, in most cases, such a dependence does exist.

The value of pK_D at 30° given in Table I for HCh agrees well with that given by Van Uitert (8.95)[6]

(6) L. G. Van Uitert and C. G. Haas, Jr., *J. Am. Chem. Soc.*, **75**, 455 (1953). The value 8.35 given in this reference is an error. See the pK_D *vs.* mole fraction dioxane plot, same reference and L. G. Van Uitert, Ph.D. Thesis, The Pennsylvania State University, 1952.

TABLE I: VALUES FOR THE THERMODYNAMIC QUANTITIES, LOG K_{fn}, $-\Delta F_n$, $-\Delta H_n$ AND ΔS_n, INVOLVED IN THE REACTION AT 10, 20, 30° (FOR LOG K_{fn} VALUES SEE REFERENCES 4 AND 5), AND 40° OF SEVERAL BIVALENT METAL IONS AND Ce^{3+} WITH THE ACETYLACETONATE ION

t, °C.	HCh	Cu^{2+}	Be^{2+}	UO_2^{2+}	Ni^{2+}	Co^{2+}	Zn^{2+}	Mn^{2+}	Cd^{2+}	Mg^{2+}	Ce^{3+}	Cu^{2+}	Be^{2+}	UO_2^{2+}	Ni^{2+}	Co^{2+}	Zn^{2+}	Mn^{2+}	Cd^{2+}	Mg^{2+}	Ce^{3+}	Ni^{2+}	Ce^{3+}
		log K_{f1}										log K_{f2}										log K_{f3}	
10	9.10	8.38 ± 0.02										7.06 ± 0.03	6.96	6.53	4.84	4.34	4.02	3.25	2.90	2.75	4.08	2.51	3.35
20	9.02	8.31 ± 0.02	7.88	7.66	6.06	5.40	5.07	4.24	3.84	3.67	5.30	6.85 ± 0.05	6.75	6.49	4.71	4.17	3.95	3.11	2.88	2.71	3.97	2.32	3.38
40	8.86	7.96 ± 0.02	7.67	7.42	5.86	5.34	5.00	4.11	3.77	3.65	5.35	6.4	6.44	6.26	4.40	3.96	3.88	2.96	2.47	2.44	3.93	1.90	ppt.
		$-\Delta F_1$ (kcal./mole)										$-\Delta F_2$ (kcal./mole)										$-\Delta F_3$ (kcal./mole)	
10	11.8	10.8	10.2	—	8.0	—	6.7	5.5	5.0	4.9	6.9	9.1	9.0	8.5	6.3	5.6	—	4.2	—	3.6	5.3		3.3
20	12.1	11.2	10.5	—	8.1	7.2	6.8	5.7	5.1	4.9	7.1	9.2	9.1	8.7	6.3	5.6	—	4.2	—	3.6	5.3		3.1
30	12.4	11.4	10.8	—	8.2	7.5	6.9	5.8	5.3	5.0	7.3	9.3	9.3	8.8	6.2	5.7	—	4.2	—	3.5	5.5		3.0
40	12.7	11.4	—	—	8.4	7.6	7.2	5.9	5.4	5.2	7.7	9	—	9.0	6.3	5.7	—	4.2	—	3.5	5.6		2.7
		$-\Delta H_1$ (kcal./mole)										$-\Delta H_2$ (kcal./mole)										$-\Delta H_3$ (kcal./mole)	
10 to 40	2.8	4.7	2.0	—	6.7	1.2	1.9	2.5	1.4	1.8	0	6.6	6.9	4.0	6.3	5.0	—	4.7	—	4.3	ca. 0–2		6.7
		ΔS (e.u.)										ΔS (e.u.)										ΔS (e.u.)	
10	32	22	29	—	12	—	17	11	13	11	24	9	7.5	16	−0.2	2.4		−1.8	—	2.5	19		−12
20	32	22	29	—	12	21	17	11	13	11	24	9	7.4	16	0	2.2		−1.9	—	2.2	18		−12
30	32	22	29	—	12	21	17	11	13	11	24	9	8.0	16	−0.4	2.4		−1.5	—	2.5	18		−12
40	32	21	—	—	13	21	17	11	13	11	24	8	—	16	−0.1	2.3		−1.5	—	2.5	18		−13

but differs considerably from the value at 30° reported by Schwarzenbach (8.88).[7] The values of pK_D at the other temperatures agree very closely with those found by Cartledge[8]: 9.14 (10°), 9.04 (20°), 8.89 (40°). The results for the metal ion–acetylacetonate ion association in general resemble those obtained by Carini and Martell[9] for the alkaline earth ions with the ethylenediaminetetraacetate ion.

Several determinations of thermodynamic data have recently been made in this Laboratory involving Cu^{2+}, Ni^{2+}, Zn^{2+} [10] and Cd^{2+} [11] with polyamines and Cu^{2+} and Ni^{2+} with amines containing oxygen and sulfur.[12]

Several comparisons between Ch^- and the amines may be noted. (1) Less negative enthalpy changes are observed in the case of Ch^- with Ni^{2+}, Cu^{2+}, Zn^{2+} and Cd^{2+}. (2) ΔS values appear, in general, to be less for the reaction of these metal ions with amines and substituted amines than with Ch^-. A large negative value of ΔS is found for the formation of the tris-(2,4-acetylacetonate)-nickelate(II) ion. McIntyre[10] also found a large negative value for ΔS in the formation of the corresponding tris-(ethylenediamine)-nickel(II) and tris-(N-methylethylenediamine)-nickel(II) ions (−10 and −13 e.u., respectively). (3) Of ten ligands studied with Cu^{2+} those containing two nitrogen atoms had the largest ΔH values (about −11 to −15 kcal./mole), those with combinations of sulfur, oxygen and nitrogen had distinctly lower ΔH values (−6.1, −5.0 and −7.4 kcal./mole), and those with Ch^- had the lowest ΔH values (−4.7 kcal./mole).

Two general conclusions appear justified on the basis of the data described above and that recently reported in the literature.[13,14] (1) The entropy changes vary regularly in the case of Ch^- as the charge types in the solution change, whereas in the case of the amines small entropy changes are observed since the charge type remains constant throughout the titration. (2) The enthalpy change in the case of each metal ion studied is considerably greater in the case of the amines than in the case of the Ch^-. This would be predicted on the basis of the relative electronegativities of the bonding oxygen and nitrogen atoms.[15] The ligands containing the less electronegative nitrogen atoms would be expected to share electrons more readily and, thus, contribute to the formation of a more covalent bond than would be the case with Ch^-. The energy changes resulting from the formation of this bond would appear in the enthalpy term.[13,14]

Several interesting facts are observed in the case of Ce^{3+}. (1) The enthalpy change in forming the first complex is approximately zero. (2) The solubility of the complex formed with Ce^{3+} increases rather markedly as the temperature decreases. For this reason values are not given for log K_{f_3} at 30 and 40° and for log K_{f_2} at 40°. Under identical experimental conditions, except for the changing temperature, precipitation was noted at pH 9.8 (10°) and pH 7.1 (40°) for $Ce^{3+} = 4.0 \times 10^{-3}$ M and $HCh = 1.95 \times 10^{-2}$ M. It has also been observed that the solubility of the rare earth sulfates decreases with increasing temperature.[16]

Acknowledgment.—The authors gratefully acknowledge financial support furnished for this work by the United States Atomic Energy Commission through Contract AT(30-1)-907.

(7) G. Schwarzenbach, H. Suter and K. Lutz, *Helv. Chim. Acta*, **23**, 1191 (1940).

(8) G. H. Cartledge, *J. Am. Chem. Soc.*, **74**, 6015 (1952).

(9) F. F. Carini and A. E. Martell, *ibid.*, **76**, 2153 (1954).

(10) G. H. McIntyre, Ph.D. Thesis, The Pennsylvania State University, 1953.

(11) H. A. Droll, unpublished results.

(12) J. R. Lotz, Ph.D. Thesis, Pennsylvania State University, 1954.

(13) C. G. Spike and R. W. Parry, *J. Am. Chem. Soc.*, **75**, 2726 (1953).

(14) C. G. Spike and R. W. Parry, *ibid.*, **75**, 3770 (1953).

(15) T. Moeller, "Inorganic Chemistry," John Wiley and Sons, Inc., New York, N. Y., 1952.

(16) D. M. Yost, H. Russell, Jr., and C. S. Garner, "The Rare Earth Elements and Their Compounds," John Wiley and Sons Inc., New York, N. Y., 1947, p. 58.

IONIZATION IN SOLUTIONS OF NITROGEN DIOXIDE IN NITRIC ACID FROM OPTICAL-ABSORBANCE MEASUREMENTS

BY SCOTT LYNN, D. M. MASON AND W. H. CORCORAN

California Institute of Technology, Pasadena, California

Received September 13, 1954

Values of the optical absorbance of solutions of nitrogen dioxide in nitric acid were measured at 0° and 1 atmosphere using light at a wave length of 425 mμ. The data obtained were applied in a study of the ionization occurring in the solutions. The numerical solution of simultaneous equations based on equilibrium expressions indicates that in nitric acid solutions containing less than 1 formal weight per cent. nitrogen dioxide the nitrogen dioxide is about 70% ionized into nitrosonium (NO^+) ions, whereas the nitric acid is about 5% ionized into nitronium (NO_2^+) ions. Although the uncertainty is high, the order of magnitude of these values is correct.

Introduction

Although Raman spectra[1,2] conductance[3,4] and cryoscopic[5] measurements have given evidence of the existence of nitrosonium (NO^+) and nitronium (NO_2^+) ions, it was believed desirable to obtain further information about the existence of these ionic species. Use of another physical property such as optical absorbance was thought to be a possible approach to the determination of the extent of their presence in solutions of nitrogen dioxide[6] and nitric acid. The optical absorbance, $-\log I/I_0$, at 425 mμ was selected as a means of analyzing the solutions since it was believed that at this wave length the nitrogen dioxide molecule could be assumed to be the only absorbing species. Two ternary systems, nitric acid–nitrogen dioxide–water and nitric acid–nitrogen dioxide–potassium nitrate, together with the binary system nitric acid–nitrogen dioxide, were used in the absorbance measurements.

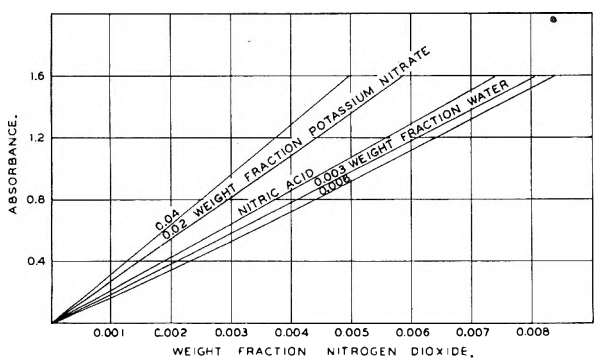

Fig. 1.

Equipment and Methods.—The equipment and the procedures used have been described in detail in a previous report.[7] The absorbance of light was measured with a Beckman model DU spectrophotometer modified to allow the cell[8] to be placed in an ice-bath.

Nitric acid was prepared by vacuum distillation at a temperature of approximately 100°F. from a mixture of pure potassium nitrate and concentrated sulfuric acid according to the procedure described by Giauque.[9] Titration of a diluted sample with sodium hydroxide indicated that the sample contained less than 0.001 weight fraction of material other than nitric acid.

Nitrogen dioxide was obtained from the Allied Chemical and Dye Corporation and was fractionated in a column provided with 16 glass plates. The central 70% portion of the overhead was collected and dried over phosphorus pentoxide. Samples similarly prepared from the same stock yielded less than 0.2 pound per square inch change in vapor pressure with a change in quality from 0.02 to 0.5 at a temperature of 160°F. The water used in the investigation was distilled and deaerated but not otherwise purified. The concentration range studied was from zero to 0.008 weight fraction nitrogen dioxide. Samples were prepared volumetrically by adding to pure nitric acid small increments of a 3 weight per cent. solution of nitrogen dioxide in nitric acid. A hypodermic syringe was used to make the additions. The weight of nitrogen dioxide added was known with a maximum uncertainty of 0.5%. The absorbance readings were reproducible within ±0.3%.

Results

Figure 1 and Table I show the effect of small amounts of water and potassium nitrate on the absorbance of solutions of nitrogen dioxide in nitric acid. These experimental data, together with other absorbance measurements, were previously reported.[7] Qualitatively the absorbance behavior is as would be expected by assuming that the absorbance is due solely to the nitrogen dioxide molecule. Furthermore, the following equilibria, which

TABLE I

WEIGHT FRACTION OF NITROGEN DIOXIDE IN NITRIC ACID SOLUTIONS FOR EVEN VALUES OF ABSORBANCE AT 425 mμ AND 0°

Absorbance $-\log I/I_0$	Nitrogen dioxide (wt. frac.) Potassium nitrate 0.02 wt. frac.	Potassium nitrate 0.04 wt. frac.	Pure nitric acid	Water 0.003 wt. frac.	Water 0.06 wt. frac.
0	0	0	0	0	0
0.200	0.00072	0.00058	0.00093	0.00102	0.00111
.400	.00144	.00120	.00185	.00204	.00220
.600	.00216	.00185	.00277	.00305	.00331
.800	.00292	.00244	.00369	.00406	.00436
1.000	.00365	.00310	.00462	.00507	.00540
1.200	.00440	.00373	.00554	.00604	.00642
1.400	.00511	.00433	.00647	.00705	.00741
1.600	.00583	.00495	.00743	.00804	.00842

(1) E. D. Hughes, C. K. Ingold and R. I. Reed, *J. Chem. Soc.*, 2400 (1950).

(2) J. D. S. Goulden and D. J. Millen, *ibid.*, 2620 (1950).

(3) G. D. Robertson, Jr., D. M. Mason and B. H. Sage, *Ind. Eng. Chem.*, **44**, 2928 (1952).

(4) E. G. Taylor, L. M. Lyne and A. G. Follows, *Can. J. Research*, **29**, 439 (1951).

(5) W. J. Dunning and C. W. Nutt, *Trans. Faraday Soc.*, **47**, 15 (1951).

(6) Unless otherwise specified, the term nitrogen dioxide refers to the formal concentration of this species. Weight fraction of other substances is also expressed on a formal basis.

(7) S. Lynn, D. M. Mason and B. H. Sage, "Optical Absorbance of the System Nitric Acid–Nitrogen Dioxide–Water at 32°F. and 1 Atmosphere," Progress Report No. 20-147, Pasadena, Jet Propulsion Laboratory, January 5, 1953.

(8) The light path in the cell was 1.000 cm.

(9) W. R. Forsythe and W. F. Giauque, *J. Am. Chem. Soc.*, **64**, 48 (1942).

were first proposed on the basis of Raman spectra,[1,2] appear to be in accord with the data

$$N_2O_4 \rightleftharpoons 2NO_2 \rightleftharpoons NO^+ + NO_3^- \quad (1)$$

$$2HNO_3 \rightleftharpoons NO_2^+ + NO_3^- + H_2O \quad (2)$$

Chédin and Fénéant[10] showed the following equilibrium to obtain

$$NO_3^- + 2HNO_3 \rightleftharpoons (HNO_3)_2\,NO_3^- \quad (3)$$

Calorimetric measurements[11] indicate another relation to be

$$HNO_3 + XH_2O \rightleftharpoons HNO_3(H_2O)_x \quad (4)$$

There is evidence that equilibrium in reactions 3 and 4 lies far to the right. Equations 1 and 3 may be combined to give

$$2NO_2 + 2HNO_3 \rightleftharpoons NO^+ + (HNO_3)_2NO_3^- \quad (5)$$

$$\downarrow\uparrow$$

$$N_2O_4$$

and a combination of reactions 2, 4 and 5 gives, where x is arbitrarily taken as unity

$$5HNO_3 \rightleftharpoons NO_2^+ + HNO_3{\cdot}H_2O + (HNO_3)_2NO_3^- \quad (6)$$

When the nitric acid contains less than 3% water, reaction 6 predominates over the ordinary ionization of nitric acid to hydronium ion H_3O^+ and nitrate ion. Qualitatively these facts seem to be supported by conductivity measurements,[3,4] freezing point measurements,[5] and absorbance measurements.[7] Considering reactions 3 and 5, it is seen that the addition of nitrate ions from potassium nitrate shifts the equilibrium shown in reaction 5 to the left, increasing the concentration of the species nitrogen dioxide and thus the absorbance for a given formal concentration of nitrogen dioxide. On the other hand, the addition of small amounts of water drives reaction 6 to the left, reducing the concentration of the $(HNO_3)_2NO_3^-$ ion and giving more nitric acid. By a reduction in the concentration of the $(HNO_3)_2NO_3^-$ ion, more of the species nitrogen dioxide ionizes according to reaction 5, thus reducing the absorbance for a given formal concentration of nitrogen dioxide.

In these considerations it was assumed that the nitrogen dioxide molecule was the only species absorbing light at the wave lengths of the measurements. It is known[12] that nitrogen tetroxide does not absorb at these wave lengths when in the gas phase and hence is not likely to absorb in the liquid phase. Nitrosonium, the only other ion not present in pure nitric acid, has an even number of electrons and forms a colorless crystalline perchlorate and bisulfate, the solutions of which in sulfuric acid are also colorless. Hence it would not be expected to absorb light in the visible range of solutions of nitric acid. Since $(HNO_3)_2NO_3^-$, $HNO_3{\cdot}xH_2O$, and the nitronium ion are present in pure nitric acid, which is colorless, these species may also be considered colorless.

(10) J. Chédin and S. Fénéant, *Compt. rend.*, **228**, 242 (1949).

(11) R. Leclerc and J. Chédin, *Mém. services chim. état (Paris)*, **32**, 87 (1945).

(12) T. C. Hall, Jr., and F. E. Blacet, *J. Chem. Phys.*, **20**, 1745 (1952).

Nomenclature

I, intensity of light transmitted by sample
I_0, intensity of light transmitted by reference blank of air
K, equilibrium constant
log, logarithm to the base 10
α, fractional ionization of nitrogen dioxide to give NO^+
β, fractional ionization of HNO_3 to give NO_2^+
γ, fractional ionization of HNO_3 to give H_3O^+
σ, standard deviation
$(\bar{\ })$, mean values

Subscripts

a, point on an absorbance curve of system containing nitric acid–nitrogen dioxide–potassium nitrate
b, point on an absorbance curve of system containing nitric acid–nitrogen dioxide
c, point on an absorbance curve of system containing nitric acid–nitrogen dioxide–water
5, Equation 5
6, Equation 6

Calculations using the absorbance data as a basis were made to establish the values of the fractional ionization of nitrogen dioxide according to equation 5 and the fraction of nitric acid giving the nitronium ion as shown in equation 6. In the calculations the following equilibrium expressions were used.

$$K_5 = \frac{(NO^+)((HNO_3)_2NO_3^-)}{(NO_2)^2(HNO_3)^2} \quad (7)$$

$$K_6 = \frac{(NO_2^+)(HNO_3{\cdot}H_2O)((HNO_3)_2{\cdot}NO_3^-)}{(HNO_3)^5} \quad (8)$$

In the use of equations 7 and 8 it was assumed that the activity coefficient for each species was independent of concentration.

Use was made of data shown in Fig. 1 to develop the necessary equations for obtaining the equilibrium constants and thereby to calculate the degree of ionization of the nitrogen dioxide and nitric acid into the species noted. Concentrations were converted from a weight-fraction basis to a volume-formality basis for use in the mass action expressions 7 and 8. These formal concentrations were obtained by assuming zero partial specific volumes of potassium nitrate, nitrogen dioxide and water in nitric acid. A value of 1.5430 g./cc. was used for the specific weight of pure nitric acid at 0°.

For one set of calculations at a given absorbance, data were taken from three curves in Fig. 1. The curve for pure nitric acid was used in each instance, together with any other pair of curves. For any arbitrary value of the absorbance in the range of Fig. 1, assuming that the nitrogen dioxide molecule is the only color-absorbing species, the following typical relationship may be written

$$(NO_2)_a = (NO_2)_b = (NO_2)_c \quad (9)$$

In this equation the subscripts designate the selected curves intersected by the line of constant absorbance. A combination of equation 9 with equations 7 and 8 gives six simultaneous equations with six unknowns which are the values of the ionization in various solutions of nitrogen dioxide and nitric acid according to equations 5 and 6, respectively. In this treatment the quantity γ, the ionization of nitric acid to give the H_3O^+ ion, was neglected as it was considered small in the calculations compared with α and β when less than 3% water was present.[3-5] The association of the species nitrogen dioxide to nitrogen tetroxide was not neglected, but it was not found mathematically

possible to consider this association independently in calculating values of α and β so that α is truly the dissociation of the combined species NO_2 and N_2O_4. Also β is the dissociation of HNO_3 and any associated[13] forms. The equilibria expressed in equations 3 and 4 were assumed to lie quantitatively to the right.

The six simultaneous equations were solved by trial and error for α_b and β_b, which are the ionizations of nitrogen dioxide and of nitric acid, respectively, in this binary system. Values were obtained at absorbances of 0.600, 0.900 and 1.200. All combinations of the curves shown in Fig. 1 fitting the described procedure were used in the calculations so that six values of α_b and β_b were obtained at each absorbance. It was found that the results were very sensitive to the relationships between absorbances and concentrations. A summary of the calculations is given in Table II.

TABLE II

DEGREE OF IONIZATION OF NITROGEN DIOXIDE AND NITRIC ACID IN SOLUTIONS OF NITRIC ACID AT 0°

Absorbance	$\bar{\alpha}_b$[a]	σ	$\bar{\beta}_b$[a]	σ
0.600	0.68	0.32	0.043	0.024
0.900	.69	.25	.045	.018
1.200	.71	.27	.048	.021

[a] Average of six values. In each group of six, one value for α_b was greater than 1.0. Since 1.0 represents complete ionization, it was taken as the maximum allowable value; and where necessary β_b was accordingly corrected.

To determine the validity of assuming γ small with respect to α and β, additional equations were developed by using four curves in Fig. 1 for each mathematical analysis. Values of α and β obtained as a first approximation in the simplified case were used in solving for γ. It was found that γ was practically zero. Thus the original assumption in regard to γ appeared valid.

Values for the degree of ionization of anhydrous nitric acid to give the nitronium ion according to equation 6 have been reported in the literature. Using cryoscopic techniques, Gillespie, *et al.*,[14] obtained a value of 0.034 at −40°, and Dunning and Nutt[5] a value of 0.08. Ingold and Millen[15] made Raman spectra measurements and found the degree of ionization to be 0.03 at −15°. These values of ionization for anhydrous nitric acid compare favorably with values of β_b shown in Table II and obtained from absorbance measurements in nitric acid containing 0.008 weight fraction of nitrogen dioxide.

Goulden and Millen[2] showed that the ionization of nitrogen dioxide when present up to 0.087 weight fraction in nitric acid solutions has a value of about 1.0 at 20°. This value compares favorably with values of α_b obtained from absorbance measurements and shown in Table II.

Analysis of Results

It is apparent from the calculations that have been made, based only on absorption data, that not all of the salient features have been taken into account. The uncertainty of the identity of all the absorbing species contributes to the possibilities of error in calculating quantities such as α_b and β_b. In addition, there would be a contribution to the error from the fact that the activity coefficient for each species in the solutions was assumed not to change with composition. Presence of species other than those stated which would affect the equilibria is another possible source of uncertainty.

Optical absorption data are difficult to interpret in describing thermodynamic equilibria since there are uncertainties as to the nature and effect of the absorbing species. It is believed, however, that by making reasonable assumptions the information on optical absorbance can at least be used to show the order of magnitude of the ionizations. It appears that the work qualitatively supports the existence of equilibria as shown in equations 5 and 6. For further investigation it would be desirable to supplement the absorption data with more direct information such as would be available in magnetic-susceptibility measurements on solutions of nitrogen dioxide in nitric acid. The fact that in this system nitrogen dioxide is the only molecule having paramagnetic properties would allow direct measurements of its presence.[16,17]

Acknowledgment.—The work described here is part of a program sponsored by the Jet Propulsion Laboratory at the California Institute of Technology under Contract No. DA-04-495 ORD-18 for the U. S. Army Ordnance Corps.

(13) R. Dalmon and R. Freymann, *Compt. rend.*, **211**, 472 (1940).

(14) R. T. Gillespie, E. D. Hughes and C. K. Ingold, *J. Chem. Soc.*, 2552 (1950).

(15) C. K. Ingold and D. J. Millen, *ibid.*, 2612 (1950).

(16) D. M. Yost and H. Russell, "Systematic Organic Chemistry," Prentice-Hall, Inc., New York, N. Y., 1946.

(17) T. Sone, *Tôhoku Imperial University Science Reports*, 5 (No. 11). 139 (1922).

GASIFICATION OF CARBON RODS WITH CARBON DIOXIDE[1,2]

BY P. L. WALKER, JR., AND F. RUSINKO, JR.

Department of Fuel Technology, Pennsylvania State University, State College, Pa.

Received September 13, 1954

The possible relation between the properties of six commercial carbons and their gasification rates with carbon dioxide at a series of temperatures between 900 and 1300° has been investigated. The following properties of the carbons have been determined: quantitative and qualitative ash analyses, hydrogen content, interlayer spacing, average crystallite size, true and apparent density, porosity, surface area and effective diffusion coefficients of hydrogen through the carbons. No general correlation between these properties and the carbon gasification rates was found.

Introduction

The heterogeneous gasification reactions of carbon are of considerable theoretical and industrial interest and have been the subject of extensive research in recent years. Although a number of comprehensive kinetic studies have been reported, where equations of the Langmuir type have been found to describe the rate data, little attention has been given toward explaining these rates in conjunction with properties of the given carbon. The authors feel that the final test toward the understanding of gas–solid reactions (be it carbon or not) is to amass sufficient data about a solid to be able to predict its relative reactivity.

A long-range program, on this basis, has been set up in this Laboratory with the present investigation serving as an exploratory look into the success of relating what are commonly considered important properties of a carbon to its gasification rate.

Experimental

Samples.—Six different commercial carbons were studied. The samples were in the form of carbon rods 2 in. long by $^1/_2$ in. in diameter, weighing approximately 10 g. All samples were extruded, using coal tar pitch as the binder. Four of the six samples used petroleum coke flour as the filler—lampblack and carbon "D" being the exception. Carbon "D" used a mixture of 13% graphitized carbon "A" and 87% carbon "C" as filler material. Graphitized carbons "A" and "B" were heated to approximately 2500 and 3000°, respectively. The lampblack and carbon samples were gas baked at approximately 1000°. A more detailed description of the manufacture of these carbon samples can be found elsewhere.[3]

Reaction Rate Apparatus.—The reactor was the same as that described in a recent gasification study.[4] Briefly, a porcelain "top plate" and "bottom cone" were cemented to the top and bottom, respectively, of the carbon rod to restrict reaction to its sides. The sample was suspended from a balance into a vertical porcelain reactor tube and the gasification rate determined by frequent weight readings. A platinum platinum–10% rhodium thermocouple, with hot junction located at a point level with the top of the sample, indicated reaction temperature, which could be maintained within 2° of the desired value. The carbon dioxide flow rate through the reactor was maintained constant within ±1%.

X-Ray Diffraction Apparatus.—A 1064° (2θ) General Electric X-ray diffraction unit, XRD-3, with copper radiation was used to determine interlayer spacings and average crystallite sizes of the carbons. Standard X-ray procedures and subsequent calculations, discussed in detail in recent papers,[5,6] have been used in the present investigation.

Gas Adsorption Apparatus.—A standard gas adsorption apparatus was employed and has been recently described.[4] Carbon dioxide (99.95% pure and bone dry) was used as the adsorbate with adsorption occurring in a bath consisting of a 50-50 mixture of carbon tetrachloride and chloroform in Dry Ice. Results[4] indicated that although the B.E.T. areas determined from carbon dioxide adsorption on carbon rods were up to 20% smaller than areas determined from nitrogen adsorption, the trends of the results were similar. In the present case, relative differences and changes in surface areas were of primary importance.

Diffusion Apparatus.—The gas-flow apparatus described by Weisz and Prater[7] was used to determine effective diffusion coefficients of hydrogen through the carbon rods. (The authors are indebted to Dr. P. B. Weisz of the Socony-Vacuum Laboratories who determined experimentally the diffusion data.) Briefly, the experimental setup consisted of heating a $^1/_8$-in. long by $^1/_8$-in. diameter carbon rod and forcing it into a piece of Tygon tubing, which fused around the sample's periphery. The Tygon tubing was mounted in the diffusion apparatus, and equal pressures of nitrogen and hydrogen applied at the adjacent ends of the rod in the form of a high-velocity gas stream. The diffusion rate of hydrogen through the carbon rod was determined by analyzing the percentage of hydrogen in the nitrogen stream, as a function of time, with a thermal conductivity cell. Effective diffusion coefficients for hydrogen were based on the geometrical dimensions of the carbon rod.

The $^1/_8$-in. long by $^1/_8$-in. diameter samples used were cut on a lathe from rods, similar to those used in the reaction rate studies. Effective diffusion coefficients were determined on six separate samples of each carbon with the average value being reported. Results on a given carbon were duplicated within ±5%.

Results

Carbon Gasification Rates.—Table I presents the gasification rates of the carbons investigated at a series of temperatures. The rate curves were similar to those previously discussed,[4] with the rate increasing sharply at the start of the run and then remaining constant over a considerable period

TABLE I

REACTION RATES OF CARBONS AT VARIOUS TEMPERATURES (G./HR.)

	Reaction temp., °C.				
	900	1000	1100	1200	1300
Graphitized carbon "A"	0.04	0.40	1.83	6.00	12.00
Graphitized carbon "B"	.24	1.15	3.40	7.10	12.30
Carbon "C"	.19	1.13	3.98	8.88	13.95
Carbon "D"	.23	0.98	4.04	8.55	13.20
Carbon "E"[a]	.20	0.44	1.71	5.50	12.72
Lampblack	.21	0.95	3.00	6.84	10.32

[a] Reaction rates taken after 1 g. weight loss.

(1) Based on an M.S. thesis submitted by F. Rusinko, Jr., to the Graduate School of The Pennsylvania State University.

(2) Presented before the Division of Gas and Fuel Chemistry at the 126th meeting of the American Chemical Society in New York, N. Y., September 12–17, 1954.

(3) H. W. Abbott, "Encyclopedia of Chemical Technology," Vol. 3, The Interscience Encyclopedia Inc., New York, N. Y., 1949, pp. 1–23.

(4) P. L. Walker, Jr., R. J. Foresti, Jr., and C. C. Wright, *Ind. Eng. Chem.*, **45**, 1703 (1953).

(5) P. L. Walker, Jr., H. A. McKinstry and J. V. Pustinger, *ibid.*, **46**, 1651 (1954).

(6) P. L. Walker, Jr., and F. Rusinko, Jr., submitted to *Fuel*.

(7) Paper #48 presented before the Division of Physical and Inorganic Chemistry at the 125th Meeting of the American Chemical Society in Kansas City, Mo., March 23–April 1, 1954.

of time. The rates reported are those over the constant rate portion of the curve with the exception of carbon "E." The rates could be duplicated within ±2.5%.

The gasification rate of carbon "E" failed to reach a constant value; instead it continued to increase with reaction time. This can probably be explained by the fact[4] that carbon "E" also failed to attain an essentially constant surface area upon reaction, although data on this point and the explanation as to why its area development should be different from the other carbons are not yet forthcoming.

At the lowest reaction temperature of 900°, where the chemical reactivity of the carbon should play its most important part in determining the gasification rate,[8] it is seen that rates of five of the carbons are very similar and considerably higher than that of graphitized carbon "A." It is noteworthy that the reaction rate of graphitized carbon "B" at 900° is slightly higher than the rates for the four ungraphitized carbons.

Over-all activation energies for the gasification of the carbons have been determined over the lower temperature range (900 to 1000°), using the Arrhenius equation.[4] They range from 43 kcal./mole for carbon "C" to 68 kcal./mole for graphitized carbon "A."

TABLE II

ANALYSES OF CARBON SAMPLES

	Analyses, %				
	C	H	Ash	H_2O	O + N
Graphitized carbon "A"	99.77	0.08	0.07	0.02	0.06
Graphitized carbon "B"	99.37	.06	.06	.01	0.50
Carbon "C"	97.37	.28	.24	.58	1.53
Carbon "D"	97.61	.13	.58	.05	1.63
Carbon "E"	98.32	.07	.32	.00	1.29
Lampblack	98.93	.09	.22	.05	0.71

Analyses of Carbons.—Table II shows the over-all analyses of the carbons with oxygen and nitrogen reported as the difference. Table III shows detailed spectrographic analyses of the carbons.

Interlayer Spacing and Average Crystallite Size of Carbons.—Table IV presents data for the interlayer spacing and average crystallite size of the carbons. Since carbon "D" was a mixture of graphitized carbon "A" and carbon "C," its X-ray diffraction peaks were all unsymmetrical in shape,[5] consisting of the superposition of the broader and weaker peak of carbon "C" onto the sharper peak of graphitized carbon "A." Its average interlayer spacing and crystallite size can be considered as being intermediate between graphitized carbon "A" and carbon "C."

In agreement with Biscoe and Warren,[9] among others, the carbon–carbon bond distance within the carbon plane was found to be constant for all carbons, having a value of 1.42 Å.

Using the Franklin correlation,[10] the carbon interlayer spacings have been related to the percentage of graphitic structure in the carbon, as seen in Table IV.

Densities and Porosities of Carbons before and after Gasification.—Table V presents data for the densities and porosities of carbons before and after the gasification. Samples gasified at 900 and 1100° reacted to one and two grams weight loss, respectively. These weight losses were selected since it placed the reaction in all cases, except carbon "E," on the constant rate portion of the reaction curve. Due to the different weight losses employed at the two gasification temperatures, unfortunately interpretation of the data for each carbon at the two temperatures is impossible. However, comparison and interpretation of the data at a particular gasification temperature for all carbons are fruitful. (Work is now in progress where carbon rods are gasified to different weight losses at a constant temperature and their change in properties investigated.)

The true densities have been calculated from the unit cell parameters of the different carbons, as determined by X-ray diffraction. Apparent densities were determined by mercury displacement at atmospheric pressure in a pycnometer. Pore volumes were calculated as the difference in the reciprocals of the apparent and true densities times the weight of carbon remaining in the rod.

TABLE III

SPECTROGRAPHIC ANALYSES OF CARBONS[c], IN %

Carbon	SiO_2	Fe_2O_3	Al_2O_3	MgO	CaO	MnO	CuO	V_2O_5	PbO
Graphitized carbon "A"	0.028	0.017[a]	0.009[a]	0.001	0.004	[b]	0.003	0.028	[b]
Graphitized carbon "B"	.023	.017[a]	.015[a]	.001	.005	[b]	.003	.029	[b]
Carbon "C"	.032	.054	.068	.008	.009	.005	.004	.038	0.04[a]
Carbon "D"	.088	.124	.068	.007	.006	.005	.004	.055	.04[a]
Carbon "E"	.051	.052	.053	.007	.009	.005	.005	.038	.04[a]
Lampblack	.044	.066	.039	.003	.006	.005	.004	.030	[b]

[a] Maximum values. [b] Not detected. [c] Ni, all samples 0.00X % except Carbon "D" which had 0.029%; Sn, present in trace amounts in graphitized carbon "B," not detected in others; Cd, may be present in trace amounts in Carbon "C," not detected in others; Cr, Na, Ti, present in all samples in trace amounts; Ag, As, B, Be, Bi, Co, Ga, Ge, Mo and Zn, sought but not detected.

TABLE IV

AVERAGE INTERLAYER SPACING AND CRYSTALLITE SIZE OF CARBONS

	d Spacing, Å.	$\bar{L}_c$, Å.	$\bar{L}_a$, Å.	Graphitic carbon content, %
Graphitized carbon "A"	3.360	900	1100	80
Graphitized carbon "B"	3.357	1200	∞	89
Carbon "C"	3.456	33	55	0
Carbon "D"	...	..	..	10
Carbon "E"	3.450	41	62	0
Lampblack	3.484	28	59	0

(8) A. Wheeler, "Advances in Catalysis," Vol. 3, Academic Press Inc., New York, N. Y., 1951, p. 286.

(9) J. Biscoe and B. E. Warren, *J. App. Phys.*, **13**, 364 (1942).

(10) Rosalind E. Franklin, *Acta Cryst.*, **4**, 253 (1951).

TABLE V

DENSITIES AND POROSITIES OF CARBONS BEFORE AND AFTER GASIFICATION

Reaction conditions	True density, g./cc.	Apparent density, g./cc.	Porosity, %	Total pore vol., cc.
Graphitized carbon "A"				
Unreacted	2.248	1.549	31.1	1.889
900°		1.390	38.2	2.364
1100°		1.189	47.1	2.897
Graphitized carbon "B"				
Unreacted	2.250	1.561	30.6	1.937
900°		1.418	37.0	2.243
1100°		1.280	43.1	2.498
Carbon "C"				
Unreacted	2.186	1.579	27.8	1.664
900°		1.438	34.2	2.070
1100°		1 390	36.4	1.854
Carbon "D"				
Unreacted	2.194	1.512	31.1	1.916
900°		1.440	34.4	1.957
1100°		1.312	40.2	2.150
Carbon "E"				
Unreacted	2.192	1 584	27.8	1.734
900°		1 447	34.0	2.162
1100°		1.362	37.9	2.257
Lampblack				
Unreacted	2.168	1.361	37.2	2.311
900°		1.224	43.6	2.761
1100°		1.074	50.5	2.983

Naturally there was a marked increase in porosity of the samples upon gasification, but differences and similarities in the degree of porosity development for the different samples should be noted. Porosity development of the two graphitized carbons was quite similar, as was the development for the comparable non-graphitized carbons "C" and "E." The unreacted lampblack rod is seen to have had a significantly higher porosity than the other unreacted samples and to have maintained its higher porosity upon gasification over the other gasified carbons.

Total Surface Areas of Carbons before and after Gasification and their Specific Gasification Rates.—Table VI presents data for the total surface area of the unreacted and reacted carbon rods. As much as a 10-fold difference is noted in the surface areas of the unreacted carbon rods. Furthermore, it is seen that there was a marked (but not a uniform) increase in surface area upon gasification. For some reason, the area of graphitized carbon "A" was increased much more markedly upon gasification than that of graphitized carbon "B." The same can be said for carbons "D" and "E," which had essentially the same original area. It is further seen that for five of the carbons the surface area developed after 2 grams weight loss at 1100° was greater than after 1 gram weight loss at 900°. Carbon "C," however, was a notable exception to this fact. Other interesting comparisons in Table VI are possible.

From a knowledge of the surface areas and the reaction rates of the carbons, as presented in Table I, the specific reaction rates can be calculated and are also shown in Table VI. In the case of carbon "E," which failed to attain a constant rate, the slopes of the tangents to the rate curves at the particular weight losses used were taken as the rates.

TABLE VI

TOTAL SURFACE AREAS OF CARBONS BEFORE AND AFTER GASIFICATION AND THEIR SPECIFIC REACTION RATES

Reaction conditions	Total surface area, m.²	Specific rate g./(hr.)(m.² of surface) × 10³	Reaction conditions	Total surface area, m.²	Specific rate g./(hr.)(m.² of surface) × 10³
Graphitized carbon "A"			Carbon "D"		
Unreacted	4.7	....	Unreacted	5.4	....
900°	24.7	1.6	900°	10.9	21.1
1100°	49.5	36.9	1100°	26.8	150
Graphitized carbon "B"			Carbon "E"		
Unreacted	3.7	....	Unreacted	5.0	....
900°	6.0	342	900°	5.3	37.7[a]
1100°	9.2	2833	1000°	14.1	180.6[a]
Carbon "C"			Lampblack		
Unreacted	36.5	....	Unreacted	27.3	....
900°	205.6	0.9	900°	63.8	32.9
1100°	116.0	34.3	1100°	111.8	26.8

[a] Reaction rates at 1 and 2 grams weight loss, respectively.

Effective Diffusion Coefficients of Hydrogen in Carbon Rods.—Table VII presents data for the effective diffusion coefficients of hydrogen in the carbon rods. These results are discussed in detail in an accompanying publication.[11]

TABLE VII

EFFECTIVE DIFFUSION COEFFICIENTS OF HYDROGEN IN CARBON RODS

	$D_{eff.}$, cm.²/sec. (H_2 at STP)
Graphitized carbon "A"	0.046
Graphitized carbon "B"	.032
Carbon "C"	.028
Carbon "D"	.035
Carbon "E"	.039
Lampblack	.049

Discussion

Perhaps the best way to analyze the results is to enumerate properties of carbon which are commonly thought to have an effect on its gasification rate and compare the present reaction rates of the carbons with their known properties.

Long and Sykes[12] postulate that the top and bottom edge atoms of a carbon crystallite are most reactive to gasification. From this, the conclusion is drawn that the smaller crystallites, with their higher concentration of edge atoms per unit weight, should be more reactive than the larger crystallites. It is seen from Table I, however, that even though the average crystallite size of graphitized carbon "B" was more than an order of magnitude larger than that of the non-graphitized carbons, its gasification rate at 900 and 1000° was larger than these carbons. On the other hand, graphitized carbon

(11) P. L. Walker, Jr., F. Rusinko, Jr., and E. Raats, THIS JOURNAL, **59**, 245 (1955).

(12) F. J. Long and K. W. Sykes, *Proc. Roy. Soc.* (*London*), **A193**, 377 (1948).

"A," which also had a much larger average crystallite size than the non-graphitic carbons, did have significantly smaller reaction rates at 900 and 1000°.

Franklin[13] raised the question as to whether non-graphitic carbons with their larger interlayer spacings would be substantially more available to attack by gases than graphitized carbons. Data in Table I indicate that this apparently was not a major factor in determining gasification rates. Graphitized carbon "B," with a smaller spacing than the non-graphitic carbons, had a higher gasification rate. Furthermore, lampblack which possessed a significantly higher spacing than either carbon "C" or "E" had a smaller gasification rate.

Long and Sykes[14] and Gulbransen and Andrew[15] have shown the marked effect which inorganic and metallic impurities have on the chemical reactivity of carbon toward gases. Comparison of Table II with reaction rate data shows, however, that the carbon with the highest ash content, carbon "D," was not the most reactive at either 900 or 1000°. Again graphitized carbon "B," with its very low ash content, gave anomalously high reaction rate results. As a matter of fact, no single constituent of the analyses listed in Table II can be correlated with the carbon reactivity.

It is generally conceded that the analysis of the ash, as well as its magnitude, is of importance in affecting chemical reactivity of carbons. However, the spectrographic analyses presented in Table III fail to indicate, among other things, why the gasification rate of graphitized carbon "B" was comparatively high. For all elements determined, their concentration level was less in this carbon than in any of the non-graphitized samples. Unfortunately the state (free metal, oxide, carbide, etc.) and location of the impurities in the carbon matrix cannot be determined and this could well be of importance in determining reaction rates.

Individual carbon particles are known to be composed of a large number of crystallites.[16] In line with previous reasoning, it would be expected that the larger the average crystallite forming the particle the fewer the number of top and bottom edge carbon atoms in the surface of the particle. If as previously reasoned, these atoms have a greater chemical reactivity for gasification than other atoms, the specific reaction rate of a carbon should decrease with increase in average crystallite size. Table VI, however, showed that such was not the case at either 900 or 1100°, with the specific reaction rates of graphitized carbon "B" having been greater in all cases and the rates of graphitized carbon "A" having been greater in three instances than those of the non-graphitized carbons. Furthermore, even though lampblack and carbon "C" had very similar crystallite sizes, the specific reaction rate of carbon "C" at 900° was markedly less than that of the lampblack. It is further difficult to explain why carbon "D," which was a mixture of 87% carbon "C" and 13% graphitized carbon "A," had considerably higher specific reaction rates than either of the original materials.

It might be thought, in light of the inability of the carbon properties which should affect chemical reactivity to satisfactorily explain differences in reaction rate, that the factor which controlled the gasification rates, even at 900°, was the resistance to mass transport of the carbon dioxide to the internal active carbon sites. However, this is not substantiated by fact if the relatively high reaction rate of graphitized carbon "B" is explained as being due to a relatively high diffusion rate of gas through its porous network. The effective diffusion coefficient of hydrogen in this carbon was lower than three of the non-graphitized carbons. Furthermore, the effective diffusion coefficient of hydrogen in lampblack was the highest of any carbon and yet it did not have the highest gasification rate. Another case was the graphitized carbon "A," through which hydrogen had the second highest diffusion rate and yet a gasification rate at 900° appreciably smaller than the other carbons.

In conclusion, it is obvious that no property or properties of the carbons investigated has satisfactorily explained differences in reaction rates. It is felt that the behavior of graphitized carbon "B" toward gasification where all of its presently discussed properties predict that it should have a relatively low reaction rate and yet it has the opposite, points most strikingly to the necessity of a more complete understanding of how the characteristics of a carbon affect its gasification rate.

(13) Rosalind Franklin, *J. chim. phys.*, **47**, 573 (1950).

(14) F. J. Long and K. W. Sykes, *ibid.*, 361 (1950).

(15) E. A. Gulbransen and K. F. Andrew, *Ind. Eng. Chem.*, **44**, 1048 (1952).

(16) W. D. Schaeffer, W. R. Smith and M. H. Polley, Paper #11 presented before the Division of Gas and Fuel Chemistry at the 124th meeting of the American Chemical Society in Chicago, Ill., Sept. 6–11, 1953.

CHANGES OF MACROPORE DISTRIBUTIONS IN CARBON RODS UPON GASIFICATION WITH CARBON DIOXIDE[1]

BY P. L. WALKER, JR., F. RUSINKO, JR., AND E. RAATS

Department of Fuel Technology, Pennsylvania State University, State College, Pa.

Received September 13, 1954

Macropore distributions in six carbon rods before and after different degrees of gasification have been determined over the pore-radius range 350 to 130,000 Å. It was found that the majority of the macropore volume is concentrated within a narrow pore-radius range, probably produced by the voids between particles composing the rods. Indications of pore constrictions in the carbon rods were found. Corrected diffusion coefficients of hydrogen through the unreacted rods are seen to be significantly lower than the comparable bulk diffusion coefficient. No correlation was found between the macropore structure of the carbons and their gasification rates.

Introduction

Wheeler[2] and Weisz and Prater[3] have made an important contribution toward the understanding of gas–solid reactions by emphasizing the importance of the physical structure of porous catalysts in determining reaction rates. They show that in the case of very fast reactions the small pores most remote from the surface of the particle play small part in catalysis of the reaction. In general, the faster the reaction and the smaller the average pore size the smaller the fraction of the internal surface of the catalyst which participates in the catalytic reaction. This is due to the fact that the rate of internal diffusion of a gas decreases with decreasing pore size.

The concepts of Wheeler and Weisz and Prater apply equally to the heterogeneous gas reactions of carbons. Since in this case the solid is continually reacting with the gas, the physical structure of the carbon should not only be important in determining gasification rates but in determining the magnitude and uniformity of the internal development of the carbon with regard to surface area and porosity.

Petersen[4] showed the increasing non-uniformity of gasification of $^1/_2$-inch graphite rods with increasing temperatures by determining bulk-density profile data, after a fixed carbon weight loss. At 900°, the profile, from the surface to the center of the rod, was uniform indicating a uniformity of reaction; but as the gasification temperature was increased in increments to 1200°, the profiles became continually more uneven, with the smallest bulk density being found at the carbon surface. Data in an accompanying paper[5] indicate that the over-all surface area and porosity development in six different carbons are in many cases not the same, which again may, in part, be attributed to differences in pore size and pore distribution in the carbons.

With these facts in mind, the nature of the internal pore structure of the six different carbons was determined in an attempt to further explain their gasification rates, internal structure development, and effective diffusion coefficients to hydrogen.

(1) Presented before the Division of Gas and Fuel Chemistry at the 126th meeting of the American Chemical Society in New York, N. Y., September 12–17, 1954.

(2) A. Wheeler, "Advances in Catalysis," Vol. 3, Academic Press Inc., New York, N. Y., 1951, pp. 249–327.

(3) P. B. Weisz and C. D. Prater, "Interpretation of Measurements in Experimental Catalysis," proposed chapter for "Advances in Catalysis," Vol. 6, contribution from the Socony-Vacuum Laboratories.

(4) E. E. Petersen, Ph.D. thesis, The Pennsylvania State University.

(5) P. L. Walker, Jr., and F. Rusinko, Jr., THIS JOURNAL, **59**, 241 (1955).

Experimental

Mercury Porosimeter.—Pore size distributions in the carbon rods were determined with a mercury porosimeter similar to that described by Ritter and Drake.[6] The main part of the apparatus was a precision bore Pyrex dilatometer tube. A carbon rod was placed in the bottom of the tube through a ground-glass joint and it in turn was placed in a lucite casing. The lucite head was screwed on the casing and the platinum–iridium wires, running through the dilatometer, were connected to the lucite head. The dilatometer, in the casing, was placed in a 24-inch long by 1.5-inch diameter mercury filling tube, and two electrical leads of the head were connected to two tungsten leads fused through the top of the filling tube. The top was placed on the filling tube and the system evacuated to 1 μ pressure. Mercury was allowed to fill the tube and spill into the dilatometer, filling it completely. By stepwise release of the vacuum back to atmospheric pressure, a series of readings of voltage drop, through the platinum–iridium wire circuit in the dilatometer, as a function of pressure was taken. Prior calibration of the dilatometer tube made possible the conversion of voltage increase to volume of mercury entering the carbon rod.

Upon reaching atmospheric pressure, the lucite casing was removed from the filling tube and placed into a pressure vessel where the leads were reconnected. By bleeding nitrogen into the system from a cylinder, corresponding readings were again taken of pressure and voltage drop across the platinum–iridium wires up to the top gas pressure of approximately 2500 p.s.i.

Using the relation between pressure and pore size, discussed by Ritter and Drake,[6] and assuming an average contact angle between mercury and carbon of 130°[7] and a surface tension for mercury of 480 dynes/cm.,[6] the results were converted into cumulative pore volume as a function of pore radius. Total pore volumes were taken from the accompanying paper.[5] With the above pressure limitation, the lowest pore radius into which mercury could be forced was 350 Å. Therefore, even though the usual dividing line between micro- and macropore size is arbitrarily taken at a pore radius of 100 Å.,[8] in the present case the dividing line is taken as 350 Å.

Results and Discussion

Macropore Distributions.—Figures 1 through 6 present the macropore distribution data for the six carbon rods before and after gasification at different conditions. As the original weight of the carbon rods was approximately 10 g., (this weight varied slightly with the apparent density of the different carbons), 1 and 2 g. weight losses represent approximately 10 and 20% burn-off, respectively.

(6) H. L. Ritter and C. L. Drake, *Ind. Eng. Chem., Anal. Ed.*, **17**, 782 (1945).

(7) Leslie G. Joyner, Elliott P. Barrett and Ronald Skold, *J. Am. Chem. Soc.*, **73**, 3155 (1951).

(8) S. Brunauer, "Adsorption of Gases and Vapors," Vol. 1, Princeton University Press, Princeton, N. J., 1943, p. 376.

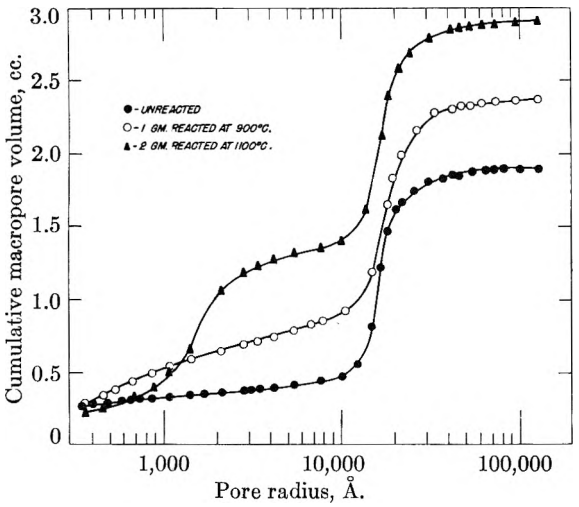

Fig. 1.—Change in macropore volume of graphitized carbon "A" rods upon gasification.

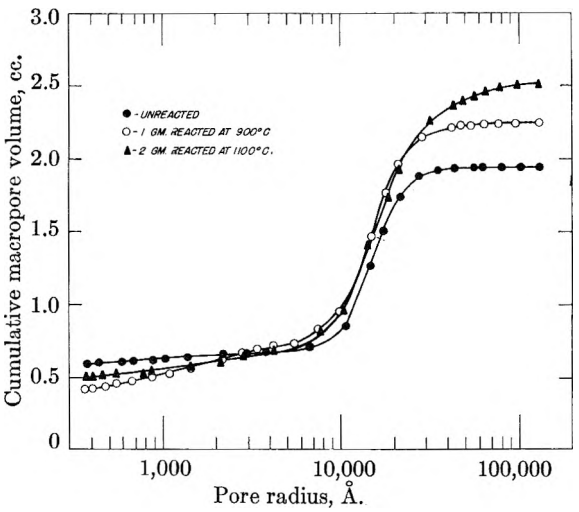

Fig. 2.—Change in macropore volume of graphitized carbon "B" rods upon gasification.

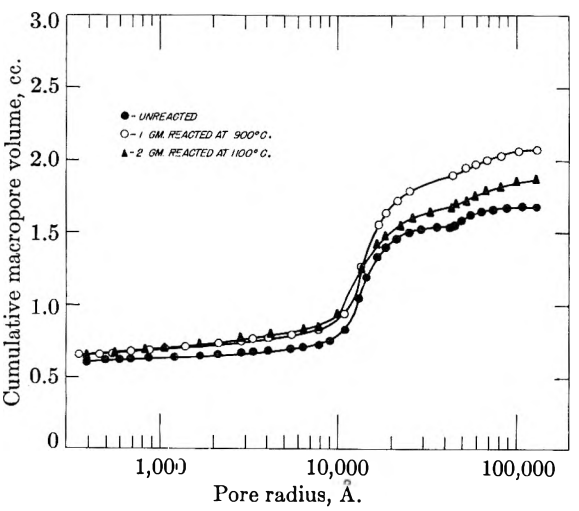

Fig. 3.—Change in macropore volume of carbon "C" rods upon gasification.

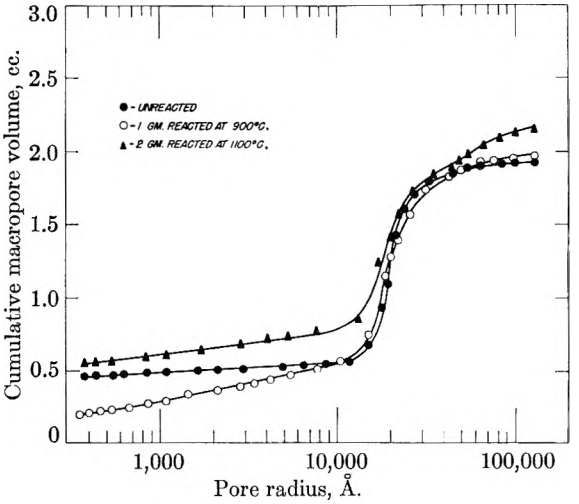

Fig. 4.—Change in macropore volume of carbon "D" rods upon gasification.

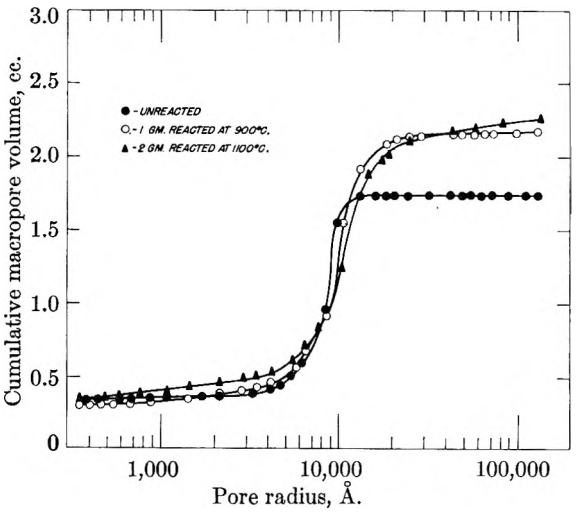

Fig. 5.—Change in macropore volume of carbon "E" rods upon gasification.

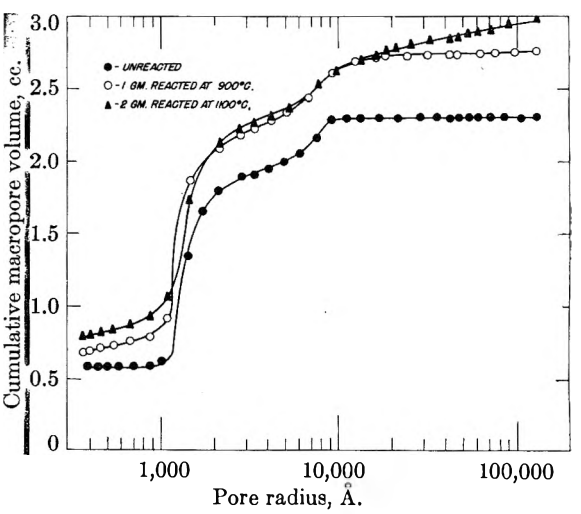

Fig. 6.—Change in macropore volume of lampblack rods upon gasification.

For all the rods, both reacted and unreacted, it is seen that the majority of the macropore volume is concentrated in a relatively narrow range of pore size. An understanding of the manufacture of carbon electrodes makes the interpretation of the above fact obvious. The original rods were a mixture of roughly 25% coal tar pitch (binder) and 75% petroleum coke flour or lampblack (filler).

TABLE I

PORE VOLUMES AND SURFACE AREAS IN MACRO- AND MICROPORES OF CARBONS

Carbon rod		All pores Vol., cc.	All pores Area, m.²	Pores over 350 Å. Vol., cc.	Pores over 350 Å. Area, m.²	Pores under 350 Å. Vol., cc.	Pores under 350 Å. Area, m.²	Pores under 350 Å. Av. radius, Å.
Graphitized carbon "A"	Unreac.	1.889	5.7	1.626	4.80	0.263	0.90	5,840
	900°	2.364	24.7	2.088	13.0	.276	11.7	472
	1100°	2.897	49.5	2.683	18.72	.214	30.78	139
Graphitized carbon "B"	Unreac.	1.937	3.94	1.356	3.63	0.581	0.31	37,500
	900°	2.243	6.0	1.829	7.43	.414	....	....
	1100°	2.498	9.2	2.019	5.49	.479	3.71	2,580
Carbon "C"	Unreac.	1.664	36.83	1.073	2.87	0.591	33.96	348
	900°	2.07	205.6	1.44	4.20	.630	201.4	62.6
	1100°	1.854	116.0	1.22	3.91	.634	112.1	113
Carbon "D"	Unreac.	1.916	5.4	1.460	2.58	0.456	2.82	3,230
	900°	1.957	10.9	1.764	6.34	.193	4.54	850
	1100°	2.150	26.8	1.605	4.42	.545	22.4	487
Carbon "E"	Unreac.	1.734	4.49	1.395	3.97	0.339	0.52	13,000
	900°	2.162	5.52	1.881	5.89	.281	....	....
	1100°	2.257	14.1	1.914	6.10	.343	8.0	857
Lampblack	Unreac.	2.311	27.3	1.733	22.15	0.578	5.15	2,245
	900°	2.761	63.8	2.077	29.92	.684	33.88	403
	1100°	2.983	111.8	2.185	24.71	.798	87.1	185

Upon baking of these rods at 950°, a considerable portion of the pitch binder was volatilized away and the residue formed into a coke. The particles of the petroleum coke were in turn coated with a thin layer of the pitch coke thereby giving strength to the carbon rod. The concentration of a large percentage of the macro-porosity in a small pore-radius increment undoubtedly represents the void volume between the particulate system. The extent of the pore radius increment over which the void volume is concentrated should be primarily determined by the range of particle size present in the carbon rods. It is seen for the rods which used petroleum coke as the filler that this large void volume is concentrated in the pore-radius range of roughly 8,000 to 20,000 Å. On the other hand, lampblack with its much smaller average particle size than petroleum coke flour, has its void volume concentrated in the region of 1,300 Å.

Figures 1 through 6 can be converted to the normal or modified Gaussian distribution plots,[6,7] if desirable. However, the present plots are adequate for both qualitative and quantitative discussion. Qualitatively, several points should be made about the macropore distributions.

1. It is seen that 4 of the 6 unreacted carbons have a normal Gaussian (or uni-modal) macropore-volume distribution over the pore range studied. Carbon "C" and lampblack are the exceptions, showing bimodal distributions. The macropore volume of carbon "C" is chiefly concentrated at a pore radius of 15,000 Å., but it also has a smaller, peak concentration of pore volume at 45,000 Å. The macropore volume of lampblack is chiefly concentrated at a pore radius of 1,300 Å., but a second distribution peak is found at 7,000 Å. Probably the bimodal pore-volume distribution is caused by bimodal particle-size distributions in these two rods. It is further seen that gasification of these two carbons at the two specific conditions did not remove their bimodal pore-volume distribution.

2. It is seen from Fig. 1 that gasification of graphitized carbon "A" to 2 grams weight loss at 1100° produced a marked bimodal pore-volume distribution; whereas, the unreacted rod showed a normal distribution. Aside from the concentration of macropore volume at a pore size of 15,000 Å., as in the unreacted rod, a second concentration of pore volume is found at 1,700 Å. Gasification of graphitized carbon "A" and graphitized carbon "B" to one gram weight loss at 900° and carbon "D" to two grams weight loss at 1100°, also produced a slight bimodal distribution of the macropore volume.

3. It is seen that the total pore volume developed upon gasification of two grams at 1100° is greater than that developed after one gram gasified at 900°, for five of the carbons. Carbon "C" is an exception.

Pore Volumes and Surface Areas in Macro- and Micropores of Carbon Rods.—Considerable information can be obtained about the internal pore structure of the carbon rods, before and after gasification, if the surface area contributions in the micro- and macropore range are estimated. Total surface areas of the carbons were reported in an accompanying paper.[5] By assuming cylindrical pores,[9] the expression $\bar{r} = 2V/A$ can be used to calculate the total surface area in the macropore range. That is, for each volume increment, shown in Figs. 1 through 6, a corresponding surface area increment can be calculated by taking the arithmetic average pore radius over the increment. Since the pore radius increments are small, this assumption of an arithmetic average pore radius is reasonably good. Table I then lists the total pore volumes and surface areas along with the pore volumes and surface areas in pores over 350 Å. for all carbon samples. It is seen that the fraction of the total surface area in pores greater than 350 Å. varies considerably with the carbon studied.

(9) P. H. Emmett and Thomas W. DeWitt, *J. Am. Chem. Soc.*, **65**, 1253 (1943).

It is well to consider what should constitute the surface areas in the micro- and macropore regions of carbon rods before continuing with the discussion. The surface area in the macropore region would be expected to be provided by the macroscopic, geometrical shape of the particles and by the major portion of their surface roughness. The surface area in the micropore region can be envisioned as being supplied primarily by internal particle porosity and by the remainder of the particle surface roughness. The internal particle porosity can be thought of as the void volume between carbon crystallites and imperfections in crystallites.[10]

It is seen for all the unreacted carbon samples, except carbon "C," that the surface area in the macropore region is an important contribution to the over-all surface area. For carbon "C," apparently due to considerable internal particle porosity, the surface area in pores over 350 Å. is less than 10% of the total surface area.

It is further seen that upon gasification there was a relatively small change of the surface-area contribution in the macropore range, graphitized carbon "A" being the exception. The indication is that a large portion of the surface area increase for five of the carbons was due to the formation of new micropores or unblocking of previously existing ones.

An idea of the extent of pore constrictions and/or bottle-neck pores in the carbon rods can be obtained by calculating the average pore size of pores under 350 Å. by knowing the pore volume and surface area under this radius. Table I also includes these data. It is seen that for all of the unreacted carbon rods, except carbon "C," the average pore radii calculated are considerably above 350 Å. At least one explanation for this fact exists. With mercury penetration, the pore volume reported to be between 130,000 and 350 Å. will only be correct if there are no pore constrictions within the solid less than 350 Å. If mercury is unable to penetrate into a fraction of the pores in the above size range because they are connected to the external surface through pores less than 350 Å., the reported pore volume will be less than the correct pore volume. Furthermore, if there are only pore constrictions in the size range of 130,000 to 350 Å., the pore volume distribution will be in error, even though the total pore volume will be correct. In this case, more of the pore volume would belong in larger pores than reported. The effect of pore constrictions on the calculations of an average pore size below 350 Å. is then twofold—too large a pore volume reported under 350 Å. and too large a surface area reported over 350 Å. Therefore, when the average pore radius below 350 Å. is estimated by the expression $\bar{r} = 2V/A$, the value could well be above 350 Å., its deviation depending upon the frequency of the pore constrictions and the pore volume blocked off beyond these constrictions.

A further understanding of the nature of the pore constrictions in the carbon rods can be obtained by observing the change in calculated, average pore radius upon gasification, as also shown in Table I. It is seen in each case, except graphitized carbon "B" and carbon "C," that the calculated, average pore radius decreased upon gasification. For these two samples, a radius could not be calculated since the calculated, surface area in pores above 350 Å. was greater than the total, experimental surface area. Previously it was noted that the calculated area in pores above 350 Å. for a sample containing pore constrictions would be greater than its true area. Furthermore, it is seen that the greater the ratio of blocked-off pore radius to pore constriction radius the more in error the calculated surface area will be. The case could well exist where the calculated area in pores over 350 Å. could exceed the total experimental surface area. In essence, the above results appear to imply that graphitized carbon "B" and carbon "C" have the largest ratio of these two radii. Apparently the reason the calculated surface area did not exceed the total area for these two unreacted carbons was that a large portion of the blocked-off volume was originally behind pores of less than 350 Å.

Relation between Pore Structure and Gas Diffusion Rate in Carbon Rods.—Experimental diffusion rates of hydrogen through the carbon rods have been reported in an accompanying paper.[5] Logically the mass transport of gas through the interior of the carbon rods should take place within the macro-void volume. To test this premise, the void volume in the particulate system has arbitrarily been taken as the volume between inflection points of the curves in Figs. 1 through 6. These data are shown in column 1 of Table II. In column 2 of Table II, the surface areas, calculated as previously discussed, between the inflection points are presented. Column 3 gives the average pore radius between the inflection points, obtained by dividing the pore radius increment in half. Column 4 shows the average pore radius in the void volume range, calculated from the expression $\bar{r} = 2V/A$. Good agreement between columns 3 and 4 is noted.

The expression given by Wheeler,[2] $L = A^2/4\pi V$, has been used to estimate the total length of the pores in the macro-void-volume region, and these data are presented in column 5 of Table II. It is seen that lampblack, because of its high surface area, has a considerably greater pore length in this range than the other carbons.

Column 6 presents the experimental data for the diffusion coefficient of hydrogen in the carbon rods. A relation between the diffusion coefficient and pore volume between the inflection points is found. The smaller the void volume, the smaller the diffusion coefficients, in the case of the unreacted carbon rods. It is noteworthy that this volume is apparently of more importance in determining diffusion rates than the average pore radius over which this void volume is concentrated. For example, lampblack has the largest void volume and the highest diffusion coefficient and yet the average pore radius over which its void volume is concentrated is from 5- to 13-fold less than the other carbons.

The diffusion coefficient of hydrogen was also determined through graphitized carbon "A" after

(10) W. D. Schaeffer, W. R. Smith and W. H. Polley, Paper #11 presented before the Division of Gas and Fuel Chemistry at the 14th meeting of the American Chemical Society in Chicago, Ill., Sept. 6–11, 1953.

TABLE II

RELATION BETWEEN PORE STRUCTURE AND GAS DIFFUSION RATES IN CARBON RODS

	Structure of pores between inflection points of distribution plots							
	V, cc.	A, m.^{2}	r, Å.	$\bar{r}$, Å.	$L \times 10^{-7}$, cm.	$D_{eff.}$, cm.^{2}/sec.	1.41 $D_{eff.}/\theta$, cm.^{2}/sec.	r_D, Å
Graphitized carbon "A"	1.43	1.739	16,500	16,270	1.72	0.0460	0.209	374
Graphitized carbon "A", 10% reacted at 900°	1.46	1.564	18,500	18,670	1.33	.0779	.288	562
Graphitized carbon "B"	1.23	1.664	15,000	14,787	1.79	.0315	.145	244
Carbon "C"	0.80	1.169	13,700	13,680	1.36	.0275	.139	232
Carbon "D"	1.31	1.347	20,000	19,450	1.10	.0350	.159	275
Carbon "E"	1.36	3.515	8,800	7,738	7.22	.0392	.199	356
Lampblack	1.72	21.94	1,500	1,568	222.3	.0486	.184	321

one gram was gasified at 900°. It is seen that even though the void volume has been increased only slightly over the unreacted sample the diffusion coefficient has been markedly increased. Furthermore, the above trend no longer holds, with this sample having a larger diffusion coefficient but a smaller void volume than the lampblack.

It is next of interest to compare the experimental hydrogen diffusion coefficients in the carbon rods with the bulk diffusion coefficient. In order to do this, the experimental, effective diffusion coefficients were corrected for the fact that they were originally calculated on the basis of the external, geometrical length and diameter of the carbon pellet ($^1/_8$-in. by $^1/_8$-in.). In solids, Wheeler[2] has shown that the internal path length, on the average, is expected to be 1.41 times the external, geometric length of the solid. Furthermore, he shows that the pore area which admits gas internally is approximately given as the external, geometrical area of the sample times its porosity. Column 7 then shows the corrected diffusion coefficients at STP conditions. These are to be compared with the bulk diffusion coefficient of hydrogen through nitrogen of 0.674 cm.^{2}/sec.

According to Wheeler,[2] for pores larger than 10,000 Å. in radius, a molecule within the pore structure will collide with other molecules far more often than with the pore wall. Hence, the diffusion coefficient will be independent of pore radius and will reach the ordinary bulk value of the diffusion coefficient. Such is seen to not be the case in the present work, with the diffusion coefficients being 3- to 5-fold less than the bulk values. It is, of course, possible that pore constrictions make the "deviousness factor," 1.41, too low and the effective porosity value too high. For example, gasification of graphitized carbon "A" to only a 10% weight loss at 900° increased the corrected diffusion coefficient by almost 50%.

An indication of the average pore size which is controlling the internal diffusion rate of gases within the carbon rods can be obtained by use of the Wheeler expression[2]

$$D = D_B(1 - e^{-2r_D\bar{v}/3D_B}) \quad (1)$$

where

D = corrected diffusion coefficient, as given in col. 7 of Table II
D_B = bulk diffusion coefficient, taken as 0.674 cm.^{2}/sec. at STP conditions
r_D = effective pore radius
$\bar{v}$ = av. mol. velocity, taken as 10^5 cm./sec.

Column 8 of Table II lists the calculated values of R_D. It is seen that they are considerably less than the values of the average pore radius in the void-volume range.

Relation between Carbon Gasification Rates and Macropore Structure.—No apparent relationships exist between the macropore structure of the carbons and their gasification rates, as presented in an accompanying paper.[5] The only inkling of a correlation that can be seen is the fact that the gasification rate of lampblack at 1300° (where mass transport would be expected to play a prominent part in controlling the gasification rate[2]) was considerably lower than the other carbons, as was its average pore radius in the macro-void-volume range. However, this comparison stops when it is noted that carbon "E" has the next smallest, average pore radius in the macro-void-volume range but yet not the next smallest gasification rate at 1300°.

It is realized that the only way to systematically study the possible effect of pore structure on gasification rate is to take a given carbon and vary its pore structure by particle size variation, etc. In the present case, there were too many variables, other than pore structure variations, which could well have affected gasification rates. Future work along the above line is planned.

Acknowledgments.—The authors wish to thank the Pittsburgh Coke and Chemical Company for their help in designing the mercury porosimeter. Also they wish to thank Dr. P. B. Weisz of the Socony-Vacuum Laboratories for his interest in the work.

THE VAPOR PHASE ASSOCIATION OF ACETIC-d_3 ACID-d[1]

BY A. E. POTTER, JR., PAUL BENDER AND H. L. RITTER[2]

Contribution from the Department of Chemistry, University of Wisconsin, Madison, Wisconsin

Received September 17, 1954

The vapor density of acetic-d_3 acid-d ($CH_3^2COOH^2$) is reported as measured in the ranges 100 to 800 mm. pressure and 80 to 170°. The data are best explained by the assumption that the vapor is an equilibrium mixture of 1-, 2- and 3-mer. The calculated heats of di- and trimerization are −14,100 and −23,200 cal./mole. The data of Ritter and Simons[3] on CH_3COOH have been recomputed on the basis of new vapor pressure values and the ordinary acid has been shown to contain the same molecular species as the deuteroacid. Corresponding values for the heats of di- and trimerization are −13,700 and −22,800 cal./mole. The difference between the heats of dimerization for $CH_3^1COOH^1$ and $CH_3^2COOH^2$ is accounted for approximately as a difference in the zero-point vibrational energies of the two dimers. A discussion is given of an observation of Johnson and Nash that the logarithm of the apparent equilibrium constant for dimerization is linearly related to the vapor density.

Changes produced in the properties of water,[4] acetic acid[5] and hydrogen fluoride[6] by deuterium substitution are believed to be largely the results of an increase in the extent of association. A study of a deuterated acetic acid by means of vapor density measurements was undertaken in this laboratory in order to obtain quantitative information concerning this effect. The completely deuterated acid, acetic-d_3 acid-d, was chosen for the study in order to eliminate the intramolecular hydrogen–deuterium exchange otherwise encountered.

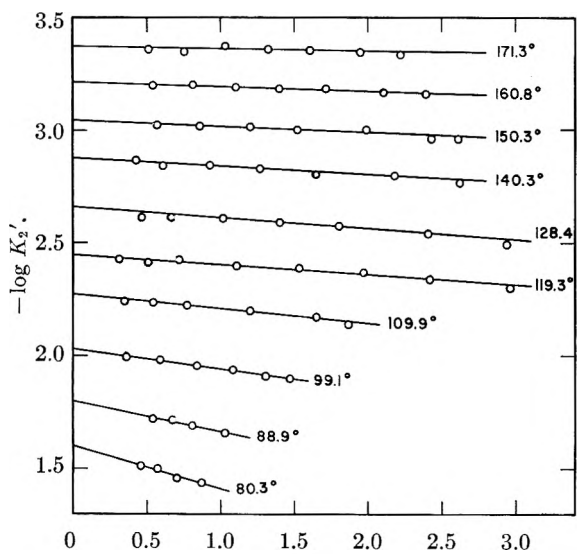

Fig. 1.—Variation of log K_2' with density for acetic-d_3 acid-d.

Materials.—Acetic-d_3 acid-d was prepared by decarboxylation of malonic-d_2 acid-d_2 formed by the reaction of D_2O and C_3O_2. The detailed method of preparation and purification, as well as the liquid density and vapor pressure of this compound, are given elsewhere.[7] The percentage of deuterium in the final product was determined by mass spectrometer as 95 ± 3% of the theoretical, corresponding to a formula weight of 63.8.

Vapor Density.—The method used for vapor density measurements has been described by Simons and Ritter.[8] The performance of the apparatus was somewhat improved by the use of a short wide buret in place of the long and narrow one as in the original design. Loss of accuracy in volume measurement due to the shortening of the buret was prevented by improved control of the buret temperature and the use of a more accurate cathetometer. As in the work of Ritter and Simons,[3] a dual system was used to correct the measurements for adsorption on the glass walls of the system. In order to facilitate analysis of the data, the vapor densities were determined at constant temperature over a range of pressures. The results of the vapor density measurements are given in Table I.

Monomer–Dimer Equilibrium.—If it is assumed that acetic acid vapor is a Dalton's law mixture of monomer and dimer, it has been shown[9] that for the dimerization equilibrium, $2AcOH \rightleftarrows (AcOH)_2$, the apparent equilibrium constant, K_2', is given by

$$K_2' = \frac{P_0 - P}{(2P - P_0)^2} \qquad (1)$$

where P is the observed pressure of the vapor, and P_0 is the pressure the vapor would exert if composed entirely of ideal monomer. It follows from the definition of P_0 that

$$P_0 = dRT/m \qquad (2)$$

where d is the observed vapor density, R is the gas constant, T is the temperature, and m is the molecular weight of the monomer. These two equations may be combined to give

$$K_2' = \frac{dRT/m - P}{(2P - dRT/m)^2} \qquad (3)$$

K_2' was calculated from experimental values of density, temperature and pressure by this equation. The results are shown in Table I, where log K_2' is tabulated. The values found for K_2' increase monotonically with pressure. The thermodynamic equilibrium constant must be obtained by extrapolation to zero pressure. In the following discussion, the apparent equilibrium constant K_2', calculated from equation 3, is distinguished from the thermodynamic equilibrium constant K_2 by an accent mark.

Johnson and Nash[9] have proposed that K_2 be found by extrapolation to zero density of a plot of log K_2' against density. Such a plot is a straight line within the precision of the experimental data, so that extrapolation is much simpler than in a plot of K_2' against pressure. In addition, graphical

(1) Abstracted from a thesis by A. E. Potter, Jr., submitted to the faculty of the University of Wisconsin in partial fulfillment of the requirements for the degree of Doctor of Philosophy, June, 1953.

(2) To whom inquiries concerning this article should be addressed at: Department of Chemistry, Miami University, Oxford, Ohio.

(3) H. L. Ritter and J. H. Simons, *J. Am. Chem. Soc.*, **67**, 757 (1945).

(4) G. N. Lewis and R. T. MacDonald, *ibid.*, **55**, 3057 (1933).

(5) G. N. Lewis and P. W. Schutz, *ibid.*, **56**, 493 (1934).

(6) W. H. Claussen and J. H. Hildebrand, *ibid.*, **56**, 1820 (1934).

(7) A. E. Potter and H. L. Ritter, THIS JOURNAL, **58**, 1040 (1954).

(8) J. H. Simons and H. L. Ritter, *Rev. Sci. Instr.*, **16**, No. 2, 23 (1945).

(9) E. W. Johnson and L. K. Nash, *J. Am Chem. Soc.*, **72**, 547 (1950).

TABLE I

VAPOR DENSITY, APPARENT DIMERIZATION CONSTANTS, TRIMERIZATION AND TETRAMERIZATION CONSTANTS FOR ACETIC-d_3 ACID-d

Pressure, mm.	Density, g./l.	$-\log K_2'$[a]	K_3, mm.$^{-2}$ × 10^6	K_4, mm.$^{-3}$ × 10^8
		80.3° Isotherm		
100.2	0.455	1.515	25.7	29.9
122.7	.570	1.499	24.2	25.2
147.2	.700	1.466	27.7	25.1
178.7	.867	1.441	26.2	21.3
		88.9° Isotherm		
124.5	0.537	1.725	11.9	
151.8	.670	1.715	11.3	
178.6	.806	1.687	12.5	
221.2	1.024	1.658	12.5	
		99.1° Isotherm		
94.9	0.359	1.992	5.58	
146.9	.587	1.984	4.02	
201.5	.841	1.956	4.73	
251.7	1.079	1.941	4.38	
296.8	1.302	1.910	4.84	
329.8	1.465	1.898	4.76	
		109.9° Isotherm		
102.6	0.354	2.247	1.58	
149.5	.542	2.238	1.44	
204.1	.772	2.225	1.52	
302.7	1.205	2.204	1.40	
398.5	1.647	2.174	1.54	
444.7	1.868	2.142	1.75	
		119.3° Isotherm		
97.8	0.311	2.433	1.46	
150.8	.508	2.412	1.45	
205.8	.717	2.430	0.711	
302.0	1.112	2.402	.841	
399.8	1.528	2.389	.811	
500.3	1.971	2.369	.798	
597.9	2.416	2.342	.860	
712.0	2.956	2.300	.982	
		128.4° Isotherm		
149.2	0.464	2.614	0.597	3.29
205.2	.663	2.613	.418	1.64
301.0	1.022	2.606	.334	1.07
397.0	1.403	2.590	.397	0.935
495.2	1.803	2.576	.378	.748
636.8	2.409	2.543	.441	.728
752.8	2.937	2.494	.560	.789
		140.3° Isotherm		
149.2	0.424	2.864	0.111	
207.9	.615	2.837	.209	
301.3	.928	2.845	.106	
397.6	1.273	2.829	.143	
497.6	1.645	2.815	.158	
636.4	2.179	2.799	.168	
748.7	2.641	2.764	.220	
		150.3° Isotherm		
206.3	0.570	3.023	0.0987	
300.0	.862	3.019	.0853	
403.5	1.202	3.009	.0891	
497.6	1.523	3.002	.0926	
632.0	1.996	2.995	.0830	
745.2	2.427	2.960	.124	
793.4	2.608	2.955	.126	
		160.8° Isotherm		
207.3	0.540	3.199	0.0785	0.258
303.0	.815	3.201	.0473	.107
399.0	1.105	3.192	.0487	.0382
493.6	1.403	3.180	.0557	.0350
593.1	1.722	3.179	.0435	.0582
708.4	2.108	3.167	.0508	.0307
790.5	2.391	3.157	.0560	.0597
		171.3° Isotherm		
206.9	0.513	3.361	0.0561	
298.1	.759	3.352	.0428	
398.5	1.035	3.373	.0193	
496.7	1.321	3.359	.0219	
592.9	1.608	3.352	.0276	
705.7	1.955	3.343	.0270	
789.2	2.220	3.333	.0334	

[a] A molecular weight of 63.8 was used for the calculation of K_2'.

extrapolation of the curved plot of K_2' against pressure tends to give special weight to the least accurate data, namely, those at low densities.

Plots of log K_2' against density for acetic-d_3 acid-d are shown in Fig. 1. The linearity of these plots is apparent. Consequently, the experimental values of K_2' found over a range of density at a particular temperature were fitted by the method of least squares to an equation of the form

$$\log K_2' = \log K_2 + Bd \qquad (4)$$

The resulting values of log K_2 and B at each temperature of measurement are tabulated in Table II. The heat of dimerization was found from the slope of a plot of log K_2 against $1/T$. The equation of the line was found by the method of least squares to be $\log K_2 = -10.322 + 3083/T$. The resulting heat of dimerization is $\Delta H_2 = -14{,}100$ cal./mole.

Dependence of log K_2' on Vapor Density.—No simple explanation has been given for the apparent linearity of a plot of log K_2' against vapor density. It was therefore thought advisable to examine the behavior of this plot. It was found possible to expand log K_2' as a power series in vapor density, the coefficients in the series involving the several equilibrium constants for i-merization. The development is given in the Appendix, the final series being

$$\ln K_2' = \ln K_2 + \frac{2K_3}{K_2}\left[\frac{RT}{m}\right]d + \left[-4K_3 - \frac{4K_3^2}{K_2^2} + \frac{6K_4}{K_2}\right]\left[\frac{RT}{m}\right]^2\frac{d^2}{2!} + \left[48K_3K_2 + \frac{12K_3^2}{K_2} + \frac{24K_5}{K_2} + \frac{16K_3^2}{K_2^3} - 48K_4 - \frac{36K_3K_4}{K_2^2}\right]\left[\frac{RT}{m}\right]^3\frac{d^3}{3!} + \ldots \qquad (5)$$

where K_2, K_3, . . . are the equilibrium constants for 2, 3, . . . -merization, defined for the equilibrium $i(AcOH) \rightleftarrows (AcOH)_i$. For sufficiently small d, the higher terms are apparently negligible within the range of density used in those experiments where the linearity has been confirmed, presumably because the higher K's are small.

Higher Polymers.—Exact definition of the nature of the higher polymers that have been shown to exist in carboxylic acid vapors[3,9,10] is exceedingly difficult. This difficulty is due primarily to the present-day practical impossibility of obtaining sufficiently accurate data. As the data obtained in

(10) F. H. MacDougall, *J. Am. Chem. Soc.*, **63**, 3420 (1941).

this research are comparable in accuracy to those recently obtained by Ritter and Simons[3] and Johnson and Nash,[9] the essential criterion used by these workers to establish the probable nature of the predominant higher polymer has been employed here also. This criterion for the predominance of a higher polymer of order i is that the equilibrium constant for i-merization should be substantially independent of pressure.

In order to calculate K_3,[11] the following procedure was used. For a Dalton's law equilibrium mixture of monomer, dimer and trimer, it may be shown[3] that

$$K_2 = \frac{m\alpha_2}{2pM\alpha_1^2} \quad (6)$$

$$K_3 = \frac{m^2\alpha_3}{3p^2M^2\alpha_1^3} \quad (7)$$

$$\alpha_1 = \frac{m}{pMK_2}\left[\{1 + pK_2(3 - M/m)\}^{1/2} - 1\right] \quad (8)$$

where α_1, α_2 and α_3 are the mole fractions of monomer, dimer and trimer, respectively, m is the molecular weight of the monomer, and M is defined as dRT/p. At each temperature the value found for K_2 was combined with each pair of experimental values of d and P for the calculation of the corresponding α_1 from equation 8. Equation 6 was then used to compute α_2. Using the further relationship that $\Sigma\alpha = 1$, it was possible to compute α_3, and finally K_3 was computed from equation 7. Inspection of these results, tabulated in Table I, reveals that K_3 exhibits only a small pressure dependence; indeed, the experimental scatter of the data generally obscures the trend of K_3 with pressure. Since the precision of the data does not justify an extrapolation to zero pressure to obtain the thermodynamic equilibrium constant, an average value of K_3 was computed at each temperature. The plot of the logarithm of the average K_3 against $1/T$ is linear. The equation of the line, as found by the method of least squares, was $\log K_3 = -18.984 + 5080/T$. The resulting value of ΔH_3 is $-23{,}200$ cal./mole.

It is possible to compute K_3 in another way. Combining equations 4 and 5 gives, to the first degree in d

$$K_3 = \frac{2.303}{2} \times \frac{BK_2}{mRT} \quad (9)$$

This relation gives an "independent" means of calculating K_3. In addition, the results of such a calculation provide some measure of the reliability of the extrapolation procedure used to compute K_2. Using the slopes given in Table II with equation 9, K_3 was found at each temperature of measurement. The equation of the straight-line plot of $\log K_3$ against $1/T$ was found by the method of least squares to be $\log K_3 = -18.755 + 4924/T$. The corresponding value of ΔH_3 is $-22{,}500$ cal./mole. The agreement between this result and that obtained previously by the more rigorous method is felt to be satisfactory.

TABLE II

LOG K_2 AND B FOR ACETIC-d_3 ACID-d

Temp., °C	log K_2	B, l./g.	Temp., °C.	log K_2	B, l./g.
80.3	−1.601	0.186	128.4	−2.648	0.047
88.9	−1.807	.145	140.3	−2.876	.039
99.1	−2.031	.089	150.3	−3.048	.034
109.9	−2.274	065	160.8	−3.216	.024
119.3	−2.453	.047	171.3	−3.374	.016

(11) The data do not justify a distinction between K_n and K_n' for $n > 2$.

The assumption that a tetramer was the predominant higher polymer was also tested, in order to make sure that this assumption would not give results as satisfactory as were found when a trimer was taken as the predominant higher polymer. Equilibrium constants for tetramerization were calculated for several isotherms by a method[3] similar to that employed for the trimer. Values of K_4 are given in Table I, where it may be seen that K_4 displays such a large pressure dependence, compared to K_3, as to make it unreasonable that the predominant higher polymer is a tetramer. In addition, the pressure dependence is in the opposite sense from that which might be expected. The fact that the experimental data produced a straight line plot of $\log K_2'$ against density is also evidence that the trimer predominates; for should the tetramer be the major higher species, $\log K_2'$ should vary as d^2 rather than d, according to equation 5. The possibility that a tetramer is present in addition to trimer has not been excluded; vapor density data of extraordinary accuracy would be required to establish the existence and nature of such higher polymers.

Acetic Acid.—Johnson and Nash have made precise density measurements for the vapors of several carboxylic acids, using a magnetically controlled gas density balance. From consideration of their data, they have concluded that a stable trimer is present in the acid vapor in addition to the dimer. This observation is in opposition to that of Ritter and Simons, who, using a procedure similar to that of this research, found the predominant higher polymer in acetic acid vapor to be a tetramer. In addition, Johnson and Nash found for acetic acid, $\Delta H_2 = -13{,}820 \pm 100$ cal./mole as compared with Ritter and Simons' value of $-14{,}500 \pm 200$ cal./mole. Both workers covered similar ranges of pressure and temperature, and the precision of their results is comparable. The lack of agreement is strange, and would appear to be due to a systematic error in one case or the other.

The calculations of Ritter and Simons involve the vapor pressure and liquid density for acetic acid; those of Johnson and Nash involve the equation of state for carbon tetrachloride. Ritter and Simons used the vapor pressure of acetic acid as determined by Ramsey and Young. The vapor pressure of acetic acid was remeasured in the course of this research,[7] and the results are considered to show that the data of Ramsay and Young are in error by about 2% at the boiling point. As an error of this magnitude in the vapor pressure causes an appreciable error in K_2' Ritter and Simons' data have been recalculated using the new vapor pressures. The recalculated values are shown in Table III. Values of $\log K_2'$ calculated from the 44.7 and 829.8 mm. isobars deviated considerably in a systematic manner from a straight line plot of $\log K_2'$ against density. Con-

TABLE III

ACETIC ACID: RECALCULATED VAPOR DENSITY DATA OF RITTER AND SIMONS

(The first column in each subtable is $M = dRT/P$; the second is the temperature, °C).

p = 44.7 mm.		p = 93.9 mm.		p = 148.2 mm.	
105.2	51.9	102.5	63.3	97.7	77.6
95.9	66.2	100.9	67.2	94.5	83.7
91.3	74.2	92.7	80.0	84.5	102.0
84.4	83.9	89.0	87.1	81.6	109.0
80.9	92.0	82.8	98.0	76.9	119.3
77.5	97.3	76.9	109.1	73.9	122.8
73.6	105.3	73.6	115.6	72.5	130.1
67.2	123.6	68.5	127.8	69.0	137.9
66.3	127.6	67.6	132.9	66.0	148.2
63.8	145.5	64.3	151.1	64.7	160.0
63.7	151.5	63.2	160.1	62.9	177.9
p = 212.8 mm.		p = 309.2 mm.		p = 433.0 mm.	
94.3	93.4	97.2	96.9	96.4	105.2
93.1	96.1	95.2	99.8	94.0	109.6
88.6	104.4	92.2	105.4	88.6	119.3
85.6	109.8	89.5	108.8	81.1	134.9
79.2	120.2	84.1	119.2	73.9	153.2
75.5	129.8	81.5	125.1	71.4	157.7
70.8	142.7	77.7	140.4	68.6	169.3
67.7	155.0	69.2	158.0	66.6	178.3
63.3	185.0	62.8	197.8	65.9	189.5
p = 612.5 mm.		p = 829.8 mm.			
96.8	114.3	93.9	129.4		
94.1	120.0	88.5	141.2		
91.2	124.8	82.8	151.5		
89.1	129.1	79.3	159.4		
85.6	135.7	74.4	171.8		
80.8	146.0	71.7	180.0		
76.5	154.9	67.9	194.8		
70.8	174.1				
66.0	193.7				

sequently these isobars were discarded in further treatment of the data. Values of log K_2 and B were determined at each temperature in the same way as for acetic-d_3 acid-d. The results are shown in Table IV. The equation of the straight line obtained by

TABLE IV

LOG K_2 AND B FOR ACETIC ACID

Temp., °C.	log K_2	B, l./g.	Temp., °C.	log K_2	B, l./g.
80.0	−1.704	0.353	130.0	−2.697	0.064
90.0	−1.901	.215	140.0	−2.876	.056
100.0	−2.109	.128	150.0	−3.060	.053
110.0	−2.301	.079	160.0	−3.232	.033
120.0	−2.504	.076	170.0	−3.349	.017

plotting log K_2 against $1/T$ was found by the method of least squares to be $\log K_2 = -10.149 + 3000/T$. The corresponding value of ΔH_2 is −13,730 cal./mole, which is in good agreement with the value obtained by Johnson and Nash. The close agreement in heat of dimerization between these two sets of data suggested that further agreement might be found concerning the nature of the predominant higher polymer. Accordingly, the pressure dependence of K_3 and K_4 was examined. K_3 and K_4 were computed in the same way as for acetic-d_3 acid-d. Some typical results are given in Table V. It may be seen from this table that the pressure dependence of K_3 is small compared to that of K_4. In addition, as with acetic-d_3 acid-d, the pressure dependence of K_4 is quite opposite to that expected. This result indicates that the trimer is the predominant higher polymer in acetic acid vapor, as well as in acetic-d_3 acid-d vapor.

TABLE V

REPRESENTATIVE VALUES OF K_3 AND K_4 FOR ACETIC ACID

	Pressure, mm.	K_3, mm.$^{-2}$ × 10^6	K_4, mm.$^{-3}$ × 10^8
90° Isotherm	93.9	12.2	13.0
	148.2	9.35	7.21
	212.8	13.7	7.91
	309.2	14.7	6.49
120° Isotherm	93.9	1.54	1.32
	148.2	1.36	0.740
	212.8	1.32	.544
	309.2	0.891	.268
	433.0	1.10	.262
	612.5	1.25	.221
160° Isotherm	93.9	[a]	[a]
	148.2	0.0332	0.0136
	212.8	.106	.0277
	309.2	.0230	.00279
	433.0	.0306	.00309
	612.5	.0568	.00721

[a] Experimental error causes K_3 and K_4 to be negative.

Values of the logarithm of the average K_3 were plotted against $1/T$ and found to fall on a straight line. The equation of the line was found by the method of least squares to be $\log K_3 = -18.591 + 4970/T$; the corresponding heat of trimerization is $\Delta H_3 = -22{,}700$ cal./mole. K_3 was also calculated using equation 9 and the slopes given in Table IV. The equation of the resulting straight-line plot of log K_3 against $1/T$ was found by the method of least squares to be $\log K_3 = -19.119 + 5090/T$. The heat of trimerization found from this slope is −23,300 cal./mole.

Comparison of the Heats of Dimerization of Acetic Acid and Acetic-d_3 Acid-d.—A primary objective of this research was the measurement of the changes produced by deuterium substitution in a compound extensively associated through hydrogen bonds. It is therefore of interest to compare ΔH_2 for acetic-d_3 acid-d with ΔH_2 for acetic acid

Acetic-d_3 acid-d	−14,100 cal./mole
Acetic acid[8,12]	−13,730 cal./mole
Acetic acid[9,12]	−13,820 cal./mole

It is seen that the energy of dimerization found for the deuterated acid is greater by about 300 cal./mole than that found for the ordinary acid. It is generally believed that replacement of hydrogen by deuterium does not affect the electronic structure of a molecule. Accordingly, the observed difference should be explicable on the basis of a mass change alone. The most important properties of the acetic acid system affected by a mass change are the zero-point vibrational energy of the dimer and the resonance energy of the hydrogen bond. Replacement of hydrogen by deuterium will decrease both of these quantities. A decrease of zero-point

(12) Other values have been reported by various workers, ranging up to −16,400 cal./mole. A recapitulation is given in reference 9. The value given here as from reference 3 is the corrected value.

vibrational energy, however, corresponds to an increase in the absolute value of the heat of dimerization, while a decrease of resonance energy results in a decrease in this quantity.

In order to calculate the effect of deuterium substitution on the zero-point vibrational energy of the dimer, equations given by Halford[13] for the normal modes of vibration of a hypothetical acetic acid dimer molecule were used. The change in zero-point vibrational energy produced by replacement of all the hydrogen by deuterium was found to be 122 to 133 cal./mole, depending upon what values of the force constants were chosen for the calculation. This difference compares favorably in magnitude and direction with the observed change of 300 cal./mole. It follows that the resonance energy of the hydrogen bond in acetic acid must be small, since deuterium substitution would be expected to change the resonance energy considerably. As an additional point of interest, the ratio of the dimerization constants of the isotopic acids was calculated and compared with the experimental ratio computed from the recalculated data of Ritter and Simons and the data of this research. The ratio of the dimerization constants is given by

$$\frac{K_2^{(h)}}{K_2^{(l)}} = \frac{Q_2^{(h)}\,[Q_1^{(l)}]^2}{Q_2^{(l)}\,[Q_1^{(h)}]^2}\, e^{-\delta\Delta H_0^\circ/RT}$$

Here, $K_2^{(h)}$ and $K_2^{(l)}$ are the dimerization constants for the heavy and light acids, $Q_2^{(h)}$ and $Q_2^{(l)}$ are the total partition functions of the heavy and light dimers, $Q_1^{(h)}$ and $Q_1^{(l)}$ are the total partition functions of the heavy and light monomers, and $\delta\Delta H_0^0$ is the difference between the heats of reaction at absolute zero. Translational, rotational, internal rotational and vibrational partition functions were included in calculation of the total partition function. The calculation was vastly simplified by the assumption that the acetic acid monomer molecule could be regarded as rigid. The structure used by Halford[13] was taken for calculation of the partition functions. Internal rotation partition functions for the hydroxyl group were calculated from the tables of Pitzer,[14] using 3000 and 10,000 cal./mole as the depth of the potential well hindering rotation in the monomer and dimer, respectively. The difference between the heats of reaction at absolute zero is the difference between the zero-point vibrational energy of the dimers, already calculated above. At 120°, (using $\delta\Delta H_0^0 = -133$ cal./mole) the ratio $K_2^{(h)}/K_2^{(l)}$ was found to be 1.23, which compares well with the observed ratio of 1.17.

From the preceding discussion, it appears likely that the differences observed between the isotopic acids, with regard to the heat of dimerization and the extent of association, are due largely to the effect of the mass increase on the zero-point energy of the dimer.

Acknowledgments.—The authors are indebted to the du Pont Company for financial assistance to one of them (AEP), and to Prof. C. F. Curtiss for many helpful discussions.

Appendix

Substituting $d = m/V$ in equation 3, where m is the molecular weight of the monomer and V is the volume occupied by one mole of monomer molecules (whether associated or not)

$$K_2' = \frac{[1 - PV/RT]}{[2PV/RT - 1]^2}\,\frac{V}{RT} \qquad \text{(i)}$$

If we now express PV/RT in terms of the virial equation of state, this equation becomes

$$K_2' = -\frac{1}{RT}\,\frac{[B + C/V + D/V^2 + E/V^3 + \ldots]}{[1 + 2B/V + 2C/V^2 + 2D/V^3 + \ldots]^2} \qquad \text{(ii)}$$

where B, C, D, . . . are the 2nd, 3rd, 4th, etc., virial coefficients. From equation ii, noting that $\ln K_2' \rightarrow \ln K_2$ as $1/V \rightarrow 0$, $\ln K_2'$ may be expanded in a Maclaurin series in $1/V$ to give

$$\ln K_2' = \ln K_2 + \left[\frac{C}{B} - 4B\right]\frac{1}{V} + \frac{1}{2!}\left[\frac{2BD + 8B^4 - C^2 - 8B^2C}{B^2}\right]\frac{1}{V^2} + \frac{1}{3!}\left[\frac{6B^3E - 6B^2CD + 2BC^3 - 24B^4D + 48B^5C - 32B^7}{B^4}\right]\frac{1}{V^3} + \ldots. \qquad \text{(iii)}$$

For a gas which is associated to form a Dalton's law mixture of polymeric forms in equilibrium, Woolley[15] has shown that the virial coefficients may be written as

$$B = -K_2RT$$
$$C = [4K_2^2 - 2K_3][RT]^2$$
$$D = [-20K_2^3 + 18K_2K_3 - 3K_4][RT]^3$$
$$E = [112K_2^4 + 18K_3^2 - 144K_3K_2^2 + 32K_2K_4 - 4K_5][RT]^4$$

By substituting these relations in equation iii and placing $d = m/V$, one obtains equation 5 of the text.

(13) J. O. Halford, *J. Chem. Phys.*, **14**, 395 (1946).
(14) K. S. Pitzer and W. D. Gwinn, *ibid.*, **10**, 428 (1942).
(15) H. W. Woolley, *ibid.*, **21**, 236 (1953).

SURFACE TEMPERATURES OF BURNING LIQUID NITRATE ESTERS

BY RUDOLPH STEINBERGER AND KENNETH E. CARDER

Allegany Ballistics Laboratory, Hercules Powder Company, Cumberland, Maryland

Received September 17, 1954

Temperature profiles of burning liquid nitrate esters have been obtained by allowing the liquid to burn past a fine wire thermocouple. The results show that the temperature at the liquid–gas interface is not appreciably above ambient. A mechanism consistent with this observation involves a free-radical attack on the nitrate ester as the initial step in the chemical reaction sequence.

In a study of the mechanism of burning of double-base propellants, knowledge of the detailed temperature distribution through the reaction zone would be very helpful. Such knowledge would supplement the scanty analytical data which are available for such systems and indicate, in rather broad fashion, the general nature of the reaction sequence.

Previous attempts in this field[1] have been successful in providing reproducible, and presumably correct, temperature profiles of double-base propellants. Some difficulty was encountered, however, in interpreting these curves, since no satisfactory method could be found for fixing a point of reference which would relate the temperature profile to observable changes within the reaction zone. The obvious point to use as an origin is the surface of the solid propellant strand. However this surface is usually somewhat irregular in shape and difficult to define, especially since the thickness of the pertinent reaction zone is on the order of 0.1 mm.

It was thought that progress could be made by making similar measurements on liquid nitrate esters burning as strands in glass tubes. These compounds have ballistic properties (burning rate levels, pressure coefficients, temperature coefficients) very similar to those of double-base propellants with comparable heats of explosion and can, therefore, be regarded as suitable models. Moreover, from the point of view of measuring temperature profiles, the liquids have several special advantages.

(1) Under suitable conditions the liquids burn with a smooth, meniscus-shaped surface, so that an easily definable reference point exists.

(2) Liquid strands are transparent, so that relatively simple photographic techniques can be used for synchronization of the physical situation with the temperature record.

(3) By means of suitable fuel-feeding mechanisms the rate of travel of the reaction zone past a thermocouple can be reduced below the normal level, so that thermocouple response times and high speed photography cease to be a problem.

Experimental

Apparatus.—Combustion was carried out in a window bomb, a horizontally mounted cylindrical vessel with 4″ diameter windows both front and rear. The fuel was contained in a 3 mm. i.d. Pyrex tube connected in U-tube fashion to a 12 mm. i.d. reservoir. The thermocouple was mounted horizontally through the smaller tube, the junction centered in the tube and the leads sealed through the glass with Armstrong A-2[2] adhesive. Ignition was obtained by means of a loop of 0.005″ platinum wire extending approximately 3 mm. into the liquid and connected to a 24 v.a.c. source. In order to get smooth ignition with some liquids it was found helpful to introduce a plug of fibrous nitrocellulose into the top of the burning tube.

The thermocouple was made of 0.0005″ Pt and Pt. 10% Rh wires fused by means of a micro-torch. The junction diameter was estimated to be approximately twice the wire size, or 25 microns. The thermocouple output was recorded by an oscilloscope–drum camera combination. Drum speed could be varied by changing synchronous motors. Such equipment is normally used for the static-testing of rockets, and characteristics such as frequency response and stability are thought to be more than adequate for the present purpose.

Photography was done by means of a Ciné Kodak Special camera, using a lens with a focal length of 2″ or 3″ and a 3″ variable extension tube. Efforts to obtain still higher magnification resulted in the use of a microscope tube with 32 mm. objective and 10× eyepiece. This combination was used without any further camera lenses, producing 40-fold magnification. When using the camera with a motor drive, it was found necessary to calibrate the framing speed for every experiment. However when the spring drive was used, only occasional recalibration was necessary. In general, a back-lighting scheme, using a #2 Photoflood bulb was found most effective for delineating the liquid meniscus and thermocouple. Synchronization between the oscilloscope and movie records was accomplished by means of a flashbulb which was actuated by the drum camera shutter and served to blank out one frame of the movie film.

Materials.—While several different nitrate esters were used in this study, the material found most suitable was triethylene glycol dinitrate (TGDN). This was prepared by mixed-acid nitration of redistilled triethylene glycol. (Nitrogen analysis by $TiCl_3$ titration: 11.96% N, theoretical 11.6% N.) Other nitrate esters were the standard commercial products, not further purified.

Experimental Conditions.—Inasmuch as some of the methods used were relatively new, experimental conditions were varied over the widest possible range in order to show up any systematic error.

1. Several different liquids were burned, including ethyl nitrate, ethylene glycol dinitrate (EGDN), and a mixture of 2,2-dimethylol-1-propanol trinitrate, 82.2%, and triacetin, 17.8%.

2. Pressures were ordinarily varied between 500 and 1000 p.s.i. (nitrogen). Some experiments were carried out, however, at pressures as low as atmospheric.

3. Burning tube and reservoir diameters were varied in order to show up effects due to rate of travel of the liquid surface, subsurface liquid turbulence caused by temperature gradients at the walls, etc. No effects were noted. Even when the reservoir was removed completely, the temperature profile retained its shape.

4. The original method of mounting thermocouples involved introduction of the leads from below, the final wires forming an inverted V at the bead. This method was thought to be inferior to the one finally adopted, which was developed by Dr. Don H. Hildenbrand of the U. S. Naval Ordnance Test Station. However, results obtained by the two methods were identical.

5. Photographic techniques were changed constantly. At first a front-lighting scheme was used, because the bomb had only one window. This served to highlight the thermocouple and leave the liquid fairly dark. A slightly different method, in which the light beam was directed at a white background, served to demonstrate the advantage of a silhouette-type photograph and led to the two-window method finally adopted. The photography can be a source

(1) R. Klein, M. Mentser, G. von Elbe and B. Lewis, THIS JOURNAL, **54**, 877 (1950).

(2) Armstrong's Products Co., Warsaw, Ind.

of considerable error in this type of experiment. However, the various approaches used here all led to the same result.

6. Inasmuch as previous work had shown that catalytic activity by the thermocouple wire can be important,[1] some experiments were done with a borax coating on the thermocouple. Results were not significantly different from the usual ones.

The range of experimental conditions quoted above covers some situations which are quite obviously more suitable for accurate observations than others. In particular it was found advantageous to work with relatively non-volatile materials at high pressure. In this way one reduces to a minimum the effect of a thin, foam-like layer which forms at the surface at low pressure and with volatile fuels and makes the location of the liquid–gas interface very difficult and somewhat meaningless. Under suitable conditions, however, the burning surface is sharply defined, and results can be quoted with considerable confidence.

Results

A typical temperature record, obtained by burning TGDN at 800 p.s.i., is shown in Fig. 1. Accord-

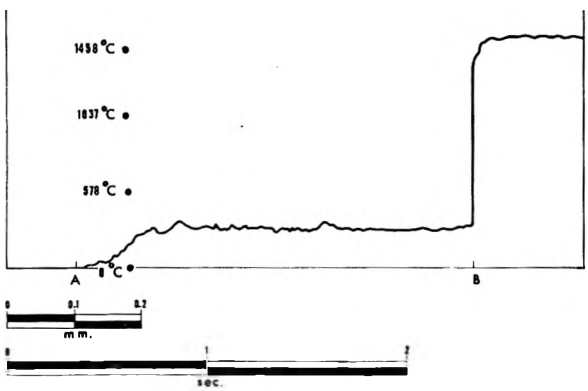

Fig. 1.—Temperature record of TGDN burning at 800 p.s.i.

ing to the movies corresponding to this record, Point A marks the moment at which the burning surface meets the thermocouple. Thus the temperature of the burning surface is equal to the ambient temperature. In only one case, EGDN burning at atmospheric pressure, an appreciably elevated surface temperature was found (70°, see Fig. 2).

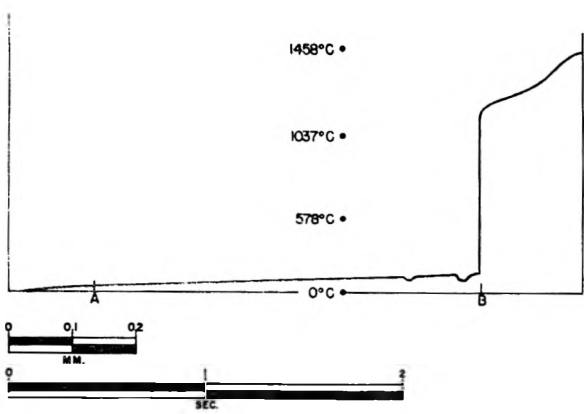

Fig. 2.—Temperature record of EGDN burning at atmospheric pressure.

These records do not give a true picture, however, of the temperature in the gas phase. It appears that as the thermocouple attempts to rise out of the liquid it drags along a cusp of liquid and remains coated through the greater part of the combustion zone. The film of liquid which coats the thermocouple is presumably burning but is replenished continually by capillary action. The recorded temperature thus approximates that of the film, which is hotter than the normal surface, because it projects into the flame zone. Eventually the film drops off, point B of Fig. 2, and the thermocouple records the flame temperature. Evidence for this picture consists of two types of observations. (1) Some of the photographic records, especially those taken at low pressure, distinctly show a rapid drop of the surface at point B. (2) Temperature records obtained with the burning surface approaching the thermocouple from below, so as to avoid the formation of the film (see Fig. 3), show a smooth, rapid temperature drop from the flame to the surface rather than the long plateau characteristic of records obtained in the normal direction.

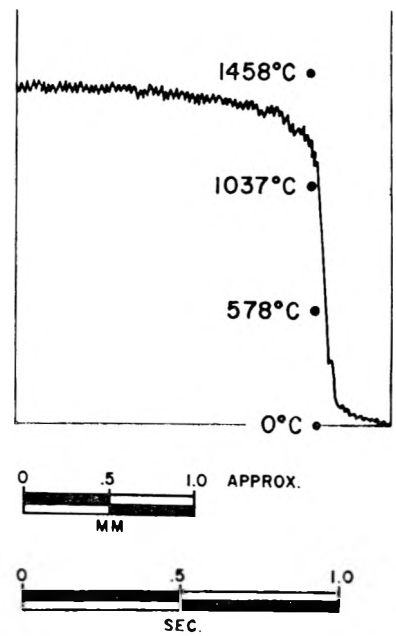

Fig. 3.—Reverse temperature record of TGDN burning at 600 p.s.i.

Thus the present work gives essentially no information as to the gas-phase temperature profile. However, the observation of a low surface temperature leads to some important conclusions.

Conclusions

Several mechanisms can be postulated for accomplishing the phase transition which occurs at the liquid–gas interface of a burning liquid. The present data can be used to distinguish between these possibilities.

1. A mechanism suggested in the past[3,4] involves the evaporation of the liquid and subsequent combustion of the vapor. The rate of burning then would depend on the rate of heat transfer by conduction from the flame. The observed temperature gradients are too low, however, to account for the burning rates of these materials. Thus the temperature gradient at point A, Fig. 1, is zero, so that no heat is flowing through this point. In the case of EGDN, burning at atmopsheric pressure (see

(3) A. F. Belajev, *Acta Physicochim. U.R.S.S.*, **8**, 763 (1938).

(4) G. K. Adams, W. G. Parker and H. G. Wolfhard, *Disc. Faraday Soc.*, **14**, 101 (1953).

Fig. 2), a constant gradient of 2000°/cm. is recorded over the entire curve up to the drop-off point, B. This leads to a rate of evaporation lower than the burning rate by a factor of 38. It is clear, therefore, that the available data do not support a phase-change mechanism involving simple vaporization of the fuel.

The calculations pertinent to this point are based on the equations

$$H_1 = H_v r$$

$$H_2 = \frac{k\,dT}{dx}$$

where H_1 is the rate of heat absorption necessary for vaporization, cal./cm.^{2} sec., H_2 is the rate of heat conduction to the surface, cal./cm.^{2} sec., H_v is the volumetric heat of vaporization of the liquid, cal./cm.^{3}; r is the burning rate, cm./sec.; k is the heat conductivity of the gas, taken to be 5×10^{-5} cal./cm. °C. sec., and dT/dx is the temperature gradient in the gas just outside the surface, °C./cm., assumed to be equal to the temperature gradient in the liquid at the surface.

In the case EGDN, $H_v = 124$ cal./cm.^{3,5} $r = 0.031$ cm.^{2}/sec., so that $H_1 = 3.8$ cal./cm.^{2} sec., whereas $H_2 = 0.1$ cal./cm.^{2} sec.

It is recognized that, if a very steep temperature gradient did exist at the surface, the thermocouple used here would be too large to record it accurately. In a purely thermal model the temperature would be expected to rise to a surface temperature of about 500° over a distance of 10 microns,[6] whereas our thermocouples are approximately 25 microns in thickness. However, since the thermocouple indicates an average temperature across its diameter,[7] the record should give evidence of such large changes in some manner. In actual fact, the records in the neighborhood of the surface are smooth, free from discontinuities, and low in slope. Therefore this difficulty would not appear to be present.

2. A second phase-change mechanism involves a chemical reaction, the usual postulate being invoked that the nitrate ester forms gaseous products by a unimolecular decomposition. However, the surface temperature necessary for this reaction to take place at the observed rate is on the order of 500°[6,8,9,10] so that this mechanism also is incompatible with the experimental observations.

3. A third mechanism, also chemical in nature, involves the attack on the nitrate ester by a second species. Such a mechanism is in accord with the temperature data, provided a material can be found which will react with the nitrate ester at the required speed at room temperature. Clearly, one is looking here for highly reactive free radicals. It is postulated that such reagents are generated in appreciable concentration in the flame and that they diffuse back to the liquid surface to initiate reaction. This type of chemical mechanism, therefore, requires that a diffusion mechanism of flame propagation be operative. Unfortunately, no unanimity exists in the literature as to the relative importance of thermal and diffusion processes in flames. The present data tend to underscore the latter. It is hoped that studies now in progress will help to clarify this point further.

Acknowledgment.—The authors wish to thank Dr. Lyman G. Bonner and Dr. Frank H. Westheimer for their continued interest and many helpful discussions. This study was sponsored by the U. S. Navy under Contract NOrd 10431.

(5) T. E. Jordan, "Vapor Pressure of Organic Compounds," Interscience Publishers, Inc., New York, N. Y., 1954.

(6) R. H. Olds and G. B. Shook, U. S. Naval Ordnance Test Station Technical Memorandum 917, 1952.

(7) N. P. Bailey, *Mech. Eng.*, **53**, 797 (1931).

(8) R. E. Wilfong, S. S. Penner and F. Daniels, THIS JOURNAL, **54**, 863 (1950).

(9) O. K. Rice and R. Ginell, *ibid.*, **54**, 885 (1950).

(10) R. G. Parr and B. L. Crawford, Jr., *ibid.*, **54**, 929 (1950).

THE SYSTEM SODIUM SULFATE–SODIUM MOLYBDATE–WATER

BY WILLIAM E. CADBURY, JR.

Contribution from the Chemistry Department of Haverford College, Haverford, Pa.

Received September 27, 1954

Solubility relationships in the system sodium sulfate–sodium molybdate–water at various temperatures are reported. At temperatures where it exists as a stable phase, the decahydrate of each of these salts takes up the other in solid solution, but the amount of sodium sulfate taken up by sodium molybdate decahydrate is very small. Boundary conditions for some of the three-phase equilibria in the system have been determined, as have the locations of two quadruple points.

The work reported in this paper is similar, in methods and in significance, to previously reported studies of the systems sodium sulfate–sodium chromate–water[1] and sodium chromate–sodium molybdate–water.[2] Ricci and Linke[3] have studied the system sodium sulfate–sodium molybdate–water at 25°.

Experimental

The salts used were C.P. grade sodium sulfate and sodium molybdate which had been recrystallized once as decahydrate. To determine solubility, the pure salt, a batch of mixed crystals prepared by crystallization as decahydrate,[4] or a mixture of salts of about the desired composition, was placed in a test-tube, 150 mm. × 25 mm. Unless solution was formed by transition, the desired amount of water was added. The tube was placed in a thermostat. After a few hours, with occasional stirring, equilibrium was reached, as indicated by agreement in analysis when the period of stirring was varied and whether the approach was from undersaturation or supersaturation.

Liquid free from solid phase, and moist solids, were obtained by filtration through paper on a small büchner funnel.

Data for the condition of equilibrium resulting when liquid and a second solid phase were formed by transition of

(1) W. E. Cadbury, Jr., W. B. Meldrum and W. W. Lucasse, *J. Am. Chem. Soc.*, **63**, 2262 (1941).

(2) W. E. Cadbury, Jr., *ibid.*, **67**, 262 (1945).

(3) J. E. Ricci and W. F. Linke, *ibid.*, **73**, 3607 (1951).

(4) Ref. 1, p. 2263; ref. 2, p. 262.

decahydrate were obtained as follows: a sample of decahydrate solid solution of suitable composition was warmed until partial transition had occurred; the tube containing the mixture was placed in the thermostat, set at approximately the desired temperature, and when the temperature of the mixture was constant, a liquid sample was filtered off and analyzed.

For analysis, the samples, whether liquid or moist solid, were transferred to weighed weighing bottles. Percentage water was determined from the loss in weight after the sample had been heated for several hours to about 150°. In samples where sodium sulfate was in excess, sodium molybdate was determined directly, and *vice versa;* the other salt was determined by difference. As a check on the analytical method, both salts were determined directly in a few cases.

Sodium molybdate was determined by the indirect Volhard method, as in ref. 3. Sodium sulfate was determined as follows. The sample, dissolved in about 100 ml. of water, was heated to boiling and a slight excess of silver nitrate solution was added to remove molybdate as insoluble silver molybdate. This precipitate was filtered off, and a slight excess of hydrochloric acid solution was added to remove excess silver. After the precipitate of silver chloride was filtered off, sulfate was determined in the usual way by precipitation as barium sulfate.

Results

In Table I are given representative data on solubility measurements at the various temperatures. The solid phases are indicated as follows: A, Na_2MoO_4; A_2, $Na_2MoO_4 \cdot 2H_2O$; A_{10}, $Na_2MoO_4 \cdot 10H_2O$; B, Na_2SO_4; B_{10}, $Na_2SO_4 \cdot 10H_2O$; S_A, decahydrate solid solution containing very little B_{10}; S_B, decahydrate solid solution containing appreciable A_{10}.

The relations covered are indicated in the polythermal diagram, Fig. 1. For clarity, the figure is distorted somewhat; correct quantitative values can be inferred from the tables and from later figures. Dotted segments of the boundary curves indicate the general direction of some equilibrium conditions possible in this system which were not investigated in this study.

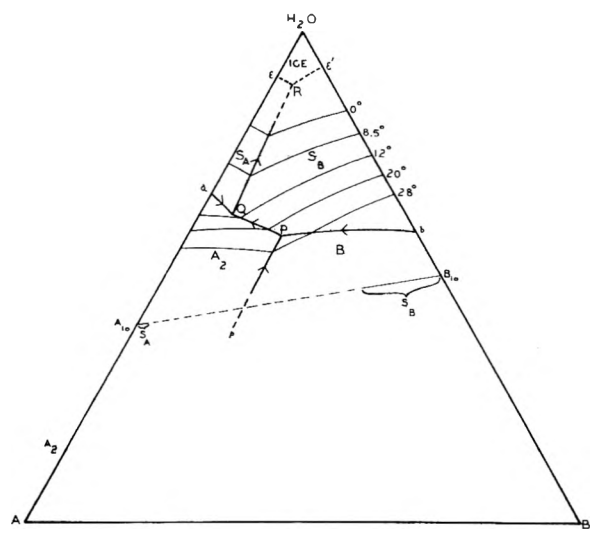

Fig. 1.—Polythermal solubility diagram for the system Na_2SO_4–Na_2MoO_4–H_2O (not to scale).

Each of the polythermal boundary curves, on which the direction of decreasing temperature is indicated by arrows, represents equilibrium among liquid solution and two solid phases. These solid phases are as follows: along bP, S_B and B; along PQ, S_B and A_2; along aQ, S_A and A_2; along QR, S_A and S_B; along pP, A_2 and B.

TABLE I

SOLUBILITY DATA: SYSTEM Na_2SO_4–Na_2MoO_4–H_2O

Temp., °C.	Satd. soln. Na_2SO_4, %	Satd. soln. Na_2MoO_4, %	Moist solid Na_2SO_4, %	Moist solid Na_2MoO_4, %	Solid phase
0	4.46	0	...	...	B_{10}
	3.32	7.00	38.48	1.11	S_B
	2.23	13.86	36.62	3.02	S_B
	1.16	29.10	33.55	8.34	S_B
	1.08	31.24	8.40	38.40	S_B, S_A
	0.81	31.52	1.02	48.80	S_A
	0.56	31.12	0.72	54.15	S_A
	0	30.60	...	...	A_{10}
8.5	7.74	0	...	...	B_{10}
	5.74	7.75	37.89	1.68	S_B
	3.40	20.66	30.71	7.73	S_B
	2.45	31.37	30.10	11.98	S_B
	1.90	36.91	6.10	41.82	S_B, S_A
	1.51	36.95	1.83	47.56	S_A
	0.81	37.67	0.89	49.32	S_A
	0	37.29	...	...	A_{10}
12.1	9.65	0	...	...	B_{10}
	8.85	2.40	40.40	trace	S_B
	6.32	12.68	36.76	3.21	S_B
	4.00	23.29	39.90	2.50	S_B
	3.02	34.03	31.46	11.36	S_B
	2.87	36.57	31.47	12.54	S_B
	2.93	36.52	0.76	73.54	A_2
	0.49	38.60	0.13	70.32	A_2
	0	39.08	...	...	A_2
20.0	15.96	0	...	...	B_{10}
	13.82	5.04	40.20	0.66	S_B
	10.97	14.22	37.15	3.48	S_B
	7.03	28.49	34.75	8.11	S_B
	6.42	34.10	27.09	22.82	S_B, A_2
	6.22	34.36	2.74	61.07	A_2
	2.99	37.28	1.58	56.78	A_2
	1.96	37.56	1.44	52.18	A_2
	0	39.30	...	...	A_2
28.0	25.54	0	...	...	B_{10}
	20.80	10.11	41.48	1.26	S_B
	17.22	17.87	36.71	5.80	S_B
	15.78	22.97	62.30	2.97	S_B, B
	12.42	28.09	90.33	3.45	B
	11.84	29.06	89.09	4.53	B
	10.06	31.56	58.63	25.36	B, A_2
	7.07	33.69	2.73	64.52	A_2
	1.78	38.17	0.78	64.09	A_2
	0	39.74	...	...	A_2

Points a and b represent transition points, A_{10} + cal. → A_2 + L, and B_{10} + cal. → B + L, respectively. The curves aQ and bP are transition curves, along which a new solid and solution, L, are formed by adding heat to a decahydrate solid solution: S_A + cal. → A_2 + L and S_B + cal. → B + L, respectively.

The curve PQ represents equilibrium among solution, S_B, and A_2: L → S_B + A_2 + cal.; *i.e.*, S_B and A_2 separate out when the saturated solution is cooled.

The points P and Q are quadruple points, invariant points at constant pressure in a three-component

system. They are transition points at which the reactions on cooling are: at P: L + B → S_B + A_2 + cal., and at Q: L + A_2 → S_A + S_B + cal.

Isothermal solubility data were obtained at five temperatures: 0, 8.5, 12.1, 20.0 and 28.0°. In their study of this system at 25° Ricci and Linke[3] observed that sodium sulfate decahydrate dissolves some sodium molybdate decahydrate in solid solution, but that sodium molybdate dihydrate does not dissolve detectable amounts of sodium sulfate. The data reported here lead to the same conclusion at these temperatures, as well as to the conclusion that sodium molybdate decahydrate dissolves a small amount of sodium sulfate decahydrate at temperatures at which the molybdate decahydrate is stable. There is no evidence that anhydrous sodium sulfate dissolves any sodium molybdate.

Figure 2 shows the data for 0°, plotted to scale on rectangular coördinates. The line EF on this and subsequent figures represents calculated compositions of decahydrate solid solutions of sodium molybdate and sodium sulfate. The tie lines, located after analysis of solutions and corresponding slightly moist solids, show that the solid phases in equilibrium along the two branches of the curve are respectively sodium sulfate decahydrate (B_{10}) containing some sodium molybdate in solid solution, and sodium molybdate decahydrate (A_{10}) containing very little sodium sulfate in solid solution. These are the phases designated above as S_B and S_A, respectively, indicated on the polythermal diagram (Fig. 1) by the solid portions of the line joining A_{10} and B_{10}. The break in the curve in Fig. 2 gives the location of the 0° point on QR of Fig. 1.

Figure 3 shows the data for 12.1°. The tie lines in this figure show that the solid phases are decahydrate solid solution, S_B, as before, and sodium molybdate dihydrate, A_2. The break in this curve gives the location of the 12.1° point on PQ of Fig. 1.

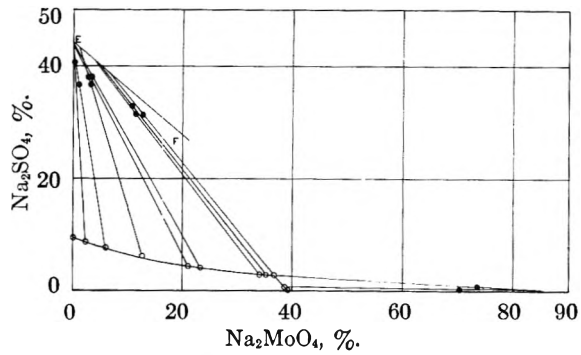

Fig. 3.—System Na_2SO_4–Na_2MoO_4–H_2O at 12.1°.

Isotherms at 8.5 and 20.0° are omitted, since they are similar in all except quantitative aspects to those at 0° and 12.1°, respectively.

Figure 4 is a plot of the data obtained at 28.0°. Three different solid phases can exist at this temperature, as indicated by the three branches of the curve. Two of these solids are S_B and A_2, the same as those which can exist at 12 and 20°; the third, represented by the middle branch of the curve, is anhydrous sodium sulfate. The break, J, in the 28° isotherm corresponds to a point on bP of Fig. 1, and the second break, K, on the same isotherm gives a point on Pp.

Other points along the curve bP were located, as described above, by analyzing the solutions formed

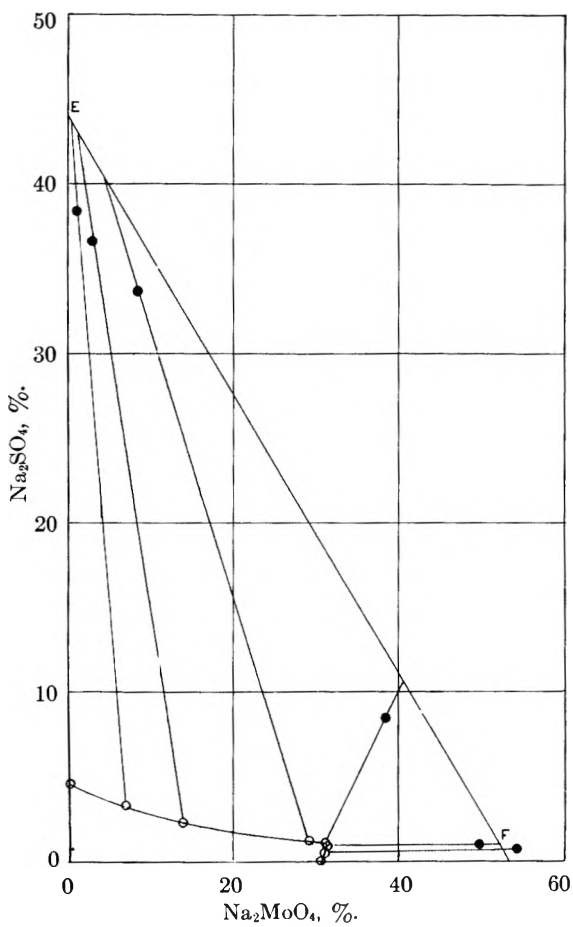

Fig. 2.—System Na_2SO_4–Na_2MoO_4–H_2O at 0°.

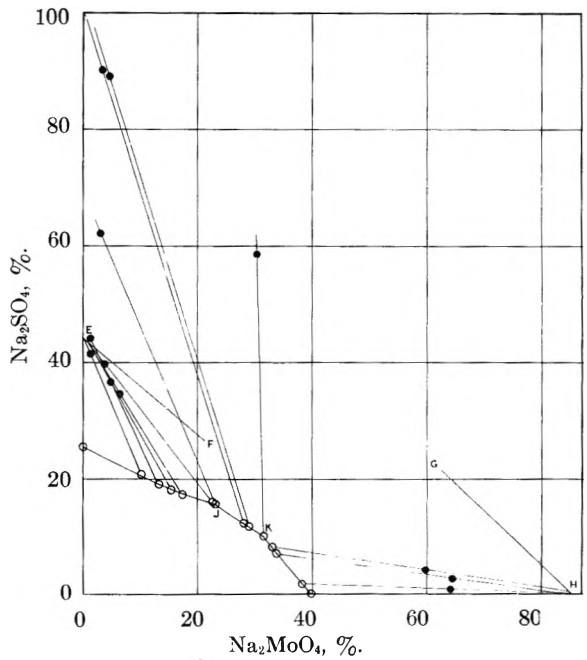

Fig. 4.—System Na_2SO_4–Na_2MoO_4–H_2O at 28°.

at measured temperatures by partial transition of decahydrate solid solutions, S_B, of various compositions.

Attempts to locate the curve aQ by an analogous method, by warming solid solutions S_A, gave results which were not satisfactorily reproducible. Since this curve is so short, however, it was located with sufficient precision by determining its extremities only, points a and Q.

Data for curves bP and aQ, Fig. 1, are given in Table II.

TABLE II

CONCENTRATIONS ALONG TRANSITION CURVES

t, °C.	Na_2MoO_4, %	Na_2SO_4, %	Solid phases
	Along curve bP		
32.4	0	33.1	B_{10}, B
31.1	8.9	26.2	S_B, B
29.0	18.5	19.0	S_B, B
27.0	25.2	14.2	S_B, B
24.8	30.3	11.0	S_B, B, A_2
	Along curve aQ		
10.3	39.0	0	A_{10}, A_2
9.8	37.3	2.2	S_B, A_2, S_B

The curve QR is the locus of points representing breaks in the appropriate isothermal solubility curves, such as those at 0 and 8.5°, where S_B and S_A can exist in equilibrium with solution. The curve PQ is the locus of points representing breaks in the isothermal curves where S_B, A_2 and solution can coexist, as at 12.1 and 20°.

The quadruple point, P, was located as follows: A mixture of B and B_{10}, together with solution of approximately the right composition, and another mixture of B and A_2, with the appropriate liquid, were prepared. These mixtures were placed in two test-tubes in a thermostat at 28°, and after equilibrium was reached, a sample of liquid was removed and analyzed. This was repeated at temperatures of 25.8 and 24°. The data obtained are given in Table III.

As the temperature goes down, the % sodium sulfate in the first mixture decreases and the % sodium molybdate increases; in the second mixture, the reverse is true. The ratio of sodium sulfate to sodium molybdate was plotted against temperature for each mixture; the temperature where the two curves cross—24.8°—is the desired point, the temperature at which a liquid phase of definite composition can exist in equilibrium with three solid phases. The composition of the liquid at this point, determined by analysis of a solution in equilibrium with the three solids at this temperature, is given in line 5 of Table II.

TABLE III

DATA FOR LOCATION OF POINT P, FIG. 1

t, °C.	Mixture L–B–B_{10} Na_2SO_4, %	Mixture L–B–B_{10} Na_2MoO_4, %	Mixture L–B–A_2 Na_2SO_4, %	Mixture L–B–A_2 Na_2MoO_4, %
28.0	15.7	23.0	10.1	31.5
25.8	12.5	27.2	10.8	30.5
24.0	9.6	30.9	11.0	30.3

The quadruple point, Q, was located by mixing the three solids, A_{10}, B_{10}, and A_2, with a little water at 9.5°. (On standing, the solids A_{10} and B_{10} were doubtless converted to solid solutions, S_A and S_B; whether diffusion is sufficiently rapid to result in internal equilibrium in the solid is immaterial, since equilibrium between the solution and the surface of the solid is established rapidly.) After this mixture had stood for some time, with occasional stirring, in a thermostat adjusted to the temperature of the mixture, the temperature became constant at 9.82°, and a sample of the solution was removed for analysis. As a further check, the rest of the liquid was returned to a tube in the thermostat, set at 9.8°, containing a mixture of the three solids. This mixture was stirred from time to time; after temporary slight changes, the temperature became constant at 9.81°. Analysis of samples of the liquid gave results not significantly different from those obtained before. The composition, which is that of point Q, is given in the last line of Table II.

The author wishes to express his thanks to the Chemistry Department of the University of Colorado for making available to him their facilities while much of this study was being made.

THE SODIUM DIFFUSION FLAME METHOD FOR FAST REACTIONS. I. THEORY OF THE EXPERIMENTAL METHOD[1,2]

BY JOHN F. REED[3] AND B. S. RABINOVITCH

Contribution from the Department of Chemistry of the University of Washington, Seattle, Washington

Received October 1, 1954

A critical analysis of the diffusion flame method for sodium atom reactions has been made. When the streaming velocity is considered in the differential equation of continuity and the flow of sodium into the system used as a boundary condition, flame shapes are distorted from spherical and calculated rate constants lowered from those calculated in the conventional manner. Consideration of halide back diffusion leads to an interpretation of the lower v/D limit which is determined by experimental variables and the reaction rate constant. Heller's lower limit is found to be a special case. Halide distribution in the flame is briefly discussed.

The reaction between metal vapor, usually sodium, and alkyl halides in the gas phase has been studied by numerous workers[4] and demonstrated to be essentially the removal of the halogen atom from the alkyl halide by the sodium atom in a bimolecular step. The reaction occurs with an activation energy generally less than 10 kcal./mole and flow systems have been used to study the kinetics of the reactions.

The system used is frequently patterned after the diffusion flame method so brilliantly pioneered by Hartel and Polanyi.[4] The usual measurements made on the system when it has attained the steady state are the halide pressure, the total pressure, the temperature of the reaction zone, the diameter of the flame and the pressure of sodium as it is fed into the system. This latter quantity is identified with the vapor pressure of sodium at the temperature of the carburetor from which the sodium is swept by carrier gas. To relate the measurements to the specific rate constant, the hydrodynamic equation of continuity has been used with approximations.[4] The original treatment of Hartel and Polanyi was semi-quantitative. Later, in an important extension, Heller[5] evaluated experimentally a number of aspects of the flow and placed some restrictions on the allowed range of variation of some of the experimental parameters.

A number of aspects of the above treatments warrant further examination. It also appears desirable to attempt a solution of a more accurate representation of the equation of continuity applied to the transport of sodium and halide. In the present paper, a number of features of the experimental method are investigated. The main conclusions apply to reactions between other materials as well.

The General Equation of Continuity.—In the flame, sodium is depleted chemically by a bimolecular step in which sodium halide is formed and a free radical liberated. Processes wherein sodium is depleted by additional reactions, *e.g.*, with halogenated free radicals, are discussed later and in a following paper.[6] The general equation of continuity for any species in an isothermal system is given by

$$\nabla(D_i \nabla p_i) - \nabla(p_i \mathbf{V}) + Q_i = \partial p_i/\partial t \qquad (1)$$

where D_i is the ordinary diffusion coefficient of the ith species in the gas mixture, p_i is the pressure of the ith species, Q_i is the rate of production of the ith species in an element of volume and $\mathbf{V}$ is the mass averaged velocity of the gas mixture at the point, *i.e.*

$$\mathbf{V} = \sum_i \gamma_i \mathbf{V}_i \qquad (2)$$

where $\mathbf{V}_i$ is the velocity of the ith component, and γ_i is the weight fraction of the ith component.

In the steady state, $\partial p/\partial t = 0$. For both sodium and halide in the flame, Q_i is given by $-kpp'$, where p and p' are the respective pressures and k is the specific rate constant. Since the pressure in the system is constant, the diffusion coefficient is taken to be constant in space. The steady-state differential equation for sodium transport is thus given by

$$D\nabla^2 p - \nabla(p\mathbf{V}) - kpp' = 0 \qquad (3)$$

A similar equation may be written for alkyl halide. The solution of these equations for various approximations and applications will now be considered.

Halide Back Diffusion. No Wall Reaction.—An important aspect of the flow of sodium is the problem of alkyl halide back diffusion into the nozzle from which the sodium streams. As a model consider that sodium streams down a uniform nozzle tube in a gas mixture traveling with constant velocity from the source (carburetor), at $z = \infty$, to the nozzle at $z = 0$. The velocity is given as $\mathbf{V} = -v\mathbf{k}$ where v is a constant scalar and $\mathbf{k}$ is the unit vector along the positive z-axis. The cross-section of the tube is taken constant and equal to πr_0^2 where r_0 is the radius. The steady-state equation of continuity for alkyl halide is

$$D' \frac{\partial^2 p'}{\partial z^2} + v \frac{\partial p'}{\partial z} - kpp' = 0 \qquad (4)$$

As a useful simplification, the pressure of sodium in the tube is considered constant and equal to the pressure in the carburetor, p^*, and wall reaction is neglected. The latter problem is discussed below. An analytic solution for the halide pressure as a function of z may be found (App. I)

$$p' = p_0' \exp[-(a + b)z/2];\ a = v/D';$$
$$b^2 = a^2 + 4kp^*/D' \qquad (5)$$

(1) Presented before the Division of Inorganic and Physical Chemistry of the American Chemical Society at the Los Angeles meeting, March, 1953.

(2) Abstracted in part from a thesis submitted by John F. Reed in partial fulfillment of the requirements for the degree of Doctor of Philosophy at the University of Washington.

(3) Department of Chemistry, Loyola University, Chicago, Illinois.

(4) H. V. Hartel and M. Polanyi, *Z. physik. Chem.*, **B11**, 97 (1930); reviews have been given by M. Polanyi, "Atomic Reactions," Williams and Norgate, London, 1932; C. E. H. Bawn, *Chem. Soc. Ann. Reps.*, **39**, 36 (1942); E. Warhurst, *Quart. Revs.*, **5**, 44 (1951).

(5) W. Heller, *Trans. Faraday Soc.*, **33**, 1556 (1937).

(6) J. F. Reed and B. S. Rabinovitch, THIS JOURNAL, to be submitted.

where p_0' is the pressure of halide at $z = 0$. Since all the halide that enters the tube is consumed, the net flow of halide into the tube is found by integrating the amount of reaction over the entire volume of the tube. Use of the sodium carburetor pressure gives the maximum flow of halide into the tube. From the net flow of sodium out of the tube, the effective pressure of sodium as it leaves the nozzle, p^e, is then given by (App. I).

$$p^e = (1 - 2kp_0'/v(a + b))p^* \qquad (6)$$

This is an upper limit to depletion since sodium pressure was set constant at the largest value, p^*.

Several conclusions may be drawn from equation 6. In line with qualitative reasoning, it is evident that the sodium pressure is depleted less for slow reactions, low halide pressure at the nozzle, low diffusion coefficient of halide into the gas mixture and high streaming velocity. In particular, it is seen that a fixed value of the v/D' (or v/D) ratio does not suffice to specify the depletion of sodium due to back diffusion of alkyl halide. Not only does one need to know the collision yield (as k), but also the halide pressure at the nozzle and, further, the actual streaming velocity. These questions arise because the conclusions of Heller[5] have frequently been assumed to imply that only the v/D ratio (for reactions with collision yields of the order of 50–5000) is needed to effectively evaluate back diffusion. Heller had selected a lower allowable limit of v/D of 5.5 cm.$^{-1}$ on the basis that it is at this value that the halide pressure in front of the nozzle, p_0' is reduced by streaming to about 10% of the halide pressure outside the flame; for some experimental conditions, this would make the halide and sodium pressures about equal at the nozzle. However, even under such circumstances, back diffusion and reaction could be sufficient to deplete the sodium pressure significantly. It is evident that a fixed lower v/D limit is too arbitrary. The finding here is that a number of additional factors enter explicitly into the determination of sodium depletion due to back diffusion.

Application of the above equation to some actual data[6] indicates that with an arbitrary allowable depletion of sodium of 2% (*i.e.*, $p^e/p^* = 0.98$) a v/D ratio of as low as 1.0 cm.$^{-1}$ could be used in some cases. By varying the parameters of a run, such as the total pressure or the streaming velocity of gas out of the nozzle, various suitable lower limiting values may be found. In particular, the above equation can be used to evaluate the net pressure of sodium as it is fed by the nozzle when the flow parameters and reactivity are known for any run.

The upper limit for v/D given by Heller is 12 cm.$^{-1}$ and corresponds to an arbitrary, practical limitation on the allowable depletion of halide in the flame just outside the nozzle due to streaming from the nozzle; Heller also suggests that turbulence in the flame becomes appreciable at higher values. In a later section a distribution function for halide in the flame, for the case $v \neq 0$, is given (equation 15). This is based on the approximation of a constant velocity averaged through the flame and has only qualitative validity. If a precise distribution function for halide in the flame were known then, for this factor, values of v/D considerably in excess of Heller's upper limit would obviously become acceptable. In the absence of such a function, the errors are limited by restraining the upper limit of v/D as much as is experimentally feasible.

Halide Back Diffusion. Wall Reaction.—The extent of wall reaction in the nozzle tube affects the sodium pressure as it issues from the nozzle. If wall reaction is insignificant, then the above calculations on the net sodium pressure at the nozzle are unaffected. The sodium nozzle pressure is less if wall reaction takes place. Some conclusions may be obtained as follows.

The steady-state equation for halide in the nozzle tube is

$$D'\nabla^2 p' + v\frac{\partial p'}{\partial z} - kpp' = 0 \qquad (7)$$

If a gradient in the direction perpendicular to the wall exists due to wall reaction, then a solution to equation 7 may be found in terms of the coördinates z and ρ. A satisfactory solution (App. II) is given by

$$p' = B' \exp[-(\lambda + v/2D)z]J_0(n\rho) \qquad (8)$$

where B' is a constant of integration, $\lambda^2 = (v/2D')^2 + n^2$, n is a separation parameter of the differential equation and $J_0(\eta\rho)$ is a zero-th order Bessel function. On the assumption that reaction at the wall is equal to the net amount of halide diffusing to the wall in the steady state, the ratio of total amount of gas phase reaction to wall reaction, w, reduces to

$$w = kp^*/D'n^2 \qquad (9)$$

The magnitude of n depends on the boundary value of the halide pressure at the wall relative to that at the center of the tube. If this ratio is designated $\bar{\alpha}$, $(1 \geq \bar{\alpha} \geq 0)$, n is determined by the first root of

$$J_0(nr_0) = \bar{\alpha} \qquad (10)$$

where r_0 is the radius of the tube.

Heller has implied that wall reaction is rapid. Unfortunately, there is no clear information on the magnitude of wall reaction, *whether indeed it is different from zero*, so it is impossible to specify the value of $\bar{\alpha}$. If $\bar{\alpha} \sim 0$, then for some reasonable values for the parameters of equation 9 wall reaction would be approximately 2000 times that of the gas phase. Such an immense amount of reaction would reduce the sodium pressure to a negligible value and essentially no sodium would issue from the nozzle. It would appear therefore that wall reaction does not occur on every collision. For $\bar{\alpha} = 0.9$, wall reaction could still be as much as 80 times the gas phase reaction, which would reduce the sodium flow out of the nozzle to a relatively small value. Polanyi and Hartel[4] suggest that heterogeneous reaction occurs with alkyl fluoride but this seems unsubstantiated.

If wall reaction in the nozzle tube, which must take place on an alkali halide coated surface, were significant with respect to gas phase depletion, then the entire treatment of sodium flames *might* be in error; inasmuch as there *may* be some nucleation of sodium halide in the flame, the presence of which would provide surface for heterogeneous reaction.

The tacit assumption seems always to have been made in the literature that either heterogeneous reaction is negligible, or else nucleation does not take place in the flame. Explicit experimental evidence on the magnitude of heterogeneous reaction is highly desirable.

Halide Distribution in the Flame.—Cvetanovic and Le Roy,[7] in an interesting extension, have examined the problem of halide distribution in the flame on the basis of diffusion as the sole transport process for both sodium and halide in the flame. The pressure of halide was obtained as an analytic function of the sodium pressure and the radial coordinates, r. This halide pressure function was not suitable for an analytic solution of the sodium steady-state aquation. However, it was possible to determine the effect of using such a variation of halide pressure in space on the value of a computed rate constant. An undetermined parameter of their result was the pressure of halide at the nozzle, *i.e.*, at $r = r_0$; in their computation it was necessary to assume a value. This pressure was taken by them to be zero, although, as they point out, other boundary values could be used. Utilizing the pressure distribution function given by Cvetanovic and LeRoy, the pressure of halide at the nozzle may be related to the sodium flow into the system.[8] The calculation shows that under the usual experimental conditions the halide pressure is not significantly reduced at the nozzle if the one transport is by diffusion. The actual halide pressure at the nozzle as shown experimentally by Heller is of course appreciably reduced, but due to streaming, a process which is usually neglected in the transport equation. It thus appears desirable to consider this type of transport since under the conventional conditions of large excess of halide over sodium this is the process which results in halide depletion in the flame.

For the case where the amount of sodium in the flame is much smaller than halide, reaction may be neglected. Then for the halide steady state

$$D'\nabla^2 p' - \nabla(p'\mathbf{V}) = 0 \qquad (13)$$

Introducing as a simplification for $\mathbf{V}$ a constant average velocity in the flame, $\mathbf{V} = \bar{v}\mathbf{k}$, the above becomes

$$D'\nabla^2 p' - \bar{v}\partial p/\partial z = 0 \qquad (14)$$

A solution to this equation possessing cylindrical symmetry and satisfying the boundary conditions $p'(\infty) = p'^*$, $p'(r_0) = p_0' < p'^*$ is

$$p' = p'^* - (p'^* - p_0')\frac{r_0}{r}\exp[(z - r + r_0)\alpha]; \quad \text{where } \alpha = \bar{v}/D' \qquad (15)$$

This function is compatible with a pressure of halide at $r = r_0$ that is significantly reduced, even to zero. This pressure function, however, when averaged over the flame gives a value only slightly less than p'^*. The pressure fall with distance is significant only in the region of the nozzle. Use of this function in the sodium equation of continuity would consequently not change the results much since the halide pressure is relatively constant, at p'^*, throughout the flame. Hence the halide distribution obtained in this approximation agrees only qualitatively with the experimental finding of Heller. Failing a solution to the equation incorporating a space dependent function of velocity it is felt that a reasonable practical approach to the nature of halide distribution is acceptance of a correction factor based on Heller's data. His data, however, appear to be unique for the conditions used. The nozzle size (or cross-section of the flux out of the nozzle) in particular does not enter expressly into his suggested correction. By a dimensional argument, this can be taken into account[8]; this analysis yields

$$f = \frac{r_H - r_0}{r_H} + \frac{r_0 f_H}{r_H} \qquad (16)$$

where f is the correction factor to be applied to yield the *average* pressure of halide in the flame, r_H the radius of Heller's nozzle, r_0 the radius of the nozzle of any other system, and f_H the correction factor deduced by Heller. The values of f_H are found in Heller's work as a function of flame size and of v_0/D.

Very recently, a calculation of the effect of atmosphere reactant distribution in the flame on rate constants has been developed by Smith[9] in which a diffusion model is used and an analytical solution obtained.

Sodium Distribution in the Flame. Pressure at the Nozzle.—Polanyi and Hartel[4] and following workers have assumed in their treatment of the sodium diffusion flame that the effect of streaming of gas out of the nozzle is negligible for the transport of sodium in the flame. To this approximation, the steady-state equation of continuity for sodium is

$$D\nabla^2 p - kpp' = 0 \qquad (17)$$

This equation was solved by using a spherical Laplacian in the radial coördinate, r, and by setting the pressure of halide, p' (present in large excess), constant in the flame. The solution subject to the boundary condition $p(\infty) = 0$ is

$$p = A\exp(-Cr)/r; \; C^2 = kp'/D \qquad (18)$$

From the second boundary condition, $p(r_0) = p_0$, there is obtained

$$p = \frac{p_0 r_0}{r}\exp[-C(r - r_0)] \qquad (19)$$

Polanyi and Hartel used the nozzle radius for r_0 and set p_0 equal to the carburetor pressure of sodium, p^*. Some question arises with regard to this latter assumption inasmuch as the locus of points for which $r = r_0$ corresponds not to the nozzle but rather to a sphere of radius r_0, and the pressure of sodium on this hypothetical sphere may correspond to some value other than p^*.

A different method of evaluating the constant A may be used as suggested by the work of Garvin and Kistiakowsky.[10] Since all of the sodium is consumed in the flame, the total amount of sodium reaction per second in the steady state is set equal

(7) R. J. Cvetanovic and D. J. Le Roy, *Can. J. Chem.*, **29**, 597 (1951).

(8) For further details, see J. F. Reed, Ph.D. Thesis, University of Washington, 1953; available on microfilm, University Microfilms, Ann Arbor, Michigan.

(9) F. T. Smith, *J. Chem. Phys.*, **22**, 1605 (1954).

(10) D. Garvin and G. B. Kistiakowsky, *ibid.*, **20**, 105 (1952).

to the flow rate of sodium into the system in moles per second, b_0. When this is done the constant A is found to have the value

$$A = \frac{b_0 RT \exp(Cr_0)}{4\pi D(1 + Cr_0)} \quad (20)$$

Further, the quantity to be taken for p_0 may be evaluated from the relation $A = p_0 r_0 \exp(Cr_0)$ and is

$$p_0 = r_0 v_0 p^*/4D(1 + Cr_0) \quad (21)$$

where v_0 is the average streaming velocity of the carrier gas at the nozzle.

In general, $Cr_0 < 1$. For a nozzle with $r_0 = 0.1$ cm. and with $v_0/D = 10$ cm.$^{-1}$, somewhat representative of values normally used, it is seen that p_0 is approximately 0.25 p^*. The evaluation of constant A by this method obviates the need to explicitly associate any particular pressure with the points $r = r_0$. From the form of this last equation, it may appear that p_0 would exceed p^* at high values of v_0. Of course this cannot occur and when velocities of this magnitude are encountered, it is apparent that the original differential equation of continuity must allow for transport by streaming.

If the pressure at the edge of the flame is the limiting detectible pressure, p_1, at $r = R$, the specific rate constant is obtained as

$$k = \frac{(\ln p_0 r_0/p_1 R)^2 D}{(R - r_0)^2 p'} \quad (22)$$

For purposes of comparison, the rate constant calculated by use of equation 22 is designated $k^{(0)}$ when p_0 is set equal to p^*, as done by Polanyi and and Hartel, and k^1 when p_0 is taken from equation 21.

Sodium Distribution in the Flame. The Case of Constant Streaming Velocity.—Measurement of the flame diameter has conventionally been made "head-on" to the flame, along the flow axis. Observations of the flame perpendicular to the flow axis however show that the flame is not actually spherical, but rather slightly oval, with the major axis along the flow axis and with the apparent center of the flame displaced along the flow axis. Since the diffusion velocity of sodium at the nozzle and the linear streaming velocity of the issuing gas mixture at the nozzle may be shown explicitly to be of the same order of magnitude under the usual conditions,[8] it is not surprising that some effect occurs due to streaming. Streaming is taken into account explicitly in the equation of continuity by a term $\nabla(p\mathbf{V})$. Unfortunately, the nature of the variation of $\mathbf{V}$ with the radius vector in the flame for a nozzle source is not known, and even for some assumed simple ideal functional forms, *e.g.*, r^{-2}, the differential equation of continuity appears analytically insoluble. Perhaps the simplest manner of introducing a term to account for the effect of streaming is by using a constant velocity in the flame. This constant velocity is to be interpreted as an average over the entire flame, and to arise from the streaming of gas out the nozzle. This velocity should be directed along the flow axis corresponding to origination of the momentum flux in the nozzle. To determine the effect of including such a term in the equation of continuity, the velocity is first included as a parameter with an unspecified value, *i.e.*, set

$$\mathbf{V} = v\mathbf{k} \quad (23)$$

where v is a constant scalar, and $\mathbf{k}$ is the unit vector along the flow axis designated as the z-axis. The equation of continuity for sodium now becomes

$$D\nabla^2 p - v\partial p/\partial z - kpp' = 0 \quad (24)$$

A solution for p, satisfying the boundary condition that at infinity the pressure of sodium is reduced to zero, is[11]

$$p = \frac{A'}{r}\exp(\alpha z - \beta r);\ \alpha = v/2D;\ \beta^2 = \alpha^2 + kp'/D \quad (25)$$

where r is the radial coördinate (App. III). The constant A' is evaluated as before by setting the flow rate of sodium into the system equal to the total amount of reaction per second. Thus

$$A' = \frac{(r_0/4)(v_0/D)p^* r_0 \exp(Cr_0)}{(1 + \beta r_0 + \alpha^2 r_0^2/2)} \quad (26)$$

The functional dependence of p on the coördinates is identical with the previous case except for a factor $\exp(\alpha z)$, the effect of which is essentially to remove some of the sodium from behind the nozzle and place it in front, which is the effect that streaming actually has on the symmetrical distribution. The solution gives the pressure contour an oval shape with an apparent center of the oval displaced along the flow axis. When the velocity parameter, v, is reduced to zero, the solution for p reduces to that obtained previously on the assumption that the velocity was negligible.

In order to put the pressure dependence in a form analogous to that used by Polanyi and Hartel, a quantity π_0 is defined corresponding to the points for which $r = r_0$, $z = 0$. Such points lie on a ring at the nozzle. Then

$$p = \frac{\pi_0 r_0}{r}\exp[\alpha z - \beta(r - r_0)];\ \pi_0 = \frac{(r_0/4)(v_0/D)p^*}{(1 + \beta r_0 + \alpha^2 r_0^2/2)} \quad (27)$$

The flame "height," P, is a measured quantity, corresponding to the maximum distance from the z-axis to the edge of the flame along the p_1 contour. This measurement is made at distance Z along the z-axis in front of the nozzle. The distance from the nozzle to the flame edge at the point in question is R. Thus

$$R^2 = P^2 + Z^2 \quad (28)$$

Further

$$(\partial p/\partial z)_{R,Z} = 0 \quad (29)$$

Using this condition on the pressure function given by equation 27, there results

$$Z = \alpha R^2/(1 + \beta r) \quad (30)$$

The value of the specific rate constant in terms of R and Z is designated $k^{(2)}$ and is given by

$$k^{(2)} = \left\{\left[\frac{\ln(\pi_0 r_0/p_1 R) + \alpha Z}{R - r_0}\right]^2 - \alpha^2\right\}\frac{D}{p'} \quad (31)$$

Equations 28, 30 and 31 give three relations among the variables k,[(2)] v (contained in α), P, R and Z; all other quantities will be known in a given experiment. Now since P is measured, only one additional measurement or quantity is needed to find the value of the specific rate constant. If the

(11) H. A. Wilson, *Phil. Mag.*, [6] **24**, 118 (1912), has treated a similar equation but with no reaction term.

parameter v is specified by means of some averaging process,[8] then the rate constant can be calculated from the usual measurements made on the system, *i.e.*, from P. However, if instead an additional measurement is made, namely, Z, then v is determined. Recourse may thus be had to the experiment for the evaluation of v. Thus k is calculable from the data of the experiment alone. It is rather obvious that the parameter v is dependent on the linear streaming velocity of gas out the nozzle, v_0; the higher the value of v_0, the greater will be the value of Z and consequently of v.

Comparison of the Various Computed Rate Constants.—The various computed rate constants have the relation

$$k^{(0)} > k^{(1)} > k^{(2)} \qquad (32)$$

The difference between the last two is small, but the difference between the first two is significant, $k^{(1)}$ being generally of the order of one-half to one-tenth $k^{(0)}$. The treatment by which $k^{(2)}$ is derived gives an oval rather than spherical shape to the flame. This last treatment corrects in principle an outstanding discrepancy of the treatment of sodium atom reaction data. It may be noted that an unreasonable result that follows from the conventional derivation of $k^{(0)}$ is that the size of the flame and total amount of reaction is independent of the amount of sodium fed to the flame. Calculation of p_0 in equation 21 and π_0 in equation 27 introduces the flow parameter v_0 into the expressions for $k^{(1)}$ and $k^{(2)}$.

Activation energies computed in the conventional manner from rate constants at a single temperature vary by as much as 2.5 kcal. depending on the extent of approximation in the treatment of the equation of continuity. In general, under usual flow conditions, the activation energy computed from $k^{(1)}$ and $k^{(2)}$ is about 1 kcal. higher than that computed from $k^{(0)}$. In making comparisons of rate data, the differences tend to disappear. The absolute magnitude of sodium atom–alkyl halide rate constants in the literature should be corrected in the direction of decreased reactivity, and the conventional activation energies raised correspondingly.

Some Other Factors.—One factor which has not been treated concerns the observation of the flame edge. It has been assumed that the edge of the flame can be distinguished at a previously determined limiting visible pressure of sodium. However, observations are generally made through a finite thickness of emitting sodium and it is the integrated intensity over the observation path length that is detected by the eye. This can simply be accounted for by assuming that emission intensity is proportional to sodium concentration and, by integrating the point intensities over the path length through which observation is made, the actual intensities can be found. This should be done for both the limiting visibility determination and for the length through the flame edge. Correcting the observations in this way would normally correct diffusion flame data so as to make the rate constant higher than conventionally reported. A rough calculation on this basis indicates that activation energies would be lowered by a few tenths of a kilocalorie when the limiting pressure calibration measurement is made through a thickness of about 6 mm. This correction disappears when differences in activation energies are calculated or compared.

A correction neglected in computing a rate constant for sodium reactions is concerned with depletion of sodium by halogenated species, other than the parent molecule, that appear in the flame, *e.g.*, halogen-containing free radicals. In the simple case where the radical contains n halogen atoms which are all removed by sodium rapidly, relative to the initial process, it is obvious that the rate constant for the primary process computed in the usual way will be in error by at most a factor of $n + 1$. An approximate treatment of the situation for radicals where there is incomplete reaction is discussed elsewhere.[6]

The diffusion coefficient of sodium into the gas mixture enters the calculations. The approximation to this quantity has been the binary diffusion coefficient of sodium into the carrier gas. Use of calculated[12] ternary diffusion coefficients for sodium in halide-carrier gas mixtures offers a more precise quantity.

It may be noted that the treatment given for the flame with a constant streaming velocity corresponds exactly to a system wherein there is diffusion from a point or spherical source into a moving stream.

Acknowledgment.—Thanks are due to the Office of Naval Research for their support. We are indebted to Professor G. H. Cady for his generous cooperation.

Appendix

I. Halide Back Diffusion. No Wall Reaction.—

$$D' \frac{\partial^2 p'}{\partial z^2} + \frac{v \partial p'}{\partial z} - kpp' = 0 \qquad (4)$$

This is a linear, second-order differential equation with constant coefficients. A solution satisfying the boundary conditions $p'(\infty) = 0$, $p'(0) = p_0'$ is

$$p' = p_0' \exp[-(a + b)z/2];$$
$$a = v/D',\ b^2 = a^2 + 4kp^*/D' \qquad (5)$$

The net flow of sodium is given by

$$\pi r_0^2 p^e v/RT = \pi r_0^2 p^* v/RT - \int_0^\infty kp^* p' r_0^2\, dz/RT$$

$$p^e = p^* - \frac{kp^*}{v} p_0' \int_0^\infty \exp[-(a + b)z/2] dz$$

$$p^e/p^* = 1 - 2kp_0'/(a + b)v \qquad (6)$$

II. Halide Back Diffusion. Wall Reaction.—

$$D'\nabla^2 p' + v\partial p/\partial z - kpp' = 0$$

Set

$$p' = \phi(z)R(\rho) \qquad (7)$$

Substituting into the above equation and dividing through by p'

$$\frac{1}{R}\frac{\partial^2 R}{\partial \rho^2} + \frac{1}{\rho}\frac{\partial R}{\partial \rho} + \frac{1}{\phi}\frac{\partial^2 \phi}{\partial z^2} + \frac{v\partial \phi}{D'\partial z} = kp/D'$$

By setting the terms in ρ equal to $-n^2$, and those in

(12) C. F. Curtiss and J. O. Hirschfelder, *J. Chem. Phys.*, **17**, 550 (1949); C. R. Wilke, *Chem. Eng. Prog.*, **46**, 95 (1950).

z equal to $kp/D' + n^2$, the resultant equations may be solved giving

$$R(\rho) = J_0(n\rho);\ \phi(z) = \exp(-vz/2D')[A' \exp(\lambda z) + B' \exp(-\lambda z)] \quad (8)$$

where

$$\lambda^2 = (v/2D')^2 + n^2 + \frac{kp^*}{D}$$

$A' = 0$ from the boundary condition $\phi(\infty) \neq \infty$

Then

$$w = \frac{\text{gas phase reaction}}{\text{wall reaction}} = \frac{\int kpp' dV}{\int_0^\infty -D' \left[\frac{\partial p}{\partial \rho}\right]_{\rho=r_0} 2\pi r_0 dz} = \frac{kp \int_0^\infty \int_0^{r_0} \phi(z) J_0(n\rho) 2\pi\rho \, d\rho \, dz}{-2D'\pi r_0 \int_0^\infty \phi(z) \left[\frac{J_0(n\rho)}{\partial\rho}\right]_{\rho=r_0} dz}$$

The integrals in dz in the numerator and the denominator are the same and thus cancel. From the properties of the Bessel function, the above ratio reduces to

$$w = kp^*/D'n^2 \quad (9)$$

The ratio of halide pressure at the wall to that at the center of the tube is given by $\bar{\alpha}$

$$\bar{\alpha} = \frac{\phi(z)J_0(nr_0)}{\phi(z)J_0(0)} = J_0(nr_0) \quad (10)$$

since $J_0(0) = 1$.

It is seen that this treatment is identical to the previous one if wall reaction is neglected, in which case $n = 0$.

III. Solution to Equation (24).—

$$D\nabla^2 p - v\frac{\partial p}{\partial z} - kpp'$$

is solved by setting $p = \exp(\alpha z)\phi(r)$, where r is the radial coördinate. Then with $\alpha = v/2D$, separation of variables is accomplished giving a solution

$$\phi = \frac{A'}{r}\exp(-\beta r) + \frac{B'}{r}\exp(\beta r)$$

where $\beta^2 = \alpha^2 + kp'/D$. Since $\beta \geqslant \alpha, r \geqslant z$, and $p(\infty) = 0$, then $B' = 0$. Thus

$$p = \frac{A'}{r}\exp(\alpha z - \beta r) \quad (25)$$

ELECTROKINETIC STUDIES ON FIBRINOGEN. V. THE DETERMINATION OF THE ISOELECTRIC POINT BY THE STREAMING POTENTIAL METHOD[1]

BY TAKESHI ABE,[2] ERWIN SHEPPARD[3] AND IRVING S. WRIGHT

The Department of Medicine, New York Hospital-Cornell University Medical College, New York 21, N. Y.

Received October 1, 1954

Streaming potential experiments were performed to determine the zeta potentials for 0.09% fibrinogen solutions (97% clottable) in contact with Pyrex capillaries as a function of *p*H and ionic strength. It is observed that the slopes of the ζ *vs.* *p*H lines decrease as the ionic strength increases and that there are no discontinuities in these lines. Within the limits of the ionic strength range investigated, 0.004–0.013 (phosphate and acetate buffers), it is found that the zero ζ for fibrinogen solutions varied from *p*H 5.85 to 5.95, respectively. These *p*H values are the isoelectric points for fibrinogen at these ionic strength levels. The *p*H of the isoelectric point extrapolated to zero ionic strength occurs at 5.80. It is found that the thickness and tenacity of fibrinogen layers adsorbed on the capillary wall will depend on the *p*H of the initial coating and the *p*H-sequence of subsequent buffer streaming. The zeta potentials observed for the fibrinogen–solid interface are due to the thickness and electrical surface properties of the adsorbed protein layer and to the concentration of electrolyte in solution.

Introduction

The evaluation of the isoelectric point of proteins by the streaming potential technique was first considered feasible by Briggs[4] in 1928. In our investigation of the electrostatic forces involved in blood coagulation,[5] the streaming potential method was used to calculate the zeta potential for fibrinogen solutions, in contact with capillary surfaces, as a function of *p*H. It was found that the zero streaming and zeta potentials occurred at *p*H 5.8 for both human and bovine fibrinogen obtained from Cohn's fraction I.[6] It was stated that this *p*H was also the isoelectric point for the adsorbed proteins.

When Laki[7] described a method to purify bovine fraction I from 40–45% clottable to better than 90%, the determination of the isoelectric point for this purified fibrinogen was undertaken in order to compare the results for the two degrees of purity. Since it has been shown[8-12] that the *p*H of the isoelectric point is dependent on the ionic strength of the solution, μ, the zeta potentials of fibrinogen solutions were determined as a function of *p*H at several low ionic strength levels. It was also of fundamental importance to investigate whether the zeta potential for fibrinogen was due entirely to the adsorbed protein on the capillary wall or to an equilibrium between the adsorbed and the soluble material or electrolyte in the bulk of the solution. Finally, the nature of the adsorbed layer on the capillary wall with respect to its thick-

(1) This is paper number 6 in the series "Electrostatic Forces Involved in Blood Coagulation." This work was supported, in part, by the Office of Naval Research, U. S. Navy under contract N6onr-264, T. O. 10 and also by grants from the Kress, Lasker, Hyde and Hampil Foundations.

(2) Department of Physiology and Pharmacology, Wayne University, College of Medicine, Detroit, Michigan.

(3) To whom inquiries concerning this paper should be addressed.

(4) D. R. Briggs, *Proc. Soc. Exptl. Biol. Med.*, **25**, 819 (1928).

(5) E. Sheppard and I. S. Wright, *Arch. Biochem. Biophys.*, **52**, 414 (1954).

(6) E. J. Cohn, L. E. Strong, W. L. Hughes, Jr., D. J. Mulford, J. N. Ashworth, M. Melin and H. L. Taylor, *J. Am. Chem. Soc.*, **68**, 459 (1946).

(7) K. Laki, *Arch. Biochem. Biophys.*, **32**, 317 (1951).

(8) E. R. B. Smith, *J. Biol. Chem.*, **113**, 473 (1951).

(9) G. Scatchard and E. S. Black, THIS JOURNAL, **53**, 88 (1949).

(10) R. A. Alberty, *ibid.*, **53**, 114 (1949).

(11) L. G. Longsworth and C. F. Jacobsen, *ibid.*, **53**, 126 (1949).

(12) S. F. Velick, *ibid.*, **53**, 135 (1949).

ness and tenacity in the presence of phosphate and acetate buffers was also studied. The results of these experiments are reported herein.

Experimental

Apparatus.—The theoretical aspects of the streaming potential technique used to determine the zeta potential, and the apparatus and methods employed in these investigations have been described previously.[5,13,14] In the work being reported, the thermionic amplifier was used exclusively since dilute protein solutions in low ionic strength buffers were studied. The *p*H of the solutions was taken with a Beckman *p*H meter. The optical densities of the fibrinogen solutions were obtained with a Beckman model DU quartz spectrophotometer.

Materials.—Bovine fraction I (Armour and Co., Chicago, Ill.) containing 42–48% clottable fibrinogen and 40% sodium citrate was purified by the $(NH_4)_2SO_4$ fractionation technique of Laki.[7] The preparations, hereafter designated B.Fr.I-L, were dialyzed against 0.3 *M* KCl and were found to contain approximately 97% clottable fibrinogen. Lorand[15] has demonstrated that during the thrombin induced polymerization of fibrinogen, 3% of the total nitrogen appears as non-protein nitrogen. Therefore, the preparations used in these investigations are to be considered pure fibrinogen. The protein concentrations for the stock B.Fr.I-L solutions were around 0.9%, the details, however, for each subsequent dilution will be given in the text.

The buffers used in these studies were the KH_2PO_4–K_2HPO_4 and sodium acetate–acetic acid combinations and were prepared at varying *p*H and ionic strength levels. The acetate system was made according to the data of Boyd[16] and the phosphate according to Cohn[17] and Green.[18] Analytical reagent grade materials and water distilled in an all Pyrex glass apparatus were used throughout.

Methods.—The clottability of the B.Fr.I-L solutions was assayed by the method of Laki.[7] The protein concentrations of these solutions were obtained by comparing the optical densities of diluted fibrinogen samples at 280 mμ with the values obtained for similar preparations whose nitrogen content had been determined by the Dumas procedure. A nitrogen to protein conversion factor of 5.9 was used.[7]

Clarification of the B.Fr.I-L solutions was achieved by centrifugation at 7000 r.p.m. for 15 min. in a Servall Model SS-1 angle centrifuge. The fibrinogen solutions were prepared prior to the streaming experiment by diluting either 0.5 or 3.0 ml. of B.Fr.I-L to 50.0 ml. with the appropriate buffer also freshly prepared. The former concentration was used in the investigation of the variation of ζ *vs.* *p*H at different ionic strength levels and the latter was used in the coating experiments. The *p*H values of the solutions were taken before and after the streaming experiment, and the mean value was recorded. It is important to point out that the temperature at which the *p*H was measured and the streaming experiments were conducted was the same, namely, room temperature. No provision was made to maintain constant temperature control since it has been reported by Bull and Gortner[19] that the zeta potential of aqueous systems has a negligible temperature coefficient in the vicinity of 25°. The zeta potential was calculated from the equation $\zeta = 4\pi\eta\kappa E/DP$ where η is the viscosity coefficient, κ is the specific conductance of the liquid in the capillary, E is the streaming potential when the liquid is forced through under nitrogen pressure P and D is the average dielectric constant of the liquid in the ionic double layer. The η and D values for water at 25° were used.

Results

The Variation of ζ for Fibrinogen Solutions as a Function of *p*H at Varying μ.—Fibrinogen solutions containing 0.09 mg. protein/ml. were prepared in 0.001, 0.0025, 0.005, 0.0075 and 0.010 ionic strength acetate and phosphate buffers of varying *p*H. The KCl solvent for the B.Fr.I-L solutions contributed an additional 0.003 to the ionic strengths of these series making the final values equal to 0.004, 0.0055, 0.008, 0.0105 and 0.013. These fibrinogen solutions were streamed in the apparatus, a clean Pyrex capillary being used for each experiment, and the zeta potentials for the fibrinogen–Pyrex interfaces were determined.

The low streaming potentials, which were produced in the higher ionic strength buffers, approached the lower limit of the thermionic amplifier's sensitivity. As a consequence, it was necessary to include more experiments in the $\mu = 0.0105$ and 0.013 series than at the lower levels in order to have a sufficient number of experimental points for the evaluation of these data. The method of least squares was used to determine the best line describing the variation of the ζ *vs.* *p*H relationship for the fibrinogen solutions at each μ level.

In Fig. 1, a plot of ζ in mv. *vs.* *p*H, are shown the experimental points for the 0.09% fibrinogen solutions in $\mu = 0.004$ and 0.013 buffers, the lowest and highest μ levels investigated. The equations describing the relationship between the dependent variable, ζ, and the independent variable, *p*H, for the fibrinogen solutions at all μ levels are shown in Table I. Also tabulated are the number of solutions studied in each series and the value of the *p*H when the zeta potential was set equal to zero in the equation. The latter is considered the isoelectric point (I.P.) for fibrinogen at that particular ionic strength.[5]

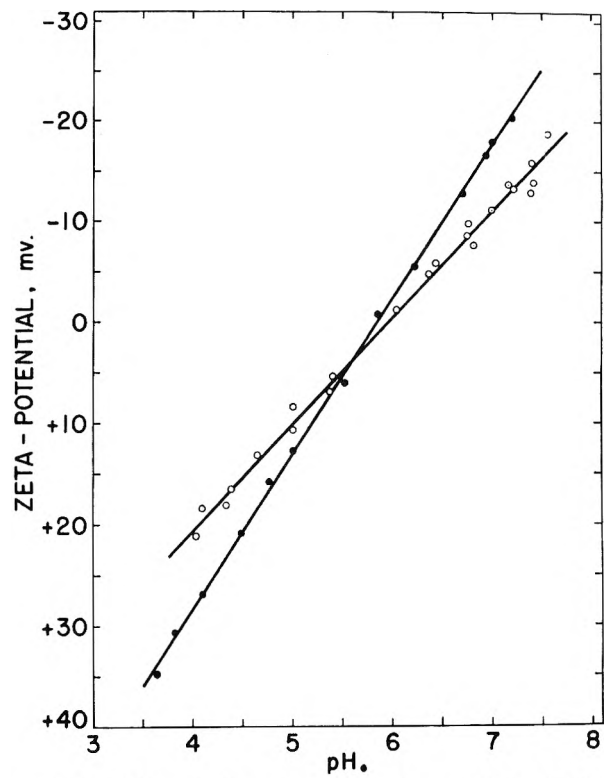

Fig. 1.—The variation of ζ as a function of *p*H for 0.09% fibrinogen solutions in phosphate and acetate buffers: ●, $\mu = 0.004$; ○, $\mu = 0.013$; lines obtained by method of least squares.

(13) F. E. Horan, F. G. Hirsch, L. A. Wood and I. S. Wright, *J. Clin. Invest.*, **29**, 202 (1950).
(14) G. Jones and L. A. Wood, *J. Chem. Phys.*, **13**, 106 (1945).
(15) L. Lorand, *Biochem. J.*, **52**, 200 (1952).
(16) W. Boyd, *J. Am. Chem. Soc.*, **67**, 1035 (1945).
(17) E. J. Cohn, *ibid.*, **49**, 173 (1927).
(18) A. A. Green, *ibid.*, **55**, 2331 (1933).
(19) H. B. Bull and R. A. Gortner, THIS JOURNAL, **35**, 456 (1931).

TABLE I

THE VARIATION OF THE ZETA POTENTIAL AS A FUNCTION OF *p*H AND THE ISOELECTRIC POINT FOR 0.09% FIBRINOGEN SOLUTIONS AT VARIOUS μ LEVELS

μ	No. of experiments	Eq. obtd. by least squares	I.P. (*p*H at $\zeta = 0$)
0.004	13	$\zeta = -15.35\ pH + 89.82$	5.85
.0055	13	$\zeta = -14.06\ pH + 82.05$	5.84
.008	13	$\zeta = -12.42\ pH + 73.50$	5.92
.0105	21	$\zeta = -10.96\ pH + 64.60$	5.89
.013	22	$\zeta = -10.52\ pH + 62.57$	5.95

It is interesting to note that as μ increases, the slopes of the lines and their intercepts on the ordinate axis decrease in a regular manner. However, the *p*H values for the isoelectric points, as calculated above, did not vary in a regular manner with μ. In order to find the isoelectric point extrapolated to $\mu = 0$, the method of least squares was employed again to establish the best line for the data describing the variation of the *p*H of the isoelectric point as a function of μ. The equation for this line was found equal to $pH = 10.88\ \mu + 5.80$. Therefore, the *p*H for the isoelectric point at $\mu = 0$ is 5.80.

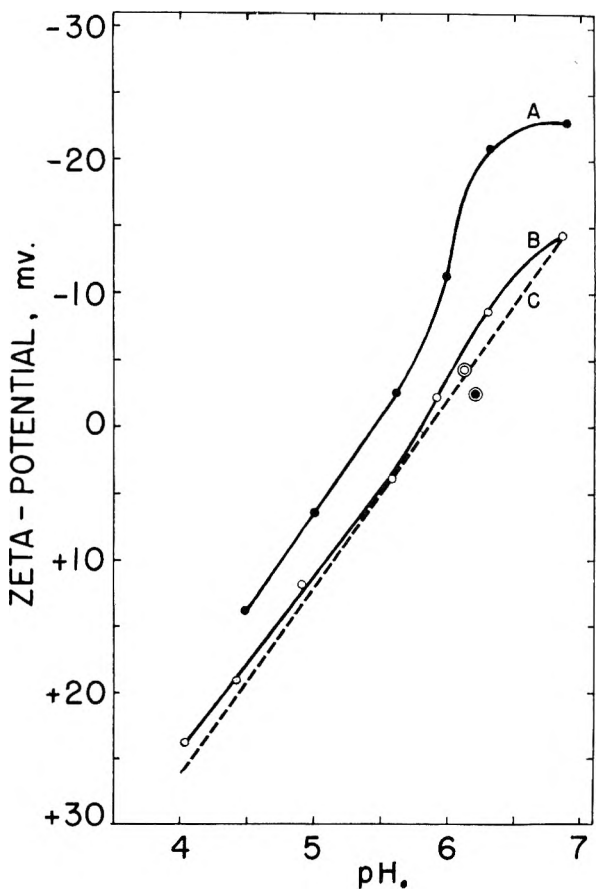

Fig. 2.—The variation of ζ *vs.* *p*H for phosphate and acetate buffers ($\mu = 0.005$) streamed through capillaries fibrinogenated at *p*H 6.1–6.2: curve A, acetate ⟶ phosphate streaming sequence, ◉, initial fibrinogen deposition; curve B, phosphate ⟶ acetate streaming sequence, ◎, initial fibrinogen deposition; dashed line C obtained by method of least squares for 0.09% fibrinogen solutions in $\mu = 0.0055$ buffer.

The Variation of ζ for Fibrinogenated Surfaces in Contact with Phosphate and Acetate Buffers at Varying *p*H and $\mu = 0.005$.—The purpose of the next series of experiments was to investigate the origin of the streaming potentials produced by the fibrinogen solutions. The problem was studied by coating a fibrinogen layer on the capillary wall and then attempting to elute the protein by subsequent streaming of buffer solutions through the apparatus. The initial fibrinogen coatings were deposited at approximately *p*H 6.1 and 4.4 by streaming solutions through the apparatus containing six times the concentration of fibrinogen previously used. At the higher *p*H, the protein has a small negative charge and would presumably adhere to the negatively charged capillary surface. In the more acid region, the fibrinogen, having a high positive charge, would be attracted to the negative wall. With a minimum of rinsing in between experiments, but following a standard procedure, buffer solutions ($\mu = 0.005$) were subsequently streamed through these fibrinogenated capillaries either from the phosphate side (*p*H 6.9, 6.3 and 5.9) to the acetate region (*p*H 5.4, 4.9, 4.4 and 4.0) or in the opposite direction starting at *p*H 4.4 and going to *p*H 6.8.

The results of these experiments are shown in Figs. 2 and 3 wherein are plotted the variation of ζ for the fibrinogenated surfaces as a function of *p*H. The series of experiments in which the initial fibrinogen coatings were deposited on the capillary surfaces at *p*H 6.1–6.2 and *p*H 4.4 are shown in Figs. 2 and 3, respectively. In these figures, curves A and D represent the results for the streaming of buffer solutions from the acetate to phosphate direction and curves B and E from the phosphate to acetate direction. For purposes of comparison, the lines obtained by the method of least squares for 0.54 and 0.09% fibrinogen solutions in 0.005 and 0.0025 ionic strength phosphate and acetate buffers are also shown and are designated curves F and C, respectively. Due to the presence of KCl in the fibrinogen stock solutions, the total ionic strengths for these solutions were 0.0055 and 0.023 for the 0.09 and 0.54% fibrinogen solutions, respectively. Finally, to serve as a control for these experiments, the phosphate and acetate buffers ($\mu = 0.005$) were streamed through an uncoated capillary. These data are shown in Table II.

TABLE II

THE ELECTROKINETIC DATA FOR BUFFER SOLUTIONS IN CONTACT WITH AN UNCOATED CAPILLARY AT VARIOUS *p*H VALUES

*p*H	*T*, °C.	$\chi \times 10^4$, mhos./cm.	*E*/*P*, mv./cm.	ζ, mv.
		Acetate, $\mu = 0.005$		
4.04	23.0	0.4493	+0.87	+37.0
4.46	24.8	.4268	+ .05	+ 1.9
4.96	24.2	.4183	− .53	−21.2
5.58	24.1	.4127	− .88	−35.2
		Phosphate, $\mu = 0.005$		
5.90	23.7	0.4794	−1.01	−46.5
6.30	24.0	.4550	−1.16	−51.0
6.86	23.5	.4155	−1.41	−56.5

These findings will be interpreted on the basis that curve C, showing the ζ *vs.* *p*H relationship for 0.09% fibrinogen in $\mu = 0.0055$ buffer, represents the electrical surface properties for surfaces in contact with a low protein concentration and a low μ solvent. The latter is comparable to the μ value for the buffer solutions streamed through the fibrinogenated capillaries in series A, B, D and E. Similarly, curve F is for the higher protein and salt concentrations; conditions which were comparable to the fibrinogen solutions streamed through the apparatus initially at *p*H 6.1 and 4.4. The low zeta potentials obtained for the 0.54% fibrinogen solutions in 0.023 μ buffers (series F) were due to the high protein and salt concentrations which presumably permitted thicker fibrinogen coatings on the capillary walls than those possible in the C series. Also to be considered are the zeta potential values obtained for the buffers streamed through the uncoated capillary.

It is interesting to note that buffers streamed in the phosphate to acetate sequence through a capillary originally fibrinogenated at *p*H 6.1 (curve B) produced zeta potentials close to the values obtained in the C series. However, when the *p*H-sequence of buffer streaming was reversed (curve A), the positive zeta potential values obtained for the first and second buffers at *p*H 4.5 and 5.0 were close to the values obtained for curve F, whereas in the phosphate region, the curve indicated a marked trend to high negative values, much higher, in fact, than the C series. This latter behavior was observed in series D and to a lesser degree in E for buffer solutions streamed through capillaries fibrinogenated in the acetate region at *p*H 4.4. Moreover, it is evident that positive zeta potential values identical to the C series were obtained at *p*H 4.4 and 4.9 for either direction of buffer streaming in series D and E.

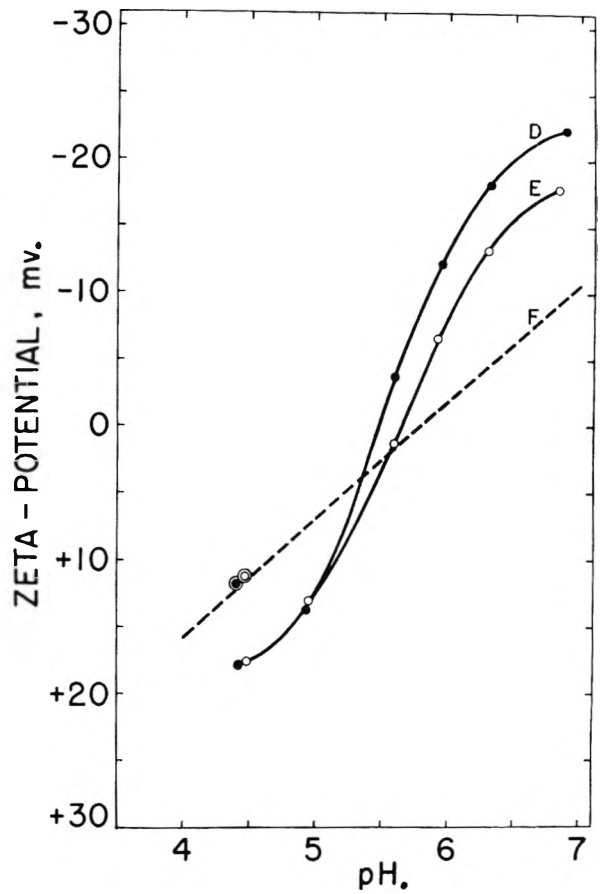

Fig. 3.—The variation of ζ *vs.* *p*H for phosphate and acetate buffers ($\mu = 0.005$) streamed through capillaries fibrinogenated at *p*H 4.4: curve D, acetate ⟶ phosphate streaming sequence, ◉, initial fibrinogen deposition; curve E, phosphate ⟶ acetate streaming sequence, ◎, initial fibrinogen deposition; dashed line F obtained by method of least squares for 0.54% fibrinogen solutions in $\mu = 0.023$ buffer.

Discussion

The variation of ζ for dilute fibrinogen solutions as a function of *p*H in the μ range of 0.004–0.013 demonstrated the influence of *p*H and μ on the magnitude and sign of the electrokinetic potential. At any given *p*H, ζ decreased as μ increased. This observation is in accordance with the inverse relationship of μ to the thickness of the diffuse double layer (the reciprocal of the Debye constant κ). The zeta potential, in turn, varies directly with the thickness of the diffuse double layer as shown by the equation $\zeta = 4\pi ed/D$ where e is the charge on the surface, d is the thickness of the diffuse double layer and D is the dielectric constant. The magnitude and sign of the charge on the capillary wall is affected by the electrical surface properties of the adsorbed protein which are influenced by the *p*H of the solution, and by the nature and extent of the ion-protein binding.

The evaluation of the *p*H at which $\zeta = 0$ for the fibrinogen solutions in contact with Pyrex surfaces was of interest since this is the *p*H of the I.P. Within the limits of the ionic strength range investigated, it was found that the I.P. at $\mu = 0.004$ occurred at *p*H 5.85 and at $\mu = 0.013$, the *p*H of the I.P. was 5.95. A similar trend, that is, increasing I.P. values with increasing μ, was reported by Smith[8] for collodion-coated ovalbumin particles in the presence of low μ levels of polyvalent cations. The uni-univalent salts exhibited the opposite effect but all lines depicting the variation of I.P. with μ extrapolated to the same value at $\mu = 0$. A decrease in the *p*H of the I.P. with increasing μ has been generally observed in mobility studies employing the moving boundary technique. In these investigations, the findings have been attributed to the variation of mobilities with ionic strength which is due, in part, both to electrostatic interaction[9] and to binding of buffer ions to the proteins.[11,12] The isoionic point, which is at a higher *p*H than the I.P. under these experimental conditions, is found when the latter is extrapolated to zero ionic strength.[9–12]

As studied by the streaming potential method, the net charge on a colloidal particle will be influenced by the ionic strength of the solvent, *p*H, and the type of electrolyte in solution. Thus, as to be expected, the slopes of the ζ *vs.* *p*H lines decreased with increasing μ. However, the increase in the *p*H of zero zeta potential (I.P.) with increasing μ and the intersection of the ζ *vs.* *p*H lines at a positive potential seemed to indicate greater binding of the solvent cations than the anions to the protein at increasing μ levels. It is interesting to note that in

the μ range employed in these studies, there were no apparent differences in binding of phosphate and acetate ions to fibrinogen since changes in slopes of the ζ *vs.* *p*H lines were not observed in the phosphate and acetate regions.

The extrapolated *p*H of the I.P. at $\mu = 0$ for 0.09% fibrinogen was found equal to 5.80. Whether this is the *p*H of the isoionic point for fibrinogen is difficult to say since isoionic fibrinogen would be insoluble in water. A *p*H value of 5.8 was previously reported[5] for the I.P. of both bovine and human fraction I, containing 42–48% and 54–60% clottable fibrinogen, respectively, in 0.001 *M* phosphate buffers. These findings seem to indicate that the protein coating out on the capillary wall, even in the presence of the non-clottable material, is fibrinogen. Edsall[20] has stated that the non-clottable component of fraction I which is similar to fibrinogen might possibly be a dimer formed from two fibrinogen molecules linked side by side since it has the same length as fibrinogen but a larger cross-section. Based on electrophoretic studies, Seegers, *et al.*,[21] have reported an I.P. of *p*H 5.5 for 1% bovine fibrinogen solutions (96% clottable) in borate, phosphate and acetate buffers (μ was not mentioned).

It was observed further in our investigations that the tenacity with which the fibrinogen layers will adhere to the capillary surface will vary depending on the initial *p*H of the fibrinogen deposition and the subsequent *p*H-sequence of buffer streaming. For example, it was found that in series B, wherein the initial fibrinogen coating was deposited at *p*H 6.2, followed by a phosphate → acetate ($\mu = 0.005$) streaming sequence, the zeta potential values were almost identical to the values found for the C series (0.09% fibrinogen in $\mu = 0.0055$ buffers). It thus appears that the fibrinogen coating adhered tenaciously to the wall during the streaming procedure. However, when the fibrinogen coating, deposited at the same *p*H, was exposed to the opposite buffer streaming sequence (curve A), it was found that the first and second acetate points at *p*H 4.5 and 5.0 were similar to the F series (0.54% fibrinogen in 0.023 μ buffers) but the zeta potentials thereafter increased significantly above the values obtained for series C and F in the phosphate region. These findings presumably are due to the removal of fibrinogen from the capillary wall, producing in effect a thinner adsorbed protein layer and consequently the zeta potential for this solid–liquid interface approaches the values found for the phosphate buffers in contact with an uncoated capillary (see Table II). A similar pattern for the phosphate region was found in series D and to a lesser degree in series E. In these experiments the initial fibrinogen coatings were deposited at *p*H 4.4. It was also found for both directions of buffer streaming through fibrinogenated capillaries in series D and E that zeta potentials identical in value to the C series occurred at *p*H 4.4 and 4.9.

From these data it is evident that a fibrinogen coating is more tenaciously held to the capillary wall when it is initially deposited at *p*H 6.2 than at 4.4. It was previously reported[5] that fibrinogen is also tenaciously bound at *p*H 7.4. The binding of fibrinogen to a surface appears to be due to adsorption since even at *p*H 8.6 in veronal buffer, $\mu = 0.05$, there is no movement of the fibrinogen boundary in plasma from the initial position on paper electrophoretograms. It was also gleaned from our studies that for protein solutions, the solid–liquid interfacial potential depends upon the electrical surface properties and thickness of the adsorbed protein layer on the solid wall, and the electrolyte concentration in the solution. Finally, it should be pointed out that the interpolated *p*H at which the acetate buffers streamed through an uncoated capillary produced a zero zeta potential occurred at about 4.6. The proximity of this value to the *pK* for acetic acid has stimulated further studies with other univalent buffer systems with the view of correlating the *p*H of the zero zeta potential to the *pK* value.

(20) J. T. Edsall, *Ergeb. Physiol. Biol. Chem. u exp. Pharmakol.*, **46**, 354 (1950).

(21) W. H. Seegers, M. L. Nieft and J. M. Vandenbelt, *Arch. Biochem.*, **7**, 15 (1945).

SPECTROSCOPIC STUDIES OF THE SOAPS OF PHENYLSTEARIC ACID. I. INFRARED ABSORPTION SPECTRA AND THE HYDROLYSIS OF SOAP FILMS

BY R. E. KAGARISE

Naval Research Laboratory, Washington 25, D. C.

Received October 8, 1954

The infrared absorption spectra of phenylstearic acid and Li, Na, K, and Ca phenylstearate have been studied in the region from 2 to 15 μ. Most of the observed frequencies have been interpreted in terms of being characteristic of either the aliphatic, aromatic or carboxyl portion of the molecule. In addition to the data for the soaps listed above, numerical values are presented for the frequency ω_2 (asymmetric stretching mode of ionized carboxyl groups) in Be, Mg, Sr and Ba phenylstearates. It is observed that for both the bivalent and monovalent metals a linear relationship exists between the frequency ω_2 and the electronegativity of the metal constituent of the molecule. From studies of the aging process in solid films of the soaps, it is concluded that the absorption of H_2O and the production of phenylstearic acid impurity increases in the order Li < Na < Ca < K. When CO_2 is excluded from the atmospheres to which films of Ca and Na soaps are exposed, the formation of phenylstearic acid is reduced to a level below the sensitivity of the spectroscopic technique (<1%). The exposure of a solid film of Na phenylstearate to an atmosphere having a relative humidity of 50% and being highly enriched in CO_2 results in the formation of phenylstearic acid and $NaHCO_3$ according to the reaction R—COONa + H_2O + CO_2 → R—COOH + $NaHCO_3$.

1. Introduction

The applicability of infrared spectroscopy to the study of the structure of aluminum soaps has been demonstrated by several investigations.[1-2] In addition, the same technique has been used to study the effects of the addition of *m*-cresol on the structure of aluminum soap–hydrocarbon gels.[3]

Recently Singleterry and co-workers[4-5] have shown that solutions of sodium phenylstearate and calcium xenylstearate in benzene are highly viscous in the absence of water or acid. The phenomenon is general for oil-soluble carboxylate soaps of a wide range of metal atoms and provides an important approach to the study of aggregation of solute and the forces responsible for micelle formation.

The purpose of this investigation was to study the purity, stability and structure of certain alkali and alkaline earth metal soaps or phenylstearic acid by means of infrared absorption techniques. The soaps were studied both as solid films and in solutions. The present paper deals primarily with the spectra of solid films, and the soap–solvent systems will be discussed in a later publication.

2. Experimental Procedure

Materials Used.—The phenylstearic acid was supplied by Edcan Laboratories, and was further purified by means of a Distillation Products Industries' molecular still. The distilled sample had a neutralization equivalent of 362.4 (theoretical 360.6). The soaps were prepared, purified and stored as previously described.[6]

ACS grade benzene was percolated through silica gel and stored over metallic sodium until used.

ACS grade chloroform was freshly percolated through a column of florosil, alumina and silica gel prior to being used.

Methods Used.—The infrared absorption spectra were observed in the 2 to 15 μ region by means of a Perkin-Elmer Model 21 double-beam spectrometer. In addition, the region from 2 to 4 μ was studied with the LiF prism instrument previously described.[7] Standard absorption cells were used for studying liquids and solutions. Films were deposited from benzene solutions on NaCl or KBr plates by spreading a uniform thickness of the jelly-like solution over the surface of the plate and allowing the solvent to evaporate. This procedure was carried out in a dry-box having a relative humidity of 10 to 20%. The soap films obtained in this manner are probably best described as being amorphous, glass-like solids.

TABLE I

INFRARED SPECTRUM OF LIQUID PHENYLSTEARIC ACID

Wave length, μ	Frequency cm^{-1}.	Intensity	Interpretation and remarks
2.31	4329	Weak	Aliphatic—combination
2.37	4219	Weak	Aliphatic—combination
2.825	3540		COOH—free OH stretching
3.240	3086	Weak	Aromatic
3.260	3067	Weak	Aromatic } C–H stretching and COOH
3.295	3035	Medium	Aromatic } OH stretch (ν_I)
3.330	3003	Shoulder	Aromatic
3.38	2960	Shoulder	Aliphatic, C–H stretch of CH_3
3.412	2930	Very strong	Aliphatic, C–H stretch of CH_2
3.48	2874	Shoulder	Aliphatic, C–H stretch of CH_3
3.500	2857	Very strong	Aliphatic, C–H stretch of CH_2
3.76	2659	Weak	COOH—bonded OH + aliphatic comb.
5.16	1938	Weak	Aromatic
5.36	1866	Weak	Aromatic } combinations
5.56	1798	Weak	Aromatic
5.68	1761		COOH—free C=O stretching
5.84	1712	Very strong	COOH—bonded C=O stretching (ν_{II})
6.23	1605	Medium	Aromatic—combination
6.31	1585	Medium	Aromatic—C–C stretching
6.70	1495	Medium	Aromatic
6.84	1462	Strong	Aliphatic, C–H bending in CH_2
6.88	1453	Strong	Aliphatic, C–H bending in CH_3
6.95	1440	Shoulder	
7.08	1412	Strong	COOH, OH bending (ν_{IV}) + α-CH_2 bending
7.27	1375	Medium	Aliphatic, C–H bending in CH_3
7.79	1284	Strong	COOH, C–O stretch (ν_{III}) + aliphatic C–H wag
8.10	1235	Strong	COOH, C–O stretch (ν_{III})
8.70	1149	Shoulder	Aromatic
8.97	1115	Medium	Aromatic
9.35	1070	Medium	Aromatic + aliphatic C–C stretch
9.72	1029	Medium	Aromatic C–H bending II to plane of ring
10.68	936	Strong	COOH, OH bending (ν_V)
11.05	905	Weak	Aromatic
11.90	840	Weak	Aromatic
13.16	760	Strong	Aromatic, C–H bending ⊥ to plane
13.86	721	Strong	Aliphatic, CH_2 rocking
14.32	698	Strong	Aromatic, C–H bending ⊥ to plane

(1) A. E. Alexander and V. R. Gray, *Proc. Roy. Soc.* (*London*), **200**, 165 (1950).

(2) W. W. Harple, S. E. Wiberley and W. H. Bauer, *Anal. Chem.*, **24**, 635 (1952).

(3) F. A. Scott, J. Goldenson, S. E. Wiberley and W. H. Bauer, THIS JOURNAL, **58**, 61 (1954).

(4) L. Arkin and C. R. Singleterry, *J. Coll. Sci.*, **4**, 537 (1949).

(5) J. G. Honig and C. R. Singleterry, THIS JOURNAL, **58**, 201 (1954).

(6) C. R. Singleterry and L. A. Weinberger, *J. Am. Chem. Soc.*, **73**, 4574 (1951).

(7) J. R. Nielsen, F. W. Crawford and D. C. Smith, *J. Opt. Soc. Am.*, **37**, 296 (1947).

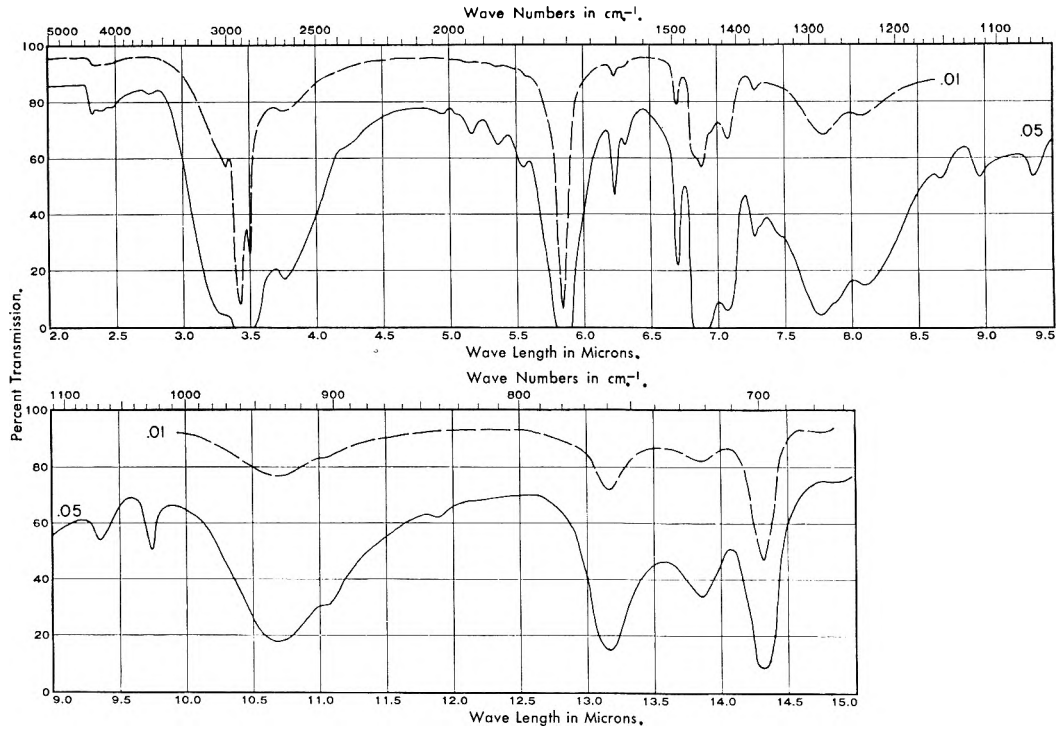

Fig. 1.—Infrared spectrum of liquid phenylstearic acid: temperature 25°, cell thicknesses in mm. as indicated.

In order to control accurately the atmosphere to which some of the soap films were subsequently exposed, a special cell was employed. This cell consisted of an aluminum spacer ($^1/_2$" thick) sandwiched between two KBr windows. The seal between the spacer and window was achieved by means of a rubber gasket. Holes were drilled in the ends of the spacer to accommodate micro-size stopcocks, which were used to control the flow of air through the system. A soap film was deposited on the inner side of one of the plates in the usual manner, and the cell was assembled immediately and evacuated to remove H_2O, CO_2 or other vapors which could conceivably react with the soap. By flowing air through various combinations of towers containing P_2O_5, Ascarite, saturated $CaCl_2$ solutions, etc., such factors as relative humidity, and CO_2 content within the cell could be varied at will.

3. Results and Discussion

Phenylstearic Acid.—The absorption spectrum of phenylstearic acid was investigated to facilitate the interpretation of the soap spectra. The spectrum obtained is shown in Fig. 1, while the wave lengths and frequencies of the absorption maxima are listed in Table I. In addition, an assignment is given for most of the bands. These interpretations are based, for the most part, on well established correlations[8-10] of characteristic group frequencies. For purposes of discussion the observed frequencies are divided into three groups according to their origin, namely, vibrations of the aliphatic portion (methyl and methylene groups), vibrations of the aromatic portion (phenyl groups), and finally vibrations localized primarily in the carboxyl group (COOH). The interpretation of the observed spectrum in terms of vibrations involving the aliphatic and aromatic portions of the molecule is, in general, straightforward and consistent with the established correlations. The only doubtful assignment is that of the bending mode of the methylene group adjacent to the COOH group. Sinclair, McKay and Jones[11] have assigned this mode to the band at 1410 cm.$^{-1}$ in the spectra of a series of saturated fatty acids. We have tentatively considered the band at 1412 cm.$^{-1}$ in the spectrum of phenylstearic acid to consist of this mode superimposed on a vibration characteristic of the COOH group.

The most interesting and important group of frequencies, from the point of view of interpreting the soap spectra, is the group due to the COOH portion of the molecule. One would expect the aliphatic and aromatic group frequencies to remain nearly constant in going from the acid to the soap or ester, whereas those frequencies due to the carboxyl portion will certainly be vastly changed.

An examination of the spectrum of phenylstearic acid in the 2 to 3 μ region shows the absence of free hydroxyl absorption in the pure compound. As expected on the basis of previous work, the OH group in phenylstearic acid is strongly bonded and is responsible for the broad absorption band which extends from roughly 3300 cm.$^{-1}$ into the region of C–H stretching absorption below 3000 cm.$^{-1}$ and presumably is responsible for the absorption maximum observed at 2600 cm.$^{-1}$. However, in dilute phenylstearic acid–carbon tetrachloride solutions (concentration = 0.002 g./10 ml.), a sharp band, which undoubtedly is due to the free OH stretching mode, appears at 3540 cm.$^{-1}$.

Hadzi and Sheppard[12] have carried out comprehensive studies of the infrared absorption bands associated with the COOH and COOD groups in dimeric carboxylic acids in the region from 1500 to 500 cm.$^{-1}$. On the basis of these studies and nu-

(8) N. Sheppard, *J. Inst. Petroleum*, **37**, 95 (1951).
(9) N. B. Colthup, *J. Opt. Soc. Am.*, **40**, 397 (1950).
(10) H. W. Thompson, *J. Chem. Soc.*, 328 (1948).
(11) R. G. Sinclair, A. F. McKay and R. N. Jones, *J. Am. Chem. Soc.*, **74**, 2570 (1952).
(12) D. Hadzi and N. Sheppard, *Proc. Roy. Soc. (London)*, **216**, 247 (1953).

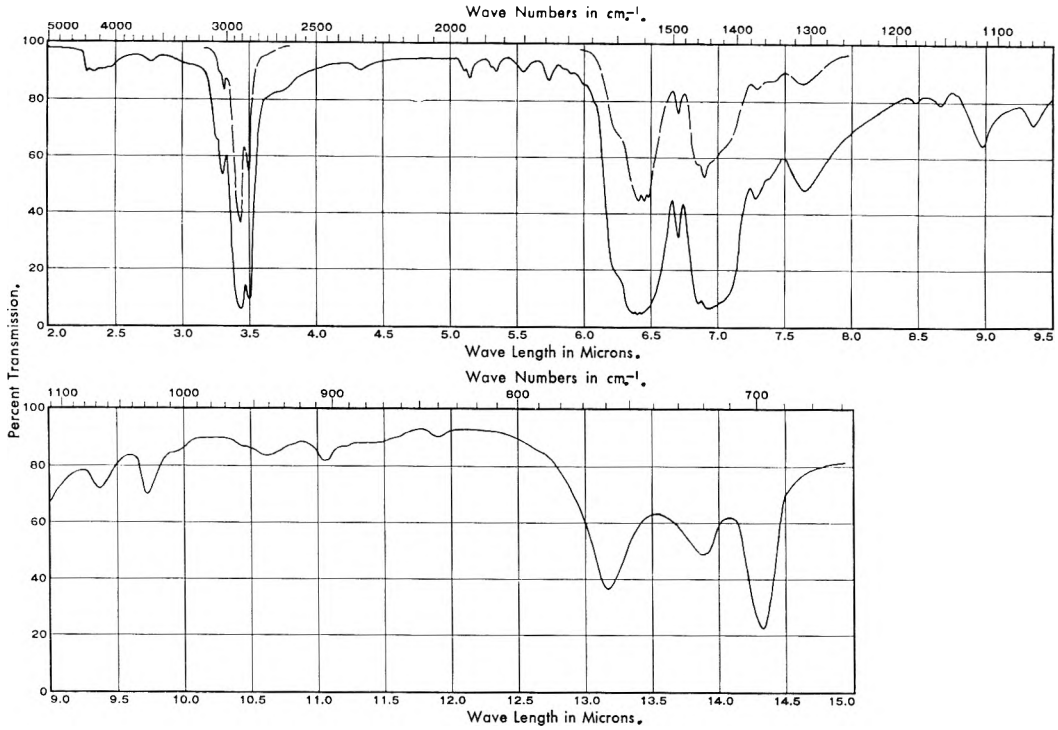

Fig. 2.—Infrared spectrum of solid calcium phenylstearate: temperature 25°, film thickness unknown.

merous earlier investigations it appears to be well established that most carboxylic acids may be represented by a dimeric structure.

The internal coördinates which might be expected to give frequencies in the region between 2 and 15 μ are (I) O–H stretching, (II) C=O stretching, (III) C–O stretching, (IV) C(=O)H angle bending and (V), the motion corresponding principally to the motion of the hydrogen atom of the OH group perpendicular to the plane of the dimer. The assignment of the first two modes to the bands at 3300 to 3000 cm.$^{-1}$ and 1712 cm.$^{-1}$ is straightforward. It is also generally accepted that the band at 935 cm.$^{-1}$ is due to mode V, *i.e.*, the out-of-plane OH deformation motion. However, there is marked disagreement in the literature concerning the assignment of modes III and IV. Shreve, Heether, Knight and Swern[13] consider the doublet absorption at 1280 and 1250 cm.$^{-1}$ to be a general characteristic of long-chain fatty acids, and conclude that one or both of these bands probably must be related to vibrations involving the C–O linkage (Mode III) in the carboxyl structure. Numerous other investigators[11,14–16] have attributed bands near 1250 and 1400 cm.$^{-1}$ to the carboxylic acid group. There is little doubt, therefore, that the infrared active C–O stretching mode and the in-plane OH deformation mode in phenylstearic acid are related to the observed bands at 1412, 1284 and 1235 cm.$^{-1}$, but the exact nature of this relationship is not apparent at the present time. Because the two modes are of similar frequency and of the same symmetry class they might be expected to interact to some degree. Thus, Hadzi and Sheppard[12] have suggested that the frequencies in question involve contributions from both C–O stretching and OH deformation.

Calcium Phenylstearate.—The infrared absorption spectrum of calcium phenylstearate is shown in Fig. 2. As expected, those frequencies which are characteristic of the aliphatic and aromatic portions of the molecule are essentially unchanged in going from the acid to the soap. However, the group frequencies related to the carboxyl group are markedly altered. One would expect, first of all, that the COOH group frequencies due to the OH group should disappear in calcium phenylstearate, and indeed such is the case with the bands at 3300, 2693 and 936 cm.$^{-1}$. Furthermore, the bands at 1712 (C=O), 1412, 1284 and 1235 cm.$^{-1}$ either disappear or change markedly in intensity. Previous investigations with compounds containing ionized carboxyl groups, *e.g.*, sodium acetate, have shown similar effects. Edsall[17] on the basis of Raman effect studies, has shown that the carbonyl frequency near 1700 cm.$^{-1}$ is always found when an un-ionized carboxyl group is present and always vanishes on ionization of the carboxyl. Davies and Sutherland[15] have pointed out that a similar situation exists in the case of the infrared spectra of compounds containing an ionized carboxyl group.

The explanation proposed by these investigators for the disappearance of the carbonyl frequency near 1700 cm.$^{-1}$ in ionized carboxyl groups is that there is complete resonance in the carboxyl group. Thus, the structure of a uni-valent metallic salt

(13) O. D. Shreve, M. R. Heether, H. B. Knight and D. Swern, *Anal. Chem.*, **22**, 1498 (1950).

(14) M. St. C. Flett, *J. Chem. Soc.*, 962 (1951).

(15) M. M. Davies and G. B. B. M. Sutherland, *J. Chem. Phys.*, **6**, 755 (1938).

(16) R. C. Herman and R. Hofstadter, *ibid.*, **6**, 534 (1938).

(17) J. T. Edsall, *ibid.*, **5**, 508 (1937).

should not be written as R—C(=O)—O—M, but rather as R—C(O⁻)=O ⁻ M⁺.

In the case of complete resonance both C–O bonds are identical and have a force constant intermediate to those of normal double and single bonds. One would expect the internal modes of vibration of an ionized carboxyl to be similar to the normal modes of a non-linear XY_2 type molecule. As such, they consist of a symmetrical valence vibration (ω_1), an asymmetrical valence mode ω_2, and a vibration of deformation ω_3.

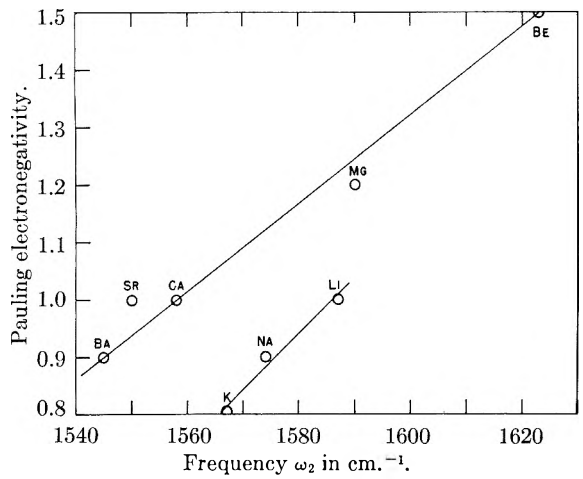

Fig. 3.—Observed stretching frequency (ω_2) *vs.* Pauling electronegativity of metal constituent of soap.

Duval, Lecompte and Douville[18] have studied the infrared absorption spectra of more than a hundred metallic salts of mono- or dibasic acids over the frequency range 600 to 1600 cm.$^{-1}$. From the results of this study they have assigned the following approximate frequency ranges to the three vibrational modes described above: ω_1 = (1350–1400 cm.$^{-1}$), ω_2 = 1550–1600 cm.$^{-1}$, and ω_3 = 800–900 cm.$^{-1}$.

In the spectrum of calcium phenylstearate the frequency ω_1 falls in the region of the C–H bending deformation modes so that only an estimate of 1430 cm.$^{-1}$ (7 μ) can be given for this frequency. The asymmetrical valence vibration (ω_2) has been assigned to the strong, broad band having its absorption maximum at 1550 cm.$^{-1}$ (6.45 μ). Although there are suggestions of structure in this band, attempts to resolve it into distinct components have been unsuccessful. Finally, the angle deformation mode ω_3 has been assigned to the weak, broad absorption at 945 cm.$^{-1}$ (10.60 μ).

Lithium, Sodium and Potassium Phenylstearate.—From the preceding discussion on the interpretation of the spectrum of calcium phenylstearate, one might expect all of the soaps of phenylstearic acid to have similar spectra except in the region of those frequencies characteristic of ionized carboxyl groups. This conclusion is verified by the experimental data, and consequently only the spectral region from 6 to 12 μ is significant for comparison purposes.

The observed frequencies of the three characteristic vibrations are summarized below in Table II.

TABLE II

CHARACTERISTIC FREQUENCIES OF IONIZED CARBOXYL GROUPS IN CERTAIN METALLIC SOAPS OF PHENYLSTEARIC ACID

Metal	ω_1	ω_2	ω_3
Li	6.96 μ, 1437 cm.$^{-1}$	6.30 μ, 1587 cm.$^{-1}$	10.69 μ, 935 cm.$^{-1}$
Na	6.94 μ, 1441	6.35 μ, 1574	10.82 μ, 924
K	7.08 μ, 1412	6.38 μ, 1567	10.93 μ, 915
Ca	6.95 μ, 1439	6.42 μ, 1558	10.62 μ, 942

Because of the coincidence of ω_1 with the C–H bending modes only an approximate value can be given for this frequency in most of the soaps studied. In addition to the data listed in Table II, the values of ω_2 for the Be, Mg, Sr and Ba soaps of phenylstearic acid were available from unpublished data obtained previously by D. C. Smith and J. M. French of this Laboratory. An interesting relationship exists between the frequency ω_2 and the electronegativity of the metal constituent of the molecule. Figure 3 shows that for both the divalent and univalent metals a linear relationship exists between the electronegativity and the frequency ω_2. This apparent relationship is in opposition to the findings of Duval, *et al.*,[18] who have concluded that no consistent relationships appear to exist between the vibrational frequencies due to the ionized carboxyl group and physical properties (*e.g.*, mass, ionic radius, etc.) of the various metals. More recently, however, Theimer and Theimer[19] have shown that in the Raman spectra of powdered salts of organic acids the frequency of the band in the 1400 to 1500 cm.$^{-1}$ region is a function of the ionic radius of the particular metal.

Spectroscopic Determination of Free Acid in Ca and Na Phenylstearate.—One of the primary objectives of this investigation was to examine the possibility of using infrared methods to determine the amount of "free" or, more precisely, unreacted acid present in the soaps of phenylstearic acid. It is well known from previous studies that the sensitivity of infrared methods in the analysis of mixtures is determined principally by the strength and disposition of the absorption bands of the various components. Because of the close similarity between the spectrum of phenylstearic acid and the spectra of its metallic salts, there are only two bands that are satisfactory for analytical purposes. These are the bands at 5.84 μ due to ν(C=O) of the acid dimer, and at 6.3 to 6.4 μ, assigned to the ω_2 mode of the soap molecules.

In order to determine the feasibility of using these bands for analytical purposes, solutions of phenylstearic acid and its calcium soap in benzene were prepared, where the concentration of acid was varied over the range 0 to 50% (by weight of total solute present) in 5% steps. From these solutions, films were deposited on KBr plates, using the procedure previously described.

Assuming that the two components obey Beer's law, it can be shown that

$$R = A(5.84\ \mu)/A(6.42\ \mu) = K(f_A/f_S) = K\beta \quad (1)$$

(18) C. Duval, J. Lecomte and F. Douville, *Ann. Phys.*, **17**, 5 (1942).

(19) R. Theimer and O. Theimer, *Monatsh.*, **81**, 313 (1950).

where the A's are the observed absorbance values at the designated wave lengths, f_A and f_S are the fractional parts of solute present as acid and Ca soap, respectively, and K is the ratio of the absorptivities at the two wave lengths. (Here we have also assumed that the soap does not absorb at 5.84 μ, nor the acid at 6.42 μ).

A plot of R *vs.* β (Fig. 4) shows that the straight line relationship predicted by equation 1 is satisfied

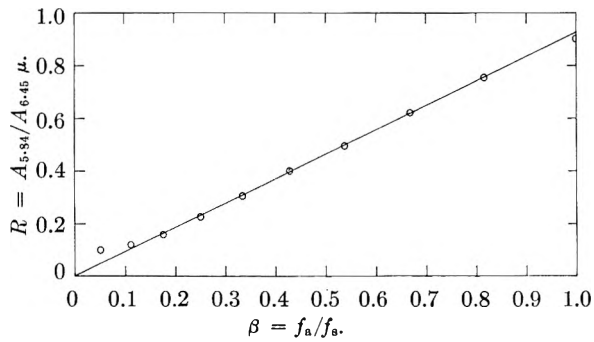

Fig. 4.—Relative absorbance *vs.* relative concentration of phenylstearic acid in films of calcium phenylstearate.

for acid concentrations greater than about 10%. The deviation of the experimental points from the theoretical curve at lower acid concentrations is due to several factors. In the first place, the absorbance values for the 5.84 μ band become less accurate at lower concentrations. A much more important factor, however, from the point of view of determining the purity of a given soap sample, is the production of acid by hydrolysis. Honig and Singleterry[5] have shown that small quantities of water exert a strong influence on the viscosity of an initially acid-free anhydrous soap–benzene system, presumably through the action of acid produced by hydrolysis. This effect was strikingly demonstrated in the process of preparing films of soap for spectroscopic studies. When the initially viscous, jelly-like, soap–benzene mixture was spread over the surface of the salt plate, it almost immediately lost this jelly-like character, and flowed readily over the surface of the plate. (This occurred in a "dry-" box having a relative humidity of about 15%). In no instance was the acid concentration of films of Ca phenylstearate prepared in this fashion found to be less than 4%. Hence, the limiting factor in the determination of acid impurity in Ca phenylstearate appears to be the sampling technique. If films can be prepared and maintained in anhydrous atmospheres, it appears probable that acid impurity in the Ca soap can be determined with an accuracy of $\pm 1\%$ (by weight).

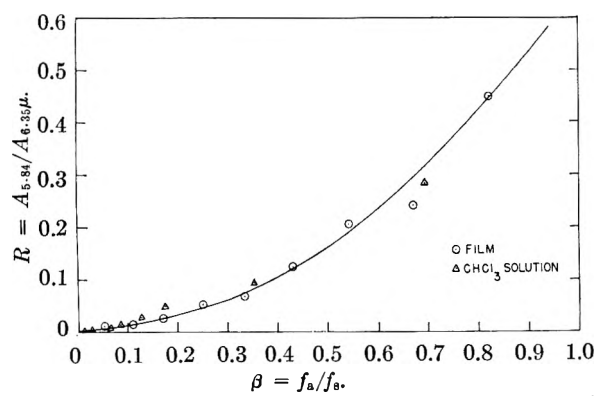

Fig. 5.—Relative absorbance *vs.* relative concentration of phenylstearic acid in films and $CHCl_3$ solutions of sodium phenylstearate.

A similar experimental procedure was carried out for a series of Na soap–acid mixtures, the results of which are shown in Fig. 5. In addition, soap–acid mixtures in $CHCl_3$ also were studied. Unlike the calcium soap, mixtures of the sodium soap and phenylstearic acid do not obey Beer's law. The interaction between soap and acid results in a diminution in the absorptivity of the acid carbonyl band at 5.84 μ and hence reduces the accuracy with which the determination of acid impurity can be made.

Hydrolysis of Li, Na, K and Ca Soaps.—In order to obtain a qualitative indication of the relative rates of hydrolysis of the various soaps, films of Li, Na, K and Ca soap were prepared and exposed to various atmospheres. Changes in the amount of absorbed water and acid impurity were followed spectroscopically for a period of 20 days.

The amount of water present was ascertained from the strength of the absorption band at 3.0 μ, while the quantity of acid impurity was estimated from the carbonyl band at 5.84 μ. The results of this experiment are shown in Figs. 6 and 7.

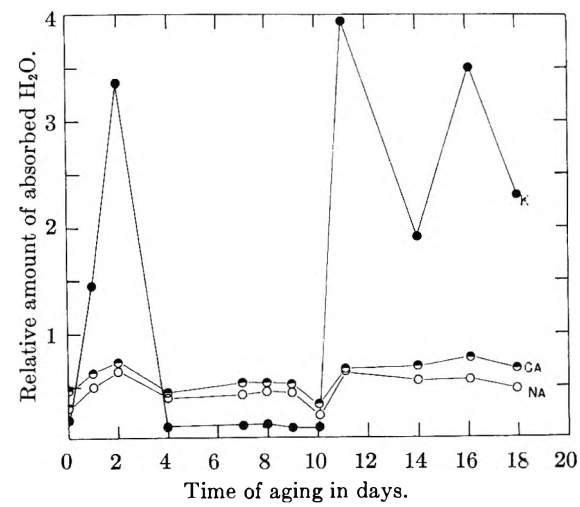

Fig. 6.—Relative amount of absorbed water *vs.* time of aging for films of Na, K and Ca phenylstearates.

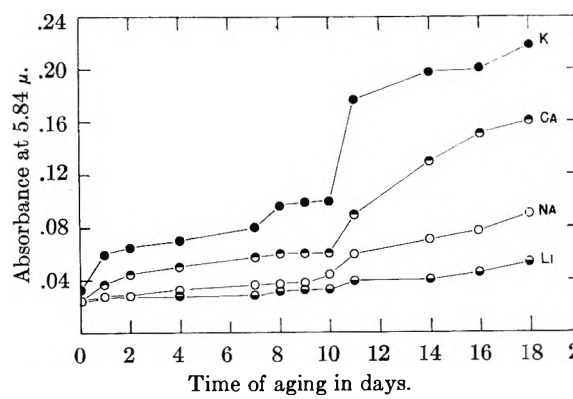

Fig. 7.—Acid carbonyl absorbance *vs.* time of aging for films of K, Ca, Na, and Li phenylstearates.

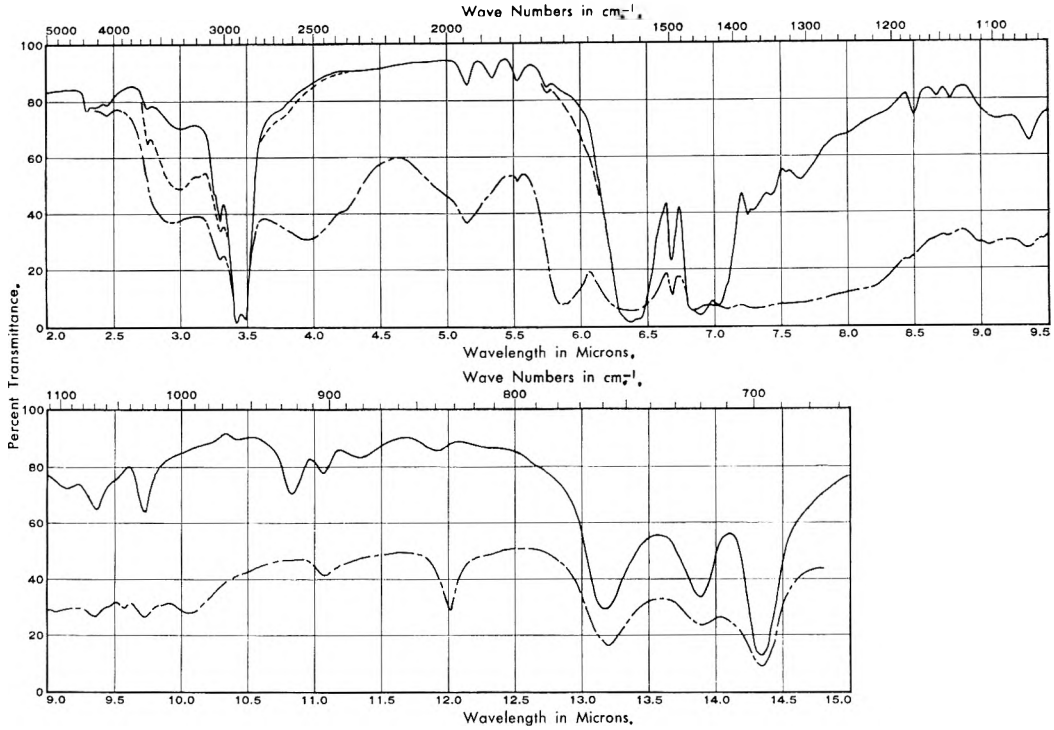

Fig 8.—Infrared spectrum of Na phenylstearate (solid film) exposed to various atmospheres: A, (——) unexposed; B, (------) exposed to normal atmosphere; C, (– – –) exposed to atmosphere enriched in CO_2.

During the first nine days the films were exposed to normal room atmospheres. On the tenth day the films were placed in a desiccator which was then evacuated (~0.1 mm.) for a period of six hours. For the remaining period of time the films were kept in an atmosphere having a relative humidity of 30%, except when the spectra were being studied. From the curve for the K soap in Fig. 6 it is apparent that the amount of water present changed markedly from day to day. These fluctuations were in all probability due to the fact that the films lost or gained water during the short period (15 min.) they were removed from the constant humidity chamber. Thus it is obvious that more refined experiments will be necessary to obtain quantitative relationships between the amount of absorbed water and the relative humidity of the atmosphere surrounding the soap films. However, certain qualitative conclusions can be made on the basis of this experiment, and are summarized as follows: (a) at no time was a detectable amount of absorbed water present in the Li soap film; (b) in general, the amount of absorbed water increased in the order of Na < Ca < K soap; (c) as indicated by the amount of water absorbed, the K soap is extremely sensitive to changes in the relative humidity.

The amount of free acid produced in the various soap films is shown in Fig. 7. From a comparison of Figs. 6 and 7, it is apparent that the rate at which acid is produced is dependent upon the amount of water present on the film. Furthermore, the amount of acid present never decreases, indicating possibly that the reaction responsible for its production is not readily reversible.

In order to control accurately the atmosphere to which the soap films were exposed, detailed studies of the hydrolysis process in Ca and Na phenylstearate were made using the special cell previously described. A film of Ca soap was deposited on a KBr plate in the normal fashion and the cell immediately assembled and evacuated for two hours to remove all water absorbed in the process of preparing the film. The spectrum was then observed and served as a standard for subsequent spectra obtained after exposure of the film to various atmospheres. The acid content initially was <1%. The film of Ca soap was then subjected to an atmosphere having a relative humidity of 30%, and which was nearly free of CO_2. This atmosphere was obtained by flowing air through towers containing Ascarite, P_2O_5 and a saturated solution of $CaCl_2 \cdot 6H_2O$ in H_2O. The film was subjected to this atmosphere for a period of 40 hours, at the end of which time the spectrum was again obtained. There was no observable increase in intensity of the 5.84 μ band, indicating that no additional free acid had been produced in the film by the action of H_2O alone.

The Ascarite tower was now removed from the system yielding an atmosphere having normal CO_2 content and a relative humidity of 30%. At the end of two hours exposure to this atmosphere, the acid band had increased perceptibly, showing that the presence of CO_2 greatly enhanced the process of acid formation. At the end of 60 hours exposure to this essentially normal atmosphere, the acid content reached a value of roughly 5% by weight.

A similar experimental procedure was carried out for a film of Na phenylstearate. The spectral results of this experiment are shown in Fig. 8. Curve a is the absorption spectrum of the film obtained immediately after preparation and evacuation of the cell. An examination of the 5.85 μ region shows little if any acid impurity present initially.

The band at 3.0 μ is indicative of residual absorbed water which was not removed by evacuation. Air having a relative humidity of 50% and essentially CO_2 free[20] was now flowed through the cell for a period of 24 hours and the spectrum reexamined. The changes from the initial spectrum are shown by the curve b of Fig. 8, the only significant ones being the increase in the water bands at 3 and 5.75–6.5 μ. After evacuation (0.1 mm.) for two hours these changes disappeared and no significant increase in the absorption at 5.84 μ was observed, indicating that little if any hydrolysis had occurred.

The Ascarite tower was now removed from the system and the film subjected to an atmosphere having a relative humidity of 50% and normal CO_2 content for a period of 15 hours. The spectrum observed at the end of this time was essentially the same as the one shown by curve b, and there was no positive indication of increased absorption at 5.84 μ, in contradistinction to the results shown by the film of Ca soap. However, this is to be expected, since the curves in Fig. 7 indicate that under similar conditions the Na soap is less susceptible to acid formation than is calcium phenylstearate. In order to accelerate the effects of CO_2 and H_2O, the film of Na soap was subjected to an atmosphere obtained by passing nearly pure CO_2 (produced by the sublimation of Dry Ice) through the $Ca(NO_3)_2$ solution. At the end of four hours the cell was evacuated and the spectrum, shown by the third curve of Fig. 8, was observed. The profound changes that occurred are reasonably explained if one considers that phenylstearic acid and sodium bicarbonate have been produced by means of the reaction

$$R—COONa + H_2O + CO_2 \longrightarrow R—COOH + NaHCO_3$$

The infrared absorption of $NaHCO_3$ has been studied by Miller and Wilkins[21] and their observed spectrum shows strong bands at about 4.0, 5.2, 6.0, 7.5, 10.0, 12.0 and 14.2 μ. Except for the band at 5.84 μ, which is due to the phenylstearic acid, these bands correspond exactly with the new bands appearing in curve C of Fig. 8.

4. Conclusions

The principal objective of this investigation was to determine the feasibility of using infrared absorption spectra to detect and quantitatively measure the acid impurity in certain metallic phenylstearates. Two phenomena have been encountered which tend to complicate the application of spectroscopic methods to this problem in varying degrees depending upon the particular soap under consideration. These are:

(a) Production of free acid, by means of the action of H_2O and CO_2, during the preparation and examination of the soap films.

(b) Interaction between the soap and acid as evidenced by the fact that certain soap–acid mixtures do not obey Beer's law. In order to obtain reliable spectroscopic data, the precautions necessitated by these two effects are:

1. The soap samples must be maintained in anhydrous, CO_2-free environments at all times. This entails the use of elaborate sampling techniques such as efficient dry-boxes for the deposition of of films from solutions, vacuum tight cells for containment of films, etc.

2. Solvents such as benzene, chloroform and carbon tetrachloride may show a strong tendency to produce acid impurity in soap solutions and must be carefully percolated prior to use.

3. In order to determine quantitatively the amount of acid present in a given soap sample, it is necessary to resort to a calibration curve based on soap–acid mixtures of known concentrations.

From studies of amorphous, solid soap films exposed to various controlled atmospheres it is concluded that the hydrolysis of Ca and Na phenylstearates in the absence of CO_2 is negligible. Thus the equilibrium strongly favors neutralization, *i.e.*

$$R—COOH + NaOH \longrightarrow R—COONa + H_2O$$

However, in the presence of CO_2, NaOH is removed by formation of sodium bicarbonate and the corresponding amount of phenylstearic acid. The effects of CO_2 on solid soaps appears to be much more pronounced than one might have anticipated on the basis of earlier hydrolysis studies of aqueous systems, and the relative acidities of carboxylic and carbonic acids. It should be emphasized that the conclusions listed above apply specifically to the solid phase, and may not be applicable to solutions.

Acknowledgment.—The author wishes to express his appreciation to Dr. C. R. Singleterry and Mr. John Honig for many helpful discussions throughout the course of this investigation, and for providing the phenylstearic acid and soap samples. Thanks are also extended to Mrs. Lorraine Weinberger, who obtained most of the infrared spectra.

(20) The atmosphere described was obtained by flowing air through a series of towers containing Ascarite, P_2O_5, and a saturated solution of $Ca(NO_3)_2$ in the presence of excess solid $Ca(NO_3)_2 \cdot 4H_2O$. The latter tower and the cell were maintained at a temperature of 25 ± 2°.

(21) F. A. Miller and C. H. Wilkins, *Anal. Chem.*, **24**, 1478 (1950).

TRANSFERENCE NUMBERS OF ELECTROLYTES UNDER PRESSURE

BY F. T. WALL AND S. J. GILL

Noyes Chemical Laboratory, University of Illinois, Urbana, Illinois

Received October 18, 1954

A method has been developed for determining transference numbers of simple electrolytes under high pressures. In this method, which is an adaptation of the conventional moving boundary technique, the movement of the ions is followed by resistance measurements. The results obtained by this procedure at 1 atm. are in good agreement with literature values for 0.1 *N* KCl, NaCl and HCl. At 1000 bars, a slight increase was observed for the cation transference number of 0.1 *N* HCl. A 2% decrease in cation transference number was observed for 0.1 *N* KCl and an even larger decrease was noted for the cation of 0.1 *N* NaCl. Cadmium chloride was employed as the "following" solution, and the transference number of Cd^{++}, calculated from the Kohlrausch regulating function and conductivity data, likewise decreased with increase in pressure.

Introduction

The effect of pressure upon transference numbers has been briefly investigated by Gans[1] for zinc sulfate. In this investigation he measured the electromotive force of an appropriate concentration cell and found a 1% change in the transference number of zinc sulfate when the pressure was increased to 1000 atm. The accuracy of this work has been questioned, however, because of the difficulties encountered in producing cells that are reversible under pressure.[2]

Numerous studies of the conductivities of solutions under pressure have been made,[3-9] but to fully interpret these data it is necessary to know the ion transference numbers under similar conditions. Accordingly, the study here reported was undertaken to develop a method for measurement of transference numbers of simple electrolytes under pressure.

Discussion of the Method.—The electromotive force method, although convenient, is unsatisfactory because of the difficulty of attaining equilibrium under pressure; hence no attempt was made to use this method in our work. The Hittorf concentration change method also appeared unattractive because it is not easily adapted to high pressure measurements. Of all the methods employed at atmospheric pressure, the moving boundary technique appeared most promising for adaptation to studies under pressure because of its precision, simplicity, and speed.[10] The method that we shall describe here is a modification of the conventional moving boundary experiment.

Observation of the boundary, which is relatively simple for transparent vessels, is quite impractical when the system is within a pressure bomb, even through use of optical windows. Accordingly, an electrical method was devised to follow the position of the boundary; this was accomplished by measuring the resistance of the column of solution through which the boundary moved (Fig. 1), using probe electrodes built into the transference cell. Suppose, for example, that the boundary is initially in the region beneath both probe electrodes and that it moves upward. The resistance measured between the probe electrodes will then be constant until the boundary moves into the region between them, after which it will change as the boundary moves, provided the conductivities of the leading and following solutions are different. If the cell is properly constructed, one can expect the resistance to be a linear function of the boundary position, thus providing a basis for accurately measuring the movement of the boundary.

In order to achieve a linear relationship between the position of the boundary and the measured resistance, it is sufficient to have a uniform cross-section, a uniform field between the measuring electrodes, and uniform compositions of leading and following solutions. These conditions can be fulfilled by proper construction. A precision bore tube gives a uniform cross-section for the region between the probe electrodes. The electric field produced by the probe electrodes will not be uniform near their surfaces unless the electrodes form the ends of a right cylinder. This inhomogeneity at the probe electrodes proves to be unimportant, for the field becomes uniform a short distance from the electrodes if the length of the cell is much greater than the diameter. The condition of uniform concentrations in the leading and following solutions is realized automatically from the Kohlrausch regulating function[11] as long as the electrolyzing electrodes are distant from the probe electrodes. An electromotive force method, related to the one described here, has been used for mobility measurements at 1 atm.[12,13]

The problem of generating a boundary under conditions of high pressure is easily solved by using an autogenic boundary produced by a cadmium anode.[14] The circuit is completed by using a silver–silver chloride cathode. For all systems studied the chloride anion was common to both the leading and the following solutions.

During electrolysis, an electric field is set up in the solution between the probe electrodes; conse-

(1) R. Gans, *Ann. Physik*, **6**, 315 (1901).

(2) E. Cohen, "Physico-Chemical Metamorphosis and Problems in Piezochemistry," McGraw-Hill Book Co., Inc., New York, N. Y., 1928, p. 144.

(3) Ernst Cohen and W. Schut, "Piezochemie kondensierter Systeme," Akademische Verlagsgesellschaft m. b. H., Leipzig, 1919.

(4) G. Tammann and W. Tofaute, *Z. anorg. allegem. Chem.*, **182**, 353 (1929).

(5) G. Tammann and A. Rohmann, *ibid.*, **183**, 1 (1929).

(6) E. Brander, *Soc. Sci. Fennica Commentationes Phys. Math.*, **6**, 1 (1932).

(7) W. A. Zisman, *Phys. Rev.*, **39**, 151 (1932).

(8) L. H. Adams and R. E. Hall, THIS JOURNAL, **35**, 2145 (1931).

(9) F. T. Wall and S. J. Gill, *ibid.*, **58**, 740 (1954).

(10) D. A. MacInnes and L. G. Longsworth, *Chem. Rev.*, **11**, 171 (1932).

(11) F. Kohlrausch, *Ann. Physik*, **62**, 209 (1893).

(12) J. Clerin, *Ann. Chim.*, [11], **20**, 244 (1945).

(13) J. Mukherjee, R. Mitra and A. K. Bhattacharya, *J. Indian Chem. Soc.*, **12**, 177 (1935).

(14) H. P. Cady and L. G. Longsworth, *J. Am. Chem. Soc.*, **51**, 1656 (1929).

quently those electrodes must be disconnected from each other while electrolysis proceeds to avoid short circuiting the current. Similarly the direct current must be stopped while a resistance measurement is made using the probe electrodes. The width of the probe electrodes (in the direction of the electrolyzing field) must not exceed a thickness above which chemical electrolysis might occur at their surfaces when current is passing through the cell.

The effect of current interruption in the determination of transference numbers by the moving boundary method has been studied by MacInnes and Longsworth.[10,15] Their findings show that interruptions in the current produce no detectable effect in the observed transference numbers and our own results support these conclusions.

Upon turning off the electrolyzing current, the boundary between the two solutions diffuses and the measured resistance changes. Reproducibility of the boundary diffusion is achieved by measuring the resistance at a fixed time after the current has been stopped.

Heat developed from electrolysis is particularly serious in any application of the moving boundary method within a pressure bomb. This effect is minimized by using a cell of short length, dilute solutions, and small currents. On the other hand, there is loss of sensitivity upon shortening the cell.

Apparatus and Procedure

Precision bore Pyrex tubing of cross section 0.0339 cm.^{2} was used for the measuring part of the cell. A ball joint was placed at one end of this tube to provide a connection to an S-shaped tube containing the silver–silver chloride electrode. The measuring electrodes consisted of #30 platinum wire inserted across the diameter of the tube. The probe electrodes were mounted in the tube with a minimum of tube distortion by the following method. Two fine holes were drilled 10 cm. apart by means of a rotating tungsten wire, while the glass was heated to its softening point at the spots where the holes were made by a hydrogen torch. The platinum wires were then sealed into the cell. This type of construction gave a cell of great strength and a region of uniform cross-section between the measuring electrodes. Other cell plans were also tried, such as using probe electrodes of washer shape, mounted with cement in a sandwich fashion between ground end pieces of precision bore tubing. The latter type of cell, although advantageous because of its high degree of electrode symmetry and the virtual elimination of capillary tube distortion, would not withstand the effects of pressure and repeated cleaning. Consequently the sealed wire electrodes were found to be more satisfactory.

The lower probe electrode must be situated far enough from the autogenic cadmium electrode so that the normal concentration build-up at this electrode would not affect the resistance measurement. This is analogous to the middle compartment requirement of the usual Hittorf cell. Our measurements indicated that this condition was fulfilled. The concentration gradient at the cadmium electrode was also observed by means of a Schlieren optical system, and the disturbed region was shown to remain beneath the probe electrode.[16]

The cell was designed to be compact, yet the cathode was kept some distance from the measuring electrodes. The silver–silver chloride electrode was fitted into the cell by means of a ground glass joint. Another opening at the top of the cell allowed pressure to be transmitted to the system. In order to isolate the cell solution from the pressurizing oil (high vacuum oil), a "Nujol" layer was placed on the solution.

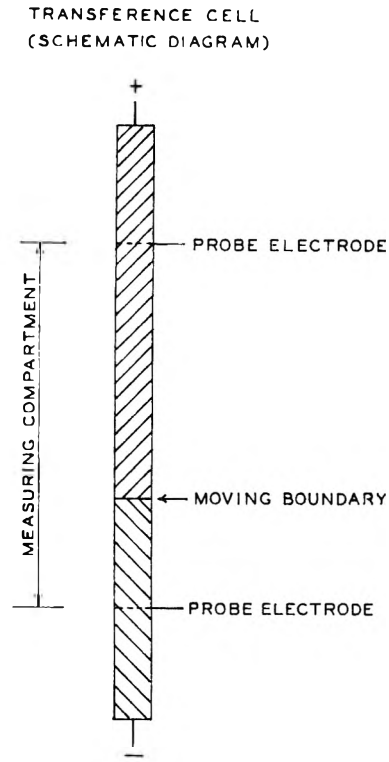

Fig. 1.—Diagram of transference–conductance cell used in pressure experiment.

This layer was found to give satisfactory protection from the pressurizing medium during the course of the experiments, since diffusion through a "Nujol" layer occurs very slowly.

The sealing technique for the cadmium electrode involves the use of a soft rubber gasket. The cadmium electrode was machined to provide a close fit into the capillary tubing and the rubber gasket was placed under a small amount of compression by the cell holder. The body of the cell holder is aluminum to provide good heat conduction. A split brass sleeve was made to fit around the measuring part of the glass cell.

The electrical connections to the cell inside the bomb were made through the usual high pressure connections. One of the major problems is that of electrical shorting within the bomb. Shorts of the order of fifty megohms or less indicated the possibility of current leakage. Electrical leads to the cell within the bomb were made of number 30 "Formex" coated magnet wire covered with polyethylene spaghetti. The soldered connections to the probe electrodes were insulated by a coating of finger nail lacquer. These leads from the cell were placed in grooves made in the aluminum cell holder. The entire cell assembly hung from the piston-like head of the bomb, thus facilitating electrical connections. It was necessary to exercise considerable care in filling the cell to avoid spilling any electrolyte into the grooves of the cell holder where possible shorts could develop. The system was tested for electrical shorts before and after each run.

The platinum measuring electrodes were platinized according to standard procedure. The silver–silver chloride electrode was made by dipping a platinum foil electrode into molten silver chloride and allowing the silver chloride to solidify upon the platinum.

The following components completed the apparatus: high pressure equipment, a conductance bridge,[9] a constant current regulator, timing switch, potentiometer with standard resistance, and temperature control bath.

A source of constant current for work of this type is highly advantageous. The circuit employed was an adaptation of two devices described in the literature.[17,18] A 0.05%

(15) D. A. MacInnes and I. A. Cowperthwaite, *Proc. Natl. Acad. Sci. U. S.*, **15**, 18 (1929).

(16) Acknowledgment is expressed to Robert L. Fischer for assisting in these measurements.

(17) P. Bender and D. R. Lewis, *J. Chem. Educ.*, **24**, 454 (1947).

(18) G. S. Hartley and G. W. Donaldson, *Trans. Faraday Soc.*, **33**, 457 (1937).

change was noted in a current of 2 ma. on changing the load resistance from 100 to 60,000 ohms, and for a fixed resistance the current was constant within 0.05% over a period of an hour. The current could be adjusted manually if larger changes occurred. The current was measured with a Leeds and Northrup K-2 potentiometer in conjunction with a Leeds and Northrup precision resistor, which upon calibration was found to have a resistance of 100.07 absolute ohms at 26°.

The timing and switching mechanism, used for switching from electrolysis to resistance measurements, was made from a "Synchrotron" motor which turned one revolution in four minutes. The motor turned a brass wheel, which has a fraction of its perimeter cut out, thus enabling a "Micro switch" to be turned off for a precise fraction of each revolution. The "Micro switch" operated a set of relays which connected either the current electrodes or the measuring electrodes into the circuit. A mechanical counter was also controlled by the switch.

The 1/4 r.p.m. motor and notched wheel provided approximately 30 seconds in which to balance the conductance bridge and to obtain an accurate resistance reading. For seven-eighths of the time, current passed through the cell. A pair of coaxial (shielded) relays controlled the measuring electrodes to prevent unnecessary noise pickup to the bridge; the relays were activated by current flowing through the cell. All of the leads into the pressure bomb were shielded and the bomb was grounded.

The cell was cleaned before each run with hot potassium dichromate–sulfuric acid cleaning solution, then rinsed several times with distilled water and with the solution to be measured. After electrical connections were made, the cell was assembled, filled with solution, and placed within the bomb. Outside electrical connections were completed and the run was started when temperature equilibrium was reached.

Calculations.—The transference cell employed in these experiments had a region of uniform cross-sectional area A with measuring electrodes a fixed distance apart. Since the measuring electrodes will not produce a uniform electric field near their surfaces, it is useful to consider an "ideal" cell of cross-section A, with measuring electrodes l cm. apart. The "ideal" electrode distance is calculated from the experimental cell constant, k, where

$$k = l/A \qquad (1)$$

Consider the measured resistance of the cell when there is a boundary in the region between the probe electrodes. The resistivity of the solution below the boundary is such that it exhibits a resistance R_1 when it completely fills the cell. The solution above the boundary produces a corresponding resistance R_2. The cell resistance when both solutions are present is given by

$$R = R_1x + R_2(1 - x) \qquad (2)$$

x is the fraction of the distance, l, through which the boundary has moved. Equation 2 rests upon the assumptions that the field and cross-section are uniform in the region in which resistance measurements are made and that the concentrations of the two solutions remain uniform.

The apparent transference number can be calculated from the equation

$$t_+ = cFdA/it \qquad (3)$$

where t_+ is the transference number of the ion determining the boundary movement, c the concentration of the same ion in equivalents per liter, F the value of the faraday, d the distance in centimeters the boundary has moved, i the current in milliamperes and t the time in seconds. Equation 3 can be rewritten in terms of the velocity v of the boundary.

$$t_+ = cFAv/i \qquad (4)$$

The velocity v can also be determined from equation 2 and the fact that $x = d/l$ using the equation

$$v = \frac{l}{R_1 - R_2} \times \frac{dR}{dt} \qquad (5)$$

where dR/dt is the time derivative of the observed resistance. Combination of equations 4 and 5 yields an expression for the apparent transference number.

$$t_+ = \frac{cFAl}{i(R_1 - R_2)} \times \frac{dR}{dt} \qquad (6)$$

A and l are determined by experimental calibration. R_1 and R_2 are the initial and final resistance readings. i is determined using a potentiometer and standard resistance. dR/dt is determined by least square computation.[19] The true transference number can be obtained when corrections are made for volume changes of transport and conductance of the solvent.[20] For 0.1 n solutions the latter correction is negligible, but the volume correction must be applied.

The cell parameters A and l, and the concentration c are affected by pressure. The product lA is a hypothetical volume, since l is an "ideal" length. The percentage change in this volume due to pressure changes should be closely approximated by the percentage change in the volume of the cell, which depends upon the compressibility of the material from which the cell is constructed. The data of Adams[21] for the compressibility of "Pyrex" show that a 0.3% correction should be made at 1000 bars.

For dilute solutions the effect of pressure upon the concentration can be determined from the Tait equation for water as given by Owen.[22] For concentrated solutions a correction can be made for solute using data given by Owen and Brinkley[23] on the effect of pressure on molar volumes.

It is also possible to determine the transference number of the following ion, in this case cadmium, by using the Kohlrausch condition. This relation, which has been used in a related application described by Hartley and Donaldson,[18] is

$$\frac{t_l}{c_l} = \frac{t_f}{c_f} \qquad (7)$$

where t_l and c_l are the transport number and concentration of the leading ion and t_f and c_f are the corresponding quantities for the following ion (Cd^{++}). When t_l and c_l are known, t_f can be determined by simply evaluating c_f. Instead of trying to determine the absolute value of t_f directly it is more expedient to determine the ratio of t_f at pressure P to its value at 1 atmosphere. This permits simplification and renders unnecessary an absolute determination of the concentrations of the

(19) This computation was performed on the University of Illinois digital computer using a code prepared by Leonard Isaacson of this Laboratory.

(20) L. G. Longsworth, *J. Am. Chem. Soc.*, **54**, 2741 (1932).

(21) J. Adams, *ibid.*, **53**, 3769 (1931).

(22) B. B. Owen, *J. Chem. Educ.*, **21**, 59 (1944).

(23) B. B. Owen and S. R. Brinkley, Jr., *Chem. Revs.*, **29**, 461 (1941).

cadmium chloride solutions. Using equation 7, this ratio can be expressed as

$$\frac{t_f^{(P)}}{t_f^{(1)}} = \frac{c_f^{(P)}}{c_f^{(1)}} \times \frac{t_1^{(P)}}{t_1^{(1)}} \times \frac{c_1^{(1)}}{c_1^{(P)}} \qquad (8)$$

where superscripts in parentheses denote the pressures. The concentration of a dilute solution at a given pressure can be related to the concentration the solution would have at atmospheric pressure by

$$c^{(1)} = c^{(P)}F(P) \qquad (9)$$

where $F(P)$ is obtained from the Tait equation for the compressibility of the solvent. Equation 9 can thus be used to simplify equation 8. It should be carefully noted that the concentration of the following ion, established at pressure P and reduced back to one atmosphere, is not the same as the concentration established in an experiment carried out at atmospheric pressure. To make this distinction clear, we shall denote the value of $c_f^{(P)}$, reduced to one atmosphere, by the symbol $c_f^{(1)p}$, which must be distinguished from $c^{(1)}$. With this understanding eq. 8 reduces to

$$\frac{t_f^{(P)}}{t_f^{(1)}} = \frac{c_f^{(1)p}}{c_f^{(1)}} \times \frac{t_1^{(P)}}{t_1^{(1)}} \qquad (10)$$

The evaluation of the ratio $c_f^{(1)p}/c_f^{(1)}$ can be made as follows. For measurements made in a given cell, we note that

$$\frac{c^{(1)p}}{c^{(1)}} = \frac{\Lambda^{(1)}R^{(1)}}{\Lambda^{(1)p}R^{(1)p}} \qquad (11)$$

where we now drop the subscript f for convenience. In eq. 11, the quantities $\Lambda^{(1)p}$ and $R^{(1)p}$ are the values, corrected to one atmosphere, of the equivalent conductance and resistance of the "following" solution as determined by an experiment carried out under pressure. $\Lambda^{(1)}$ and $R^{(1)}$ are the corresponding quantities for the experiment carried out at one atmosphere. It is found experimentally that the relative change in resistance with pressure is quite insensitive to the concentration. By using such an experimentally determined factor, $R^{(1)p}$ can readily be obtained from the resistance observed in a pressure experiment. As a first approximation we can assume $\Lambda^{(1)p} = \Lambda^{(1)}$ since the equivalent conductance of a dilute solution of a strong electrolyte is not strongly dependent on concentration. This enables us to calculate a first approximation to the desired ratio $c^{(1)p}/c^{(1)}$. From that ratio and a knowledge of $c^{(1)}$ determined by experiments at one atmosphere, one can compute an improved value for the ratio $\Lambda^{(1)}/\Lambda^{(1)p}$, using literature values for the equivalent conductance of cadmium chloride as a function of concentration. The calculation using eq. 11 is then repeated as often as necessary to get a consistent answer. In practice the second or third approximation is sufficient to give a satisfactory value of the ratio $c^{(1)p}/c^{(1)}$ to use in eq. 10.

Calculations.—The cross-sectional area A and the hypothetical length l were determined by calibration. The region between the measuring electrodes was tested for uniformity of cross-section by measuring the length of a small slug of mercury at several positions. By this means the tube was found to be uniform to within one part per thousand over a length of 8 to 9 cm. This test for uniformity necessarily included some averaging of small deviations, but it did show that no gross defects in cross section were present. Deviations were apparent near the probe electrodes, which were sealed into the glass at points about 10 cm. apart.

The following method of measuring the cross-sectional area was employed. Two slugs of mercury of different lengths were measured and weighed. The difference in volume of these two slugs, assuming similar end effects for each, was equal to their difference in lengths times the cross-sectional area which was shown to be constant. The cross-section was so determined to be 0.03390 cm.^{2}.

The ideal cell length l was calculated after determining the cell constant by measurements on a standard 0.1000_0 demal solution of potassium chloride, prepared according to the directions of Jones and Bradshaw.[24] The conductivity water used to prepare this solution was distilled from permanganate and had a specific conductance of 9.66×10^{-7} mho cm.$^{-1}$ at 25°. A solvent correction was applied in determining the value of the cell constant. The cell constant was 293.0 and the calculated length l was 9.932 cm.

It was also necessary to calibrate the time per revolution during which the timing switch was in a position that permitted passage of current through the cell. This time value was determined both by stop-watch and by a stop-clock whose magnetic clutch was connected into the actual cell circuit for a typical run. The average time for several determinations was 210.35 seconds. Individual determinations deviated from this average value by no more than 0.10 second.

Preparation of Solutions.—Solutions of potassium chloride, sodium chloride and hydrochloric acid were prepared from purified materials. Reagent grade potassium chloride was precipitated from a concentrated hot solution by cooling, dried for 12 hours at 110°, then fused in a platinum crucible and cooled in a platinum dish before being bottled. The sodium chloride was purified from reagent material by twice precipitating with pure hydrogen chloride gas, drying at 110° for 12 hours and then drying at 450° in a Richards drying tube[25] with a nitrogen sweep for two hours. Solutions of these materials were then made up using the densities given by the International Critical Tables to give the desired normalities. Corrections for buoyancy were made in all cases. Solutions of hydrochloric acid were prepared from a constant boiling mixture of hydrochloric acid and water as specified by Foulk and Hollingsworth.[26] The standard solutions were diluted to desired concentrations using calibrated pipets and volumetric flasks. The cadmium chloride solutions, used for determining the pressure coefficient of resistance of this material, were prepared from reagent cadmium chloride, and standardized by silver chloride titration using dichlorofluorescein indicator. The precise concentrations for the cadmium chloride solutions were not needed. All solutions used were prepared with conductivity water of specific conductance 9.6×10^{-7} mho cm.$^{-1}$ at 25°.

Discussion of Errors.—From equation 6 an estimate can be made of the magnitude of error to be expected in t_+. The concentration is subject to a small error due to preparation of solutions. It may be affected noticeably, however, in the process of filling the cell or through possible contamination

(24) G. Jones and B. C. Bradshaw, *J. Am. Chem. Soc.*, **55**, 1780 (1933).

(25) T. W. Richards and H. G. Parker, *Proc. Am. Acad. Sci.*, **32**, 59 (1896).

(26) C. W. Foulk and M. Hollingsworth, *J. Am. Chem. Soc.*, **45**, 1223 (1923).

with the high pressure system. The latter errors cannot be estimated. The value for the cross-section A was determined within 0.1%. The error in the values for the resistance measurements due to diffusion is of the order of 0.1%. The variation in the current for a given run is about 0.05%. The slope of the resistance *versus* time curve has an error of about 0.05% when approximately ten points are used for determining the slope. Considering these possible errors in the determined parameters, the transference number given by our measurements should be accurate within 0.3%.

There is a small uncertainty in the concentration, because of the assumption that the Tait equation for pure solvent can be applied to the solution. The correction of cell constant and cross-sectional area for the compressibility of the glass tube could be more serious because the cell dimensions may not change reversibly with pressure. Happily we noted excellent reproducibility in resistance measurements with standard solutions, indicating that the application of pressure has no permanent effect upon the cell constant.

It is of interest to examine the sensitivity of the resistance method for measuring boundary position. The total resistance difference between the measuring cell filled with 0 1 N KCl and the cell filled with the following cadmium chloride solution is about 30,000 ohms. This figure of 30,000 ohms corresponds approximately to 10 cm. of boundary movement. Since the resistance can be read to ± 10 ohms, the uncertainty in boundary position attributable to resistance errors is only 0.003 cm.

Results and Discussion

The resistance measurements for a typical run are shown in Fig. 2. It will be observed that the

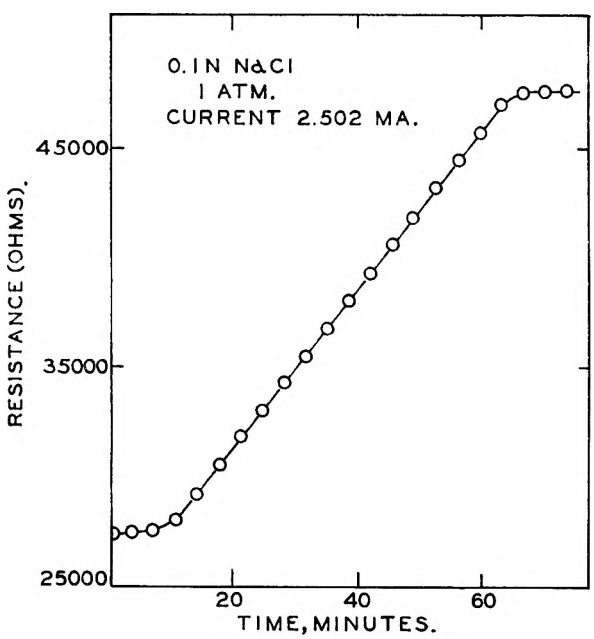

Fig. 2.—Typical resistance *vs.* time plot using cell illustrated in Fig. 1.

graph has three distinct parts. First a horizontal portion representing the resistance of the leading solution; second a linearly increasing portion representing movement of the boundary; finally another horizontal portion characteristic of the "following" solution. The time required for the boundary to travel between the two probe electrodes is thus clearly established. The cation transference numbers for 0.1 N solutions of HCl, KCl and NaCl at 25° are shown in Figs. 3, 4 and 5. For all of the experiments, the concentration refers to that of the solution prepared at 1 atm. pressure. It will be observed that for HCl, the cation transference number increases from 0.831 to about 0.835 in going from one to about 1000 atm. In the cases of KCl and NaCl, decreases of 2–3% are observed. The most general statement that can be made is that the transference number is not much affected by pressure. This is reasonable since the transference number represents a fraction and not an absolute quantity.

To calculate the effect of pressure upon the transference number of cadmium chloride, values of the equivalent conductance at 25° were taken from the "International Critical Tables."[27] Measurements of the effect of pressure and current passage upon the

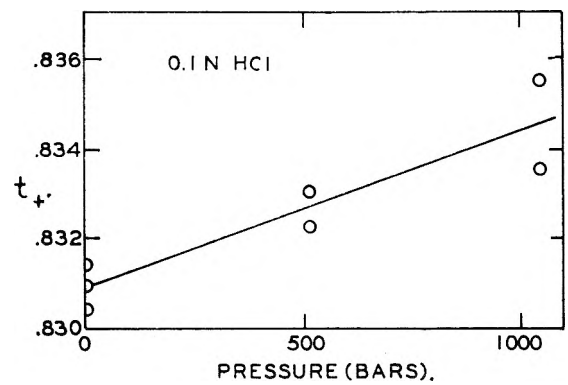

Fig. 3.—Cation transference number of 0.1 N HCl as function of pressure.

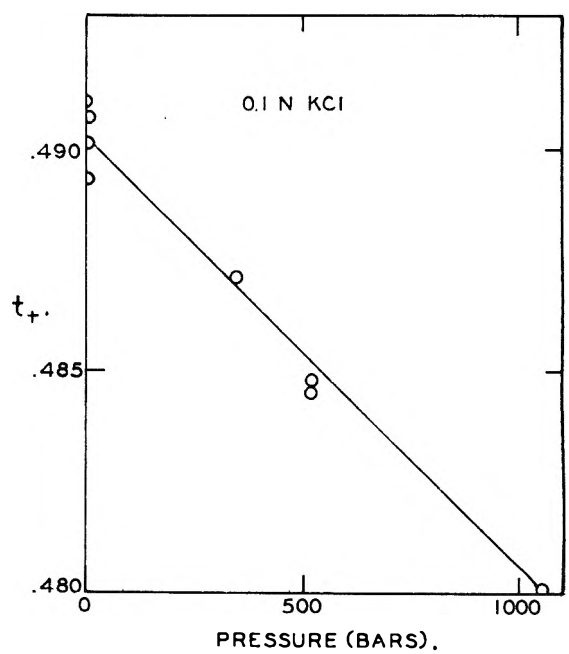

Fig. 4.—Cation transference number of 0.1 N KCl as function of pressure.

(27) "International Critical Tables," Vol. 6, McGraw-Hill Book Co., New York, N. Y., 1929, p. 232.

resistance of 0.144 and 0.072 N $CdCl_2$ solutions showed that the actual resistance measured in the transference cell can be corrected to 1 atmosphere by the factors 1.002 at 1 bar, 1.005 at 517 bars, and 1.095 at 1051 bars. The effect of pressure upon the cation transference number in $CdCl_2$ as determined from the Kohlrausch regulating function is shown in Table I. It will be observed that for this salt also, the cation transference number diminishes with pressure by about 3% for 1000 atm.

TABLE I

RATIO OF CATION TRANSFERENCE NUMBER OF $CdCl_2$ AT PRESSURE p TO THAT AT ONE ATM.

Leading soln.	$c_f^{(1)p}$	$t^{(p)}/t^{(1)}$ 517 bars	1051 bars
0.1 N KCl	0.088	0.982	0.966
0.1 N NaCl	0.110	.987	.971
0.1 N HCl	0.051	.984	.969

Assuming the Onsager equation[28] to be applicable to KCl and NaCl, the observed decreases in transference number with pressure cannot be accounted for by the increase of concentration with pressure, nor by changes brought about in the viscosity and dielectric constant. Thus we can expect that the transference number at infinite dilution will change with pressure. For the salts mentioned this dependence should be approximately that observed for the 0.1 N solutions.

The increase of cation transference number of HCl with pressure is consistent with recent theories for the conductance mechanism of the hydronium ion.[29] It has been suggested that the number of linear water chains increases with pressure, thus promoting hydronium ion transport. Protons presumably add on to one end and are ejected at the other, thus providing rapid transport.

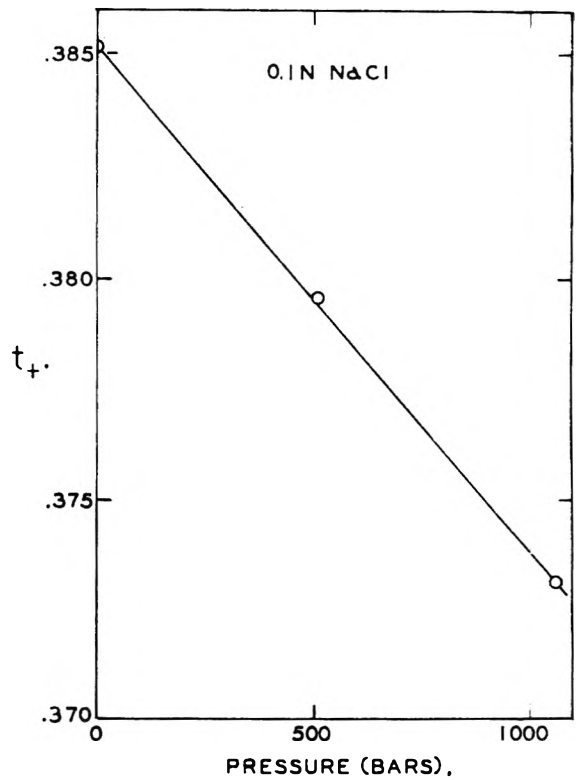

Fig. 5.—Cation transference number of 0.1 N NaCl as function of pressure.

(28) H. S. Harned and B. B. Owen, "Physical Chemistry of Electrolytic Solutions," Reinhold Publ. Corp., New York, N. Y., 1943, p. 162.

(29) A. Gierer and K. Wirtz, *Ann. Physik.*, **6**, 257 (1949).

NOTES

NOTE ON THE KINETICS OF THE REACTIONS OF THE PROPYL RADICAL WITH OXYGEN

BY CHARLES N. SATTERFIELD AND ROBERT C. REID

Department of Chemical Engineering, Massachusetts Institute of Technology, Cambridge, Mass.

Received July 19, 1954

Previous experimental studies of the partial oxidation of propane have led to the hypothesis that the propyl radical, which is initially formed, reacts in the homogeneous phase essentially in three alternate directions,[1] reaction 1 predominating at relatively low temperatures, below about 300°, reaction 2 at intermediate temperatures, and reaction 3 at high temperatures, above about 550°

$$C_3H_7\cdot + O_2 \longrightarrow C_3H_7OO\cdot \longrightarrow \text{oxygenated organic species} \quad (1)$$

$$C_3H_7\cdot + O_2 \longrightarrow C_3H_6 + HO_2\cdot \quad (2)$$

$$C_3H_7\cdot \longrightarrow C_2H_4 + CH_3\cdot \quad (3)$$

Arguments for this mechanism and reasons for discarding alternate reactions have been discussed in detail.[1,2] All of the propylene isolated is believed to result from reaction 2. Products isolated which are formed *via* the propyl peroxy radical (with possible intermediate formation of propyl hydroperoxide and other species) are formaldehyde, acetaldehyde, methanol and the carbon oxides,[3-7]

(1) C. N. Satterfield and R. E. Wilson, *Ind. Eng. Chem.*, **46**, 1001 (1954).

(2) C. N. Satterfield and R. C. Reid, "Fifth International Symposium on Combustion," Pittsburgh, Pa., September 1954, proceedings to be published by Reinhold Publishing Corp., New York, N. Y.

(3) B. Lewis and G. von Elbe, "Combustion, Flames and Explosions of Gases," Academic Press, Inc., New York, N. Y., 1951.

(4) F. E. Malherbe and A. D. Walsh, *Trans. Faraday Soc.*, **46**, 824, 835 (1950).

(5) N. C. Robertson, "The Partial Oxidation of Hydrocarbons," Chapter in B. T. Brook's book "Hydrocarbon Reactions" (to be published).

(6) E. R. Bell, J. H. Raley, F. F. Rust, F. H. Seubold and W. E. Vaughan, *Disc. Faraday Soc.*, No. **10**, 242 (1951).

(7) A. D. Walsh, *J. Chem. Soc.*, 331 (1943).

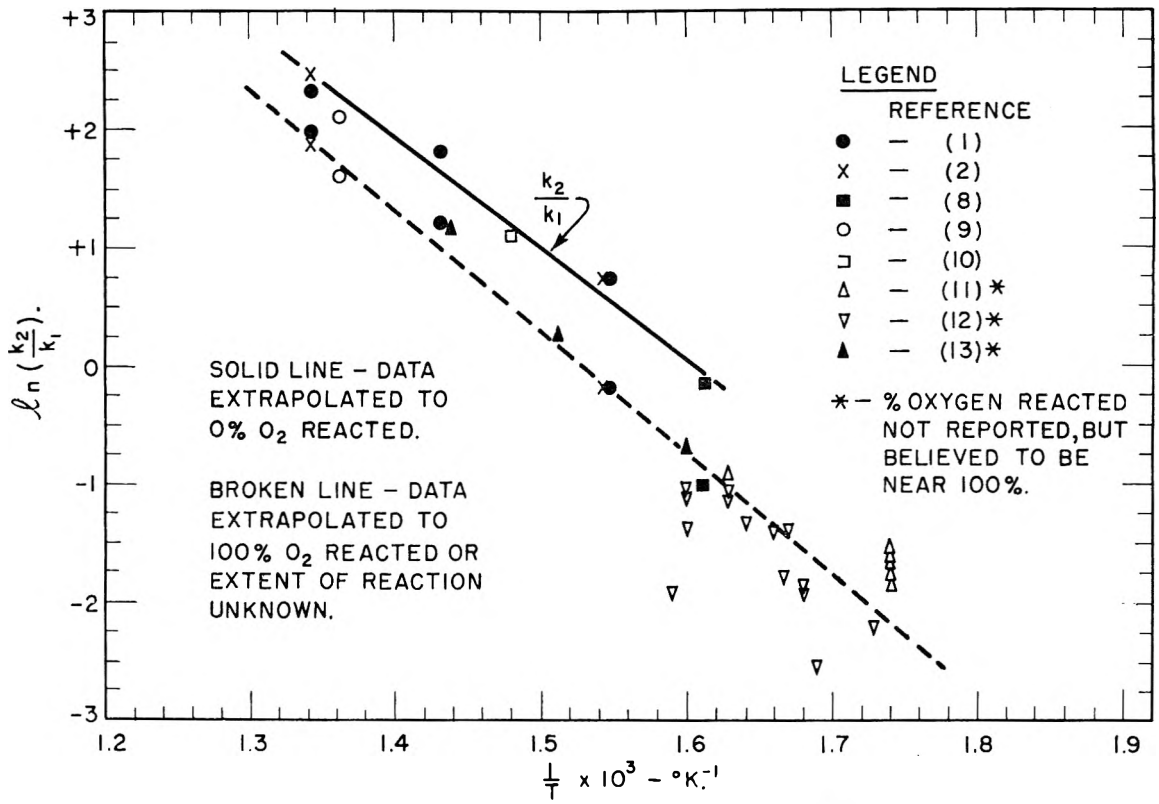

Fig. 1.—Effect of temperature on ratio k_2/k_1.

and these are referred to here collectively as oxygenated organic species.

By dividing the rate expression for reaction 2 by that for reaction 1, the following relationship is found

$$\frac{\text{moles propylene formed}}{\text{moles of propane forming oxygenated organic species}} = k_2/k_1 = \text{constant}$$

or since all of the propane which reacts proceeds through the propyl radical which either thermally decomposes to ethylene or reacts with oxygen, the fraction

$$\frac{\text{moles propylene formed}}{\text{total moles of propane reacted, less moles ethylene formed}}$$

called F, is the fraction of propyl radicals reacting with oxygen which do so to form propylene, and equals $k_2/(k_1 + k_2)$. The ratio $k_2/(k_1 + k_2)$ should be independent of the propane/oxygen ratio, but would be a function of temperature.

The above neglects further reaction of oxygen with products from reactions 2 and 3. If relatively high ratios of propane to oxygen are studied, as has frequently been the case, the ratio, F, as calculated from the products actually isolated is found to vary only slightly with the extent of reaction. If values of this ratio, for various fractions of oxygen reacted, are calculated from the experimental data[1,2,8-10] and extrapolated to zero per cent. reaction, the value of F at this limit equals the true value of $k_2/(k_1 + k_2)$. These values may be used to calculate k_2/k_1 which may be expressed in terms of an Arrhenius-type expression to give the relationship

$$\ln (k_2/k_1) = (P_2/P_1) + (E_1 - E_2)/RT$$

where P represents the probability factor. The collision number is the same for the two reactions and does not appear in the final expression. Values of $\ln (k_2/k_1)$ are plotted in the figure *versus* the reciprocal of the temperature, as the solid line.

In some investigations, product compositions were reported only for conditions under which the oxygen was substantially completely reacted. Therefore, they could not be used directly to calculate k_2/k_1. However, they can be compared with the studies used to construct the k_2/k_1 line, by considering the latter data as extrapolated to 100% reaction. The comparison is shown by the broken (lower) line of the figure which includes the data used to construct the k_2/k_1 line plus values of Pease,[11] Harris and Egerton,[12] and Antonovski and Shtern.[13] The percentage of initial oxygen reacted was not given by the last three groups of authors but it is believed it was near 100%. The ordinate for the broken line is the ratio of propylene to oxygenated organic species isolated at approximately 100% reaction of oxygen.

The slope of the line for k_2/k_1 gives a value of $-19{,}000$ cal. for the difference between the energy of activation of reaction 1 and of reaction 2. The ratio P_2/P_1 has a value of about 4×10^5, which indicates that in an activated collision the probability is very small that the propyl radical and oxygen

(8) N. Chernyak and V. Shtern, *Doklady Akad. Nauk, S.S.S.R.*, **78**, 91 (1951).
(9) P. L. Kooyman, *Rec. trav. chim.*, **66**, 205, 217, 491 (1947).
(10) D. M. Newitt and L. S. Thorne, *J. Chem. Soc.*, 1656 (1937).
(11) R. N. Pease, *J. Am. Chem. Soc.*, **57**, 2296 (1935).
(12) E. J. Harris and A. Egerton, *Chem. Revs.*, **21**, 287 (1937).
(13) V. L. Antonovski and V. Shtern, *Doklady Akad. Nauk, S.S.S.R.*, **78**, 303 (1951).

will meet with the proper orientation and favorable distribution of the activation energy at the moment of collision to allow the union of the two species to occur. On the other hand the abstraction of a hydrogen atom by oxygen here should not require a highly unusual set of conditions if the requisite activation energy is available, and P_2 is probably of normal magnitude.

Two interesting observations proceed from the above. (1) It is remarkable how closely this large group of experimental studies agree with one another when analyzed in this fashion, as shown on the figure, particularly in view of the complex nature of hydrocarbon oxidation mechanisms. (2) The probability factor deduced for reaction 1 by this method of analysis has the abnormally low value frequently found in similar bimolecular reactions where a more complicated structure is formed by combination of reactants.

These results lend additional support to the hypothesis that reactions 1, 2 and 3 are the predominating reactions of the propyl radical in the oxidation of propane.

THE THREE-COMPONENT SYSTEM BENZALDEHYDE–WATER–ACETIC ACID

By Alexander R. Amell and Thomas Teates

A Contribution from the Chemistry Department, Lebanon Valley College, Annville, Penna.

Received September 25, 1954

During a study of the oxidation of certain alcohols being carried out in this Laboratory, it became necessary to determine the distribution of benzaldehyde in an acetic acid–water system. Since a search of the literature revealed no data on this system, a study of the three-component system benzaldehyde–water–acetic acid was made.

Experimental

Benzaldehyde exposed to the atmosphere for a short time was found to contain about 2% benzoic acid. Eastman Kodak white label benzaldehyde was distilled at a pressure of 3 to 7 mm. of mercury under a nitrogen atmosphere. The benzaldehyde purified in this way had a refractive index of 1.5443 at 20° (lit. value corrected to 20° is 1.5456).[1] Titrations of aliquots of this benzaldehyde in water showed that it still contained 0.1% acid. This content was considered satisfactory for this study and benzaldehyde was used without further purification. It was stored in a nitrogen atmosphere and all transfers were made in a nitrogen atmosphere. Glacial acetic acid and distilled water were used throughout.

Temperatures of all reactions were held constant to within 0.5°. Known weights of benzaldehyde and acetic acid were buretted into a flask and titrated with water to the appearance of the second phase. In the titrations in which the water concentration was very high, benzaldehyde was titrated into known weights of acetic acid and water to improve the sharpness of the end-points.

Various known mixtures in the two-phase region of the three components were thoroughly mixed and the layers separated. The densities of the layers were determined and each layer titrated with standard sodium hydroxide. From these data the tie lines were determined at each temperature by standard procedures.[2] At 25° a number of tie lines were determined but only one tie line each at 15 and 40°. These showed the tie lines at all temperatures to be essentially the same.

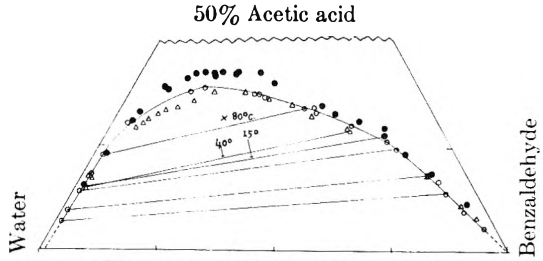

Fig. 1.—○, 25°; ●, 15°; △, 40°.

Experiments were carried out at 15, 25 and 40°. Data are given in the graph. Because of the small temperature coefficient of solubility over this range one point was determined at 80° and also is given on the graph.

(1) N. A. Lange, "Handbook of Chemistry," Handbook Publishers, Inc., Sandusky, Ohio, 1952, p. 1312.

(2) Daniels, Mathews and Williams, "Experimental Physical Chemistry," McGraw-Hill Book Co., Inc., New York, N. Y., 1949, pp. 117–120.

ACTIVATION ENERGY AND ENTROPY FOR ADSORPTION

By Takao Kwan[1]

The Research Institute for Catalysis, Hokkaido University, Sapporo, Japan

Received October 16, 1954

It is well known that there is a regular relationship between the activation energy and the frequency factor of the Arrhenius equation, $k = Ae^{-E/RT}$, expressed by $\log A = c + bE$ (c and b are constants),[2] when a chemical reaction takes place over a series of catalysts of a similar type. This means that the rate constant does not change as much as might be expected from the change of E because the term A acts simultaneously in a compensating manner.

There are many other examples of this phenomenon. The Richardson formula for electron emission, $i = AT^2e^{-\epsilon\varphi/kT}$, is subject to a compensatory effect between the work function φ and the constant A when the metal surface is covered by various gases.[3] The specific conductivity of a semiconductor which has the form $\sigma = ae^{-\epsilon/kT}$, and substitution reactions in organic chemistry sometimes show a similar trend.[4,5]

This effect also has been observed for the adsorption of gases on solid catalysts. Here we shall investigate the effect for the adsorption of nitrogen on a promoted iron catalyst. The rate of the adsorption of nitrogen on the catalyst can be expressed by[6,7]

$$k \equiv -\frac{1}{p} \times \frac{dp}{dt} = k_a\theta^{-\alpha} \qquad (1)$$

where p is the pressure of nitrogen at time t, θ the fraction of surface covered, and α, k_a are constants. As shown in Fig. 1 α varies linearly with the reciprocal of absolute temperature within a range

(1) Fulbright scholar, now visiting lecturer, University of Washington, Seattle, Washington.

(2) G. M. Schwab, H. S. Taylor and R. Spence, "Catalysis," Van Nostrand Co., New York, N. Y., 1937, p. 286.

(3) J. H. de Boer, "Electron Emission and Adsorption Phenomena," Cambridge Press, New York, N Y., 1935, p. 152.

(4) W. Meyer and H. Neldel, *Physik. Z.*, **38**, 114 (1937).

(5) For example see I. Meloche and K. J. Laidler, *J. Am. Chem. Soc.*, **73**, 1712 (1953).

(6) T. Kwan, *J. Res. Inst. Catalysis*, **3**, 16 (1953).

(7) T. Kwan and K. Yamamori, *Kagaku*, **23**, 533 (1953).

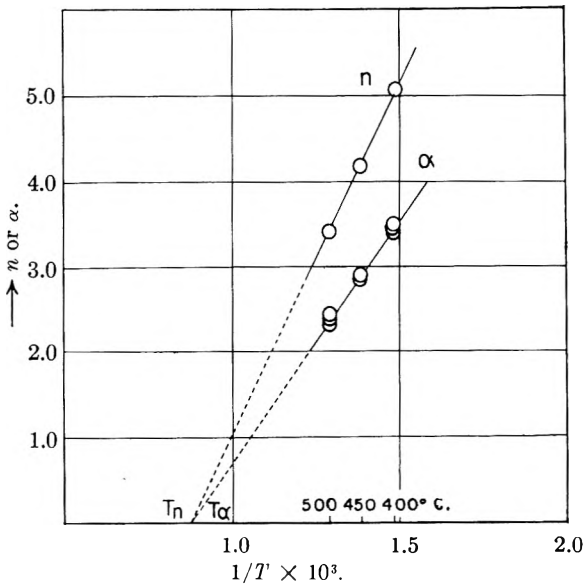

Fig. 1.—Temperature dependencies of n and α for the adsorption of nitrogen on a promoted iron catalyst.

from 400 to 500°. Let the slope of this straight line be g/R (R is the gas constant); we have then

$$\alpha = \frac{g}{RT} - \frac{g}{RT_\alpha} \qquad (2)$$

From equations 1 and 2 we have

$$E \equiv RT^2\left(\frac{\partial \ln k}{\partial T}\right)_\theta = g \ln \theta + E_a \qquad (3)$$

for the Arrhenius activation energy. Here $E_a \equiv RT^2(\mathrm{d} \ln k_a/\mathrm{d}T)$. According to the theory of absolute reaction rates[8] k is given by

$$k = \frac{kT}{h} e e^{\Delta S^*/R} e^{-E/RT} \qquad (4)$$

$$k_a = \frac{kT}{h} e e^{\Delta S_a^*/R} e^{-E_a/RT} \qquad (5)$$

Substitution of (2), (3) and (5) in (1) yields

$$k = \frac{kT}{h} e e^{\Delta S_a^*/R} e^{g \ln \theta/RT_\alpha} e^{-E/RT} \qquad (6)$$

From (4) and (6) the entropy of activation becomes

$$\Delta S^* = \frac{g \ln \theta}{T_\alpha} + \Delta S_a^* \qquad (7)$$

$$\text{or} \quad \Delta S^* = \frac{E}{T_\alpha} - \frac{E_a}{T_\alpha} + \Delta S_a^* \qquad (8)$$

The equation 8 indicates that E and ΔS^* are "compensatory." For the expression of the free energy of activation the thermodynamic definition gives

$$\Delta F^* = g\left(1 - \frac{T}{T_\alpha}\right) \ln \theta + \Delta F_a^* \qquad (9)$$

These thermodynamic quantities vary linearly with $\ln \theta$. This result conflicts however with the recent report[9] that these quantities vary linearly with θ.

(8) S. Glasstone, K. J. Laidler and H. Eyring, "The Theory of Rate Processes," McGraw-Hill Book Co., New York, N. Y., 1941, p. 199.

(9) P. Zwietering and J. J. Roukens, *Trans. Faraday Soc.*, **49**, 543 (1954).

Now the Arrhenius frequency factor A is given by (6) and thus the compensation effect, $\log A = c + bE$, requires that expressions

$$c = \log \frac{kT}{h} e + \frac{\Delta S_a^*}{2.3R} - \frac{E_a}{2.3RT_\alpha} \qquad (10)$$

$$b = 1/2.3RT_\alpha \qquad (11)$$

The values of the constants are $c = 3$ (500°) and $b = 1.9 \times 10^{-4}$ mole/cal. The latter value is approximately the same as those for catalyzed reactions[2] or specific conductivity of semiconductors.[4] This suggests that some common mechanism is operating in these reactions.

The adsorption isotherms of this system observed in the range of temperature from 400 to 500° and at equilibrium pressures ranging from 0.01 to about 30 mm. were found to obey the Freundlich equation except for low coverage. The log-log straight lines of these isotherms have a common intersection, if extrapolated linearly, $p = 320$ mm. Assuming the adsorption reaches a saturation or $\theta = 1$ at the intersection, we may express the adsorption isotherms as

$$\ln \theta = \frac{1}{n} \ln \frac{p}{p_s} \qquad (12)$$

where p_s is the equilibrium pressure at $\theta = 1$, a constant independent of temperature. The n of equation 12 is a linear function of reciprocal of absolute temperature as shown in Fig. 1. So it can be expressed by

$$n = \frac{\gamma}{RT} - \frac{\gamma}{RT_n} \qquad (13)$$

where γ/R is the slope of the straight line in the plot of n against $1/T$. We get from (12) and (13)

$$q \equiv RT^2\left(\frac{\partial \ln p}{\partial T}\right)_\theta = -\gamma \ln \theta \qquad (14)$$

for the isosteric heat of adsorption, and from (12), (13) and (14) we have

$$-q = -q\frac{T}{T_n} + RT \ln \frac{p}{p_s} \qquad (15)$$

Using the thermodynamic relation, $\Delta H = T\Delta S + \Delta F$, and remembering that $-q = \Delta H$ and $\Delta F = 0$, we have

$$\Delta S = \frac{\Delta H}{T} = \frac{\Delta H}{T_n} + R \ln \frac{p}{p_s} \qquad (16)$$

for the differential entropy of adsorption. If we take the standard state in the gas phase as 1 atm. and allow the perfect gas law, (16) becomes

$$\Delta S^0 = \frac{\Delta H}{T_n} - R \ln p_s \qquad (17)$$

The above equation indicates that ΔS^0 and ΔH are "compensatory" similarly as ΔS^* and E in the equation 8. Incidentally, T_n is approximately coincident with T_α, as shown in Fig. 1.

The compensation effect perhaps may be explained because the freedom of the system increases, due to loosened bonds with the surface and other adsorbed molecules, as the energy of the system increases.

COMMUNICATIONS TO THE EDITOR

A COMPARISON OF SORPTION CHARACTERISTICS OF SOME MINERALS HAVING A LAYER STRUCTURE

Sir:

The report by Young and Healey[1] showing that unactivated chrysotile adsorbed approximately twice as much water as nitrogen, expressed in units of surface area, is of interest to the science and technology of some minerals possessing a layer structure. It has recently been reported[2] that the mineral tobermorite ($4CaO \cdot 5SiO_2 \cdot 5H_2O$) the probable binder of autoclaved concrete block, also adsorbed approximately twice as much water as nitrogen. Because tobermorite has a layer structure the large adsorption of water compared to that of nitrogen became of interest regarding the drying shrinkage of concrete. Theoretical considerations indicate that the shrinkage is not a capillary phenomenon. Bernal[3] suggested that tobermorite may undergo the swelling-shrinkage changes similarly as do some clays which also have a layer structure. Such volume changes in clays are easily demonstrated by X-ray results on clays before and after drying. A similar hypothesis on concrete shrinkage was studied in these laboratories but it could not be demonstrated[2] that the water involved in volume change was inter-layer water. X-Ray results obtained subsequently[4] show that phases closely related to tobermorite may undergo significant structural changes during in-vacuum drying and subsequent re-saturation, but it has not yet been shown how such structural changes may be due to the movement of water or what effect they produce on the properties of concrete.

The present comments are being presented because similar sorption results on minerals having the layer structure have been interpreted differently by the writer, and Young and Healey. The sorption behavior of tobermorite (and antigorite as mentioned by these authors) shows that a portion of the water is accommodated differently than is nitrogen. Because these minerals generally occur as flat plate-like crystals explanations based on capillary phenomenon do not apply.

Young and Healey pointed out that chrysotile occurs in the form of capillaries having a bore of approximately 150 Å. and a diameter of about 350 Å. They postulate formation of water plugs at the ends of the capillaries which are permeable to polar substances, water and ammonia, but not to non-polar adsorbents as nitrogen. The water required to fill the pores would account for the much larger sorption of water than nitrogen.

Results on properties of chrysotile and antigorite components of serpentine, now being prepared for publication, included density measurements on several kinds of chrysotile in form of relatively large "bundles" of fiber and also in highly micronized form; the samples were tested as received. Water and carbon tetrachloride were used as immersion media. The density results were the same within limit of experimental error for both media and regardless of the degree of subdivision of the fiber. The spread in values amounted to about 2% but generally the differences were less than 1%. If the ends of the capillaries were plugged with water, the density results obtained with carbon tetrachloride, a non-polar medium, would be approximately 15 to 20% lower than in water. These results, and others on the crystal habits of antigorite and chrysotile which will be submitted for publication, suggest that water plugs probably do not form in the tube-shaped crystals of chrysotile.

Antigorite and chrysotile are either the same in compositions and atomic structure or very closely related. It would seem, therefore, that the sorption characteristic should be the same for both. The mechanism of adsorption-desorption of these two minerals may be the same as that for tobermorite, presumably that of movement of structural water. As mentioned, however, this hypothesis remains to be resolved experimentally. It would appear that careful studies on sorption characteristics and surface energy changes such as those being conducted at the Surface Chemistry Laboratories at Lehigh University, should provide an unequivocal proof on the manner in which the excess water is adsorbed by the layer structure minerals. Such basic information will be of great help to concrete technology, to mention only one field of application.

Owens-Illinois Company
1700 North Westwood
Toledo, Ohio
G. L. Kalousek

Received January 27, 1955

(1) G. J. Young and F. H. Healey, This Journal, **58**, 881–884 (1954).

(2) G. L. Kalousek, *J. Amer. Concr. Institute*, **26**, 233–248 (1953).

(3) J. D. Bernal, "Structures of Cement Hydration Compounds," *Proc. 3rd International Symp. on Chemistry of Cements*, p. 216–236 (1952).

(4) G. L. Kalousek, "Tobermorite and Related Phases in the System CaO–SiO_2–H_2O," *J. Amer. Concr. Institute*, accepted for publication.

FORMATION OF DIBORANE DURING THE SLOW OXIDATION OF PENTABORANE

Sir:

When dry air was admitted slowly to a gas absorption cell containing pure pentaborane at 25° and a pressure of 50 mm., partial oxidation took place and diborane, hydrogen and a white solid were formed. The reaction was conducted in a cell 10 cm. in length, with a volume of 150 ml. Absorption measurements were made with a Perkin-Elmer Model 21 double-beam infrared recording spectrometer. The progressive disappearance of pentaborane and the simultaneous accumulation of diborane were followed by infra-

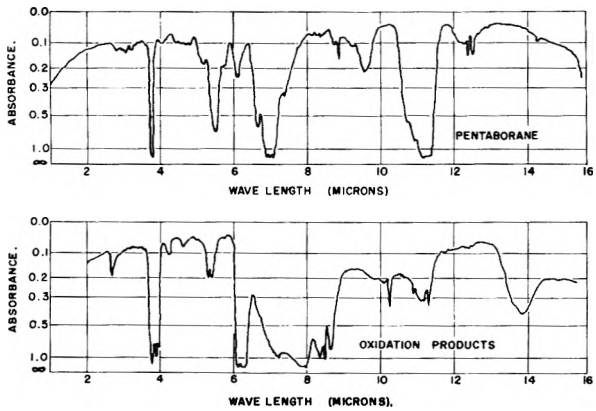

Fig. 1.—Infrared spectra of pentaborane and of the products formed during its slow oxidation.

red absorption measurements, made possible because of the differing spectra of the two hydrides.[1] At the end of the reaction, after six hours, when the total pressure approached 1 atm., the partial pressure of diborane was approximately 10 mm. The initial absorption spectrum of the pentaborane and the final absorption spectrum of the reaction mixture after the reaction was complete are shown in Fig. 1.

It is evident that initial reaction of oxygen with pentaborane results in incomplete oxidation. Unstable residues of the partially oxidized pentaborane molecules may be the source of the diborane formed. At the temperature and pressure at which the reaction took place, diborane–oxygen mixtures are well below the spontaneous explosion limit.[2,3] The spectrum of the white solid reaction product, which absorbs strongly at 7.9 and 13.8 microns, differs from that of boric acid and the higher boron hydrides. The solid is presumed to be HBO_2 or B_2O_3.

DEPARTMENT OF CHEMISTRY
RENSSELAER POLYTECHNIC INSTITUTE
TROY, N. Y.

HARRY C. BADEN
STEPHEN E. WIBERLEY
WALTER H. BAUER

RECEIVED FEBRUARY 5, 1955

(1) L. V. McCarty, G. C. Smith and R. S. McDonald, *Anal. Chem.*, **26**, 1027 (1954).

(2) W. Roth and W. H. Bauer, *Fifth Symposium on Combustion*, John Wiley and Sons, Inc., following publication.

(3) F. P. Price, *J. Am. Chem. Soc.*, **72**, 5361 (1950).

ANNOUNCING

New Schedule of Back Issue Prices

Effective January 1, 1955

American Chemical Society Journals

RATES FOR SINGLE COPIES OF CURRENT ISSUES AND BACK NUMBERS

Single copies or complete volumes of nearly all the ACS journals listed below may be purchased at these prices.

NOTE: In the event an issue appears in two or more parts, a special issue price will apply.

Journal	Current Year	Back Years	Foreign Postage	Canadian Postage
ANALYTICAL CHEMISTRY				
(formerly Analytical Edition)				
Volumes 1–4	...	$2.00	$0.15	$0.05
Volumes 5–8	...	1.25	.15	.05
Volume 9 et seq.	$1.00	1.50	.15	.05
CHEMICAL ABSTRACTS, Volumes 11–30				
Numbers 1–22	...	1.25	.15	.05
Numbers 23 and 24 (Author & Subject Index)	...	3.00	.45	.15
CHEMICAL ABSTRACTS, Volume 31 et seq.				
Numbers 1–22	2.00	2.25	.15	.05
Number 23 (Author Index)	12.00*	12.00*	free	free
Number 24 (Subject Index)	24.00*	24.00*	free	free
CHEMICAL AND ENGINEERING NEWS, Vols. 1–24	...	.25	.05	free
CHEMICAL AND ENGINEERING NEWS, Vol. 25 et seq.	.40	.50	.05	free
INDUSTRIAL AND ENGINEERING CHEMISTRY	1.50	2.00	.15	.05
JOURNAL OF AGRICULTURAL AND FOOD CHEMISTRY	1.00	1.25	.15	.05
JOURNAL OF THE AMERICAN CHEMICAL SOCIETY				
Volumes 32–73	...	1.75	.15	.05
Volume 74 et seq.	1.00	1.50	.15	.05
JOURNAL OF PHYSICAL CHEMISTRY				
Volume 56 et seq.	1.00	1.75	.15	.05

* A special rate of 50% of these amounts applies to orders from ACS members for personal use.

RATES FOR VOLUMES OF BACK NUMBERS

		Foreign Postage	Canadian Postage
ANALYTICAL CHEMISTRY			
(formerly Analytical Edition)			
Volumes 1–8	$7.50	$0.75	$0.25
Volume 9, et seq.	15.00	.75	.25
CHEMICAL ABSTRACTS			
Volumes 11–30	25.00	2.40	.80
Volume 31, et seq.	65.00	2.40	.80
CHEMICAL AND ENGINEERING NEWS			
Volumes 1–24	5.00	2.25	.75
Volume 25 et seq.	20.00	2.25	.75
INDUSTRIAL AND ENGINEERING CHEMISTRY			
Volume 1 et seq.	20.00	2.25	.75
JOURNAL OF AGRICULTURAL AND FOOD CHEMISTRY			
Volume 1 et seq.	10.00	1.50	.50
*JOURNAL OF THE AMERICAN CHEMICAL SOCIETY			
Volume 32 et seq.	20.00	1.50	.50
*JOURNAL OF PHYSICAL CHEMISTRY			
Volume 56 et seq.	15.00	1.20	.40

* Prior Volumes—Order from Walter Johnson, 125 East 23rd Street, New York 10, N. Y.

American Chemical Society

Back Issue Department

1155 Sixteenth Street, N.W. Washington 6, D.C.